SOIL RESTRAINTS ON STEEL BURIED PIPELINES CROSSING ACTIVE SEISMIC FAULTS

by

MANUEL MONROY-CONCHA

B.Sc., Universidad Nacional de San Agustín, Arequipa, Peru, 2000
M.Sc. (Eng). Pontificia Universidad Católica del Perú, Lima, Peru, 2004

A THESIS SUBMITTED IN PARTIAL FULFILLMENT OF

THE REQUIREMENTS FOR THE DEGREE OF

DOCTOR OF PHILOSOPHY

in

THE FACULTY OF GRADUATE AND POSTDOCTORAL STUDIES

(Civil Engineering)

THE UNIVERSITY OF BRITISH COLUMBIA

(Vancouver)

August 2013

© **Manuel Monroy-Concha, 2013**

ABSTRACT

The quantification and prediction of soil restraint on buried pipelines are essential for the design of pipeline systems crossing seismic faults, and in turn to reduce the risk of pipeline damage due to geotechnical earthquake hazards. Full-scale soil-pipe interaction tests were undertaken to better simulate the mobilization of soil restraints under controlled conditions and to provide insight on a number of currently unresolved technical issues that so far have been investigated only based on small-scale tests. In particular, an existing full-scale testing chamber was significantly modified to simulate pipeline breakout from its soil embedment on one side of a strike-slip fault and on the footwall side of a reverse fault in an effort to characterize lateral, combined axial and lateral, and vertical oblique soil restraints. The experimental system was also used to assess the effectiveness of reducing soil loads on pipelines using geotextiles. The following was noted: (1) approaches based on limit equilibrium reasonably well predict maximum values of lateral soil restraint for shallow pipelines backfilled with sand, with mixture of crushed gravel and sand, and with crushed limestone; (2) the lateral soil restraint on pipes in geotextile-lined trenches increased with increasing relative pipe displacement and could even be higher than the restraint without the geotextile lining. A procedure was developed to capture this behaviour; (3) experimental and numerical results for geotextile-lined trenches suggest that the shear resistance is not controlled solely by the geotextile interface; as such, there is no clear benefit in using geotextile-based mitigation measures for reducing soil loads; (4) the results from tests on combined axial and lateral soil restraints provided limited clarification on whether or not these soil restraints should be considered independent for fault crossing designs. This was due to the difficulty in selecting an axial soil restraint value to anchor existing soil restraint interaction relationships. No axial soil restraint tests were conducted in this work; and (5) values for the maximum vertical oblique soil restraint diminish as the inclination of the angle of breakout of buried pipelines increases with respect to the horizontal.

PREFACE

This dissertation contains details of a research program conducted in the Civil Engineering Department of the University of British Columbia during the period from 2009 – 2012. Professor Wijewickreme was the supervisory author on this project. Author also acknowledges the constructive comments from the members of the supervisory committee to improve the readability and presentation of results.

The design of the full-scale soil-pipe interaction testing chamber presented in Chapter 3 was done mainly by myself, with suggestions from Professor Wijewickreme and Dr. D. Nyman (for vertical oblique tests), as well as support from Mr. Harald Schremp and Mr. Doug Smith.

The preparation of samples and development of full-scale tests in Chapter 4, Chapter 5 and Chapter 6 were performed by myself, with assistance from many other collaborators. The analysis of test data, concept formation and interpretation of the results for cases with trench wall in Chapter 4 are my original work. The interpretation of results in Chapter 5 was mainly done by myself in coordination with Professor Wijewickreme and Mr. Doug Honegger. I did the numerical analyses described in Chapter 7, while Professor Byrne and Professor Wijewickreme provided consultation and review.

Following is a list of publications arisen to date from the studies presented in this dissertation. Also presented next to the publication is the corresponding chapter(s) of the dissertation in which the work is located.

Monroy M., Wijewickreme D., Honegger D. (2012) Effectiveness of Geotextile-Lined Pipeline Trenches Subjected To Relative Lateral Seismic Fault Ground Displacements, *Proceedings 15th World Conference on Earthquake Engineering*, 2534, Lisbon, Portugal. (Chapter 4).

Monroy M., Wijewickreme D., Honegger D. (2013) Effectiveness of Geotextiles in Reducing Levels of Soil Restraint for Buried Pipelines Crossing Seismic Faults, *21st Vancouver Geotechnical Society Symposium on Foundation and Lifeline Engineering*, B.C., Canada. (Chapter 4 and 6).

TABLE OF CONTENTS

ABSTRACT ii
PREFACE iii
TABLE OF CONTENTS iv
LIST OF TABLES ix
LIST OF FIGURES x
NOMENCLATURE xviii
ACKNOWLEDGMENTS xx
DEDICATION xxii

CHAPTER 1: INTRODUCTION 1
1.1 Geotechnical Earthquake Hazards and Buried Pipeline Performance during Earthquakes 3
1.1.1 Geotechnical Earthquake Hazards 3
1.1.2 Buried Pipeline Performance during Earthquakes 9
1.2 Mitigation Measures for Reducing Soil Restraint at Fault Crossings 11
1.3 Objectives and Organization of the Thesis 13
1.3.1 Objectives 13
1.3.2 Organization 15
CHAPTER 2: LITERATURE REVIEW 17
1.4 Horizontal and Axial Soil Restraints on Buried Pipes 18
1.4.1 Horizontal Soil Restraint 19
1.4.2 Axial Soil Restraint 31
1.5 Interaction of Horizontal and Axial Soil Restraint on Buried Pipes 37
1.6 Interaction of Horizontal and Upward Vertical Soil Restraint 45
1.7 Effects of Trapezoidal Trench on Levels of Lateral Soil Restraint 50
1.8 Use of Geotextile to Reduce Soil Restraint on Buried Pipelines 52
CHAPTER 3: EXPERIMENTAL ASPECTS 57
3.1 Experimental Apparatus 58
3.1.1 Original Soil-Pipe Interaction Testing Chamber 58
3.1.2 Modified Soil-Pipe Interaction Testing Chamber 60
3.2 Loading System 64
3.3 Description of Materials 71
3.3.1 Backfill Materials 71
3.3.2 Pipe specimens 80

3.3.3 Geotextile and Soil-Geotextile Interface Materials 81
3.4 Experimental Procedures 84
3.4.1 Backfill Placement and Density Control 84
3.4.2 Pipe Specimen Placement and Coupling System 87
3.4.3 Trench with Sloping Surface (“Trench Wall”) 89
3.4.4 Trench Wall Lining Configurations 92
3.5 Instrumentation and Data Acquisition 96
3.5.1 Measurement of Loads (Soil Restraints) 96
3.5.2 Measurement of Pulling Angle 98
3.5.3 Measurement of Pipe Displacement 99
3.5.4 Measurement of Geotextile Displacement 99
3.5.5 Measurement of Soil Pressure on Pipe Surface 101
3.5.6 Measurement of Backfill Density 102
3.6 Development of the Testing Program 102
3.6.1 Lateral Soil Restraints 105
3.6.2 Reduction of Lateral Soil Restraints by Geosynthetic Fabric 108
3.6.3 Horizontal Oblique Soil Restraints 109
3.6.4 Vertical Oblique Soil Restraints 111
3.7 Experimental Limitations and Associated Errors 112
3.7.1 Control of Backfill Density 113
3.7.2 Boundary Conditions 114
3.7.3 Loading System Mechanisms 118
3.8 Summary of the Chapter 119
CHAPTER 4: LATERAL SOIL RESTRAINT ON BURIED PIPELINES 122
4.1 Summary of Test Parameters 123
4.2 Results of Lateral Soil Restraint Tests on Pipe Buried in Sand Backfill 124
4.2.1 Normalised Load-Displacement Response on Sand 125
4.2.2 Recorded Contact Pressure for Sand Backfill 127
4.2.3 Observed Backfill Soil Deformation Geometry for Sand 130
4.3 Results of Lateral Soil Restraint Tests on Pipe Buried in Road Mulch Backfill 136
4.3.1 Normalised Load-Displacement Response on Road Mulch 136
4.3.2 Recorded Contact Pressure for Road Mulch Backfill during Lateral Pulling 137
4.3.3 Observed Backfill Soil Deformation Geometry on Road Mulch 139

4.4 Results of Lateral Soil Restraint Tests on Pipe Buried in Crushed Limestone Backfill 141

4.4.1 Normalised Load-Displacement Response – Crushed Limestone 141

4.4.2 Recorded Contact Pressure for Crushed Limestone Backfill during Lateral Pulling 142

4.4.3 Observed Backfill Soil Deformation Geometry for Crushed Limestone. 144

4.5 Results of Tests on Reduction of Lateral Soil Restraint by Geosynthetic Fabrics - Sand Backfill..... 146

4.5.1 Normalised Load-Displacement Response for Geotextile-Lined Pipeline Trench - Sand Backfill..... 147

4.5.2 Recorded Contact Pressure for Geotextile-Lined Pipeline Trenches - Sand Backfill..... 152

4.5.3 Observed Sand Backfill Deformation Geometry for Geotextile-Lined Pipeline Trench – Sand Backfill..... 154

4.5.4 Recorded Movement of Upper Geotextile - Sand Backfill 158

4.6 Results of Tests on Reduction of Lateral Soil Restraint by Geosynthetic Fabric - Road Mulch Backfill..... 159

4.6.1 Normalised Load-Displacement Response for Geotextile-Lined Pipeline Trench - Road Mulch Backfill 160

4.6.2 Recorded Movement of Upper Geotextile - Road Mulch Backfill..... 161

4.7 Evaluation of Test Results..... 163

4.7.1 General Comments on Maximum Lateral Soil Restraint 163

4.7.2 Estimation of Maximum Lateral Soil Restraint for Cases with no Trench 168

4.7.3 Estimation of Lateral Soil Restraint for Cases with Trench Wall..... 178

4.8 Summary of the Chapter 190

CHAPTER 5: HORIZONTAL OBLIQUE SOIL RESTRAINT ON PIPELINES 193

5.1 Summary of Test Parameters..... 194

5.2 Framework for Interpreting Horizontal Oblique Tests 196

5.3 Results of Horizontal Oblique Tests – β = 75 degrees..... 199

5.3.1 Soil Restraint-Displacement Response 199

5.4 Results of Horizontal Oblique Tests – β = 60 degrees..... 203

5.4.1 Load-Displacement Response 203

5.5 Results of Horizontal Oblique Tests – β = 45 degrees..... 205

5.5.1 Load-Displacement Response 205

5.6 Discussion on Horizontal Oblique Pipe-Soil Interaction 207

5.7 Summary of the Chapter 221

CHAPTER 6: VERTICAL OBLIQUE SOIL RESTRAINT ON PIPELINES 224

6.1 Summary of Test Parameters 225

6.2 Results of Vertical Oblique Soil Restraint Tests Using Sand Backfill (θ = 45°) 228

6.2.1 Normalized Soil Restraint-Displacement Response: Sand Backfill - θ = 45° 228

6.2.2 Recorded Soil Restraint Angle: Sand Backfill - θ = 45° 229

6.2.3 Observed Soil Deformation Geometry: Sand Backfill - θ = 45° 232

6.3 Results of Vertical Oblique Soil Restraint Tests on Crushed Limestone Backfill (θ = 45°) 234

6.3.1 Normalized Load-Displacement Response: Crushed Limestone Backfill - θ = 45° 234

6.3.2 Recorded Soil Restraint Angle: Crushed Limestone Backfill - θ = 45° .. 236

6.3.3 Observed Soil Deformation Geometry: Crushed Limestone Backfill - θ = 45° 238

6.4 Results of Vertical Oblique Soil Restraint Tests in Crushed Limestone Backfill (θ = 35°) 240

6.4.1 Normalized Load-Displacement Response: Crushed Limestone Backfill - θ = 35° 240

6.4.2 Recorded Soil Restraint Angle: Crushed Limestone Backfill - θ = 35° .. 242

6.4.3 Observed Backfill Soil Deformation Geometry: Crushed Limestone Backfill - θ = 35° 244

6.5 Results of Vertical Soil Restraint Tests Using Sand or Crushed Limestone Backfill (θ = 90°) 247

6.5.1 Normalized Load-Displacement Response: Sand or Crushed Limestone Backfill (θ = 90°) 247

6.5.2 Observed Backfill Soil Deformation Geometry: Sand and Crushed Limestone Backfill (θ = 90°) 249

6.6 Summary of Soil Restraint Tests 252

6.7 Summary of the Chapter 254

CHAPTER 7: NUMERICAL SIMULATION OF LATERAL SOIL 257

RESTRAINT 257

7.1 Numerical Simulation Procedure 258

7.1.1 Constitutive Models for Soil Backfills 259

7.2 Numerical Simulation of Lateral Soil Restraint on Pipelines 273

7.2.1 Numerical Simulation for Cases with no Trench 273

7.2.2 Numerical Simulation for Cases with Geotextile-lined Trench Wall 285

7.3 Summary of the Chapter 307

CHAPTER 8: SUMMARY, FINDINGS AND FURTHER STUDIES 310
8.1 Testing Apparatus for Soil-Pipe Interaction 311
8.2 Lateral Soil Restraint on Buried Pipelines 311
8.3 Combined Axial and Lateral Soil Restraints on Buried Pipelines 313
8.4 Vertical Oblique Soil Restraint on Buried Pipelines 315
8.5 Numerical Simulation of Lateral Soil Restraint 317
8.6 Further Studies..... 319
REFERENCES..... 321
APPENDICES 333
Appendix A: Direct Shear Test Results on Backfill Materials..... 334
Appendix B: Direct Shear Test Results on Backfill-Geotextile Interface 337
Appendix C-1: Lateral Soil Restraint vs. Pipe Displacement 343
Appendix C-2: Horizontal Oblique Soil Restraint vs. Pipe Displacement 353
Appendix C-3: Vertical Oblique Soil Restraint vs. Pipe Displacement 357
Appendix D: Cysoil Model..... 365
Appendix E: Additional Photographs 372
Appendix F: Soil Pressure Sensor Calibration..... 394

LIST OF TABLES

Table 3.1: Identification of Testing Chamber Test Equipment 68

Table 3.2: Test Pipe Sizes Used in the Test Program..... 80

Table 3.3: Summary of Friction Angles from Laboratory Direct Shear Testing 83

Table 3.4: Testing Matrix for the Experimental Work 107

Table 3.5: List of Conducted Tests for Lateral Soil Restraints..... 108

Table 3.6: List of Conducted Tests for Reduction of Lateral Soil Restraint by Geotextiles 109

Table 3.7: List of Conducted Horizontal Oblique Soil Restraint Tests..... 110

Table 3.8: List of Conducted Vertical Oblique Soil Restraint Tests..... 112

Table 4.1: Summary of Parameters for Lateral Soil Restraint Tests[2]..... 124

Table 4.2: Summary of Predicted Values for Maximum Lateral Soil Restraint (Region 2) 177

Table 4.3: Measured Versus Calculated Lateral Soil Restraint for Geotextile-Geotextile Interface Conditions 187

Table 4.4: Measured versus Calculated Lined Trench Lateral Soil Restraint..... 188

Table 5.1: List of Conducted Horizontal Oblique Soil Restraint Tests..... 195

Table 5.2: Summary of Parameters for Horizontal Oblique Soil Restraint Tests 195

Table 5.3: Normalized Axial Soil Restraint Values Available in the Literature..... 216

Table 5.4: Normalized Axial Soil Restraint Values Predicted by PRCI (2004)[1] and ASCE (1984)[1] 216

Table 5.5: Maximum Horizontal Oblique Soil Restraint Values from This Work..... 217

Table 6.1: Summary of Parameters for Vertical Oblique Soil Restraint Tests 226

Table 6.2: List of Vertical Oblique Soil Restraint Tests 227

Table 6.3: Summary of Vertical Oblique Soil Restraint Test Results (H/D=1.6) 253

Table 7.1: Mohr-Coulomb Model Parameters Used in the Numerical Simulation for No Trench Cases 267

Table 7.2: Cysoil Model Parameters Used in the Numerical Simulation 270

Table 7.3: Interface Model Parameters Used in the Numerical Simulation 288

LIST OF FIGURES

Figure 1.1.a: Shallow skewed buried pipeline movement due to right lateral strike-slip fault displacement..... 6

Figure 1.1.b: Schematic of a shallow buried pipeline movement due to thrust/reverse fault displacement..... 6

Figure 1.2: Main patterns of soil–pipeline interaction triggered by permanent ground displacements. After O'Rourke 1998..... 7

Figure 1.3: Modes of soil restraints on pipelines due to different directions of relative movement. 8

Figure 1.4: Schematic of geotextile-line pipeline trench as a mitigation measurement for fault crossings. 12

Figure 2.1: Failure model used by Hansen (1961)..... 20

Figure 2.2: Comparison between the vertical restraint assumptions in: (a) Hansen (1961) method and (b) Ovesen (1964) method (from Trautmann and O'Rourke, 1983) 20

Figure 2.3: Prediction of horizontal bearing capacity on buried pipes. From Audibert and Nyman (1977)..... 23

Figure 2.4: Prediction of horizontal soil restraint on buried pipes. From Trautmann and O'Rourke (1983) following method suggested by Ovesen (1964). 25

Figure 2.5: Lateral soil bearing capacity on buried pipes for dry and moist sand (Turner 2004). ..... 27_Toc366064472

Figure 2.6: Assumed forces for estimating horizontal load using a log-spiral failure surface (O'Rourke et al. 2008)..... 29

Figure 2.7: Axial soil restraint vs. axial pipe displacement, after Karimian (2006)..... 35

Figure 2.8: Dilation effect concept for axial soil-pipe interaction, after Wijewickreme et al. (2009)..... 35

Figure 2.9: Angle of movement for defining horizontal oblique ground displacement with respect to pipeline axis (top view)..... 37

Figure 2.10: Test Arrangement Used by Hsu et al. (2006). From Hsu et al. 2006..... 38

Figure 2.11: Horizontal and axial soil restraint interaction envelops proposed by Hsu et al. (2006), C-CORE (2008) and Daiyan et al. (2010). 39

Figure 2.12: Lateral soil restraint vs. lateral pipe displacement as a function of oblique angle (α). From Ha et al. (2008)..... 43

Figure 2.13: Variation maximum of soil restraint for loose sand as a function of oblique angle proposed by Hsu et al. (1996) (90° horizontal direction)..... 46

Figure 2.14: Interaction relationship for pipes buried in clay subjected to vertical oblique (lateral and upward vertical) displacements (Guo 2005)..... 47

Figure 2.15: Comparison between vertical, oblique and horizontal soil restraints in loose/contractive soils. After Vanden Berghe et al. (2005)..... 48

Figure 3.1: Soil chamber used in previous studies at the University of British Columbia. 59

Figure 3.2: General view of the modified soil-pipe interaction testing chamber built for this study. 62

Figure 3.3: Construction and structural system of the soil-pipe interaction testing chamber. 63

Figure 3.4: Control system layout. 66

Figure 3.5: Testing chamber to study horizontal oblique soil restraints – XY plan view layout (Displacement vector in X-direction) 69

Figure 3.6: Testing chamber to study horizontal oblique soil restraints – XZ lateral view layout (Displacement vector in X-direction) 69

Figure 3.7: Testing chamber to study vertical oblique soil restraints – XY plan view layout (Displacement vector in XZ plane). 70

Figure 3.8: Testing chamber to study vertical oblique soil restraints – XZ lateral view layout (Displacement vector in XZ plane). 70

Figure 3.9: Fraser River sand grain size distribution before and after testing in the soil pipe interaction chamber (after Karimian 2006). 72

Figure 3.10: Results of direct shear testing on Fraser River sand (after Karimian 2006). 73

Figure 3.11: Peak friction angle for Fraser River sand from triaxial test results (after Karimian 2006). 74

Figure 3.12: Initial elastic modulus for Fraser River sand from triaxial test results (after Karimian 2006). 75

Figure 3.13: A photograph of the crushed sand and gravel material supplied by AT&H. 76

Figure 3.14: Grain size distribution for crushed sand and gravel (road mulch). 77

Figure 3.15: A photographic image of the crushed limestone material supplied by Lafarge. 78

Figure 3.16: Grain size distribution for crushed limestone backfill material. 79

Figure 3.17: Photograph showing the NPS16 test pipe used in pipe soil restraint testing. 80

Figure 3.18: Use of the forklift to lift batches of backfill material. 85

Figure 3.19: Density measurement of backfill (left), and use of a static roller for backfill compaction (right). 85

Figure 3.20: Soil-pipe interaction test specimen prior to testing. 86

Figure 3.21: Pipe specimen placement procedure. 87

Figure 3.22: Coupling system for soil restraint testing – a) pipe-cable connection system; b) pipe-rod connection system. 88

Figure 3.23: Coupling system for soil restraint testing – cable to actuator connection system. 89

Figure 3.24: Trench wall built in native soil (road mulch) – a) view from rear to front b) view from right to left..... 90

Figure 3.25: Trench wall constructed to simulate hard boundary conditions..... 91

Figure 3.26: Schematic of the geotextile-lined trench wall constructed to study lateral soil restraints due to relative horizontal ground displacements. 92

Figure 3.27: Schematic of the geotextile-lined trench wall constructed to study vertical oblique soil restraints for buried pipelines crossing reverse faults. 94

Figure 3.28: Typical configuration of geosynthetic slip surface used in the test program..... 95

Figure 3.29: Axial load cell installed on internal pipe mount. 97

Figure 3.30: Axial load cell bearing on steel plate wall. 97

Figure 3.31: Load cell arrangement for the study of vertical oblique soil restraints. ... 98

Figure 3.32: String potentiometers (SP) arrangement for the study of vertical oblique soil restraints. 100

Figure 3.33: Photograph of inclinometers and string potentiometers arrangement for the study of vertical oblique soil restraints. 100

Figure 3.34: Buried string potentiometers to record geotextile displacement..... 101

Figure 3.35: Components of test naming convention. 105

Figure 3.36: Arrangement of horizontal oblique pipe specimens in the testing chamber. 110

Figure 3.37: Free development of soil failure zones during the testing program. 116

Figure 3.38: Calculation of sidewall friction (from Karimian 2006). 117

Figure 4.1: Normalised load-displacement relationships for NPS16 pipe specimen with H/D=1.6 buried in moist sand during lateral pulling..... 125

Figure 4.2: Normalised load-displacement relationships for NPS18 pipe specimen with H/D=1.9 buried in moist sand during lateral pulling..... 127

Figure 4.3: Pressure readings as a function of pipe displacement - Test 16-1.6-90H-MS-MS-GN..... 128

Figure 4.4: Pressure readings as a function of pipe displacement - Test 18-1.9-90H-MS-MS-GN-1..... 130

Figure 4.5: Backfill soil deformation during Test 16-1.6-90H-MS-MS-GN – Y'=0.07D. 132

Figure 4.6: Backfill soil deformation during test 16-1.6-90H-MS-MS-GN – Y'=0.25D. 133

Figure 4.7: Backfill soil deformation during test 16-1.6-90H-MS-MS-GN – Y'=0.8D. 135

..... 135

Figure 4.8: Surface deformation of sand backfill Test 16-1.6-90H-MS-MS-GN – Y'=0.8D (looking towards the front of the chamber). 135

Figure 4.9: Normalised load-displacement relationships for NPS18 pipe specimen with H/D=1.9 buried in road mulch during lateral pulling 137

Figure 4.10: Pressure readings as a function of pipe displacement - Test 18-1.8-90H-RM-RM-GN-1. 138

Figure 4.11: Pressure readings as a function of pipe displacement - Test 18-1.8-90H-RM-RM-GN- 2. 138

Figure 4.12: Backfill soil deformation during test 18-1.9-90H-RM-RM-GN-1 – Y'=0.75D. 140

Figure 4.13: Surface deformation of road mulch backfill Test 18-1.9-90H-RM-RM-GN-1 – Y'=0.75D (looking towards the front of the chamber). 140

Figure 4.14: Normalised load-displacement relationships for NPS16 pipe specimen with H/D=1.6 buried in limestone during lateral pulling 142

Figure 4.15: Pressure readings as a function of pipe displacement - Test 16-1.6-90H-LM-LM-GN. 143

Figure 4.16: Surface deformation of crushed limestone backfill - Test 16-1.6-90H-LM-LM-GN – Y'=0.1D. 144

Figure 4.17: Surface deformation of crushed limestone backfill - Test 16-1.6-90H-LM-LM-GN – Y'=0.94D. 145

Figure 4.18: Backfill soil deformation during Test 16-1.6-90H-LM-LM-GN – Y'=0.94D. 145

Figure 4.19: Schematic of hard boundary test arrangement. 146

Figure 4.20: Lateral soil restraint in sloped trench walls with moist sand backfill and with (GY) and without (GN) geotextile lining. 148

Figure 4.21: Lateral soil restraints in sloped trench walls with S=1D with moist sand backfill and with (GY) and without (GN) geotextile lining. 149

Figure 4.22: Lateral soil restraints in sloped trench walls with S=2D with moist sand backfill and with (GY) and without (GN) geotextile lining. 150

Figure 4.23: Lateral soil restraints in sloped trench walls with moist sand backfill and with geotextile lining. 151

Figure 4.24: Pressure readings as a function of pipe displacement - Test 18-1.9-90H-HB-MS-GY-45-0.5D-2. 153

Figure 4.25: Pressure readings as a function of pipe displacement - Test 18-1.9-90H-HB-MS-GY-45-0.5D-3. 154

Figure 4.26: Observed soil deformations for tests with moist sand backfill at Y'=0.05D. Note that grid on Plexiglas is 0.1 x 0.1 m. 155

Figure 4.27: Observed soil deformations for tests with moist sand backfill at Y'=0.45D. Note that grid on plexiglass is 0.1 x 0.1 m. 156

Figure 4.28: Patterns of soil deformation and inferred log-spiral failure surface developed for trench wall-pipe distance S = 2D (grid 0.1 x 0.1 m). 157

Figure 4.29: Displacement of upper geotextile for moist sand and hard trench boundary tests. 159

Figure 4.30: Lateral soil restraints in sloped trench walls with sand and gravel backfill. 161

Figure 4.31: Displacement of geotextile fabric for road mulch tests..... 162

Figure 4.32: General normalised load-displacement relationship for pipelines crossing strike-slip faults without a trench boundary..... 164

Figure 4.33: General normalised load-displacement relationship for pipelines crossing strike-slip faults with a trench boundary..... 165

Figure 4.34: Assumed forces for estimating lateral soil restraint using a log-spiral failure surface (based upon O'Rourke et al. 2008)..... 169

Figure 4.35: Pipe displacement trace and log-spiral failure surface from O'Rourke et al. (2008)'s approach for test 16-1.6-90H-MS-MS-GN..... 172

Figure 4.36: Log-spiral failure surface from O'Rourke et al. (2008) approach and soil deformation for Test 18-1.9-90H-RM-RM-GN-1..... 174

Figure 4.37: Log-spiral failure surface from O'Rourke et al. (2008)'s approach and soil deformation for Test 16-1.6-90H-LM-LM-GN – peak friction angle 54°..... 175

Figure 4.38: Log-spiral failure surface from O'Rourke et al. (2008)'s approach and soil deformation for Test 16-1.6-90H-LM-LM-GN – peak friction angle 46°..... 176

Figure 4.39: Sliding block mechanisms for geotextile-lined trench wall after Karimian et al. (2006) (a) sliding only at geotextile interface (left); (b) sliding at geotextile interface and shear failure through soil between pipe and trench wall (right)..... 179

Figure 4.40: Observed patterns of soil deformation for Test 18-1.9-90H-HB-MS-GY-45-0.5D-2: (a) Y'=0.05D, and (b) Y'=0.45D. 181

Figure 4.41: Evolution of lateral soil restraint and geotextile displacement as a function of time for Test 18-1.9-90H-HB-MS-GY-45-0.5D-2..... 183

Figure 4.42: Evolution of lateral soil restraint and geotextile displacement as a function of time for Test 18-1.9-90H-RM-RM-GY-35-0.5D. 183

Figure 4.43: Sliding block mechanism for quantifying F_y for pipeline systems with geotextile-lined trench walls. $\phi_i = \phi_{interface}$. 185

As can be observed from Figure 4.44 and, the computed lateral soil restraint from Equation 4.5 using the interface friction angle between the geotextile fabric layers ($\phi_{interface}$ = 21°) substantially under predicts the plateau load observed during the tests. 186

Figure 4.44: Comparison between lateral soil restraint from tests and soil restraint from Equation 4.5 for different interface friction angles..... 186

Figure 4.45: Lateral soil restraint-displacement from Equation 4.6 and 4.7 vs. tests results. 189

Figure 5.1: Photograph insets show general arrangement and direction of oblique (F) and axial (A) reaction forces. 197

Figure 5.2: Forces acting on horizontal oblique pipe test specimens..... 198

Figure 5.3: Load-displacement relationships measured for β = 75° with H/D=1.9 buried in moist sand during horizontal oblique pulling. 201

Figure 5.4: Axial and lateral soil restraint-displacement for β = 75° with H/D=1.9 buried in moist sand during horizontal oblique pulling. 201

Figure 5.5: Effect of the sliding friction factor on the computed axial and lateral soil restraint values. 202

Figure 5.6: Load-displacement relationships measured for β = 60° with H/D=1.9 buried in moist sand during horizontal oblique pulling. 203

Figure 5.7: Axial and lateral soil restraint-displacement relationships for β = 60° with H/D=1.9 buried in moist sand during horizontal oblique pulling. 204

Figure 5.8: Load-displacement relationships measured for β = 45° with H/D=1.9 buried in moist sand during horizontal oblique pulling. 206

Figure 5.9: Axial and lateral soil restraint-displacement relationships for β = 45° with H/D=1.9 buried in moist sand during horizontal oblique pulling. 207

Figure 5.10: Axial-lateral soil restraint interaction envelopes proposed by Hsu et al (2006); C-CORE (2008) and Daiyan et al. (2010, 2011). 208

Figure 5.11: Axial load-displacement response from Karimian (2006) (H/D = 2.5, NPS18, dry density = 16 kN/m^3; Fraser River sand). 213

Figure 5.12: Horizontal oblique test results compared to Hsu et al. (2006) interaction relationship. 218

Figure 6.1: Normalized Load-displacement relationships for NPS16 pipe specimen with H/D=1.6 buried in moist sand during vertical oblique displacement (θ = 45°). .. 229

Figure 6.2: Reference points trajectory during Test 16-1.6-45V-MS-MS-GN-2 - vertical oblique pulling (θ = 45°) a) upper graph: left side of pulling cable; b) lower graph: right side of pulling cable. 231

Figure 6.3: Average pulling angle during Test 16-1.6-45V-MS-MS-GN-2 from inclinometers. 232

Figure 6.4: Backfill soil deformation during Test 16-1.6-45V-MS-MS-GN-1 – a) Y'=0; b) Y'=0.25D; c) Y'=0.57D; d) Y'=0.73D. 233

Figure 6.5: Normalized load-displacement relationships for NPS16 buried in crushed limestone with hard trench wall during vertical oblique displacement (θ = 45°). 235

Figure 6.6.a: Reference points trajectory during Test 16-1.6-45V-HB-LM-GN - vertical oblique pulling (θ = 45°) - Left side of pulling cable. 236

Figure 6.6.b: Reference points trajectory during Test 16-1.6-45V-HB-LM-GN - vertical oblique pulling (θ = 45°) - Right side of pulling cable. 237

Figure 6.7: Average pulling angle during Tests 16-1.6-45V-HB-LM-GN & 16-1.6-45V-HB-LM-GY from inclinometers. 237

Figure 6.8: Backfill soil deformation during Test 16-1.6-45V-HB-LM-GY – a) Y'=0; b) Y'=0.25D; c) Y'=0.65D; d) Y'=1.23D. 239

Figure 6.9: Photos of geotextile slip surface at the end of Test 16-1.6-45V-HB-LM-GY. 240

Figure 6.10: Normalized load-displacement relationships for NPS16 buried in crushed limestone with hard trench wall during vertical oblique displacement (θ = 35°). 242

Figure 6.11: Reference points trajectory during Test 16-1.6-35V-HB-LM-GY - vertical oblique pulling (θ = 35°) a) Left side of pulling cable; b) Right side of pulling cable. 243

Figure 6.12: Average pulling angle during Tests 16-1.6-35V-HB-LM-GN from inclinometers. 244

Figure 6.13: Backfill soil deformation during Test 16-1.6-35V-HB-LM-GY – a) Y'=0; b) Y'=0.34D; c) Y'=0.72D; d) Y'=1.23D. 246

Figure 6.14: Photos of geotextile slip surface at the end of Test 16-1.6-35V-HB-LM-GY 247

Figure 6.15: Normalised load-displacement relationships for NPS16 pipe specimen buried in crushed limestone and sand during vertical displacement (θ = 90°) 249

Figure 6.16: Backfill soil deformation during Test 16-1.6-90V-LM-LM-GN – a) Y'=0; b) Y'=0.22D; c) Y'=0.83D. 251

Figure 6.17: Backfill soil deformation during Test 16-1.6-90V-MS-MS-GN – a) Y'=0; b) Y'=0.38D; c) End-of-test condition 252

Figure 7.1: Basic explicit calculation cycle used by FLAC (Itasca 2012) 258

Figure 7.2: Initial Youngs modulus for Fraser River sand from triaxial test results (after Karimian 2006). 265

Figure 7.3: Comparison between measured and simulated response of Fraser River sand tested in drained triaxial compression. Data from Karimian (2006). Dry density = 1576 kg/m^3 (D_r=69%) and confining stress of 25 kPa. 272

Figure 7.4: Grid configuration for simulating tests with NPS16 274

Figure 7.5: Grid configuration for simulating tests with NPS18 274

Figure 7.6: Vertical (a) and horizontal (b) stresses (kPa) prior to lateral pulling for Test 16-1.6-90H-MS-MS-GN. 277

Figure 7.7: Simulation of Tests 18-1.9-90H-MS-MS-GN-1 and 18-1.9-90H-MS-MS-GN-2 using bilinear Mohr-Coulomb and CYSOIL models. 278

Figure 7.8: Simulation of Test 16-1.6-90H-MS-MS-GN using bilinear Mohr-Coulomb and CYSOIL models. 279

Figure 7.9: Displacement and maximum shear strain field predicted by the CYSOIL model at Y'=0.07D (failure condition) for Test 16-1.6-90H-MS-MS-GN. 281

Figure 7.10: Distribution of mobilised friction and dilation angle by CYSOIL model at Y'=0.07D (failure condition) for Test 16-1.6-90H-MS-MS-GN. 282

Figure 7.11: Simulation of Tests 18-1.9-90H-RM-RM-GN-1 and 1.9-90H- RM-RM - GN-2 using bilinear Mohr-Coulomb and CYSOIL models. 283

Figure 7.12: Simulation of Test 16-1.6-90H-LM-LM-GN using bilinear Mohr-Coulomb and CYSOIL models. 285

Figure 7.13: Grid configuration for simulating tests with NPS18 pipe specimen and trench conditions at 45°. Some nodes (at Line 1, Line 2 and Line 3) and soil element (Element A) selected to observe the mobilisation of responses at selected locations are also shown. 286

Figure 7.14: Simulation of Test 18-1.9-90H-HB-MS-GY-45-0.5D-2 using bilinear Mohr-Coulomb and CYSOIL models. 290

Figure 7.15: Displacement (left) and maximum shear strain (right) field by the CYSOIL model for Test 18-1.9-90H-HB-MS-GY-45-0.5D a) at Y'<0.002D; b) at Y=0.003D; c) at Y' = 0.05D (Region 2, plateau level)..... 292

Figure 7.16: Mobilisation of inner-outer geotextile interface friction angle for Test 18-1.9-90H-HB-MS-GY-45-0.5D-2 using CYSOIL model..... 295

Figure 7.17: Mobilisation of outer geotextile-sand interface friction angle for Test 18-1.9-90H-HB-MS-GY-45-0.5D-2 using CYSOIL model..... 295

Figure 7.18: Evolution of inner geotextile, outer geotextile and sand backfill nodes along L1 for Test 18-1.9-90H-HB-MS-GY-45-0.5D-2……295

Figure 7.19: Evolution of inner geotextile, outer geotextile and sand backfill nodes along L2 for Test 18-1.9-90H-HB-MS-GY-45-0.5D-2…… 2957

Figure 7.20: Evolution of inner geotextile, outer geotextile and sand backfill nodes along L3 for Test 18-1.9-90H-HB-MS-GY-45-0.5D-2…… 2958

Figure 7.21: Normal and shear forces along the geotextile-geotextile and the soil-geotextile interfaces for Test 18-1.9-90H-HB-MS-GY-45-0.5D-2 using CYSOIL model. 298

Figure 7.22: Volumetric strain – normalised pipe displacement relationship for Test 18-1.9-90H-HB-MS-GY-45-0.5D-2 using CYSOIL model..... 299

Figure 7.23: Spread of mobilised friction angle (ϕ_m) by CYSOIL model for Test 18-1.9-90H-HB-MS-GY-45-0.5D a) at Y'=0.001D; b) at Y'=0.003D; c) at Y' = 0.05D. 300

Figure 7.24: Simulation of Test 18-1.9-90H-RM-RM-GY-45-0.5D using bilinear Mohr-Coulomb and CYSOIL models. 302

Figure 7.25: Simulation of Test 18-1.9-90H-RM-RM-GY-35-0.5D using bilinear Mohr-Coulomb and CYSOIL models. 303

Figure 7.26: Mobilisation of N_{qh} for different soil backfill friction angles(ϕ'_p) – Friction angle along trench wall of 21° - Configuration for Test 18-1.9-90H-HB-MS-GY-45-0.5D using CYSOIL model. 306

NOMENCLATURE

ϕ'_p	soil peak effective friction angle
γ	total unit weight of soil
ν	poisson ratio
ψ	soil dilation angle
ϕ_m	mobilized soil friction angle
ε_v	volumetric strain in a soil element
B	bulk modulus
C_u	coefficient of uniformity of sand
D	outside pipe diameter
d_{50}	average grain size
D_r	soil relative density
E_i	initial Young modulus
E_{max}	maximum elastic modulus
F_n	normal force per unit length on geotextile interface
F_S	shear force per unit length on geotextile interface
F_y	lateral soil restraint at the plateau level
G	shear modulus
G_p	plastic shear modulus
H	depth from the ground surface to the centerline of a buried pipeline
K_0	coefficient of lateral earth pressure “at rest”
k_E	Young’s modulus number
k_G	shear modulus number
k_G^e	elastic shear modulus number
k_n	interface stiffness in the normal direction
k_s	interface stiffness in the shear direction
L	length of pipe test specimen
L_H	moment arm between horizontal soil force and center of rotation
L_P	moment arm between pipe weight and center of rotation
L_S	moment arm between soil mass and center of rotation
m	shear modulus exponent
n	Young modulus exponent
N_{qh}	normalized lateral soil restraint per unit length of pipe

N_{qv}	normalised vertical soil restraint per unit length of pipe
N_{vo}	normalised vertical oblique soil restraint per unit length of pipe
p’	mean normal effective stress
P_a	atmospheric pressure
P_a	reference pressure (100 kPa)
P_H	horizontal lateral soil restraint on pipe
P_{qv}	measured vertical load
P_{vo}	measured vertical oblique load
R_f	failure ratio
S	trench-wall pipe distance
T	axial force on pipe
T_a	normalised axial soil restraint per unit length of pipe
W	weight of the front passive wedge
W_P	pipe weight (including contents)
Y	measured pipe displacement in direction of ground movement
Y’	dimensionless pipe displacement (Y/D)
Y'_p	normalised horizontal displacement necessary to develop F_y
Y_p	ground displacement parallel to the lateral restraint P
Y_T	ground displacement parallel to the axial restraint T
$\phi_{interface}$	interface friction angle
β	angle between horizontal and r_1 or calibration factor in CYSOIL model
θ	angle between r_0 and r

ACKNOWLEDGMENTS

I would like to express my gratitude to all those who gave me unconditional support in completing this thesis. After spending four years at UBC, the people that made this journey possible, and to which I am grateful, is not short.

My thanks are due to my advisor Professor Dharma Wijewickreme. The comments, large debates and exchanges of opposite ideas that we had during my time at UBC gave shape to this thesis. I also greatly appreciate the support given by the supervisory committee members comprising of Professor Peter Byrne and John Howie for providing valuable comments to improve the content and readability. Furthermore, I greatly appreciate the comments given by Professor Richard Brachman of the Civil Engineering Department of Queen's University, Canada.

I am grateful to Mr. Douglas Honegger of D.G. Consulting for providing continuous support, ideas and review to the findings of this work. His comments and technical support were also an important help towards the completion of this thesis. The gratitude is also extended to Dr. Douglas Nyman of D.J. Nyman and Associates and Dr. Jean Audibert for sharing their large experience in earthquake pipeline engineering.

My experience at UBC was enriched through the interaction with a great group of geotechnical, structural and mining engineering students with whom I have been able to build good friendships and shape some ideas. Among them: Matthias Busslinger, Dr. Lalinda Weerasekara, Ruslan Amarasinghe, Antone Dabeet, Eduardo Salfate, Jose Sanchez, Jose Centeno, Manuel Archilla, Seku Samori and Miguel Fraino. Their friendship and support have been significant.

My thanks are also extended to technical staff of the Department of Civil Engineering. These include Mr. Harald Shrempp, Doug Smith, Scott Jackson, and John Wong. During the research program, I was grateful to get assistance

from some of my fellow graduate students and undergraduate students. I would like to thank Ruslan Amarasinghe, Dave Lee, Andrew Critchley and Kyle Ford.

While at UBC, I shared my time providing support to the Global Earthquake Engineering Team of Golder Associates. This experience was particularly rewarding as I had the opportunity to combine academic and professional perspectives on earthquake topics. A special gratitude is extended to Dr. Alan Hull from Golder Associates for his advices, care, unconditional support and more importantly his friendship.

Financial support for this investigation was provided by Pipeline Research Council International. The Terra and Aqua Continued Learning Awards offered by Golder Associates are also gratefully acknowledged.

I cannot express with words my gratitude towards my wife Ana. Her patient and willingness to share with me this long journey from Arequipa, to Lima, to Toronto and finally to Vancouver allowed me to navigate safely through the ocean of knowledge. Her understanding, love and care during all these years were really the true motor of my life. This work could not have been completed without her presence. The support of my parents and parents-in-law has been also important. Thank you.

DEDICATION

Esta tesis está dedicada a mi esposa Ana y mis padres Elard and Gilda.

Chapter 1: Introduction

This thesis deals with the estimation and characterisation of soil restraints on pipes and the effectiveness in reducing levels of soil restraint of geotextile-lined pipeline trenches crossing seismic faults. Because buried pipeline performance to earthquake effects depends on mobilized levels of soil restraint, their appropriate estimation is an important step for designing pipeline systems against ground displacement. Soil restraints depend on the direction and level of relative displacement, between the buried pipeline and its surrounding soil, imposed by a particular ground movement and the amount of deformation of the soil surrounding the pipe. Such displacements can induce bending, shear, tension or compression demands on segments of buried pipeline systems.

In an effort to characterize soil restraints, an existing full-scale testing chamber at the University of British Columbia was improved and significantly modified. In particular, the newly modified test chamber allows applying relative pipe displacements in different oblique directions from horizontal to vertical planes and provides opportunity for continuous observation of soil deformation patterns. For example, lateral displacement could be applied to a buried pipe specimen aligned at different angles with respect to the induced displacement on the horizontal plane; in turn, this permits simulation of the oblique lateral breakout of buried pipelines from their soil embedment on one side of a strike-slip fault or abrupt ground displacements arising from a landslide. Similarly, the simulation of the vertical oblique angle breakout of buried pipelines from their soil embedment on the footwall side of reverse/thrust faults could be achieved by applying vertical oblique displacement to a steel pipe specimen at angles of 35° and 45° degrees from the horizontal.

Using the above loading modes, the development of a coupled condition between axial and lateral soil restraints was assessed by displacing laterally a buried pipe specimen oriented at different angles with respect to the direction of simulated strike-slip fault type displacement condition. This was performed with the aim of studying the validity of the assumption used in current state of practice (PRCI 2004, 2009; ASCE 1984) that lateral and axial soil restraints act independently of each other (e.g., lateral and axial soil restraints react only to components of displacement in the lateral and axial directions, respectively).

Current design guidelines recommend the use of geotextile-lined pipeline trenches to reduce soil restraints on buried pipelines, and therefore, increase their capacity and performance. The effectiveness of this recommendation was assessed by studying the backfill soil and geotextile interaction behaviour during large lateral and vertical oblique pipe displacements. The side slope of a pipeline trench with a trapezoidal cross-section (usually called a trench wall) lined with two layers of geosynthetic materials was built for this purpose. The size of the trapezoidal trench had typical dimensions and inclinations used in current field practice. The trench was backfilled using selected backfill material after placement of the pipe segment chosen for testing. In addition to studying the effectiveness of geotextile-lined trench walls, the effect of the presence of trench wall on the development of levels of lateral soil restraint was also studied.

Soil restraints for the above-mentioned directions of pipe movement were characterized and expressed in terms of pipe displacement and its correspondent axial, lateral, and oblique soil restraint loads. Geotextile movement was also observed, and related to mobilised levels of soil restraint. The soil response observed during the tests that simulate pipeline breakout during lateral strike-slip fault conditions, was further studied by a set of 2D numerical analysis. By combining the above measurements with the patterns of soil deformation observed during the tests, a new procedure was developed

to predict lateral soil restraint vs. pipe displacement for geotextile-lined pipeline trenches. The prediction of lateral soil restraint by approaches based on limit equilibrium was also verified against the observed deformation of the soil mass and measured soil restraint.

To place the thesis into context, this first chapter describes the major geotechnical earthquake hazards that affect pipeline systems and observed pipeline performance during those hazards and presents an overview of common mitigation approaches used in practice to improve pipeline performance. The objectives as well as the organization of the thesis are also described.

1.1 Geotechnical Earthquake Hazards and Buried Pipeline Performance during Earthquakes

1.1.1 Geotechnical Earthquake Hazards

Buried pipeline systems such as oil and gas pipelines, water distribution networks and sewage systems are linear systems (many hundreds of kilometers long) that cover a large geographical region. As such they are exposed to a wide variety of geotechnical earthquake hazards and soil conditions that may induce significant disruptions to sections of a pipeline. These disruptions in turn translate into undesirable impacts on the environment, economies, and/or the living conditions of citizens.

The oil and gas pipelines are usually buried with a soil cover of 0.6 to 1.5 m. The overburden ratio (defined as H/D where D = diameter of pipe, H = soil cover above springline of pipe) for these types of pipelines varies in the range of 1 to 5. The critical soil loads on pipelines with this level of soil cover typically arise from geotechnical earthquake hazards such as ground shaking, liquefaction or lateral spreading. However, it is the ground rupture and relative movement along faults or landslide zones the ones that pose the major risk to

the pipeline performance (Kennedy et al. 1977; O'Rourke and Liu 1999; O'Rourke and Bonneau 2007; PRCI 2004, 2009; Abdoun et al. 2009; Xie et al. 2012).

The above listed geotechnical earthquake hazards impart lateral, vertical bearing or uplifts or axial loads on sections of pipeline systems. Therefore, identifying the geotechnical earthquake hazards and understanding soil behavior associated with these hazards provides the ability to conduct appropriate designs and mitigation controls of a pipeline system in an effort to withstand anticipated relative ground movements.

In high geotechnical earthquake hazard regions, the routes of major pipeline transmission system inevitably encounter events related to active faults or large scale ground movements generated, for example, by landslides. While a pipeline route can in theory avoid a region of seismic hazard, this is rarely the case in practice. Rights-of-way for pipeline corridors are increasingly difficult to obtain due to more stringent land use policies or environmental concerns that pose limits on the choices for routes that avoid ground movement hazards (PRCI 2009). Thus, because pipeline fault crossings are one of the major geotechnical earthquake hazards that rarely can be avoided, the following paragraphs will briefly discuss the main aspects of seismic faults and the loading conditions they impose on buried pipelines.

A seismic fault is characterised either in terms of its movement along the strike or dip. However, faults with movement in both directions are also possible (Cluff et al. 1970; Taylor and Cluff 1977; Bolt 2003). A fault movement that occurs parallel to the strike (i.e. the two sides of a fault move past each other) with horizontal relative motion is called strike-slip fault. Strike is the angle from the north to the horizontal line defined by the intersection of a fault plane with the surface of the earth. Depending on the sense of the relative motion along the strike, a strike-slip fault could be further categorized into left lateral or right lateral strike-slip fault.

When the two sides of a fault press against each other or pull away from each other, the relative motion has a vertical component and the fault is called a dip-slip fault. Dip is the angle formed by the plane of the fault with the surface of the earth. If the upper rock block or hanging wall moves upward relative to the lower rock block or foot wall in a dip fault, then the fault is called a reverse or thrust fault. The movement along a reverse fault is therefore of a compressional type. Conversely, if the upper rock block or hanging wall moves downward relative to the foot wall, the fault is called a normal fault. The relative movement of a normal fault is extensional.

Depending on the type of fault crossing (i.e. strike-slip or dip-slip) or a similar event characterised by directional relative motion (e.g. landslide events), different modes of soil restraint arise on sections of the pipeline. These modes of soil restraint and corresponding loads and strains distribution in pipe sections depend on the orientation of the pipeline with respect to the direction of relative ground movement, the amount of ground displacement and the specific site soil conditions along the pipeline.

When the pipeline direction is skewed to the strike of a right lateral strike-slip fault the lateral and axial restraint imposed by the soil mass on the pipeline applies lateral and axial loads to sections of the pipeline which results in tension, compression or shear strains in different sections of the pipeline, as shown in **Figure 1.1.a**. This figure also shows the side of the fault that was modeled in this thesis (See **Section 3.2.1**).

For pipelines closely aligned with the direction of the strike of a thrust fault as depicted in **Figure 1.1.b**, the pipeline is subjected not only to different levels of vertical oblique soil restraint due to the upward movement of the pipeline, but also to longitudinal-axial soil restraint. Therefore, different sections of the pipe will experience bending moment and shear stress in a vertical plane and either tension or compression stresses in a horizontal plane. Other causes of

relative permanent ground displacement and their effects on pipeline behavior are described by O'Rourke (1998) and are shown in **Figure 1.2**.

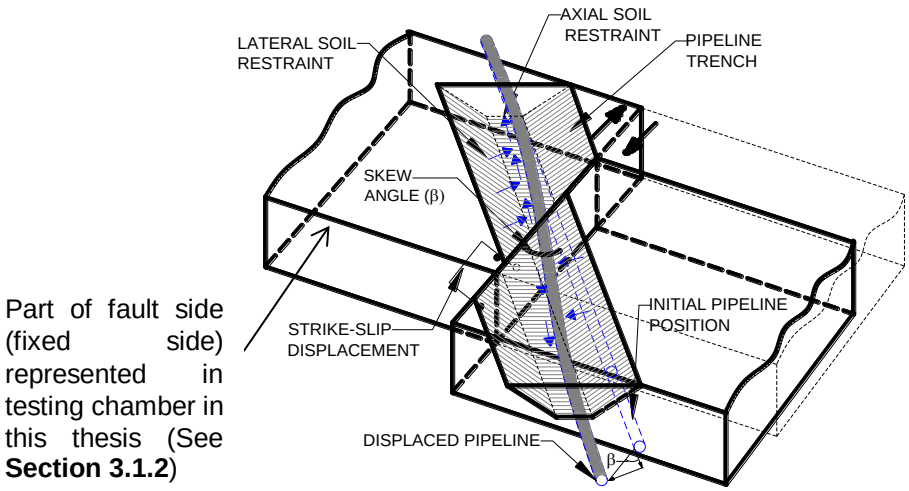

Figure 1.1.a: Shallow skewed buried pipeline movement due to right lateral strike-slip fault displacement.

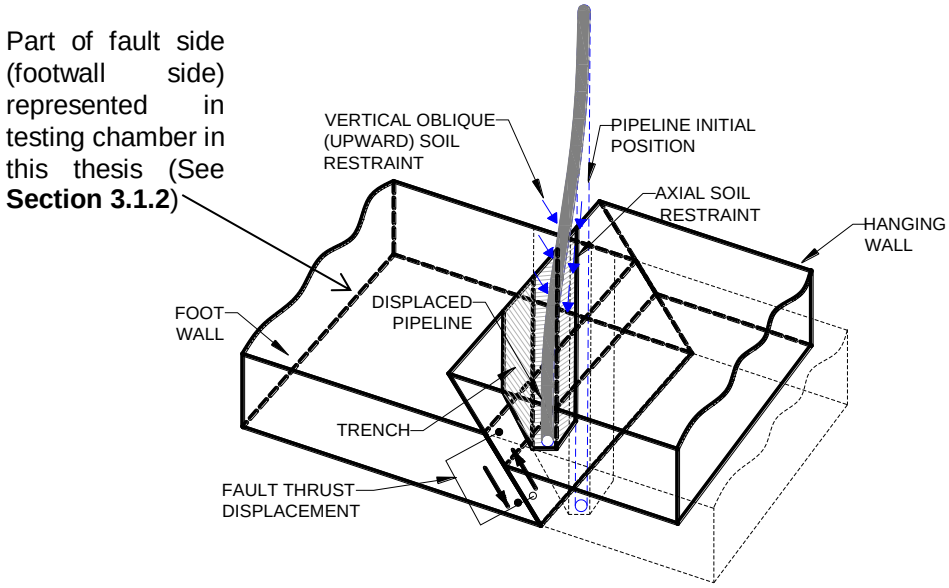

Figure 1.1.b: Schematic of a shallow buried pipeline movement due to thrust/reverse fault displacement.

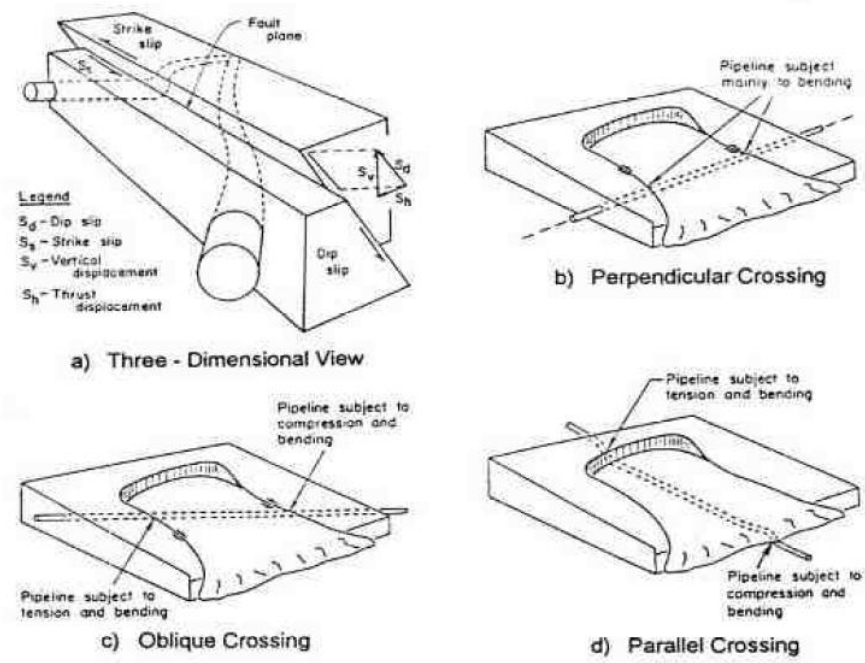

Figure 1.2: Main patterns of soil–pipeline interaction triggered by permanent ground displacements. After O'Rourke 1998.

O'Rourke (1998) showed that pipelines crossing a fault plane subjected to oblique slip as in **Figure 1.2a** may promote compression and tension, depending on the angle of intersection between the pipeline and the fault. Likewise, **Figure 1.2b** shows a pipeline crossing a lateral spread or landslide perpendicular to the general direction of soil movement that may subject the pipeline to bending strains and extension. As shown in **Figure 1.2c**, the pipeline will undergo bending and either tension or compression at the margins of the slide when the crossing occurs at an oblique angle. In Figure 1.2d a pipeline is oriented parallel to the general direction of soil displacement. At the head of the zone of soil movement, the pipeline will be subjected to both bending and tensile strains. At the toe of the slide, the pipeline will be subjected to compressive strains.

In essence, a buried pipeline subjected to different direction of relative movement might experience one or a combination of different soil restraint conditions. Therefore, based on the direction of relative displacement between the soil embedment and the pipeline, soil restraints can be categorized into four different modes (ASCE 1984; PRCI 2004, 2009) as shown in **Figure 1.3**: (a) vertical-uplift; (b) vertical-bearing; (c) horizontal-lateral; and (d) longitudinal-axial. Any relative movement can be identified as one or a combination of these modes.

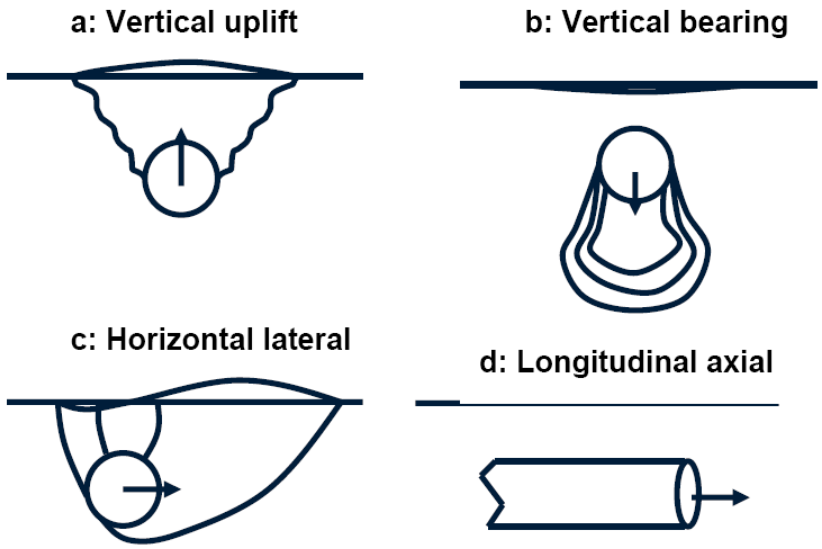

Figure 1.3: Modes of soil restraints on pipelines due to different directions of relative movement.

Other source of geotechnical earthquake hazard to buried pipelines arises from transient ground shaking. Although this is not as significant for buried pipelines as the permanent ground movements are, this geotechnical earthquake hazard is particularly significant for aboveground sections of pipeline transmission systems (Kennedy et al. 1977; Kennedy et al. 1979; Trautmann and O'Rourke 1983; O'Rourke and Liu 1999).

Transient ground shaking is characterised by the strain and curvature in the ground due to travelling wave effects (O'Rourke and Liu 1999) and can cause surficial soil cracks and fissures. Hence, in most instances, designing a pipeline against permanent ground deformation would automatically provide resistance against transient ground shaking.

Soil liquefaction hazard is also less severe and abrupt than the movements at fault crossings. Pipeline river crossings are a good example of zones exposed to high liquefaction potential. Liquefaction hazard can be caused by lateral spread, flow failure, local subsidence, post-liquefaction consolidation, buoyancy effects, and loss of bearing (Kennedy et al. 1979; O'Rourke 1998; PRCI 2004). Lateral spread is the most pervasive and damaging one (Kennedy et al. 1977; O'Rourke and Bonneau 2007).

While it is possible to apply soil stabilization measures to these liquefaction-induced hazards, the large extent of the pipeline make this measure not practical. Other options include locating the pipeline aboveground, below the lowest depth of liquefiable soil, within the liquefiable soil or within competent soil above liquefiable layers (Kennedy et al. 1979; PRCI 2004). Thus, relative pipe movements resulting from soil liquefaction should be accounted for in design. However, as shown in previous paragraphs, the design criteria employed for fault crossings will cover pipeline crossings of liquefiable soil regions.

1.1.2 Buried Pipeline Performance during Earthquakes

The observed performance of buried pipelines in zones of surface faulting during past earthquakes evidences the vulnerability of these systems to earthquake effects (O'Rourke and Liu 1999). Even though after 1972 the design of buried pipeline systems incorporated stringent seismic design requirements, the damage observed during recent earthquakes evidences the complex nature of seismic hazard demands usually faced in pipeline

earthquake engineering (Kennedy et al. 1979). Pipeline damage was reported during the earthquakes of San Francisco (1906), Long Beach (1933), Kern County (1952), Alaska (1964), Niigata (1964), Parkfield (1966), San Fernando (1971), Guatemala (1976), Imperial Valley (1979), Whittier Narrows (1987), Loma Prieta (1989), and Northridge (1994). Recent pipeline damaged has been reported during the 1999 Koaceli and 1999 Duzce earthquakes in Turkey and the 1999 Chi-Chi earthquake in Taiwan. A brief summary of the documented pipeline damage during some of the above earthquakes is presented below. A more complete description can be found in T. O'Rourke et al. (1985).

Extensive gas and water pipeline damage was reported during the Great Alaskan earthquake of 1964. Most of the rupture or severe distortions of pipelines were associated with fault movements, landslides or ground squeeze associated with fault zones. 200 breaks in gas pipelines and 100 breaks in water distribution pipelines were observed at Anchorage.

The San Fernando earthquake of 1971 produced over 2,400 breaks of water, natural gas, and sewer pipelines in the area of permanent fault displacement. The pipelines were buried at a nominal depth of 0.9 m (from the surface to the top of the pipe). The soils in the region of observed damage are mostly silty sands and gravels. The pattern of pipeline damage during the earthquake revealed that the pipeline damage is related to the orientation of the pipelines with respect to the fault trace. For example pipelines oriented at a position that produced compressive strains on them from fault movement reported the most damaged compared to the ones oriented in a perpendicular direction.

The performance of pipeline systems subjected to ground shaking has been satisfactory. However, there have been some events where pipe damage has been due only to wave propagation. An example was observed during the 1985 Michoacan earthquake in Mexico City. In addition, O'Rourke et al. (1985) reported that approximately half the pipe breaks in the 1906 San Francisco

event occurred due to liquefaction-induced lateral spreading zones while the other half occurred apparently due to wave propagation over a somewhat larger area.

1.2 Mitigation Measures for Reducing Soil Restraint at Fault Crossings

For pipelines located in tectonically active regions, sources of large ground displacements include surface faulting, triggered landslides, and lateral spreading. These large ground displacements (larger than 1 m) can mobilise high levels of soil restraint and can impose large levels of demand which may greatly exceed established pipeline acceptance criteria. Therefore, mitigation measures are focused on reducing levels of soil restraint on buried pipelines and therefore increasing the pipeline capacity to resist ground displacement.

A common mitigation measure undertaken to reduce soil loads in situations of abrupt ground movement such as pipeline fault crossings is the installation of pipelines in a trapezoidal trench with loose to moderately dense sand backfill. Where suitable low-cost sand backfill is not readily available or drainage and erosion issues preclude the use of sand, the use of a mixture of silty sand and gravel or the use of polystyrene (EPS) geofoam blocks as a backfill material is accepted in current practice (PRCI 2004, 2009; Wook et al. 2007).

Other recommended mitigation option given by design guidelines (PRCI 2004, 2009) is the use of geosynthetic fabric on sloped trench walls for pipelines buried in native soils. This recommendation is based on the concept that improved flexibility can be achieved by slippage in the form of a contiguous soil blocks that would be promoted due to the low frictional properties prevalent at the geosynthetic fabric interfaces.

The concept of improved flexibility and performance given by a geotextile-lined pipeline trench with soil backfill is sketched in **Figure 1.4**. The figure

shows a pipeline crossing a strike-slip fault. The pipeline is embedded in loose granular material which has the purpose of allowing the pipeline to breakout the backfill material with minimal soil resistance. The function of the sloped trench wall is to allow the pipe to ride along the side of the trench so that the pipe can eventually come above ground if the earthquake-induced displacement is large enough. The recommended geotextile lining is used to further improve this mitigation concept. For pipelines crossing reverse faults, a similar concept applies.

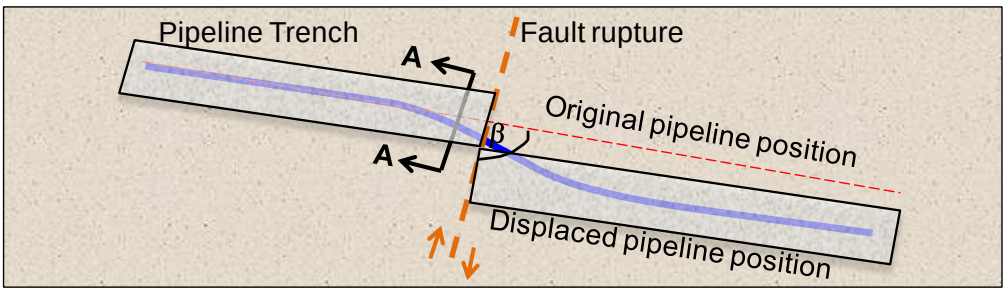

Plan View of Fault Crossing

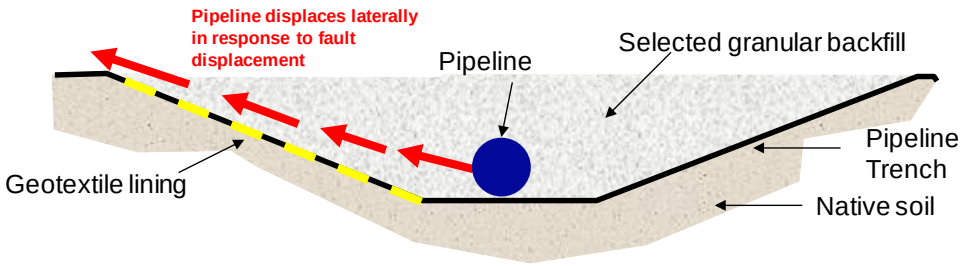

Section A-A

Figure 1.4: Schematic of geotextile-line pipeline trench as a mitigation measurement for fault crossings.

Other pipeline design mitigation alternatives not based on reducing values of soil restraint include increasing pipe strength and modifying the pipeline alignment by reducing the length of exposed pipeline, maximizing the unanchored length or isolating pipelines from ground displacement to mention a few. In general, the selection of a pipeline design mitigation strategy

depends on the consequences of ground movement activity, the consequence of damage to the pipeline, the frequency or importance of the ground movement and the cost of implementing the design mitigation alternative.

1.3 Objectives and Organization of the Thesis

1.3.1 Objectives

Because extensive damage due to geotechnical earthquake hazards has been observed and reported in several occasions, the quantification and prediction of soil restraint on pipelines subjected to different directions of relative displacement are essential for pipeline earthquake engineering. In previous sections, it was emphasized that buried pipeline performance to earthquake effects depends on mobilized levels of soil restraint and therefore their appropriate estimation is an important step for designing pipeline systems against ground displacement and deformation.

While the mobilisation and maximum levels of soil restraint for pipelines buried in clean sand and subjected to relative lateral movements has been the subject of study by many researchers (Trautmann and O'Rourke 1983, 1985; Audibert and Nyman 1977; Hsu 1994, 2001; Paulin et al. 1996, 1997, 1998; Turner 2004, Karimian 2006), levels of soil restraint on materials other than sand has not received much attention from the technical community due to the difficulty of conducting full-scale testing or of extrapolating data from small-scale testing. Similarly and to the author's best knowledge, information on experimentally-based vertical oblique soil restraint is not available in current technical literature.

Furthermore, to date very little has been done to understand and validate coupling effects under axial and lateral conditions in full-scale testing environments. It is clear that there is a great need for such validation if

coupling effects are to be included in the fault crossing design of pipeline systems. Likewise, existing concepts for mitigation options based on geotextile-lined pipeline trenches for pipelines crossing reverse or strike-slip faults are not fully understood, tested and verified. With this philosophy, the objectives of this research are as follows:

1. Design, improve and significantly modify an existing full-scale testing chamber at the University of British Columbia to facilitate applying different directions of displacement to pipe specimens with the aim of simulating the lateral or vertical oblique angle breakout of buried pipelines from their soil embedment on one side of a strike-slip fault or on the footwall side of reverse/thrust faults, respectively.

2. Conduct a set of full-scale tests to examine lateral and vertical oblique soil-pipe interaction behavior with different backfill soil materials used in current practice (e.g. sand, crushed sand and gravel or crushed limestone materials).

3. Assess the applicability of available analytical approaches to estimate maximum lateral soil resistance on pipes buried in road mulch or crushed limestone material by comparing the results from the full-scale tests with those obtained from analytical approaches.

4. Conduct a set of full-scale tests of pipes buried in sand to study axial and lateral coupling effects that arise during the soil-structure interaction of segments of buried pipeline systems subjected to horizontal oblique relative displacements and compare the coupled axial and lateral soil restraint relationships obtained in this work with currently available relationships.

5. Conduct a set of full-scale tests to study the effectiveness of geotextile-lined pipeline trenches subjected to simulated strike-slip or reverse fault displacement type. This is achieved by building a trench wall with

inclinations of 35 degrees and 45 degrees from the horizontal and by comparing measurements taken with and without geotextile. Factors such as pipe-trench distance and backfill materials on the effectiveness of this mitigation technique were investigated.

6. Develop a solution procedure to predict the lateral soil restraint vs. pipe displacement relationship for cases of geotextile-lined pipeline trenches and compare the full-scale tests measurements with those predicted by the analytical solution.

7. Conduct a 2D numerical analysis to assess the role of soil and geotextile interface behaviour on the measurements observed during the full-scale tests of relative lateral pipe displacement by using the commercially available software FLAC V7.0.

1.3.2 Organization

This work is divided into eight main chapters:

- **Chapter 1** describes geotechnical earthquake hazards, the loading conditions they impose on buried pipelines, some mitigation measurements for reducing soil restraint at fault crossings and the objectives as well as the organization of the thesis.

- **Chapter 2** discusses and reviews existing research work and findings on lateral, axial, horizontal oblique and vertical oblique soil restraints on buried pipelines or similar structures in terms of physical, analytical and numerical modelling.

- **Chapter 3** describes the design criteria for the testing chamber (2.45 m x 3.8 m) used to conduct full-scale pipe-soil interaction tests to study soil restraints on relatively large diameter steel pipe specimens. The

equipment used, setup, methodology, measurements, and limitations of the experimental setup are presented in detail.

- **Chapter 4** presents in detail the results of lateral soil restraint on pipe specimens buried in Fraser River sand, sand and gravel mixture and crushed limestone in different trench configurations. The results are compared with commonly used analytical approaches and previous studies. The effectiveness of geotextile-lined pipeline trenches subjected to simulated strike-slip fault conditions is also discussed and evaluated. An approach to estimate lateral soil restraint for this geotextile-lined condition is presented and verified.

- **Chapter 5** presents the results of horizontal oblique soil restraints and deals with axial-lateral coupling effects obtained in this study and the different approaches suggested by other researchers.

- **Chapter 6** describes the measurements obtained from tests that simulated the vertical oblique angle breakout of buried pipelines from their soil embedment on the footwall side of reverse/thrust faults. The effectiveness of geotextiles to reduce vertical oblique soil restraints on buried pipes is also discussed.

- **Chapter 7** discusses the numerical analysis procedure used in this study and the calibration of the constitutive models for soil materials. This chapter also compares the numerical simulation of the lateral soil restraint tests with and without geotextile-lined trench walls with the full-scale measurements.

- **Chapter 8** summarizes the work done in this research, the conclusions drawn from the test results, and points out important issues related to this study that require further attention and work.

Chapter 2: Literature Review

Pipeline earthquake engineering is an emerging engineering field in which geotechnical engineers play an important role in the soil-structure interaction component of the practice. While there is a good understanding of pipeline behavior buried in sand and subjected to lateral ground displacements and in less scale to axial ground displacements, the practice still has some shortcomings particularly in cases in which the findings are based on small-scale tests. Therefore, results from full-scale tests can find a useful place in the practice and shed light on the current unresolved technical issues that exist in the literature. For example, the soil-pipe interaction under lateral pipe displacement for granular materials other than sand has not been properly tested and verified due to the difficulty in conducting full-scale testing or in extrapolating to actual field conditions if the tests are conducted at a reduced scale.

Along the same line, the influence of axial-lateral coupling on the mobilisation of levels of soil restraint has generally not been considered in the design of pipeline systems and its behaviour has not been fully validated and characterized. In particular, no information seems to exist from full-scale tests on the interaction characteristics of axial and lateral levels of soil restraint on pipelines subjected to horizontal oblique or skew displacements.

For pipelines located in active geological regions, large ground displacements (larger than 1 m) can mobilise high levels of soil restraint which impose large levels of demand on pipeline segments. In an effort to reduce such high levels of demands, the Oil and Gas Industry is working closely with researchers to evaluate potential mitigation options and to assess the effectiveness of existing ones. For example, one mitigation option is to bury pipelines in shallow geotextile-lined trenches excavated in native soils and backfilled with loose geomaterials or the same material as the native soil. While the use of loose material is preferable, dense and strong material are sometimes used in

practice, particularly for cases controlled by high levels of traffic condition. However, the study of soil restraint for pipelines buried under such conditions has not received much attention not only under geotextile-lined pipeline trench conditions but also for plain conditions.

For cases in which the dominant relative ground movement direction applied to the buried pipeline is a combination of horizontal and vertical ground movements (vertical oblique displacements), such as those produced by reverse faults, the amount of reported tests data on levels of soil restraint is even more limited and not properly validated.

With this overview, the next sections of **Chapter 2** will describe findings from the currently available published information particularly obtained from experimental and analytical studies carried out to understand the development of soil restraint on buried pipelines subjected to different modes of ground displacement. Currently used methods for estimating maximum levels of soil restraint on buried pipelines are also summarized and discussed. The conclusions or observations on the soil restraint characteristics are arising from the past work then presented with the view of identifying the existing knowledge gaps and areas for further research work.

1.4 Horizontal and Axial Soil Restraints on Buried Pipes

Levels of lateral and axial soil restraints are one of the most studied cases of soil-structure interaction for pipeline systems. Horizontal lateral soil restraints on rigid pipelines are based upon a relative large number of laboratory, numerical, and field experimental investigations on soil-pipe interaction response in buried sand and also studies on related structures such as piles, strip footings, and especially anchor plates.

For levels of axial soil restraint, the available technical literature seems to be less than those for horizontal lateral cases and appears to point out that this topic has not reached a proper consensus yet. Likewise, there is a limited amount of experimental and analytical data reported for soil restraints which develop from conditions different than purely axial or horizontal lateral relative ground movements.

1.4.1 Horizontal Soil Restraint

Initial attempts to estimate levels of lateral soil restraint for buried pipelines were based on Hansen's study (1961). Hansen (1961) developed a model to determine ultimate lateral resistance for deep and shallow rigid piles by assuming restrained vertical movement for the piles and by only satisfying horizontal equilibrium.

For shallow rigid piles, Hansen (1961) assumed a behavior similar to that used for the analysis of retaining walls. For deep rigid piles, he considered a strip footing model. At intermediate depths, the ultimate lateral resistance was determined by an empirical interpolation function. This function assumes full mobilisation of frictional forces along a hybrid failure surface, which consists of a straight line starting from the base of the pile combined with a Rankine and logarithmic spiral Prandtl zone as shown in **Figure 2.1**.

Further studies (Ovesen 1964; Trautmann and O'Rourke 1983, 1985) have shown that the above vertical restraint assumption by Hansen (1961) leads to higher lateral soil restraints on buried pipes due to the imposed restriction to the upward movement tendency of buried pipes when subjected to lateral ground displacements (see **Figure 2.2**). However, Hansen's (1961) model can still be found to be used in current technical guidelines such as the ASCE (1984) and PRCI (2004).

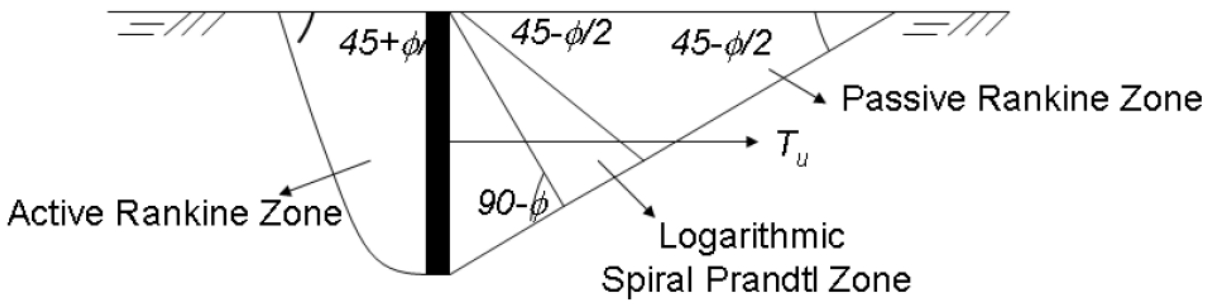

Figure 2.1: Failure model used by Hansen (1961).

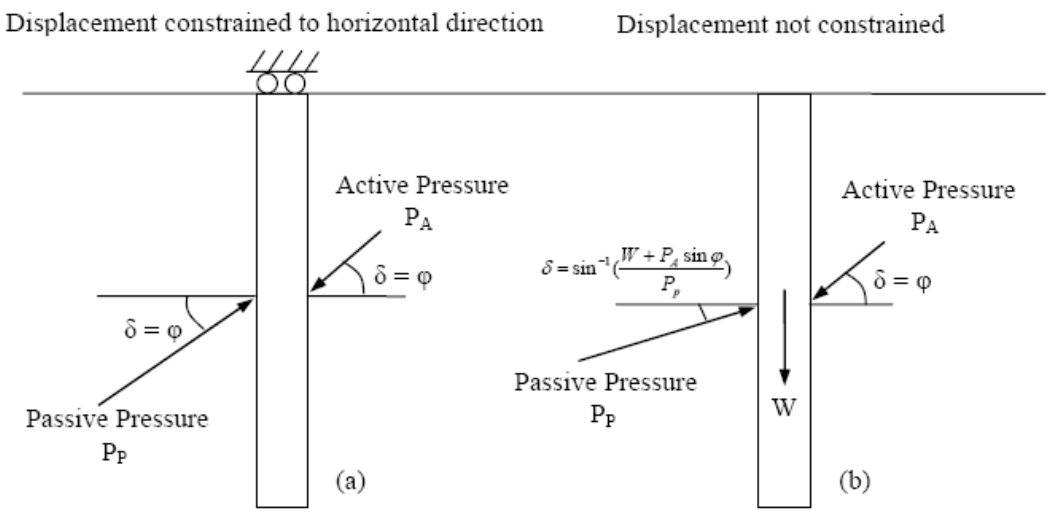

Figure 2.2: Comparison between the vertical restraint assumptions in: (a) Hansen (1961) method and (b) Ovesen (1964) method (from Trautmann and O'Rourke, 1983)

Ovesen (1964) conducted experimental tests on 15 cm high plate anchors subjected to lateral ground displacements. His tests were developed in loose and dense sand and simulated a plane strain condition. By using the results of tests with overburden ratios from 1 to 10, he developed an analytical model to determine passive soil loads on anchors. The model showed a reduction in soil loads compared to Hansen's (1961) model. The reduction was attributed to the free development of vertical displacement of the vertical anchor.

Neely et al. (1973) and Das and Seeley (1975) conducted similar investigation to estimate the effect of aspect ratio (i.e., ratio between width and height of the anchors) on soil resistance in vertical anchor plates. Das and Seeley (1975) observed that the measured resistance per unit width of the anchor decreases with increasing aspect ratio. This finding is of relevance to pipes because it shows the importance of geometry in determining lateral soil resistance.

Besides these observations on the magnitude of the soil resistance, the displacement corresponding to the peak soil resistance is also an important aspect when developing bilinear soil-springs. From the tests conducted on vertical anchors buried in loose sand, Neely et al. (1973) observed that for tests with presumed plain strain conditions (i.e., aspect ratio larger than 5), the displacement at failure varied from 0.1 to 0.2 times the height of the anchor plate when the overburden ratio ranges from 1 to 5.

The study conducted by Audibert and Nyman (1977) appears to be the first experimental study to deal with the direct characterization of soil-pipe interaction behavior and the quantification of levels of lateral soil restraint against horizontal lateral pipe displacement. By performing tests in a small-scale apparatus (0.38 m x 0.46 m x 0.71 m), they showed that the mobilisation of soil restraint depends on factors such as the burial depth, pipe diameter and soil density. The tests were conducted on small-specimen pipes with diameters of 25, 60, and 111 mm buried in both loose and dense air-dried Carver sand. Embedment ratios (ratio of the buried depth at the springline to the pipe diameter) of 1, 3, 6, 12, and 24 were considered for pipe diameters other than 111 mm, and embedment ratios of 1 and 2 for the pipe with 111 mm diameter.

Audibert and Nyman (1977) showed that the relationship between lateral soil restraint and pipe displacement is nonlinear and the soil restraint reaches a maximum value at certain level of pipe displacement. They demonstrated that the soil restraint and pipe displacement relationship approximate a rectangular

hyperbolic curve and that this relationship can be predicted by a set of non-dimensional parameters relating a normalized force ($\bar{p}$) with normalized displacement ($\bar{y}$) as shown in **Equation 2.1**.

$$\bar{p} = \frac{\bar{y}}{0.145+0.855\cdot\bar{y}} \qquad [2.1]$$

Where:

$$\bar{p} = \frac{p}{p_u} \; and \; \bar{y} = \frac{y}{y_u} \qquad [2.2]$$

p_u is the maximum soil restraint mobilized at displacement y_u. The level of p_u depends on soil friction angle, depth to embedment and unit weight of soil. By assuming that the soil-pipe failure mechanism resembles those of model footing tests, they proposed to use the Hansen (1961) capacity factor N_{qh} to predict the maximum soil restraint p_u. The variation of N_{qh} versus the ratio of depth to center of pipe (H) to diameter (D) is shown in **Figure 2.3**.

Rowe and Davis (1982) developed a numerical model to investigate the behaviour of anchor plates buried in sand. They studied the effects of burial depth, friction angle, dilation, initial soil stress conditions, and surface roughness on the anchor plate response. They concluded that the capacity of the anchor plate is modified by dilatancy effects, especially for deep embedment. For shallow embedment conditions, the anchor roughness was found to produce the greatest effect on the anchor's capacity. They also indicated that the effect of initial lateral soil stress on anchor capacity is insignificant. Their work was summarized in a series of charts that could be used to estimates capacity of vertical anchors. Correction factors are also available for modifying the estimated anchor capacity due to surface roughness, soil dilatancy, and initial stress conditions.

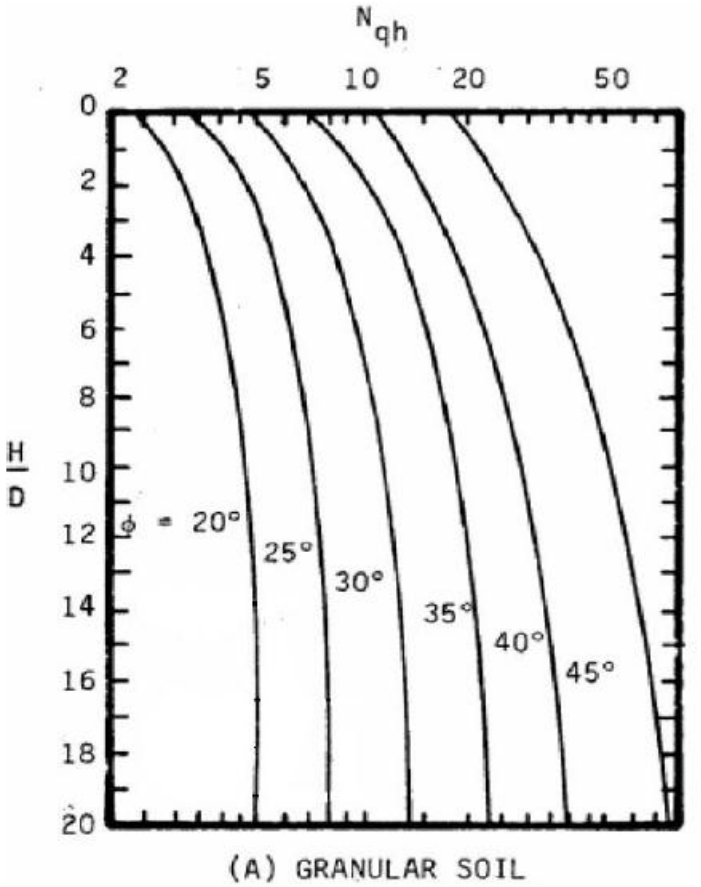

Figure 2.3: Prediction of horizontal bearing capacity on buried pipes. From Audibert and Nyman (1977).

Trautmann and O'Rourke (1983, 1985) performed a series of experimental tests on pipes buried in Cornell filter sands and subjected to relative lateral ground displacements in order to evaluate the effect of soil density, pipe burial depth, pipe roughness, and pipe diameter on levels of lateral soil restraint. Pipe specimens of 102-mm and 324-mm diameter were tested at burial depth ratios of 1.5, 3.5, 5.5, 8, and 11. Backfill densities of 14.8 kN/m^3, 16.4 kN/m^3, and 17.7 kN/m^3 were used to simulate compact, medium, and loose density conditions.

Trautmann and O'Rourke (1983, 1985) defined the lateral soil restraint by a non-dimensional force (N_h) and the evolution of pipe displacement was presented in terms of the ratio of recorded pipe displacement, Y, to diameter, D, (Y/D). The maximum level of lateral soil restraint was found to be much lower than that predicted by Hansen (1961) capacity factor N_{qh}. The size of the difference was about 150 - 200%. The reason for the difference was attributed to the assumption regarding the level of vertical restraint during lateral movement. The capacity factor N_{qh} of Hansen (1961) was based on fully restraining the vertical displacement; while the N_h values of Trautmann and O'Rourke (1985) was based on permitting the pipe to move vertically as the pipe was pulled horizontally. Trautmann and O'Rourke (1985) further compared their results with those of Ovesen (1964) and Rowe and Davis (1982) for anchors plates buried in soil and that accounted for vertical equilibrium. The comparison showed very good agreement. The soil restraint-displacement relationships were approximated by using an equation based on a rectangular hyperbola as expressed by **Equation 2.3**.

$$F'' = \frac{Y''}{0.17 + 0.83 \cdot Y''} \qquad [2.3]$$

Where F" = (F / γ·H·L·D) / N_h; Y" = (Y / D) / (Y_f / D); Y is the actual pipe displacement, Y_f is the pipe displacement at failure (maximum load) and F is the lateral soil restraint associated with Y. By using appropriate values of Y_f/D ratio and N_h, which depend on pipe burial depth and soil friction angle, force-displacement relationships can be obtained for design purposes. The N_h values as a function of embedment ratio (H/D) and friction angle (ϕ) are shown in **Figure 2.4**.

Hsu (1994) found levels of lateral soil restraint that lie between those obtained by the experimental studies of Audibert and Nyman (1977) and Trautmann and O'Rourke (1985). By conducting tests on pipe specimens buried in Da-Du riverbed sand, he investigated the effect of soil density, burial depth, pipe

diameter and relative ground movement velocity on levels of lateral soil restraint. Hsu (1994) used pipe specimens with outside diameters of 38 mm up to 229 mm in a large-scale drag box of 1.83 m x 1.83 m x 1.22 m. The increase of pullout rate leaded to an increase in lateral soil restraint of less than 5%. He also proposed a series of rectangular hyperbola relationships between lateral soil restraint and pipe displacements for different strain rates. These relations are in line with those proposed by Audibert and Nyman (1977), Das and Seeley (1975), and Trautmann and O'Rourke (1985). Hsu concluded that a limit equilibrium model with the assumption of a planar failure surface could be used successfully to predict the maximum lateral soil restraint.

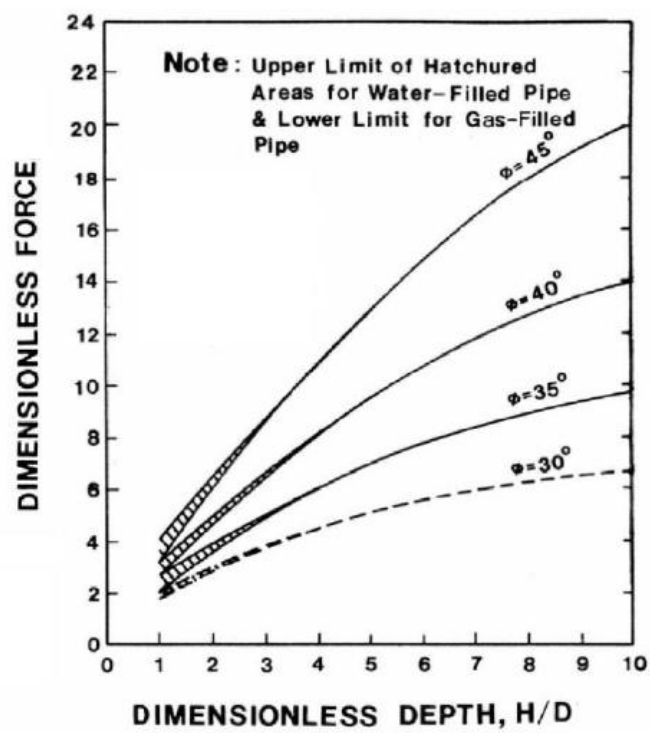

Figure 2.4: Prediction of horizontal soil restraint on buried pipes. From Trautmann and O'Rourke (1983) following method suggested by Ovesen (1964).

Paulin et al. (1996, 1997 and 1998) conducted a series of full-scale tests on a pipe with outside diameter of 324 mm buried in sand at the testing facility of the Centre for Cold Oceans Resources Engineering (C-CORE), Memorial University of Newfoundland, Canada. C-CORE used the test results to calibrate numerical models. The soil restraints were presented in terms of percentage of the maximum load and no absolute value for the results was reported.

By testing small pipe specimens buried in saturated sand, Calvetti et al. (2004) found values of lateral soil restraints higher than those from Trautmann and O'Rourke (1985) and Hsu (1994) and in good agreement with the Hansen (1961) capacity factor N_{qh}. They conducted a series of small scale tests on pipe specimens with diameters ranging from 20 mm to 50 mm to investigate levels of soil restraints during relative lateral ground movement. A Distinct Element Method model developed with Particle Flow Code (PFC2©) software was carried out to further validate their experimental test results.

Yimsiri et al. (2004) calibrated a finite element numerical model to investigate soil-pipe behaviour in sand for deep embedment conditions by using the experimental results of Trautmann and O'Rourke (1983) with overburden ratios of 2 to 11. They used two different constitutive models: Mohr-Coulomb model and Nor-Sand model. They extended the result of numerical model to overburden ratios of 100 and suggested limiting values for dimensionless load for different friction angles.

Turner (2004) investigated the effect of moisture content on levels of lateral soil restraint. He conducted experimental tests on buried steel pipes with external diameter of 119 mm buried at a depth that ranges from 6 to 20 diameters in sand with different moisture content and densities. He concluded that the maximum lateral soil restraint in moist sand was approximately two times greater than the lateral soil restraint in dry sand condition. From the observation of the deformational characteristics of the sand mass during his

tests, he claimed that different failure patterns exist in dry and moist sand conditions. In dry sand conditions, the failure pattern showed distinct regions of heave and subsidence; while the soil deformation pattern in moist sand conditions showed a single soil mass movement moving up and forward as a rigid body. The results of his work are summarized in **Figure 2.5**.

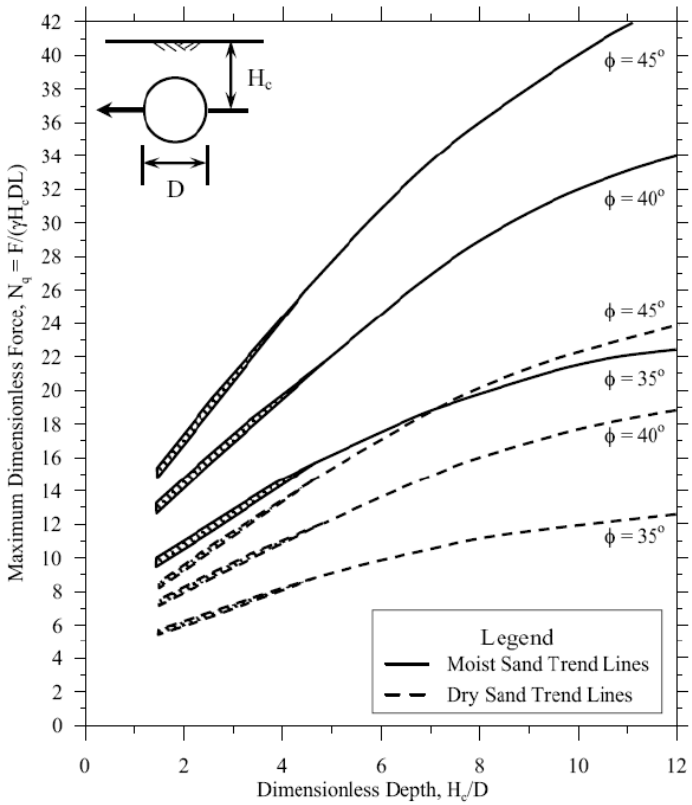

Figure 2.5: Lateral soil bearing capacity on buried pipes for dry and moist sand (Turner 2004).

Karimian (2006) conducted a series of full-scale tests on rigid steel pipes at the University of British Columbia to determine longitudinal and horizontal lateral levels of soil restraint. The tests were performed in pipe specimens with 32.4 mm (12.75”) and 45.7 mm (18”) outside diameter buried in Fraser River sand. The effect of density on levels of soil restraint was investigated by using sand with average dry densities of 1430 kg/m^3 to 1600 kg/m^3 (loose and

dense, respectively). The influence of moisture content on levels of lateral soil restraint was studied by performing tests on moist sand with 1% to 10% moisture content. He concluded that moisture content has no influence on the magnitude of lateral soil restraint and therefore dry and moist sand exhibits the same level of lateral soil restraint. This conclusion is contrary to that from Turner (2004).

O'Rourke et al. (2008), after re-evaluating the data from Turner (2004), concluded that moisture content has no influence on the magnitude of lateral soil restraint. This revised assessment by O'Rourke et al. (2008) corroborates the observations by Karimian (2006).

The effect of soil dilatancy and scale effect on levels of lateral soil restraint developed on pipes buried in sand subjected to lateral ground movements was studied by Guo and Stolle (2005) using a numerical model. By using ABAQUS software and a Mohr-Coulomb model with constant dilation angle and constant friction angle, they investigated the effects of geometrical factors such as burial depth and overburden ratio, pipe specimen scale, and sensitivity analysis of soil parameters on lateral soil restraint. They also used an elasto-plastic hardening model. The effect of soil dilatancy showed that it increases the horizontal bearing capacity factor (N_h) and a equation was proposed to take this effect into account. Regarding the scaling effect, they concluded that this effect depends on pipe diameter and not on overburden ratio.

O'Rourke et al. (2008) proposed an analytical approach to estimate lateral soil restraint for pipelines buried in cohesionless soils. They validated their approach by comparing the values from their analytical model with values from full-scale experimental test data and those given by ASCE (1984). Their approach is based on a trial method using log-spiral failure surfaces. By changing the center of rotation of the log-spiral failure surface along a predefined trajectory, a critical failure surface can be found that corresponds

to the minimum value of P_H as depicted in **Figure 2.6**. The lateral soil restraint (P_H) is found by satisfying moment equilibrium about the center of rotation and shown in **Equation 2.4**:

$$P_H = \frac{W_S L_s + W_p L_p}{L_H} \qquad [2.4]$$

Where:

P_H	=	horizontal soil force;	W_S	=	weight of soil mass;
W_P	=	pipe weight (including contents);			
L_H	=	moment arm between horizontal soil force and center of rotation;			
L_S	=	moment arm between soil mass and center of rotation;			
L_P	=	moment arm between pipe weight and center of rotation;			
β	=	angle between horizontal and r_1;			
ϕ	=	internal friction angle; θ = angle between r_0 and r;			
ψ	=	soil dilation angle			

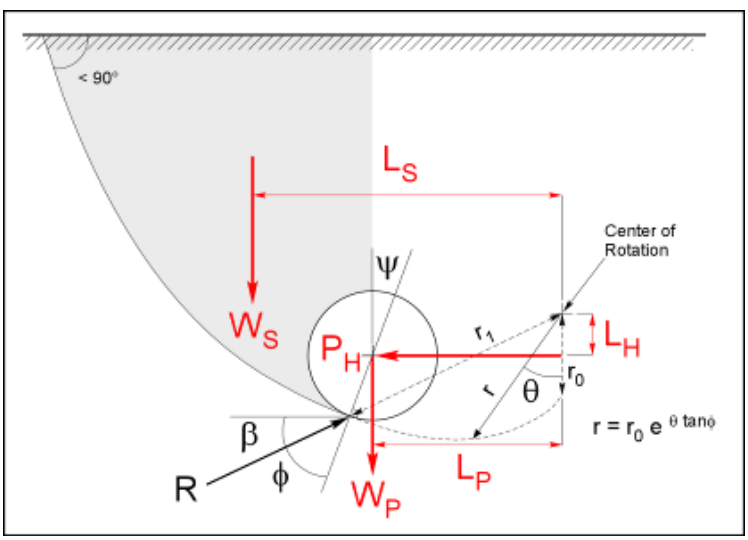

Figure 2.6: Assumed forces for estimating horizontal load using a log-spiral failure surface (O'Rourke et al. 2008).

Based on the foregoing observations, the following conclusion can be drawn:

1. It seems that the fundamental behaviour of pipelines buried in sand and subjected to different levels of horizontal relative ground displacement has received considerable attention from the research community and therefore its behaviour is fairly well understood. Parameters such as soil friction angle, soil density, pipe diameter, soil dilatancy, surface roughness and overburden ratio have been studied and their effects on soil-pipe interaction have been quantified by experimental and numerical models.

2. The existing methodologies and approaches to quantify levels of lateral soil restraint are influenced by definitions and criteria developed for retaining walls, laterally loaded piles, and vertical anchors.

3. Literature suggests that still there are differences in the way to estimate maximum lateral soil restraint on buried pipelines, which partly appear to be related to the assumed level of vertical constraint during lateral horizontal pipe displacement. Several investigators have concluded that the load-displacement relationship observed from both small and large-scale experimental tests follows the shape of a rectangular hyperbolic function.

4. Simple analytical models based on limit-equilibrium approaches with planar and log-spiral-shaped failure mechanisms forming in the soil mass during lateral pipe movement have been widely used to predict the maximum level of lateral soil restraint on buried pipes observed during experimental tests. Comparisons performed by researchers between the observed and predicted maximum lateral soil restraints showed good agreement.

It is of relevance to note that most of the research summarized earlier in this section was done on pipe elements buried in sand using small-scale tests or numerical modeling. Therefore, there is a good understanding of pipe behavior buried in sand and subjected to lateral ground displacements. However, the behavior of lateral soil restraint for granular materials other than sand has not been properly tested and verified due to the difficulty in conducting full-scale testing or in extrapolating to actual field conditions if the tests are conducted at a reduced scale.

In this study, other natural geomaterials, besides using sand as backfill material, such as crushed gravel and sand and crushed limestone were used to simulate soil conditions usually found in practice. By conducting full-scale tests on such soil conditions, levels of lateral soil restraint can be obtained and their values can be compared to those predicted from existing analytical models (e.g. O'Rourke et al. 2008). In this way, the portability of the analytical models to conditions different than sand can provide further validation of the models to uses that cover a wider range of practical cases.

1.4.2 Axial Soil Restraint

Newmark and Hall (1975) and Kennedy et al. (1977) pioneered the development of practical approaches to estimate levels of axial soil restraint for pipelines crossing active seismic faults. The approaches are based on frictional soil-pipe interface properties and average normal effective soil stress in at rest conditions. The axial soil restraint per unit length is estimated using **Equation 2.5** as shown below:

$$F_a = \pi \cdot D \cdot (\sigma'_n)_{av} \cdot \tan(\delta) \qquad [2.5]$$

where:

$$(\sigma'_n)_{av} = \left(\frac{1+Ko}{2}\right) \cdot \gamma \cdot H \qquad [2.5\text{-A}]$$

$(\sigma'_n)_{av}$ is the average normal soil stress on the pipe in at rest conditions; H is the height of the soil over the pipe springline; D is the nominal diameter of the pipe; δ is the soil-pipe interface friction angle; K_0 is the coefficient of lateral earth pressure at rest; and γ is the soil density. The normalised axial soil restraint per unit length, T_a, can be expressed as:

$$T_a = F_a / (\gamma \cdot D \cdot H) \qquad [2.6]$$

Equation 2.5 is recommended for the computation of axial soil loads in ASCE (1984) "Guidelines for the Seismic Design of Oil and Gas Pipeline Systems", American Lifeline Alliance (2001) "Guidelines for the Design of Buried Steel Pipe", and PRCI (2004) "Guidelines for the Seismic Design and Assessment of Natural Gas and Liquid Hydrocarbon Pipelines".

The existing available current literature also shows other equations proposed for estimating axial soil restraint. McAllister (2001) proposed **Equation 2.7** for determining the axial frictional resistance, which includes the weight of the pipe (W_p). The Danish Submarine Pipeline Guidelines (1985) proposed **Equation 2.8** for estimating the frictional force per unit length of pipe. **Equation 2.8** is based on the integration of shear stresses around the pipe.

$$Fa = \left\{2D\overline{\gamma}\left(H - \frac{D}{2}\right) + W_p\right\} tan\delta \qquad [2.7]$$

$$Fa = \left\{\frac{D\overline{\gamma}}{2} tan\varphi \left(H + \frac{D}{2}\right)\pi(1 + Ko) + \frac{4}{3}\frac{W_p}{\pi}(2 + Ko) - \frac{D\overline{\gamma}}{3}(2 + Ko)\right\} tan\delta \qquad [2.8]$$

Having illustrated the recommended approaches to estimate levels of axial soil restraint in pipeline engineering practice, it will be beneficial for this study to compare these values with those from experimental and analytical studies.

The following paragraphs will describe existing studies and refer to comparisons, where appropriate.

Paulin et al. (1998) conducted full-scale testing on a 324 mm steel pipe buried in loose and dense sand. The length of the testing chamber was 5.2 m. By comparing their test results with those predicted by **Equation 2.5**, they concluded that the axial soil restraint is different for loose and dense sand. For loose sand, the comparison showed test values lower than those predicted by **Equation 2.5**. For dense sand, the test values are higher. Furthermore, the axial soil restraint on buried pipe in loose sand is about 30% to 50% of that in dense sand.

Hsu et al. (2006) used pipe specimens with outside diameters of 152.4 mm, 228.6 mm, and 304.8 mm buried in dense sand. Hsu et al. (2006) reported a maximum normalised axial soil restraint, T_a, of about 1.1 for a pipe specimen (diameter of 228.6 mm) buried in sand with peak friction angle of 42°, soil-pipe interface friction angle of 26° and for H/D = 2. As indicated by Hsu et al. (2006), this value is close to that obtained from **Equation 2.6**. However, the axial displacement to failure reported by Hsu et al. (2006) is much larger than the usual range of about 3 mm expected for dense sand (PRCI 2004). They reported an axial displacement of around 0.2D.

Anderson (2004) performed a series of tests on Polyethylene (PE) gas pipelines buried in sand with the aim of determining levels of axial soil restraint along the pipe. He investigated longitudinal soil restraints on straight and branch PE pipes with diameter of 60 mm and 114 mm buried in loose and dense Fraser River sand. He concluded that the equations given by ASCE (1985), ALA (2001) and PRCI (2004) could not satisfactorily predict his test results. No detailed information was presented on the reasons under which the discrepancies were found.

The work presented by Karimian (2006) and Wijewickreme et al. (2009) on their tests on longitudinal soil restraint showed values comparable to those predicted with the equations from ASCE (1984) guidelines, but only for loose sand cases. For cases of pipes buried in dense sand, his results showed values three times higher than those predicted by the ASCE (1984) guidelines. The difference was attributed to constrained soil dilation which occurred during shear–induced volumetric expansion within a thin annular shear zone around the pipe. They claimed that the outward movement of the soil particles is constrained by the surrounding soil mass, and therefore the normal stress on the pipe increases. A summary of their axial pullout test results is shown in **Figure 2.7**.

Karimian (2006) and Wijewickreme et al. (2009) concluded that the coefficient of earth pressure at rest (K) should be used with caution for cases in which dense geomaterials are involved. The test results were further compared with 2D numerical simulations, in which a cross section of the pipe specimen buried in soil was modelled using FLAC. By expanding the diameter of the pipe by the same thickness of an observed shear zone during axial pullout test (1.2 to 2.8 mm, see **Figure 2.8)**, normal soil stresses around the pipe were computed and compared with those from normal stress measurements recorded during the axial pullout tests. Relatively similar results were found.

Relatively similar evidence of the volume-induced mechanism claimed by Karimian (2006) and Wijewickreme et al. (2009) has also been observed in piles (Kraft 1990; Jardine and Lehane 1993; Randolph et al. 1994; Jardine and Overy 1996; Foray et al. 1998; Lehane et al. 1993). For example, Lehane et al. (1993) observed an increase of around 50% in the values of normal stress on piles. However, the increment was not as high as that observed by Karimian (2006) and Wijewickreme et al. (2009). Evidence from CPT measurements in calibration chambers suggests that chamber boundaries increase the penetration resistance in dense dilatant soils (Parkin et al. 1980; Parkin and Lunne 1982).

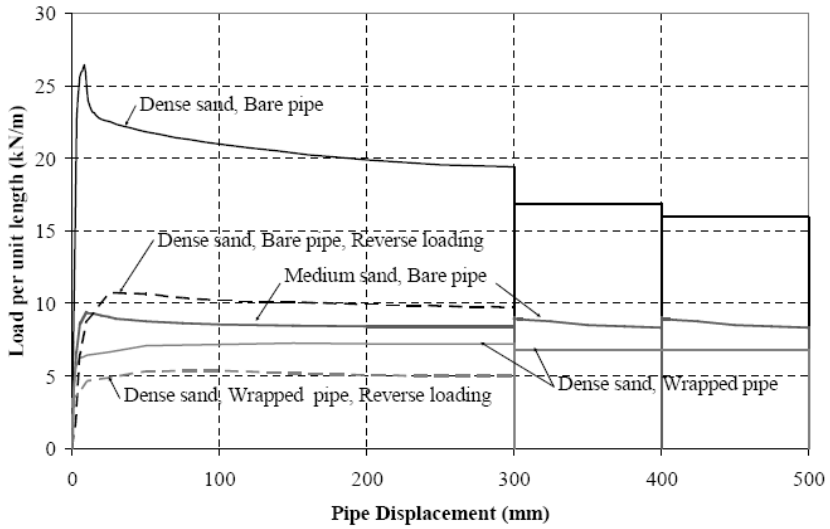

Figure 2.7: Axial soil restraint vs. axial pipe displacement, after Karimian (2006).

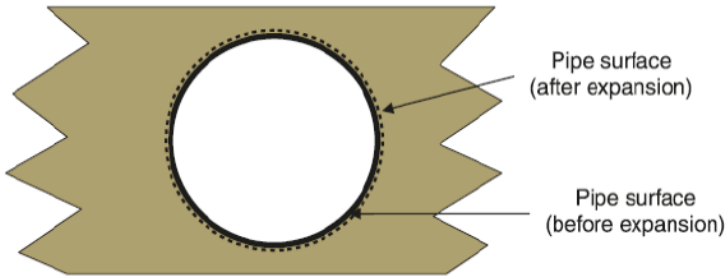

Figure 2.8: Dilation effect concept for axial soil-pipe interaction, after Wijewickreme et al. (2009).

Weerasekara and Wijewickreme (2008) performed full-scale experimental tests on buried MDPE (medium-density polyethylene) natural gas pipeline subjected to axial and lateral ground displacements. By testing pipe specimens with diameters of 60 mm and 114 mm buried in Fraser River sand, they observed that that the axial soil restraint on MDPE pipes depends on the flexibility of the pipe. They developed analytical closed-form formulations to determine the longitudinal and transverse response of MDPE pipes that adequately simulated the experimental test results.

Daiyan et al. (2011), based on their results from centrifuge tests, reported a maximum normalised axial soil restraint of about 2.0 for a pipe specimen buried in sand with peak friction angle of 43°, unit weight of 16 kN/m^3, soil-pipe interface friction angle of 24°and H/D = 2. Daiyan et al. (2011) acknowledged that the purely axial soil loads measured in their centrifuge tests for H/D = 2 on dense sand were approximately two times higher than that given by **Equation 2.6**.

Daiyan et al. (2010, 2011) concluded that the high axial soil restraint is attributed to dilation and increased normal stress on the pipe related to end bearing of the pipe specimen loading system, flexibility of the frame to which the pipe specimen was attached and the high weight of the pipe loading system.

A numerical simulation without the additional weight from the loading mechanism was carried out by Daiyan et al. (2010, 2011) to further verify their results. They found a normalised axial soil restraint of about 1.1 for a pipe specimen buried in sand with H/D = 2. Their maximum normalised value for axial soil loads is very similar to the value of 0.92 calculated following **Equation 2.6**.

Another feature of particular interest is the extremely large pipe displacement value required to reach maximum axial soil restraint in small-scale tests, when compared to full scale test results. Axial load-displacement response in the Daiyan et al. (2010, 2011) tests showed a pipe displacement value of 14 mm at model scale (0.34D at prototype scale), against values less than approximately 5 mm to 10 mm (less than 0.05D) that were observed in full-scale pipe tests (NOVA 1995; Wijewickreme et al. 2009).

1.5 Interaction of Horizontal and Axial Soil Restraint on Buried Pipes

Interaction or interdependence of horizontal and axial soil restraints arises when the buried pipeline axis is oriented with an angle with respect to the main direction of ground displacement (e.g., plane of a strike-slip fault) and therefore is subjected to horizontal oblique ground movements as depicted in **Figure 2.9**.

Initial discussions on the interaction between horizontal and axial soil restraints can be found in Kennedy et al. (1977). Kennedy et al. (1977) determined that an increase in the maximum axial soil restraint of about 2 to 3 was appropriate to account for the increased in normal stress on a 42" (1.06 m) pipeline buried in moderately dense sand and subjected to strike-slip fault displacement type. The axial soil restraint in regions with relative lateral ground displacement was determined by multiplying the soil-pipe interface friction angle, δ, and the maximum lateral soil restraint.

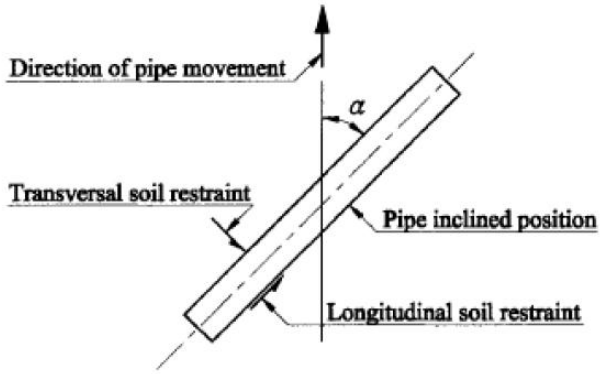

Figure 2.9: Angle of movement for defining horizontal oblique ground displacement with respect to pipeline axis (top view).

Investigations into the interaction of horizontal and axial soil restraint on rigid pipes have been reported by Hsu et al. (2001, 2006) and investigators at C-CORE (C-CORE 2003, 2008; Phillips et al. 2004; Daiyan et al. 2010, 2011). However, notable differences between their corresponding interaction relationships exist.

The experimental work by Hsu et al. (2001, 2006) used pipe specimens with outside diameters of 152.4 mm, 228.6 mm, and 304.8 mm buried in loose and dense sand. The experimental apparatus used in the Hsu et al. tests held an active pipe section (segment exposed to soil loading) with an specially designed load cell to measure axial and horizontal loads (see **Figure 2.10**).

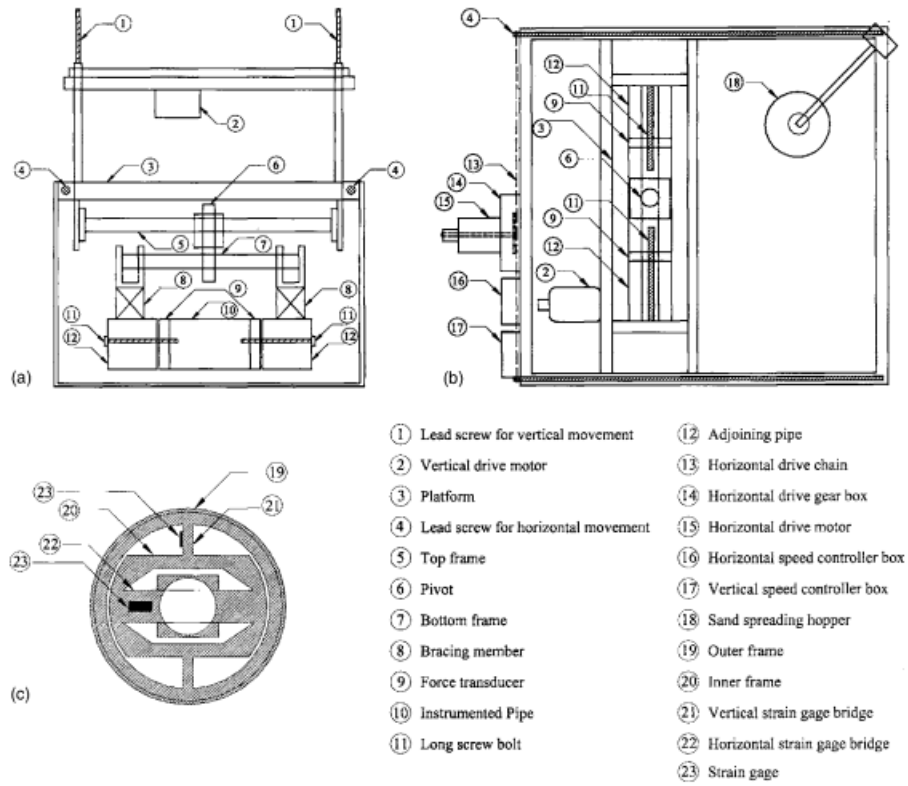

Figure 2.10: Test Arrangement Used by Hsu et al. (2006). From Hsu et al. 2006.

From the description of the test apparatus, it is unclear whether or not the pipe test specimen was prevented from upward movement during the tests. Based upon observed trends in test results with the oblique direction of horizontal ground displacement relative to the pipeline axis (0° being purely axial and 90° being purely horizontal), Hsu et al. (2001, 2006) suggested that axial and lateral soil restraint vary as the cosine and sine of the oblique angle, respectively. This relation is shown in **Figure 2.11**.

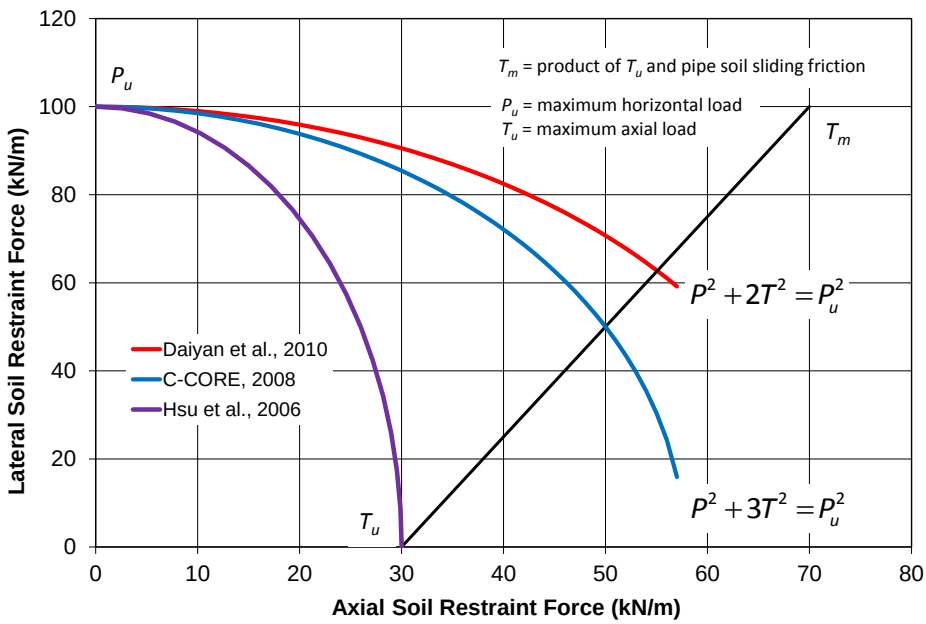

Figure 2.11: Horizontal and axial soil restraint interaction envelops proposed by Hsu et al. (2006), C-CORE (2008) and Daiyan et al. (2010).

Daiyan et al. (2010, 2011) and C-CORE investigators performed centrifuge tests on pipe specimens with a diameter of 41 mm at 12.3 g to study the lateral-axial interaction under ground movements oblique to the pipe alignment. The test specimen length-to-diameter ratio was 8 and a load cell was mounted at each end. For the C-CORE tests, the pipe test specimen was rigidly held at each end and moved through a bed of sand. Vertical movement of the pipe specimen was allowed during the testing but, as noted in Daiyan et

al. (2010, 2011), the weight of the test assembly largely restricted vertical upward movement of the test specimen and resulted in much higher lateral soil restraint.

The interaction between axial and lateral soil restraint recommended by C-CORE (2003, 2008) is defined in terms of an interaction envelop illustrated in **Figure 2.11**. A similar interaction envelope is recommended by Daiyan et al. (2010) for sand with the only difference being a factor of 2 applied to the variable *T* instead of the factor of 3, suggested by Phillips et al. (2004) based on their tests on clay, as in **Figure 2.11**.

C-CORE (2003, 2008), Phillips et al. (2004) and Daiyan et al. (2010, 2011) claimed that the value of axial soil restraint during axial-lateral soil restraint coupling is more than the pure axial condition; with a factor of even 2.5 for oblique angles less than 40°. The observed higher axial soil restraint by C-CORE (2003, 2008), Phillips et al. (2004) and Daiyan et al. (2011) is attributed to an increase in normal or lateral pressure due to the lateral component of oblique relative displacement. This claim is in line with the suggestions made by Kennedy et al. (1997). Daiyan et al. (2010, 2011) also observed large increments of axial soil restraint for oblique angles of even 1° (pipe misalignment) during their 3D numerical simulation. However, this condition required oblique displacements larger than 1D.

Daiyan et al. (2010, 2011) acknowledged that both the purely horizontal soil restraint and purely axial soil loads measured in their tests were approximately two times higher than those reported in the literature (such as Trautmann and O'Rourke 1983, 1985). As noted above, the high horizontal soil load was attributed to the restriction on vertical movement of the pipe specimen and the high weight of the pipe loading system.

Daiyan et al. (2010, 2011) considered their centrifuge tests as valid because their 3D numerical simulation resulted in comparable peak load values when

the weight of the pipe and loading mechanism were incorporated in the simulation. However, there was substantial difference between the computed horizontal load versus displacement behavior and that observed in the experimental tests. This poor relationship between measured and simulated horizontal load-displacement behavior was not considered relevant by Daiyan et al. (2010, 2011).

Given the similarity in loading arrangement between Hsu et al. (2001, 2006) and Daiyan et al. (2010, 2011), the results presented in Hsu et al. (2001, 2006) were carefully reviewed. The horizontal bearing factor N_h reported for loose sand by Hsu et al. (2001) for an H/D ratio of 2 was approximately 5. For tests in dense sand and for an H/D ratio of 2, Hsu et al. (2006) reported a horizontal bearing factor N_h of approximately 7.5 which is similar to values of approximately 7 to 8 reported by others (Trautmann and O'Rourke 1985; O'Rourke et al. 2008; Karimian 2006). Therefore, the Hsu et al. (2001, 2006) tests on both loose and dense sand do not appear to have been affected by restraining vertical displacement of the pipe test specimen.

Axial tests conducted by Hsu et al. (2001, 2006) exhibited the same problems as noted by Daiyan et al. (2010, 2011) in that the maximum axial soil restraint did not develop until pipe displacement reached 0.2D to 0.55D for dense and loose sand, respectively. For the data presented by Hsu et al. (2001, 2006), these displacement ratios correspond to actual displacements of 46 mm to 126 mm, which appear to be extremely large when compared to those from full-scale tests (NOVA 1995; Wijewickreme et al. 2009). The above may suggest interference of the loading system with the soil around the pipe specimen.

As noted above, the load-displacement relationship results of Hsu et al. (2001, 2006) appear to exhibit the same anomalies in test results related to the testing hardware as noted in Daiyan et al. (2010, 2011). The similarity in the small-scale testing apparatus used by Hsu et al. and Daiyan et al. raises a

possibility that the anomalous test results reported by Daiyan et al. were related to some artifact of centrifuge testing.

Ha et al. (2008) presented results from four centrifuge tests designed to investigate the influence of pipe-fault orientation on HDPE pipe behavior under earthquake faulting. The pipes were buried in dry sand which had a friction angle ϕ=35° and unit weight of 18.9 kN/m^3. The tests were conducted at 50 g (50 times Earth's gravity) with the pipe and fault oriented 85° and 63.5°, relative to each other, and a pipe burial depth of 1.2 m in prototype scale.

The Ha et al. (2008) test results show that, as expected, pipe axial strain is strongly influenced by the pipe-fault orientation angle, whereas the influence of pipe-fault orientation angle on pipe bending strain is minor. Likewise, the measured pipe strains were shown to follow the trend predicted by the Kennedy et al. (1977) model. The peak axial force measured for pipes oriented at 85° and 63.5° was about 140 kN and 330 kN, respectively. The peak pipe lateral force from the 85° test was higher than that from the 63.5° test by about 20%. **Figure 2.12** shows the lateral force vs. displacement relationship from the Ha et al. tests. However, no lateral-axial interaction relationship was developed.

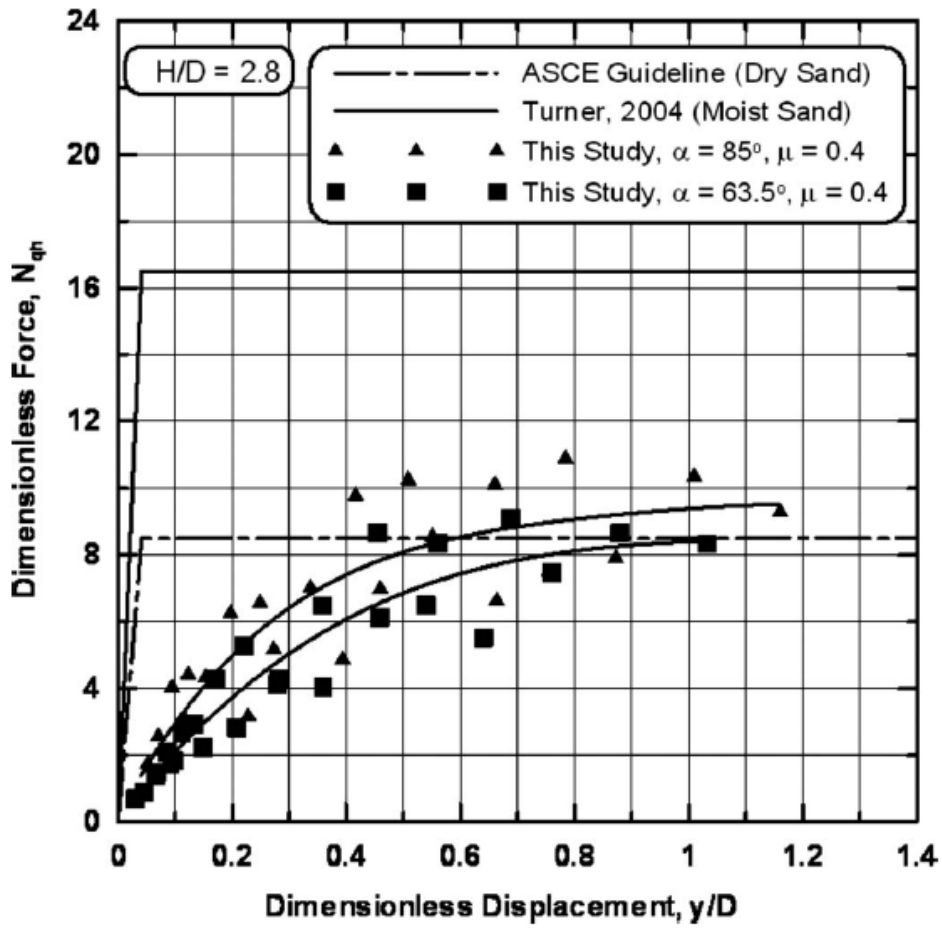

Figure 2.12: Lateral soil restraint vs. lateral pipe displacement as a function of oblique angle (α). From Ha et al. (2008).

From the foregoing very limited data the following observations can be made regarding the interaction of horizontal and axial soil restraint:

1. Existing lateral-axial soil restraint interaction relationships are reported by Hsu et al. (2001, 2006) and investigators at C-CORE (Phillips et al. 2004; Daiyan et al. 2010, 2011). These interaction relationships are based on the values of maximum lateral and axial soil restraint and were developed upon a limited number of small scale tests, centrifuge

tests and finite element modeling, where sand was used as the surrounding soil.

2. Hsu et al. (2001, 2006) argued that the relation between axial and lateral soil restraint during relative oblique displacements is a function of the cosine and sine of the oblique angle. C-CORE investigators claimed that the interaction between axial and lateral soil restraint do not fit in the pattern of cosine and sine of oblique angle relationship for oblique soil-pipe interaction. They claimed that the value of axial soil restraint component during axial-lateral soil restraint coupling is more than that for the pure axial condition with a factor of even 2.5 for oblique angles less than 40°. No information exists on the reason for the differences in the proposed interaction curves by Hsu et al. (2001, 2006) and Daiyan et al. (2010, 2011), shown in **Figure 2.11**.

3. Conflicting results exist on the relative pipe displacement values required to reach maximum axial soil restraint under small-scale and full-scale test conditions. Axial pipe displacement from small-scale was shown to be in the range of 0.2D to 0.55D. The results from full-scale tests exhibited values less than 0.05D.

4. Given the issues related to the test results in work by Hsu et al. (2001, 2006) and Daiyan et al. (2010, 2011) and the lack of a demonstrated ability to replicate load-displacement behavior observed in the small-scale experimental tests with numerical analyses, the conclusions drawn so far with respect to the interaction between lateral and axial soil restraint should be treated with caution.

In view of the above mentioned limited and often contradictory data, it was decided to compare the interaction between lateral and axial soil restraints of buried pipelines as a part of the research work undertaken in this thesis. A number of full-scale tests conducted on pipe segments buried in sand was

designed in view of obtaining clarification of soil-pipe interaction response to horizontal oblique soil loading. In particular, a proper understanding of the correlation between lateral and axial soil restraints would permit clarification on whether or not an increase in axial soil restraint should be considered in design.

1.6 Interaction of Horizontal and Upward Vertical Soil Restraint

By using the experimental data from Meyerhof (1973) for anchor plates, Nyman (1982) developed an analytical model to include the horizontal and upward vertical soil restraint interaction when pipelines are subjected to vertical oblique ground movement. The interaction model depends on maximum values of soil restraint in each orthogonal direction and the inclination angle with respect to the vertical direction. The relationship is presented in **Equation 2.9**:

$$p_{u-\alpha} = (1-k)q_{u0} + kp_{u0} \qquad [2.9]$$

$$k = \frac{0.25\alpha}{90-0.75\alpha} \qquad [2.10]$$

Where p_{u0} is the maximum horizontal soil restraint per unit length, q_{u0} is the maximum upward vertical soil restraint per unit length, and α is the inclination angle with respect to the vertical that controls the direction of pipe displacement. Later, Das (1985) found that a value of $k = (\alpha/90)^2$ in **Equation 2.9** approximate better his small-scale experimental test results on anchor plates buried in clay.

Hsu et al. (1996) conducted large-scale experimental tests to study horizontal and upward vertical soil restraints on pipelines subjected to vertical oblique

ground displacements. 1.22 m pipe specimens with diameters of 38.1, 76.2, 152.4, and 228.6 mm and normalized burial depth of 1.5 and 3.5 were tested with inclination angles between 0 (vertical direction) to 90 degrees (horizontal direction) with angular increment of 10 degrees.

The pipe specimens used by Hsu et al. (1996) were buried in loose sand with internal friction angle of 33° and an average density of 15.2 kN/m^3. The dimensions of the chamber were 1.83 m x 1.83 m x 1.22 m. The maximum lateral soil restraints and corresponding displacements increased as the oblique angle increased from the vertical to the horizontal direction. Oblique soil restraints were predicted by means of a simple limit equilibrium model based on planar failure surfaces. By fitting his experimental data to a rectangular hyperbola (constants "*a*" & "*b*"), he reproduced force-displacement relationship as function of oblique angle. Based on his observations, the "*a*" value increases with oblique angle (measured from vertical direction) while the constant "*b*" decreases. The lateral and upward vertical interaction proposed by Hsu et al. (1996) is shown in **Figure 2.13**.

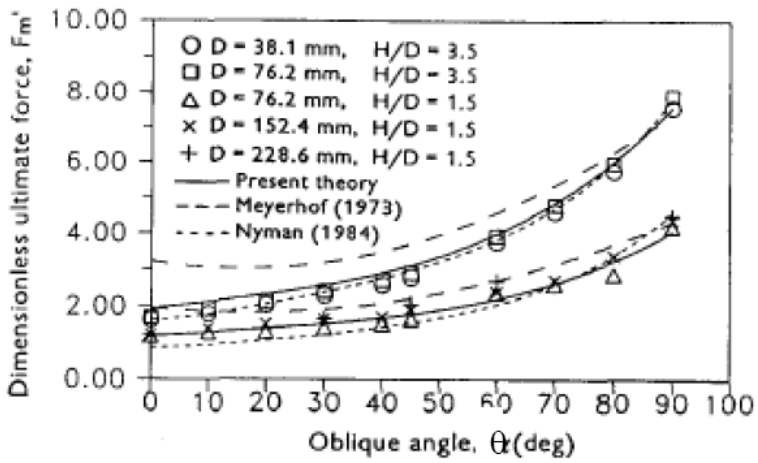

Figure 2.13: Variation maximum of soil restraint for loose sand as a function of oblique angle proposed by Hsu et al. (1996) (90° horizontal direction).

Guo (2005) developed an associative, hardening elastoplastic constitutive model in load space suitable for the analysis of pipes buried in clay subjected to oblique (lateral and upward vertical) displacement by extending the model proposed by Martin and Houlsby (2001) for shallow foundations. His proposed model involves seven parameters, which can be obtained from experimental data or from recommendations of the ASCE (1984) guidelines. He validated his model by comparing his results to the results of continuum finite element analysis. The comparison is shown in **Figure 2.14**. Finally, he recommended the development of experimental studies to further validate his model.

Vanden Berghe et al. (2005) found small differences in upward vertical soil restraint values on pipelines when the direction of pipe displacement is less than 30° from the vertical. This conclusion is based on results from finite element analysis which simulates a pipe buried in very loose sand. The vertical soil restraint as a function of direction is shown in **Figure 2.15**. This finding is consistent to that of Hsu (1996).

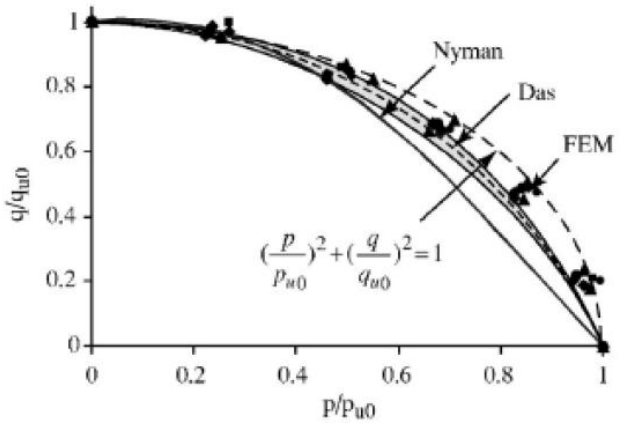

Figure 2.14: Interaction relationship for pipes buried in clay subjected to vertical oblique (lateral and upward vertical) displacements (Guo 2005).

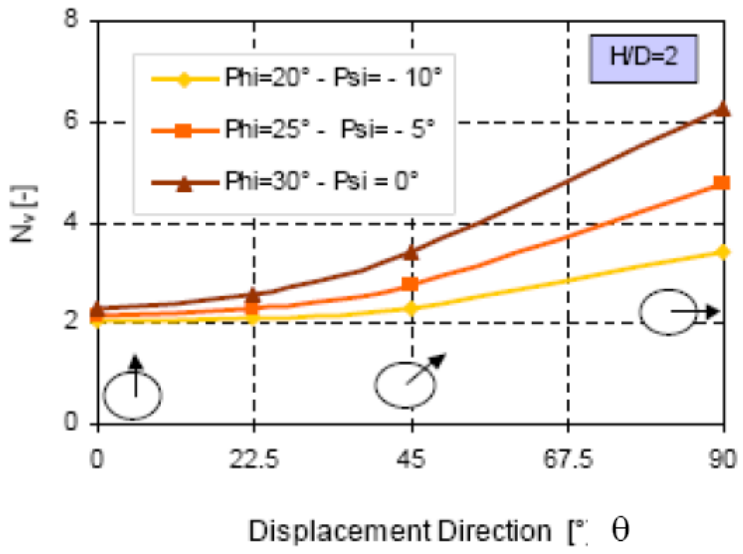

Figure 2.15: Comparison between vertical, oblique and horizontal soil restraints in loose/contractive soils. After Vanden Berghe et al. (2005).

Jung J. et al. (2012) carried out numerical simulations to estimate maximum force and force-displacement relationships, including post-peak performance, during soil-pipeline interaction subjected to vertical upward ground movements. The results from the numerical simulations were compared against results from full-scale tests carried out by Trautmann and O'Rourke (1983). Good agreement was found. Simulations were later conducted to cases with various sand densities and depth-to-diameter ratio up to 100. Results showed that maximum force occurred at a depth-to-diameter ratio of 30. An elasto-plastic model with Mohr-Coulomb (MC) strength parameters under plane condition was adopted for the modeling. Peak strength parameters from direct shear tests were converted to plane strain strength parameters. Furthermore, soil migration that occurs beneath the pipe during upward pipe displacement was incorporated in the model.

On the basis of the very limited data, the following observations can be made regarding the interaction of lateral and vertical (upward) soil restraints:

1. Coupling horizontal and vertical soil deformations develops due to permanent vertical oblique ground displacements.

2. The magnitude of soil restraint on buried pipe gradually increases as the direction of relative ground displacement changes from vertical to horizontal direction according to the results of different investigators from tests on clay and loose sand.

3. The ratio of vertical and horizontal soil restraint corresponding to a given direction of oblique pipe displacement appears to vary within a narrow range and therefore no significant differences or conflicting results appear to exist in the literature for practical purposes and for the cases evaluated (i.e. clay and loose sand).

4. Maximum oblique soil restraint for loose sand can be predicted by means of a simple limit equilibrium model based on planar failure surfaces.

5. Numerical modeling based on continuum mechanics and well established elasto-plastic models seems to predict appropriately soil restraints for vertical upward ground movements observed from full-scale tests, when appropriate modification are incorporated.

The above observations indicated that the values of maximum vertical oblique soil restraint available in the literature have been developed mainly for pipelines buried in plain clay or loose sand and are based on small-scale testing. No information appears to exist on maximum vertical oblique soil restraint for pipelines buried in trenches and backfilled with dense sand or other geomaterial.

The above vertical oblique pipe-soil restraint properties are mainly needed to estimate pipeline segments performance for reverse/thrust fault crossing design.

Because the pipeline earthquake engineering practice has not benefited from appropriate information on soil restraint modeling parameters for reverse/thrust fault displacement, these soil restraint parameters are usually inferred on the basis of horizontal and vertical restraint. This invariably requires a large degree of extrapolation tuned with conservative engineering judgment. This thesis is an attempt to measure vertical oblique soil restraint by applying relative vertical oblique ground displacements to a real-scale pipe specimen in an effort to simulate the oblique angle breakout of buried pipelines from their soil embedment on the footwall side of reverse/thrust faults.

1.7 Effects of Trapezoidal Trench on Levels of Lateral Soil Restraint

Buried pipelines are generally placed in shallow trenches backfilled with loose geomaterials or the same material excavated from the pipeline trench. The use of loose material for the backfill is preferable; however, the use of a denser and stronger material than the surrounding soil is sometimes used in practice. For example, the use of compacted granular backfill or the use of controlled-density fill in trenches excavated in soft clay or peaty soils (PRCI 2009).

As reported in PRCI (2009), C-CORE (2003) presented results from analytical and experimental investigation on the effects of clay backfill soils with lower strength than the surrounding soil. They presented an approach in which the lateral soil restraint can be defined using the strength properties of the backfill until the relative horizontal displacement between the pipeline and the soil exceeds the distance between the pipe and the trench wall. At larger relative horizontal displacements, the lateral soil restraint should be representative of the surrounding soil. This approach is illustrated schematically in **Figure 2.16**.

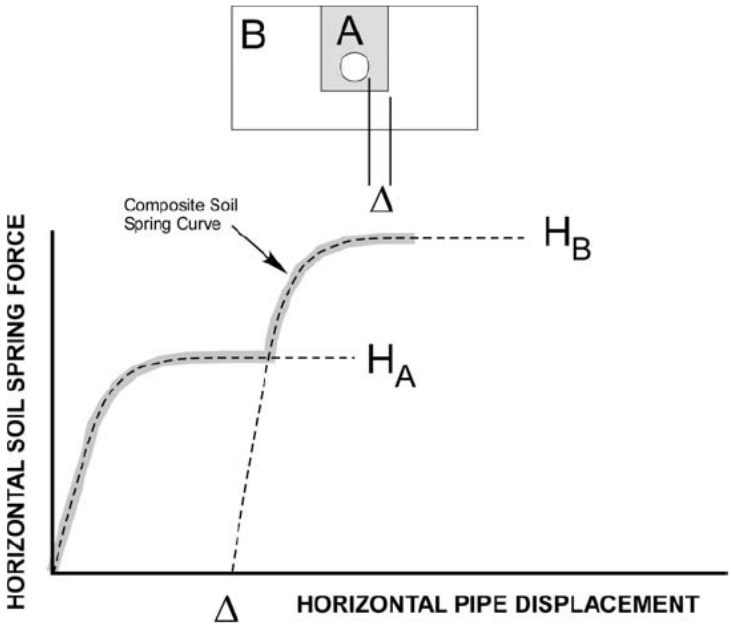

Figure 2.16: Approach for defining lateral soil restraint for pipelines buried in trenches (C-CORE, 2003).

Using a two dimensional finite element model in ABAQUS, Phillips et al. (2004) investigated the effect of lateral ground movement on pipes buried in trenches. Both backfill and native soil materials were modelled as cohesive materials. The results of numerical modeling were supported by physical centrifuge tests. The effects of rate of ground movement and trench wall inclination were investigated. It was shown that a decrease in trench surface slope from vertical position to 60° does not noticeably affect the soil load on the pipe while trench wall inclination of 45° and less can result in reduction of soil loads on pipes significantly (depending on relative density of native soil and backfill material and distance of the pipe from the trench surface).

Karimian (2006) performed a series of experimental tests on pipes buried in trench-configurations. Compacted Fraser River sand was used for the trench backfill as well as native soil. The tests were performed with trench slope

angles of 45° and 35°. A constant maximum lateral soil restraint was reported similar to tests performed without trench configurations.

Furthermore, Karimian (2006) performed a series of experimental tests to simulate the soil response under lateral loading of pipes buried in trench configurations with hard native soil conditions (e.g., pipe buried in glacial till-like material or bedrock). Five full scale tests were performed with a trench slope of 35°. Compacted dry Fraser River sand was used as backfill to capture the effect of cohesionless material in trench backfill. The results of the tests showed a continuous increase of lateral soil restraint above the expected maximum lateral soil restraint. Karimian (2006) indicated that the increase is due to the close distance between the pipe and the rigid trench reached during the test.

1.8 Use of Geotextile to Reduce Soil Restraint on Buried Pipelines

The use of geotextiles as a means to reduce axial and lateral soil restraints dates back to the early 90's and is a recommended mitigation option in pipeline engineering design guidelines (e.g. PRCI 2004, 2009). For axial soil restraints, the reduction is achieved by using low-friction coating or by wrapping the pipe with two layers of geofabric with the aim of reducing the pipe-soil friction. For lateral soil restraints, the basis of reduction is similar (i.e. by reducing friction). However, for the latter, the geotextiles are placed on the sloped walls of the trench constructed to build the pipe. The following paragraphs present results from previous experimental and analytical approaches developed to characterize the effectiveness of the geotextile-based mitigation option.

NOVA Gas Transmission Ltd. (1995) performed a series of field axial tests with the aim of studying the reduction of soil restraint by wrapping a pipe with different geosynthetic materials. A 0.4 m diameter steel pipe and a constant

overburden ratio of approximately 3 were used for all field tests. Only the load and displacement of the pipe were recorded during the tests. Test results indicated that using proper wrapping material might decrease the load on pipe to 40% of that on bare pipe. The NOVA tests led to a recommendation of a combination of geotextiles as a means to reduce axial soil loads.

Karimian (2006) performed a series of experimental tests on bare and geotextile-wrapped pipelines subjected to axial ground movements. He found that wrapping a pipeline with two layers of geotextile can substantially reduce the axial soil restraint on buried pipelines. The use of two separate layers of geotextile was found to be much superior to an overlapping spiral placement. Contrary to the findings from the NOVA tests, axial soil restraints for a configuration consisting of an inner layer of geonet and an outer smooth woven-geotextile were greater than the configuration with two smooth geotextile layers.

Karimian et al. (2006) reports results from physical model tests simulating lateral soil loading of buried pipes in trenches where the trench slope is lined with two layers of geotextile fabric. A case with a “flexible” sloped trench wall (a trench constructed in sand) a backfilled with dry sand and a case with a rigid sloped trench (a trench constructed with wood elements and braced to prevent deformations on the trench plane) with sand as backfill were performed by Karimian et al. (2006). The rigid boundary trench wall had an inclination of 35° with respect to horizontal. The position of the pipe at the initial of the test was 0.7D from the sloped trench wall.

The results from the Karimian et al. (2006) tests on the geotextile-lined sloped flexible-trench wall were similar to those from test on which the trench wall was absent (note that the flexible trench wall was constructed over the native soil).

Furthermore, a number of tests were performed in moist sand by Karimian et al. (2006) in the belief that moist sand would behave more like a block and improve the likelihood of slippage at the geotextile interface. However, it was found that tests with moist sand backfill exhibits the same reduction in horizontal soil restraint than their dry sand counterparts (i.e. 15% to 20%).

For all tests under rigid sloped trench wall, Karimian et al. (2006) found that the geotextile configuration provided a reduction of horizontal soil restraint of about 15% to 20% with respect to the case without geotextile. They also found a continuous increase in lateral soil restraint, regardless of the use of geotextile on the sloped trench, as the pipe approached the trench wall. Karimian et al. (2006) concluded that the development of local shearing of sand between the front of pipe and trench wall is the reason for the low effectiveness of the geotextile interface in reducing soil loads.

Karimian et al. (2006) proposed an equation based on a rigid block and a limit equilibrium approach to quantify the observed lateral loads under the assumption that soil-pipe behaviour under trench conditions is controlled by one failure mode. The formulation depends on the weight of a passive wedge, geotextile interface friction angle (δ) and the backfill soil friction angle (ϕ). The approach is shown in **Figure 2.17**.

The two formulations are shown in **Figure 2.17** which differ in whether the sliding friction between the pipe and the trench wall is characterized by the friction between two layers of geotextile fabric (**Figure 2.17-a)** or by the internal friction of the soil **(Figure 2.17-b)**. Karimian et al. (2006) postulated that as the pipe approaches the trench wall the soil restraint increases as a result of soil confinement and forces shear failure through the soil instead of the geotextile interface. This is accounted for by the term tan(ϕ) in the denominator of the equation for P in **Figure 2.17-b**.

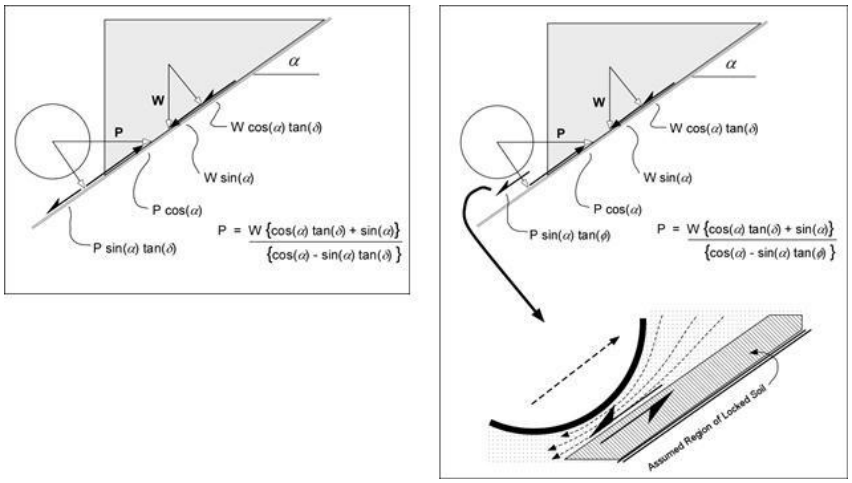

Figure 2.17: Sliding block mechanisms for geotextile-lined trench wall (a) Sliding only at geotextile interface (left); (b) Sliding at geotextile interface and shear failure through soil between pipe and trench wall (right).

Karimian et al. (2006) indicated that their equation is not able to estimate the horizontal soil resistance for dual-geotextile lined trench configurations. They pointed out the hypothesis that relative movement of the pipe within the backfill is the main reason for this inability.

On the basis of the above information, the following observations can be made regarding the effectiveness of geotextiles in reducing axial and lateral soil restraints:

1. Wrapping a pipeline with two layers of geotextile can effectively reduce the axial soil restraint on buried pipelines according to the results of different investigators.

2. The soil-pipe interaction behavior of pipelines buried in geotextile-lined trenches appears to be studied only by Karimian et al. (2006). This study reported marginal levels of reduction of lateral soil restraint (less than 20%). No difference was found on the levels of lateral soil restraint reduction under backfills with moist or dry sand.

3. No proper mechanical models or equations are available to quantify levels of lateral soil restraint for pipelines buried in geotextile-lined trenches. The nature of the equation proposed by Karimian et al. (2006) is rooted in their test results and cannot be applicable to conditions different than their tests. Furthermore, the equation does not take into account the rate of change of lateral soil restraint with horizontal pipe displacement, which developed during the Karimian et al. (2006) tests as the pipe approached the sloped trench wall.

In view of the foregoing observations, it seems that the nature of the soil-pipe interaction in the analysis of pipelines placed in geotextile-lined trenches under relative horizontal displacement is rather complex and needs to be studied further. On the other hand, the response of pipelines wrapped with two layers of geotextile is simpler and appears to show effective reductions of levels of axial soil restraint.

The understanding of the lateral soil-pipe interaction problem in geotextile-lined trenches and the study of the effectiveness of geotextiles in reducing levels of lateral soil restraint would be improved by observations from carefully conducted full-scale physical experiments, in which appropriate engineering parameters are measured and supported by numerical modeling.

This thesis is an attempt to contribute to the above understanding by simulating experimentally and numerically the lateral breakout of geotextile-lined buried pipelines from their soil embedment. Several pipe-trench distances will be experimentally tested to find the distance that fully mobilises the geotextile interface friction. The effectiveness of geotextiles in reducing levels of soil restraint will be studied by comparing the response of pipe specimens buried in trenches lined with and without geotextiles and subjected to lateral and vertical oblique ground displacements.

Chapter 3: Experimental Aspects

The development of experimental studies is crucial for the understanding of soil-pipe interaction aspects, its mitigation effectiveness and validation of approaches used in current practice of pipeline earthquake engineering. A large testing chamber, designed and constructed for this work, was used to conduct experimental tests and to understand these aspects of soil-pipe behavior.

The testing apparatus that was used for soil-pipe interaction research over the past 11 years at the University of British Columbia to study the behavior of rigid and extensible pipes subjected to axial and lateral ground displacements, as well as the behaviour of soil-cable interaction (Anderson 2003; Karimian 2006; Weerasekara 2008, 2011; Ahmadnia 2012; Wijewickreme et al. 2009) was suitably redesigned and modified to meet the current testing requirements.

The previous testing apparatus was largely modified and improved in a way that the testing can: a) accommodate loading conditions different than those imposed by purely axial and lateral relative ground movements; b) be easily relocated to any space (it includes a “self-sustained” foundation pad unanchored to a concrete floor); and c) provide continuous visual inspection and observation of patterns of deformation and geometric changes in the soil mass coupled with the change in position of the pipe specimen during the full-scale tests.

This chapter describes the experimental aspects of a set of full-scale tests conducted in the new testing chamber to study the development of soil restraint on rigid steel pipe specimens due to a variety of relative ground displacement directions and the effectiveness of geosynthetic-based mitigation measurements in reducing levels of soil restraint. In particular,

displacement types and modes that are expected to be generated in strike-slip and reverse faults were simulated.

Details about the design of the testing chamber, tests setup, mechanism of displacement application to pipe specimens, testing approach and instrumentation (i.e., instrumentation for the measurement of soil restraint, spatial pipe displacement, and geotextile displacement) will be described in detail in the following sections. This chapter also presents specific details on material properties such as friction angle of backfill materials used for the tests; index properties for geomaterials (e.g. soil density, moisture content, etc.); and soil-geotextile interface friction properties.

3.1 Experimental Apparatus

3.1.1 Original Soil-Pipe Interaction Testing Chamber

Previous work on soil-pipe interaction conducted at the Civil Engineering Department of the University of British Columbia was based on a soil chamber as described in detail by Anderson (2004) and Karimian (2006). The apparatus allowed investigating force-displacement relationships for segments of buried pipeline subjected to only axial and horizontal lateral ground displacements.

This original soil chamber is shown in **Figure 3.1** and was built upon the published experience of the work performed at Cornell University (Trautmann and O'Rourke 1983), and Centre for Cold Ocean Resources Engineering, C-CORE (Paulin et al. 1997). The internal plan dimensions of the soil chamber measured approximately 2.45 m x 3.8 m. The design of the chamber provided for up to 2 m of soil cover above the test pipe specimen. The following criteria were considered in the design of the soil chamber (Karimian 2006):

1. Full development of active and passive soil wedges during tests for pipe specimens with diameters up to 500 mm;

2. Minimal effects from the end walls and sidewalls during tests;

3. Promoting essentially plane strain conditions in horizontal lateral loading including rigid boundary wall conditions and minimum side friction;

4. Flexible dimensions and configuration to allow extensions to meet alternative test configuration requirements.

Figure 3.1: Soil chamber used in previous studies at the University of British Columbia.

3.1.2 Modified Soil-Pipe Interaction Testing Chamber

The development of earthquake pipeline engineering projects in regions, such as those characterized by active natural hazards or congested urban environments, challenges our current approaches and requires reliable information on soil-pipe interaction aspects different from the traditionally considered axial and lateral ground displacement conditions. For example, the design of pipelines crossing active reverse faults or the design of pipelines crossing strike-slip faults or landslides, in which the pipeline axis is not perpendicular to the direction of ground displacement requires relevant information on levels and on mobilization of soil restraints that are not readily available in the current technical literature.

Therefore, the design and construction of a testing chamber that is able to impose several directions of ground displacement on representative pipe specimens and that is able to simulate and replicate the mobilization of soil restraint on segments of pipelines that are imposed by different modes of ground displacement is of special interest for this study.

The mobilization of soil restraint on segments of pipelines depends on the direction and level of relative displacement imposed by a particular ground movement and the amount of deformation of the soil surrounding the pipeline. Therefore, by applying displacements to pipe specimens buried in different types of backfill soil in the direction of a particular ground movement (e.g. those occurring on a fault or other natural hazard condition), the corresponding levels of soil restraint can be measured, quantified and studied in a reliable, practical and economical way.

This work focuses specifically on investigating soil restraint on segment of pipelines imposed by ground movements that follow the type of displacement associated with strike-slip (lateral displacements) and reverse fault systems (lateral and vertical displacements). It is importance to note that it is not the

intent of this work to reproduce fault rupture conditions. Rather, the intent of this work is to simulate specific directions of ground displacement that would occur during fault rupture and the effect of this ground displacement on the mobilization of soil restraint.

Another loading full-scale soil-pipe simulation facility exists at the George E. Brown, Jr. Network for Earthquake Engineering Simulation (NEES) at Cornell University (Palmer et al. 2006; O'Rourke and Bonneau 2007). This facility allows a pipe buried in soil be subjected to an abrupt ground displacement using a split-box testing apparatus (i.e. the pipe moves in accordance with the displacement of the soil mass in the movable side of the slip box). By displacing the pipe in this way, the soil and pipe portion in the fixed part of the slip box start to interact and therefore levels of horizontal soil restraint are measured and quantified.

The split-box testing at Cornell University resembles abrupt ground displacement at strike-slip faults or at the margins of lateral spreads and landslides. In essence, the device simulates the soil pipe interaction condition at the location of the abrupt ground movements as well as its vicinity. The device is also useful in studying pipes with elbows or connectors. In contrast, in this study the displacement of the pipe is achieved by a set of cables that pull the pipe in a predefined direction (e.g. lateral, oblique or upward), rather than pushing it from the back or below. In this way the soil pipe interaction problem is mimicked in a 2-dimensional manner.

The modified soil-pipe interaction testing chamber can impose not only displacements along a horizontal plane, but also displacements along planes that go from horizontal to vertical under 2D and plain strain conditions. The testing chamber is based on the same size (2.45 m x 3.8 m) and main steel frame components of the previous soil chamber. A general view of the modified soil-pipe interaction testing chamber is shown in **Figure 3.2**. The

orientation of the 2D condition is defined with respect to the X-Z Cartesian coordinate system.

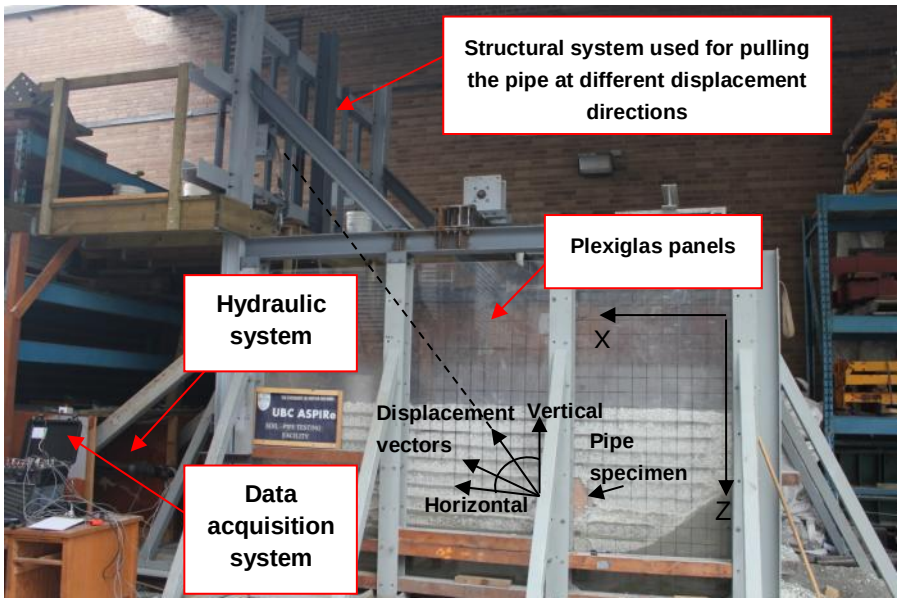

Figure 3.2: General view of the modified soil-pipe interaction testing chamber built for this study.

In particular, the following major modifications were made to the existing soil chamber to accommodate the demands of this study:

1. Removal of the bolted anchor system used to connect the previous soil chamber to the concrete floor of the structural laboratory of the Civil Engineering Department at UBC.

2. Relocation of the previous soil chamber from the structural laboratory to a site adjacent and outside this facility.

3. Design and construction of a new foundation system. The foundation system incorporates a new “floating” foundation pad formed by ½” steel plates resting on a grid of C-shape steel sections.

4. Design and placement of lateral members to provide stability to the modified soil-pipe interaction testing chamber testing chamber.

5. Incorporation of Plexiglas panels on one side of the testing chamber to allow visual observation of trench configuration, formation of failure wedges, patterns of deformation and geometric changes in the soil mass that are coupled with the changes in position of the pipe specimen during the full-scale tests.

6. Design and placement of a structural system that enables the application of loading on the pipe at different angles to the horizontal. The structural system consists of a vertical steel frame, a sheave system, several connections and a group of steel braces that provide appropriate lateral stiffness to the system (see **Figure 3.3)**.

Some stages of the construction process and the structural system are illustrated in **Figure 3.3**.

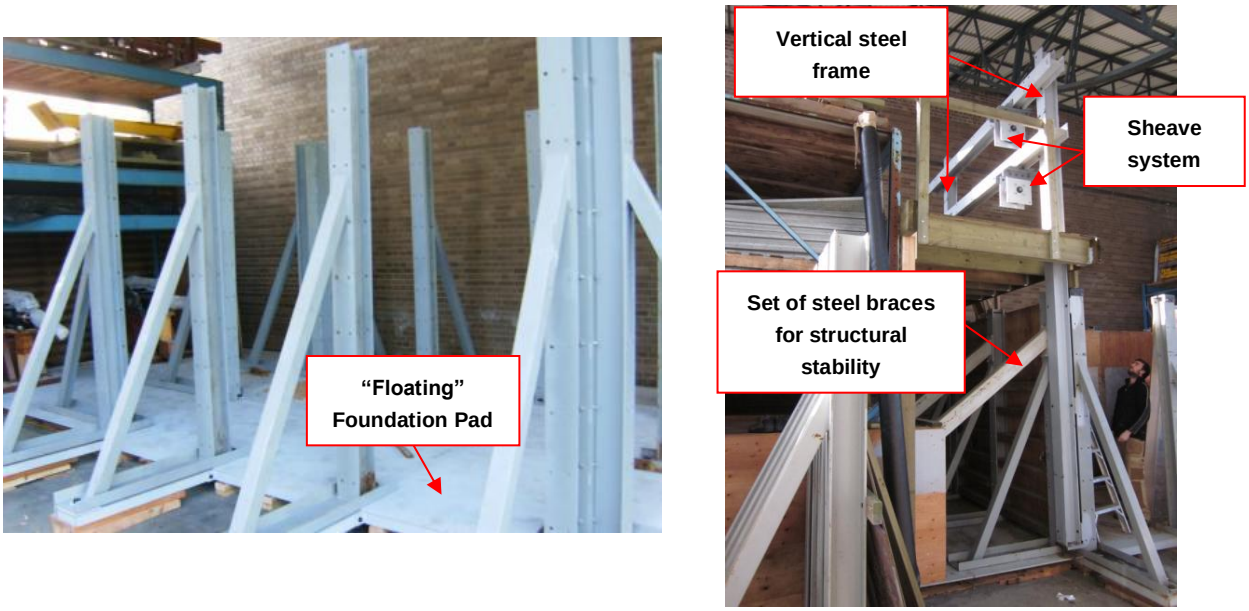

Figure 3.3: Construction and structural system of the soil-pipe interaction testing chamber.

3.2 Loading System

The pipe specimens were displaced by a system of pulling cables connected to hydraulic actuators. The pipe specimens were loaded in a displacement-controlled manner at a rate of 2.5 mm/s. The available displacement rate was controlled by the capacity of the hydraulic pumps and operating limitations of actuators. Prior test results have confirmed that displacement rates less than 50 mm/s applied in a direction perpendicular to the pipe and along the pipe axis, respectively, have no noticeable effect on the results (Karimian 2006).

The loading system consisted of two double-acting hydraulic actuators with a digital hydraulic control system. Actuator displacement was monitored by an externally mounted Temposonic SSI probe with a resolution of 2 microns. Both actuators were trunnion-mounted to a loading pedestal attached to the rigid steel floor pad system which supports the soil-pipe interaction testing chamber. The actuators were positioned in the loading pedestal in a way that they imposed displacement in the horizontal direction; however, they were free to move in a vertical plane, if required.

The capacity of the actuators was 418 kN (93 kips) at 21 MPa (3000 psi) working pressure and a pressure drop of 5.6 MPa (800 psi) through the control valve. The hydraulic actuators, manufactured by Royal Cylinders Inc., had a 200-mm (8-in) bore diameter, with a full stroke of ±305 mm (±12 in) and a 90-mm (3.5-in) rod diameter.

The control system for the hydraulic actuator system consisted of the following components:

- Delta RMC controller, model RMC100-S2-ENET, with SSI interface to the probe and analog command output to the valves, manufactured by Delta Computer Systems Inc., Vancouver, WA, USA;

- Ethernet communication link to PC for data acquisition;
- Analog input card for reading of pressure transducer for pressure control;
- SSI feedback probe, Temposonic RP with captive sliding magnet;
- Servo proportional valve, 10 GMP, for speeds up to 25 mm/s; and
- Servo life filters manufactured by PQ Systems ltd;

RMCWin software by Delta Computer Systems Inc., Vancouver, WA, USA, was employed to interface with the RMC controller. The SSI probe has the ability to check the position of each cylinder so that actual and target positions are being compared continuously. The controller sends command signals to the servo valve to adjust the valve opening, and consequently the actual position of the loading ram to match the target. The controller can provide synchronized or proportional movements of up to four control axes. The movement of one of the actuators was geared to the 2nd axis to provide uniform and steady loading at each end of the pipe during the tests. A layout of the control system is schematically shown in **Figure 3.4**.

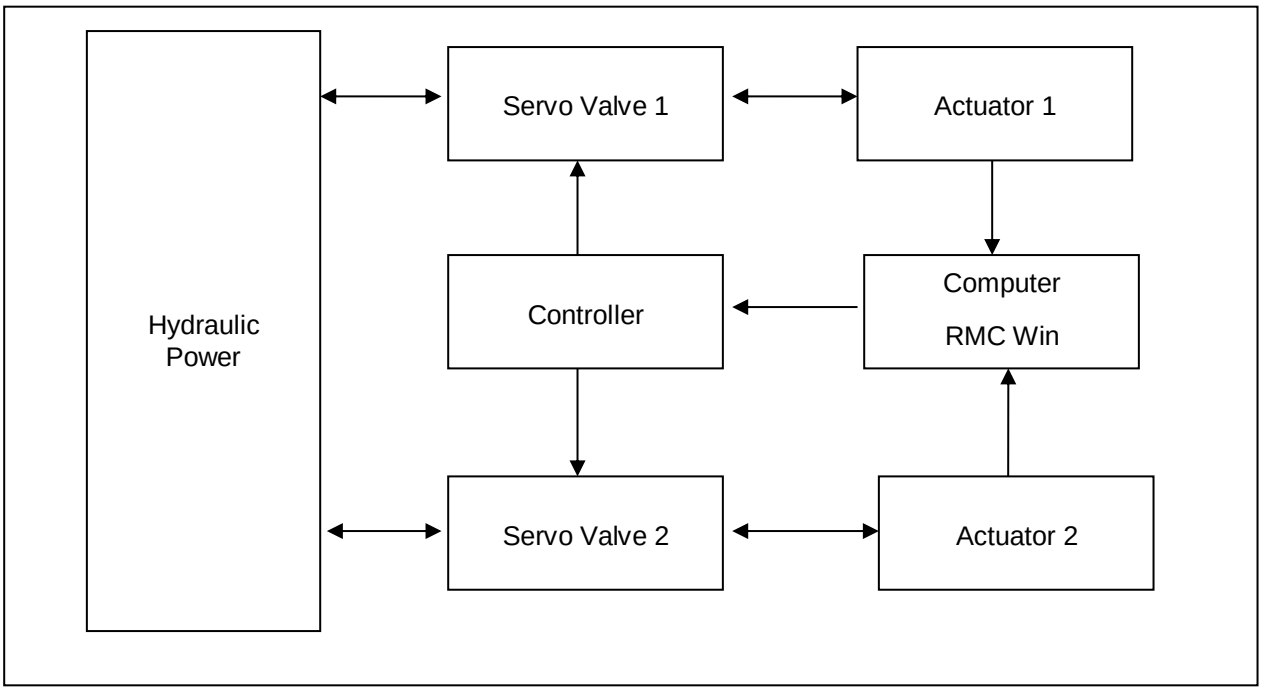

Figure 3.4: Control system layout.

The volume of the hydraulic fluid pumped into the actuator could also be controlled manually using a knob on the control box. This manual control allowed movement of the actuator during initial positioning as well as loading. A stop-button on the control box was available for emergency shutdown, if needed.

The study of soil restraints in this thesis required the application of displacement vectors to buried pipe specimens not only in the horizontal direction but also in directions that lie on the XZ plane (see **Figure 3.2**). This was achieved by attaching each end of the hydraulic actuators by means of 28.6 mm (1 1/8”) steel cables to connectors at the end of the pipe specimens. Whenever needed, the steel cables were passed through a system of sheaves which were hanging from a vertical steel frame (see **Figure 3.2 and Figure 3.3**) in order to guide the pipe displacement in a desired direction from a horizontal plane. For example, displacement in the X-direction can be applied to pipe specimens by simply connecting the ends of both hydraulic actuators

to the pipe connectors (without the sheave system) as shown in **Figure 3.5** and **Figure 3.6**. This type of loading mechanism was used to investigate the development of lateral and coupled lateral-axial or horizontal oblique soil restraints that occur during pipe-soil interaction of segments of pipelines crossing strike-slip faults.

A plan and lateral view layout of the testing chamber used to mimic reverse-fault displacement type and therefore to study vertical oblique soil restraint is depicted in **Figure 3.7** and **Figure 3.8**, respectively. These figures show the connections made through the sheave system with the aim of applying displacements to a buried pipe specimen with a predefined orientation with respect to the horizontal. In particular, 35° and 45° displacement angles were applied to pipe a specimen. Also, a similar connection can be made through the sheave system to apply displacements in the vertical direction.

The general components of the testing chamber, loading mechanism, and data acquisition equipment used in this endeavor to study soil restraints are described in **Table 3.1**. The location of each piece of equipment, identified by the corresponding number next to the equipment description in **Table 3.1**, can be observed in **Figure 3.5** to **Figure 3.8**. Connection characteristics, backfill and geotextile materials and particular details about the overall testing configurations will be covered in the following sections.

Table 3.1: Identification of Testing Chamber Test Equipment

No.	Description	No.	Description
1	Soil chamber	14	Turn-buckle
2	Plexiglas panel	15	Load cell for oblique soil restraint & inclinometer
3	Pipe specimen	16	Sheave system for oblique pulling
4	Load cell for lateral soil restraint	17	Vertical steel frame system
5	Load cell for axial soil restraint	18	Steel brace for lateral stiffness
6	1 1/8” Steel cable	19	Data acquisition system & computer
7	String Potentiometer	20	Control system
8	Hydraulic actuator system	21	Steel foundation pad
9	LVDT	22	Hydraulic system pedestal
10	Servo controller	23	Sheave system for vertical pulling
11	To hydraulic power	24	Crane
12	Steel cable to pipe connector	25	Trench wall
13	Reaction steel plate	26	Collar steel beam

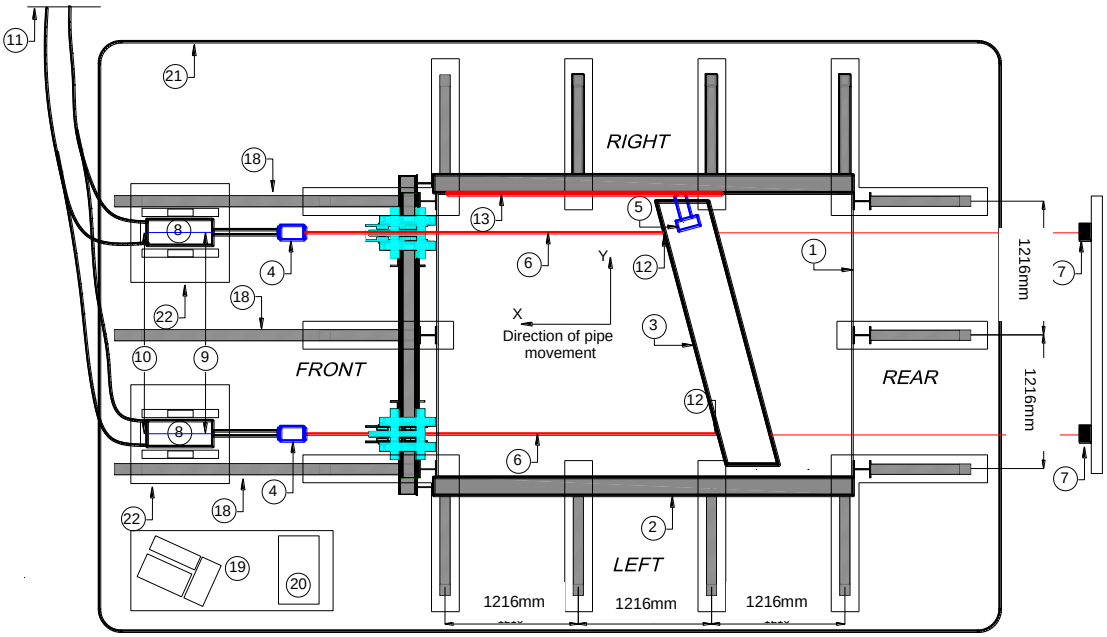

Figure 3.5: Testing chamber to study horizontal oblique soil restraints – XY plan view layout (Displacement vector in X-direction)

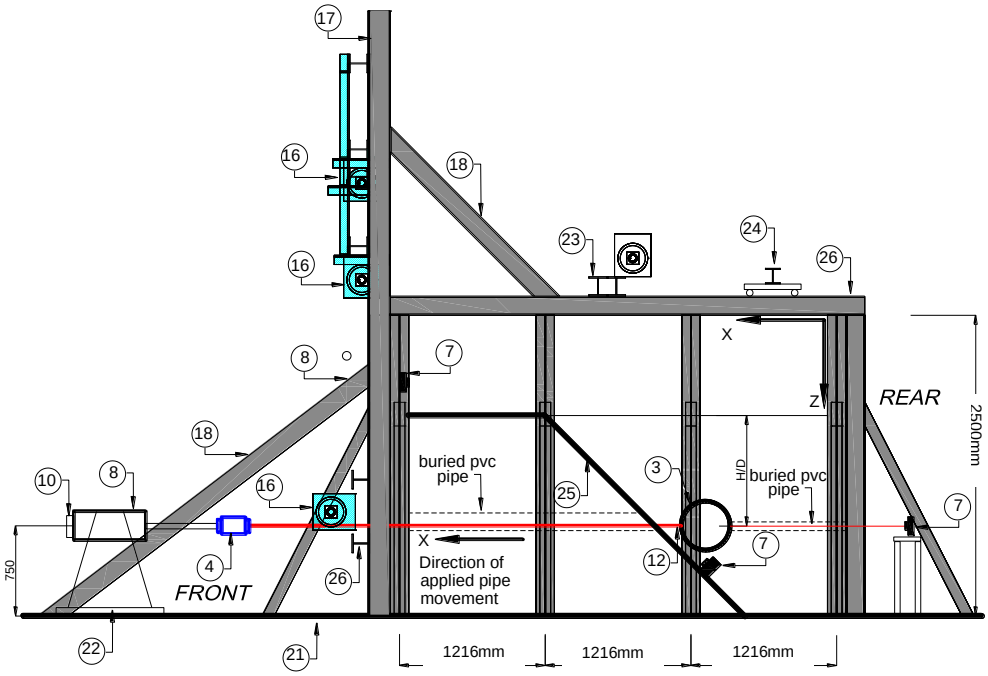

Figure 3.6: Testing chamber to study horizontal oblique soil restraints – XZ lateral view layout (Displacement vector in X-direction)

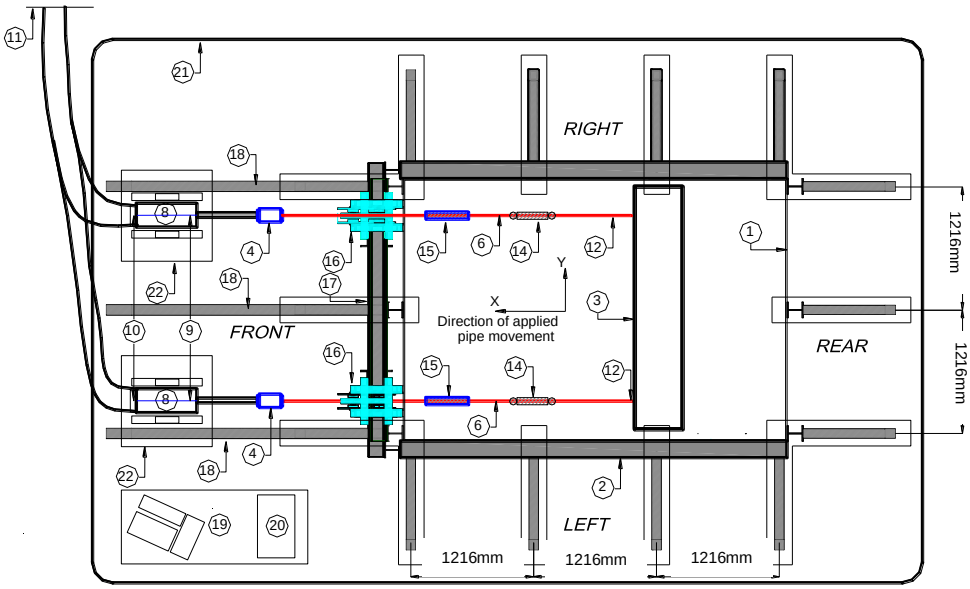

Figure 3.7: Testing chamber to study vertical oblique soil restraints – XY plan view layout (Displacement vector in XZ plane).

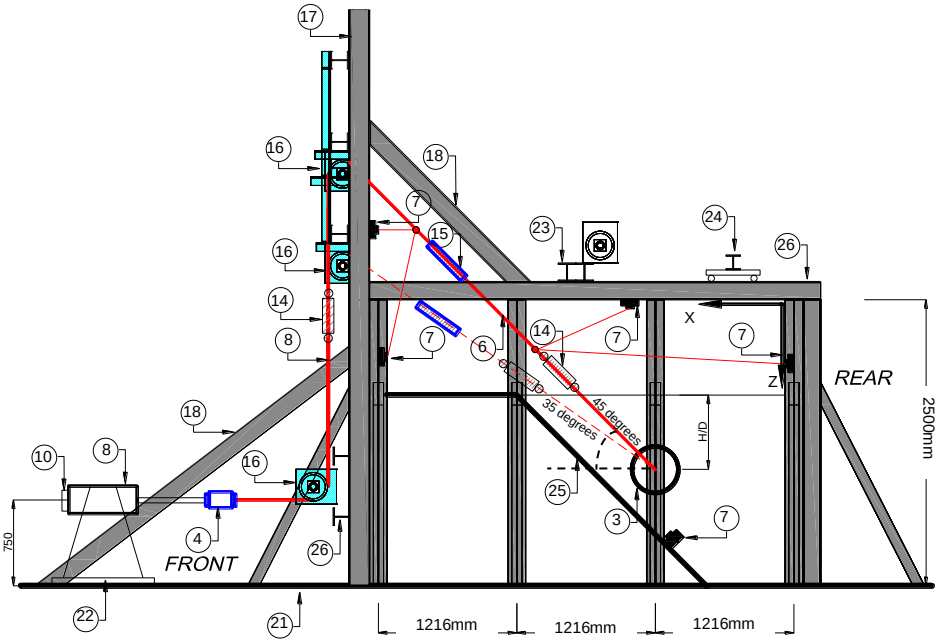

Figure 3.8: Testing chamber to study vertical oblique soil restraints – XZ lateral view layout (Displacement vector in XZ plane).

3.3 Description of Materials

Three locally-available materials were employed for the testing program as backfill soils:

i) Fraser River sand;

ii) Crushed mixture of sand and gravel (road mulch); and

iii) Crushed limestone.

Details of their characteristics in terms of appropriate soil parameters are described in this section. The selection of backfill materials for the pipe-soil restraint testing of this study was made on the basis of using closely equivalent backfill materials found in current practice and that are available in Vancouver.

3.3.1 Backfill Materials

3.3.1.1 Fraser River Sand

Dredged sand from the Fraser River supplied by AT&H industries, Maple Ridge, B.C. was used as one of the backfill soils for the research program. Approximately 20 m^3 of sand material deposited in several 0.9 m^3 bulk-storage bags were transported and stored in an area immediately outside the research chamber. Fraser River sand has been extensively studied at UBC over the past 20 years. Therefore, in this study, no attempt was made to characterize this material.

As described by Karimian (2006), Fraser River sand can be characterized as a fine to medium sand with sand grains that are generally angular to sub-rounded in shape. The composition of Fraser River sand is 40% quartzite and

chert, 11% feldspar, 45% unaltered rock fragments, and 4% other minerals (Garrison et al. 1969). Previous tests of Fraser River sand indicate an average particle size, D_{50}, of 0.23 mm, a minimum particle size of 0.074 mm, a coefficient of uniformity, C_u, of 1.5, and a specific gravity, G_s, of 2.70. The minimum and maximum void ratios, determined in accordance with American Society for Testing and Materials Standards ASTM-4254 and ASTM-4253, are reported to be 0.62 and 0.93, respectively (Anderson 2004).

Karimian (2006) performed a grain size distribution for the Fraser River sand at the start and end of his test program. The work undertaken by Karimian (2006) suggests that repeated moving and compaction of the sand does not significantly alter the grain size distribution of the sand (see **Figure 3.9**).

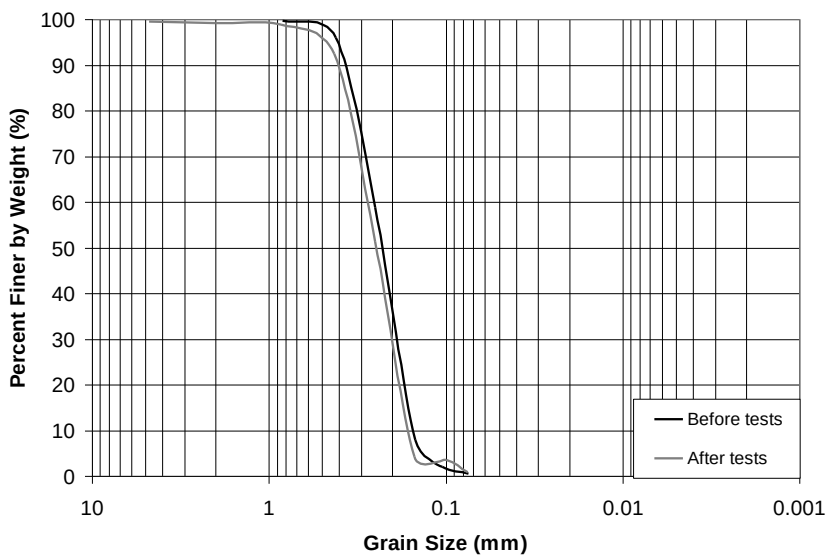

Figure 3.9: Fraser River sand grain size distribution before and after testing in the soil pipe interaction chamber (after Karimian 2006).

Based upon numerical modeling of horizontal tests in sand and contact pressure measurements made by Karimian (2006), the mean stress imparted on the soil from lateral pipe movements during testing, for the H/D ratios covered in his test program, does not exceed 100 kPa.

Because the prediction of maximum soil restraint values on buried pipelines is highly dependent upon the peak effective friction angle (ϕ'_p), Karimian (2006) performed several conventional direct shear (DS) and triaxial (TX) tests on Fraser River sand (FRS) specimens in an effort to characterize ϕ'_p and therefore to interpret the results from his large-scale experimental tests.

For the DS tests, Karimian (2006) compacted the FRS to a dry unit weight of 15.75 kN/m^3 (relative density D_r=68%) and the tests were conducted with effective normal stress from 20 kPa to 100 kPa. The lower value of effective normal stress corresponds to the normal stress at a pipe burial depth of 1.3 m. The measured peak and large-strain shear stress versus normal stress values from the DS tests performed by Karimian (2006) are shown in **Figure 3.10**. The ϕ'_p of Fraser River sand varied between 44° and 41° (average of 42°). The average friction angle at large strain was 36°. In addition, constant volume internal friction angles (ϕ_{cv}) reported for Fraser River sand in the literature range from 32° to 34° (Uthayakumar 1996; Sivathayalan 2000).

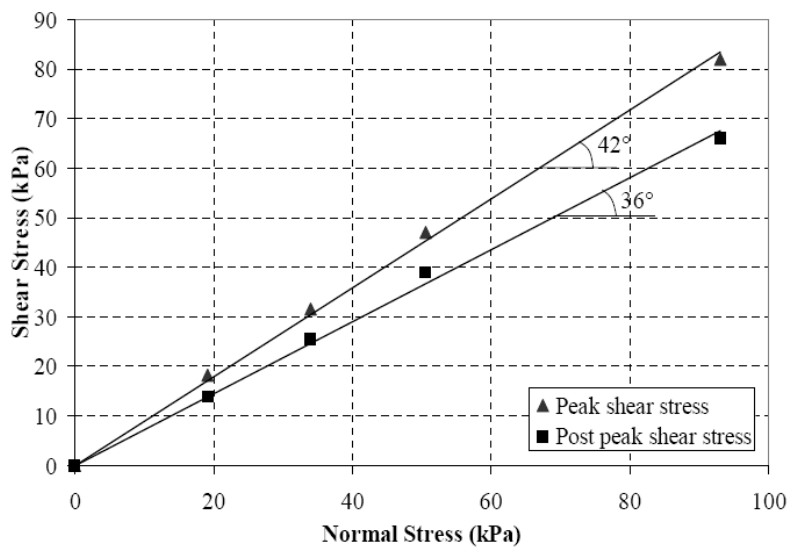

Figure 3.10: Results of direct shear testing on Fraser River sand (after Karimian 2006).

Likewise, Karimian (2006) carried out eight (8) TX tests on FRS to characterize peak friction angles and parameters for developing stress-strain relationships to feed numerical simulations of lateral and axial soil restraints. Soil response was evaluated at dry densities of 1,575 kg/m^3 and 1,665 kg/m^3 with effective confining stress levels of 15 kPa, 25 kPa, 35 kPa and 50 kPa. This range of confining stress corresponded to those recorded during his large-scale testing program.

Peak effective friction angles computed from TX testing by Karimian (2006) are shown in **Figure 3-11**. The peak friction angle varied with both density level and effective confining stress. The ϕ'_p of Fraser River sand ranged from 42° to 46°. In addition, it dropped by about 2° to 3° when the confining stress increased from 15 kPa to 50 kPa. By assuming a linear variation of ϕ'_p with density level, Karimian (2006) approximated a curve that relates ϕ'_p and confining stress for FRS with a dry density of 1600 kg/m^3 (D_r = 75%). This study uses this same density for the backfill material in the testing program.

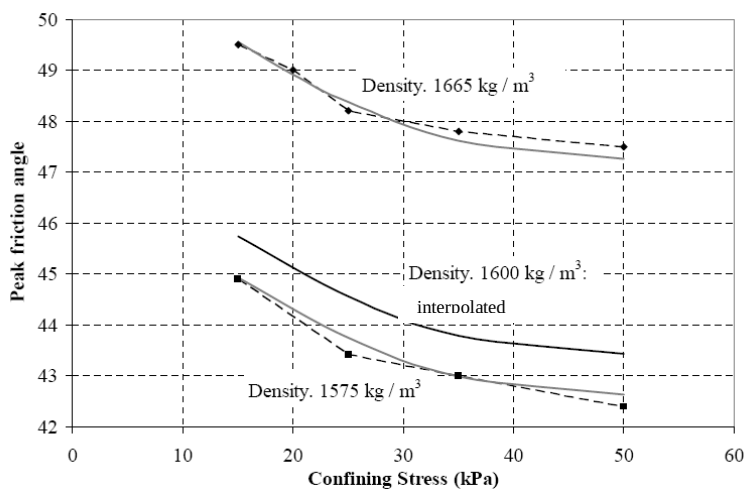

Figure 3.11: Peak friction angle for Fraser River sand from triaxial test results (after Karimian 2006).

Karimian (2006) also estimated initial elastic modulus (E_i) from the results of triaxial tests used to determine friction angles. He followed the approach proposed by Duncan et al. (1980) for obtaining these moduli. The calculated initial elastic moduli for different tests are shown in **Figure 3-12** together with the curve-fitted power law equations to calculate initial elastic modulus as a function of confining stress.

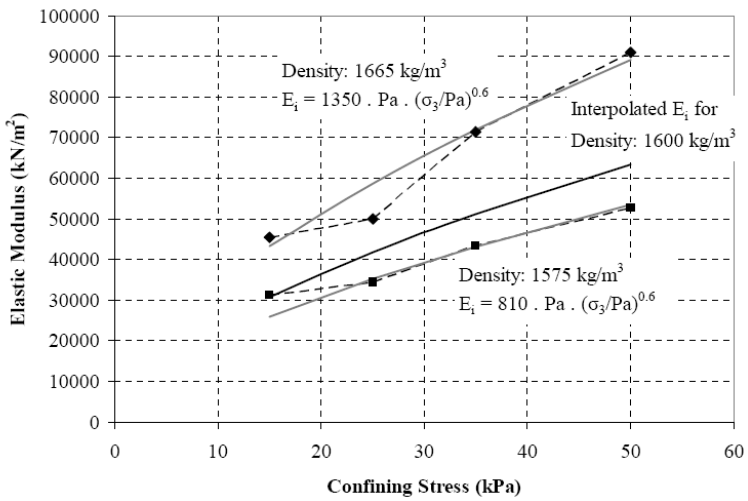

Figure 3.12: Initial elastic modulus for Fraser River sand from triaxial test results (after Karimian 2006).

3.3.1.2 Crushed sand and gravel (Road Mulch)

A mixture of crushed sand and gravel (road mulch) was obtained from AT&H industries, Maple Ridge, B.C. 15 m^3 of road mulch deposited in several 0.9 m^3 bulk-storage bags were transported to and stored in an area immediately outside the research chamber. This material is usually used in Vancouver as base course material underneath shallow foundations and road construction. Therefore, the material was selected as suitable to simulate stiff to hard overconsolidated native soil conditions.

A photographic image of the crushed sand and gravel material supplied by AT&H is presented in **Figure 3.13**. A grain size distribution for this material is shown in **Figure 3.14**. The data from this figure indicate an average particle size, D_{50}, of 1.7 mm, a minimum particle size of 0.074 mm, a coefficient of uniformity, C_u, of 40 and a coefficient of curvature, C_c of 0.86.

Figure 3.13: A photograph of the crushed sand and gravel material supplied by AT&H.

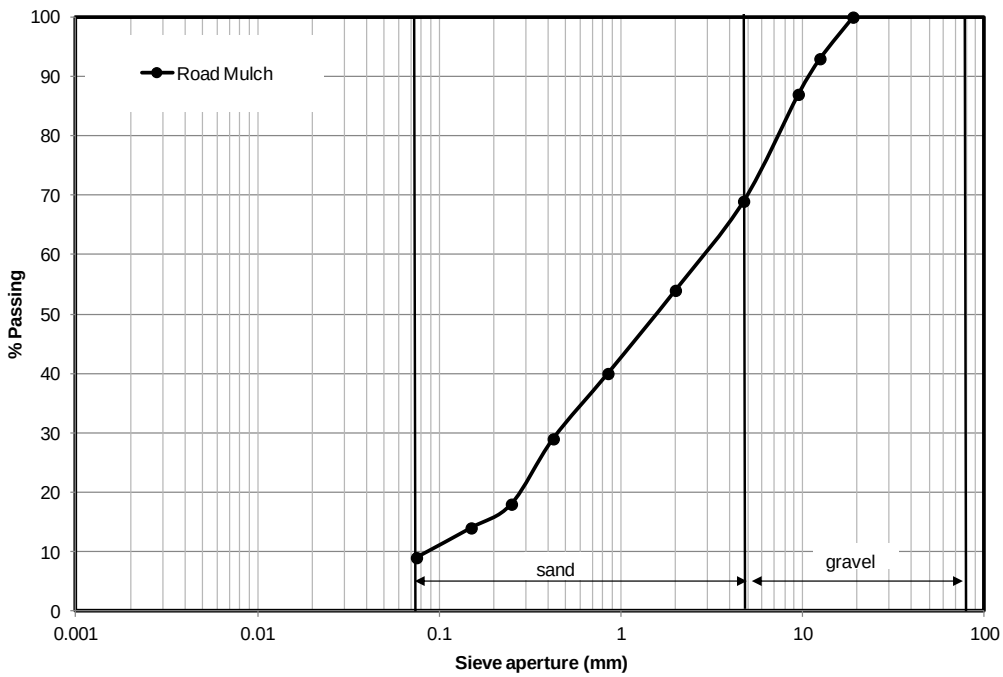

Figure 3.14: Grain size distribution for crushed sand and gravel (road mulch).

Due to the size of the gravel particles in the road mulch material, it was decided to conduct a series of direct shear tests using the 300 mm x 300 mm shear box equipment at the Geotechnical Laboratory of Golder Associates under the close supervision of the author. Three tests subjected to normal stresses of 20, 40, and 70 kPa were carried out with a dry unit weight of about 18 kN/m^3.The results show an internal friction angle ranging between 59º (at ~20 kPa stress level) and an average of 49º (at ~40 to 70 kPa stress level). Details of the results are shown in **Appendix A**.

3.3.1.3 Crushed Limestone

Crushed Limestone was obtained from Lafarge Aggregates and Concrete, Vancouver, BC. 15 m^3 of crushed limestone deposited in several 0.9 m^3 bulk-storage bags were transported to and stored in an area immediately outside the research chamber. This material was selected because of its considered

use as a backfill material with respect to real-life projects in places where sand is not readily available.

A photographic image of the processed crushed limestone material supplied by Lafarge is presented in **Figure 3.15**. The grain size distribution analysis is shown in **Figure 3.16**.

Figure 3.15: A photographic image of the crushed limestone material supplied by Lafarge.

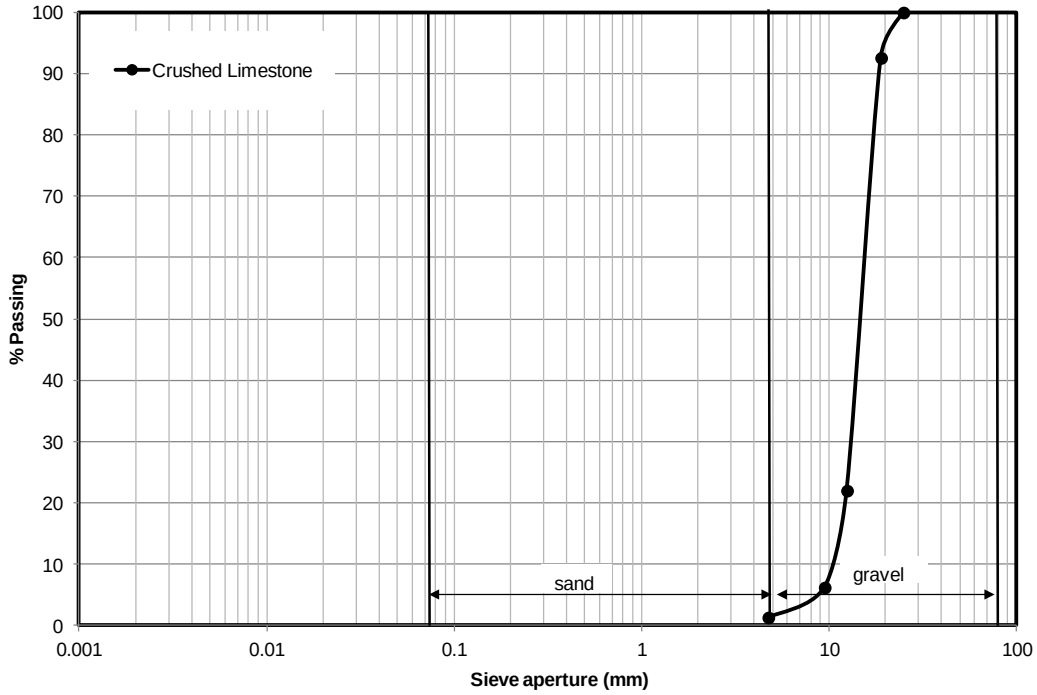

Figure 3.16: Grain size distribution for crushed limestone backfill material.

As in the case for the road mulch material, a series of direct shear tests using the 300 mm x 300 mm shear box equipment at the geotechnical laboratory of Golder Associates, Vancouver, BC, were conducted on specimens that were initially subjected to approximate normal stresses of 20, 40, and 70 kPa with dry density values prior to shear (after applying vertical stress on the specimen) in the order of 1700 kg/m^3. The results are presented in Appendix A and indicated that the crushed limestone material has a peak internal friction angle ranging between 68º (at ~20 kPa stress level) and 58º (at ~70 kPa stress level).

3.3.2 Pipe specimens

Both NPS18 and NPS16 were used in the testing program of this study. Each test pipe was procured from North American Pipe & Steel (Napsteel), Surrey, BC. The list of test pipe sizes and their dimensions are given in **Table 3.2.**

Table 3.2: Test Pipe Sizes Used in the Test Program

Nominal Pipe Size (NPS)	Yield Strength (MPa)	Outer Diameter inch (mm)	Wall Thickness inch (mm)	Weight (kN/m)
NPS18	320	18 (457)	0.5 (12.7)	1.44
NPS16	320	16 (406)	0.5 (12.7)	1.28

A photograph of the NPS16 steel pipe is shown in **Figure 3.17**. As may be noted from this figure, one end the test pipe was equipped with two "marker-pen holders" located circumferentially so that the displacement path of the test pipe would be marked on the transparent Plexiglas screen of the testing chamber. This in turn will provide means of obtaining a visual observation of the movement of the test pipe in a given test.

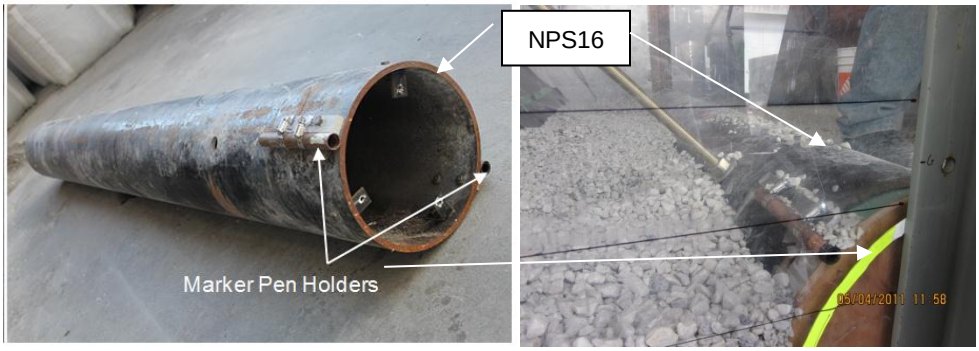

Figure 3.17: Photograph showing the NPS16 test pipe used in pipe soil restraint testing.

Only the surface of the pipes used for the study of horizontal oblique soil restraints was prepared by sand blasting (using coarse sand). This is because only the horizontal oblique tests have an axial component of movement; and therefore, it was possible to use the steel/sand interface measured by Karimian (2006) for his pipe axial movement tests for the interpretations in this study. The diameter of "pits" due to sand blasting on the pipe surface had a maximum size of approximately 0.8 mm (0.030 in) and an average size of approximately 0.4 mm (0.015 in).

Karimian (2006) noted that the average peak interface friction angle for the sand-blasted steel and sand interface as 36° and 33° for the cases of dense sand and loose sand, respectively, and for a normal stress between 20 to 40 kPa. The average interface friction angle at large strains was determined to be 30.5°, for both dense and loose sand. Based upon these tests, the interface friction factor is about 0.85 at both peak and large strains.

3.3.3 Geotextile and Soil-Geotextile Interface Materials

TC Mirafi Filterweave 700 woven geotextile, manufactured by Mirafi Construction Products, Georgia, USA, was used as the geosynthetic fabric material in the tests where geosynthetic lined trenches were simulated. As described by the manufacturer, the material is composed of high-tenacity monofilament polypropylene yarns, which are woven into a stable network such that the yarns retain their relative position. The wide-width tensile strength is 26 kN/m to 40 kN/m and the apparent opening size and percentage of open area are 0.212 mm and 4% to 6% respectively (http://www.tencate.com/TenCate/Geosynthetics/documents/FW%20Series/TDS_FW700.pdf last accessed 11-10-11).

3.3.3.1 Geotextile-Geotextile Interface Friction

For the evaluation of interface friction characteristics between two layers of TC Mirafi Filterweave 700 woven geotextile fabric, Karimian (2006) used the 100 mm x 100 mm direct shear box available at the Department of Civil Engineering at UBC. In this work, two blocks of wood were fitted into the bottom and top halves of the direct shear box. The two wooden blocks were lined with the geotextile fabric with a very thin layer thickness of Fraser River sand introduced between the wooden blocks and geosynthetic fabric; the introduction of this thin sand layer simulated a case of field interface conditions of a double-geotextile fabric interface sandwiched in a sand mass. Five geotextile/geotextile interface tests were performed using this set up under normal effective stress conditions between 10 kPa to 20 kPa. The average peak and large-strain interface friction angles were determined to be 20.8° and 19.8° respectively. Karimian (2006) mentioned that his results were in line with those reported by the manufacturer (Texas Research International Company) for the range of normal stress between 27 kPa and 40 kPa (21.1° for the peak and 19.7° for residual interface friction angle).

3.3.3.2 Fraser River Sand-Geotextile Interface Friction

The interface behavior of Fraser River sand and TC Mirafi 700 geotextile fabric was also assessed using the UBC 100 mm x 100 mm direct shear box. A piece of geosynthetic fabric was glued to the top portion of a steel plate machined to fit in the bottom half of the direct shear box. This geotextile-lined steel plate was mounted so that its top surface was flush with the top level of the bottom half of the direct shear box. The upper part of the direct shear box was filled with Fraser River sand in layers of about 5 to 10 mm in thickness. Then each layer was compacted using a square-shaped wooden tamper essentially covering the footprint of the specimen and vibrated using a small vibrator. An average density of 1600 kg/m^3 (D_r = 75%) was used in the tests. Five tests were performed at a normal stress between 20 kPa to 100 kPa.

The average peak and large-strain interface friction angles were determined to be 32±1° and 30±1°, respectively. These values are in the range of data reported in the literature (Lee and Manjunath 2000; Anubhav and Basudhar 2010). Details of the results are shown in **Appendix B**.

3.3.3.3 Road Mulch-Geotextile Interface Friction

The interface behavior of road mulch material and TC Mirafi 700 geosynthetic fabric was assessed using the same equipment and procedure as the one for Fraser River sand and TC Mirafi 700 geosynthetic fabric. Five tests were performed at a normal stress between 20 kPa to 100 kPa with an initial road mulch density of 18 kN/m^3. The average peak and large-strain interface friction angles were determined to be 31±1° and 29±1°, respectively. Details of the results are shown in Appendix B.

3.3.3.4 Summary of Interface behavior

The interface friction angles between the geosythetics and different granular soils (or other material) from the tests above are compared with the internal friction angle of Fraser River sand alone in **Table 3.3**.

Table 3.3: Summary of Friction Angles from Laboratory Direct Shear Testing

Slippage Surface	Dry Density (kN/m^3)	Peak (ϕ'_p)	Large Strain
Sand[1]	16	43°	36°
Road Mulch	18	49°	49°
Limestone	17	54°	54°
Sand-Sand Blasted Steel[1]	16	36°	31°
Geotextile- Geotextile[1]	-	21°	20°
Sand – Geotextile	16	32°±1°	30°±1°
Road Mulch-Geotextile	18	31°±1°	29°±1°

Note: [1] Data from Karimian (2006)

3.4 Experimental Procedures

3.4.1 Backfill Placement and Density Control

The backfill materials were stored in bulk-storage bags, each of which contained approximately 0.9 m^3 of soil, that were moved using a forklift. Backfilling of the chamber was carried out as follows: (i) filling a tipping bucket with the soil material; (ii) lifting the tipping bucket with soil using a forklift to a level above the top edge of the chamber; and (iii) releasing the material into the testing chamber and leveling using a shovel and a rake. In releasing the material into the testing chamber, the material was dropped from an average free-fall height of about 1.5 m; this drop height was selected to meet safety concerns, minimize the generation of dust, and achieve a relatively uniform as-placed density across the soil box. After approximately two batches of material were released into the chamber and levelled (yielding ~200 mm to 300 mm lifts), it was compacted manually by using a number of passes of a hand-pushed static drum-roller. The static drum-roller has dimensions of 61 cm in length and 46 cm in diameter, and has a weight of approximately 100 kg.

Compaction of soil in the vicinity of the pipe was difficult due to accessibility constraints. In these zones, a hand-held plate tamper weighing ~ 13 kg and having dimensions of 25 cm x 21 cm x 2.54 cm (1" plate) was used. In this process, the tamper was raised about 15 cm and allowed to freely fall on the soil that is in the vicinity of the pipe. The number of repetitions of tamping used varied depending on the backfill material. Limestone and road mulch were tamped 15 times and sand 30 times. Some photographs taken during backfill placement and compaction are presented in **Figures 3.18** and **3.19**.

Figure 3.18: Use of the forklift to lift batches of backfill material.

Figure 3.19: Density measurement of backfill (left), and use of a static roller for backfill compaction (right).

The mass density of the sand and road mulch was measured at random locations during the filling process using a nuclear densometer. The mass

density of the crushed limestone was not measured using the nuclear densometer due to significant scatter; alternatively, the density of the as-compacted backfill was calculated from mass-volume measurements that were taken with the aid of aluminum containers of known volume placed within the fill prior to compaction and retrieved carefully after compaction. The aluminum containers were also used to verify the density given by the nuclear densometer when both sand and and road mulch backfill were used.

In order to make visual observations of the deformation pattern of the fill during the tests, a series of parallel strip-zones of soil having a contrasting color were introduced into the backfill immediately adjacent to the Plexiglas wall every 0.10 m. The soil in the strip zones essentially comprised road mulch or white coloured fine sand. **Figure 3.20** presents a typical completed test specimen prior to testing with the soil strip-zones clearly visible through the Plexiglas window. The Plexiglas remained smooth throughout the test program. This was verified by visual inspection. No roughness measurements were carried out.

Figure 3.20: Soil-pipe interaction test specimen prior to testing.

Upon completion of a given test, the material was removed through an access-hole provided near the base of the modified soil-pipe interaction testing chamber, on the rear sidewall. The access-hole measured approximately 450 mm by 300 mm, and was covered by a plywood panel during the tests. The materials were transferred from the access holes back into the bulk-storage bags using a conveyor belt mechanism to be reused for subsequent tests.

3.4.2 Pipe Specimen Placement and Coupling System

The pipe specimen for a given test was carefully placed in the chamber using a forklift. Then, the pipe was carefully positioned at the specified location and elevation using a set of steel chains, a small crane system, which was specially built for this purpose and a 2-ton "come along" tool. **Figure 3.21** illustrates this procedure.

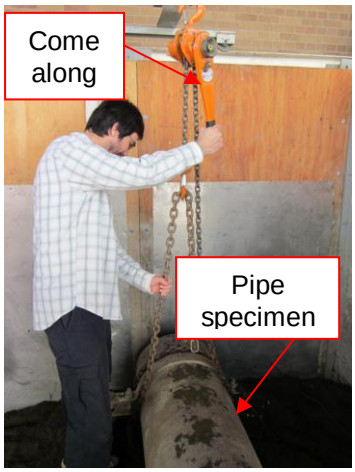

Figure 3.21: Pipe specimen placement procedure.

Coupling of the pull cables to the test pipe was initially carried out using a shackle arrangement as shown in **Figure 3.22.a**. During the initial part of the testing program, it was felt that the failure mechanism observable through the

Plexiglas sidewall may have been distorted by the soil moved by the clamps and not depicting the likely mechanism of soil failure (i.e., introducing an end-effect not representing the real soil movement by the pipe). In consideration of this, the shackle arrangement was replaced by a set of two diametric steel rods passing through each test pipe as shown in **Figure 3.22.b** as connectors to the cables that were used for displacement transfer to the test pipe. However, it was found that the shackle arrangement produced no noticeable distortion or effect to the tests.

For horizontal tests, each pull cable was passed through vertical slots located in the front wall of the box. The vertical slots were provided to permit vertical movement of the cables in the event of vertical pipe uplift during the tests. Cell foams were used to seal the vertical slots. The cables extending out of the box were attached to load cells using shackles, which in turn where attached to the actuators (see **Figure 3.23**). The cable system provided a loose connection during test preparation and prevented damage in the event of unexpected movement of the actuator.

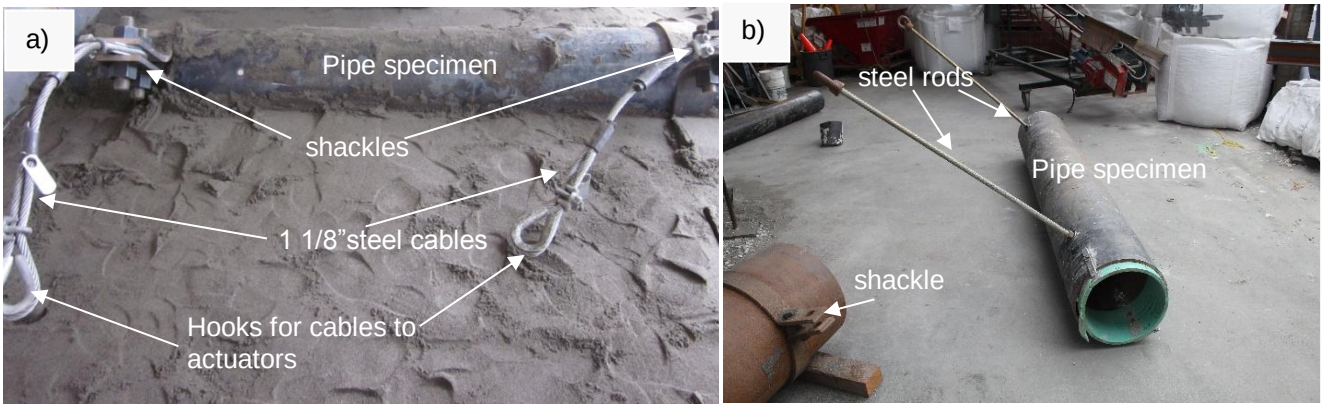

Figure 3.22: Coupling system for soil restraint testing – a) pipe-cable connection system; b) pipe-rod connection system.

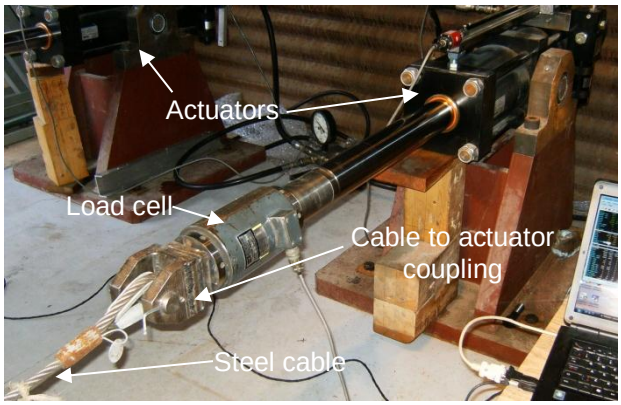

Figure 3.23: Coupling system for soil restraint testing – cable to actuator connection system.

For vertical oblique restraint tests, the cable originating from each actuator passed through the corresponding bottom level sheave and then was attached through a turnbuckle-shackle arrangement as shown schematically in **Figure 3.8** to a pulling cable which passed through the respective top level sheaves and on to the test pipe. Connection of the pulling cables to the pipe-rod connection system was carried out once the filling was complete.

3.4.3 Trench with Sloping Surface ("Trench Wall")

A full-scale trench with a trapezoidal cross-section had to be carefully constructed inside the soil chamber for some of the tests. In particular, for the study of horizontal and vertical oblique soil restraints under trench conditions, trenches with side slope angles ("trench wall" slope angles) of 35° and 45° to the horizontal were constructed. These trench side-wall slope angles were selected because they simulate the trench wall angles typically used in current practice. The trench wall slope angle of 45° was considered to represent a limiting value for measurable benefit. Side-wall slope angles less than 35° were not considered based upon what was believed practical limit on the size of the trench in practice.

The trench wall material was selected so that it would simulate a trench wall with stiff native soil boundary conditions or hard trench soil conditions. The pulling cables used for the pipes had to penetrate through the trench wall during horizontal lateral restraint tests; as such, free passage for the pulling cables was facilitated by installing them through PVC pipes appropriately placed in the trench wall. This allowed the pulling cables to move freely inside the PVC pipes in the horizontal and vertical directions.

The approached used herein for the trench construction allowed re-use of the rigid and stiff trench walls for multiple tests - only the backfill material and pipes needed to be replaced while the built trench remained unchanged between tests. A photograph of a typical trench wall constructed to simulate the stiff native soil boundary condition is shown in **Figure 3.24**. As indicated in Section 3.3.1.2, well compacted 19-mm minus well-graded crushed sand and gravel (road mulch) was used to represent a trench wall encountered in stiff native soil conditions. The construction work was undertaken with specific care and effort to maintain a well-defined slope angle for the trench surface.

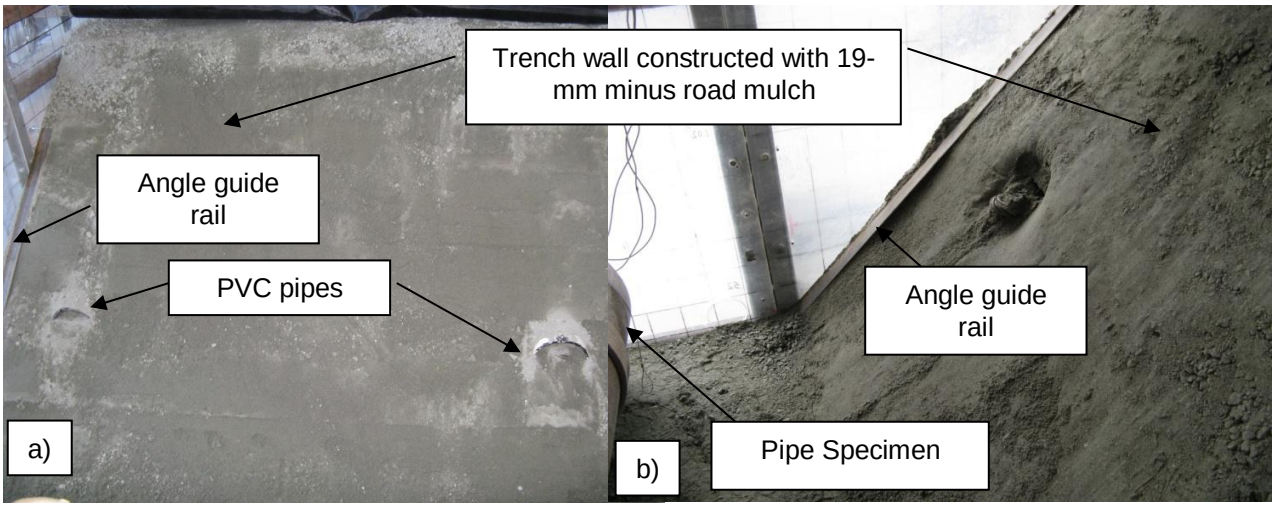

Figure 3.24: Trench wall built in native soil (road mulch) – a) view from rear to front b) view from right to left

For the tests requiring the simulation of a hard boundary condition, the trench wall was constructed as follows:

- Six lengths of 50 mm x 300 mm (2 inch x 12 inch) rough Douglas Fir timber boards were spanned across angle guide rails set at appropriate inclination angles;
- The timber boards spanning the angle guide rails were braced against the front wall of the test chamber using sixteen, evenly spaced, 100 mm x 200 mm (4 inch x 8 inch) timber boards.
- The space between the timber board bracing and the front wall was backfilled with sand or road mulch and compacted.
- A layer of Fraser River sand was glued to the surface of the timber boards spanning the angle guide rails to simulate the roughness of an excavated soil trench wall.

A photograph of a typical trench wall constructed to simulate the hard soil boundary condition is shown in **Figure 3.25.**

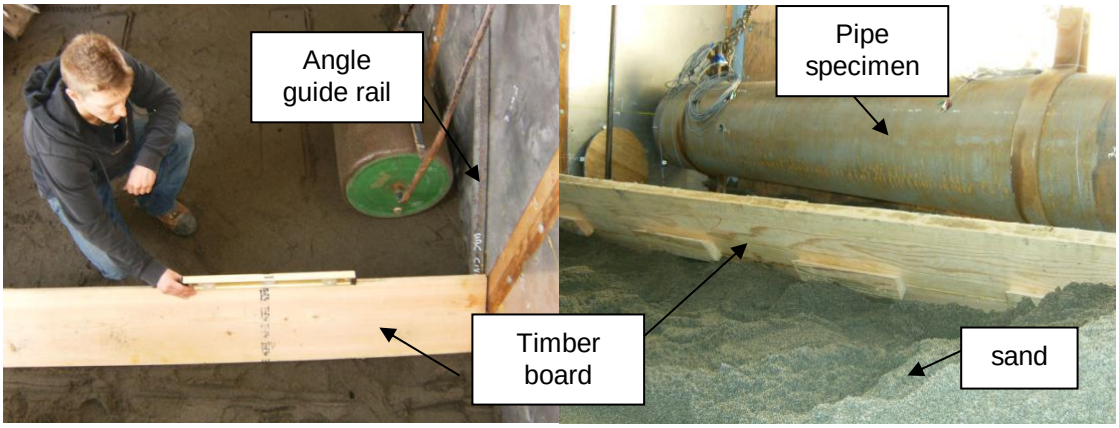

Figure 3.25: Trench wall constructed to simulate hard boundary conditions.

3.4.4 Trench Wall Lining Configurations

In tests with the trapezoidal trench, the trench wall was lined with selected different geotextile interface configurations, to study the effectiveness of such configurations in reducing levels of soil restraint. For the study of lateral soil restraints under geotextile-lined pipeline trenches subjected to relative horizontal fault displacements, a dual layer of TC Mirafi Filterweave 700, woven geotextile was used as a lining material. The dual layer of geotextile spanned the length of the trench wall. Only the overlying geotextile layer (i.e., the geotextile in contact with backfill material) was allowed to move, therefore, it extended across the slope of the trench wall from the top of the trench wall to a depth that coincided with the bottom of the pipe specimen. The underlying geotextile layer (i.e. geotextile in contact with the native material) was anchored 20 cm below the pipe bottom. A schematic of the lining arrangement is shown in **Figure 3.26**.

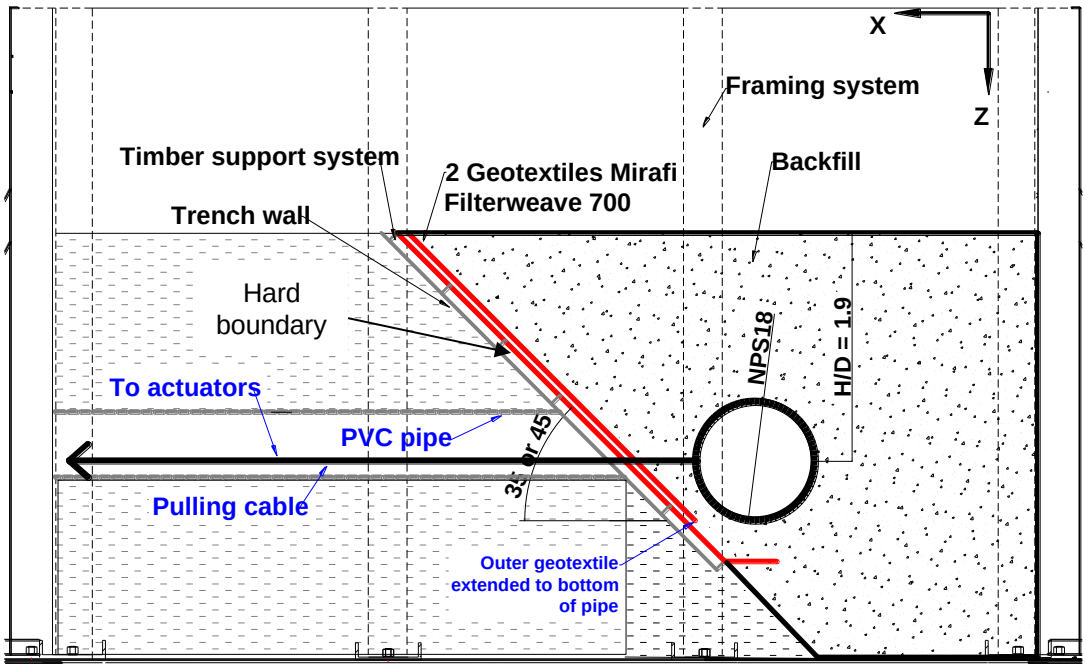

Figure 3.26: Schematic of the geotextile-lined trench wall constructed to study lateral soil restraints due to relative horizontal ground displacements.

Similarly, a trench wall lined with TC Mirafi Filterweave 700, woven geotextile fabric over a GSE HDE 080A000 (80mil HDPE) geomembrane was constructed with the aim of studying the geotextile effectiveness in reducing soil restraints for pipelines crossing reverse faults. During the development of the testing program, it was judged important to provide minimal constraints to the freedom of slippage between the geotextile and geomembrane during the movement of the pipe and associated soil mass.

Given that the direction of the pipe displacement vector crossing reverse faults is not horizontal as in the case from strike-slip faults, the location of the shear transfer between the lower portion of the overlying geotextile and soil during pipe movement is not well known. Therefore, it was suspected that the lower portion of the overlying geotextile may lock in place and constrain the freedom of the geotextile to movement.

On the basis of the above considerations, it was decided to lay the lower portion of the overlying fabric in a segmental manner. A schematic of this lining arrangement is shown in **Figure 3.27.** Essentially, the geotextile was initially cut into five 150-mm horizontal strips and with a 2.38 m length (i.e., to span the full width of the soil chamber). Each cut strip was then placed one at a time on the geomembrane spanning across the full width of the soil chamber beginning with Strip 1 placed at the base of the trench; each subsequent strip was then placed to have an overlap of approximately 25 mm with the previous strip (overlap to be measured along the direction of the trench slope).

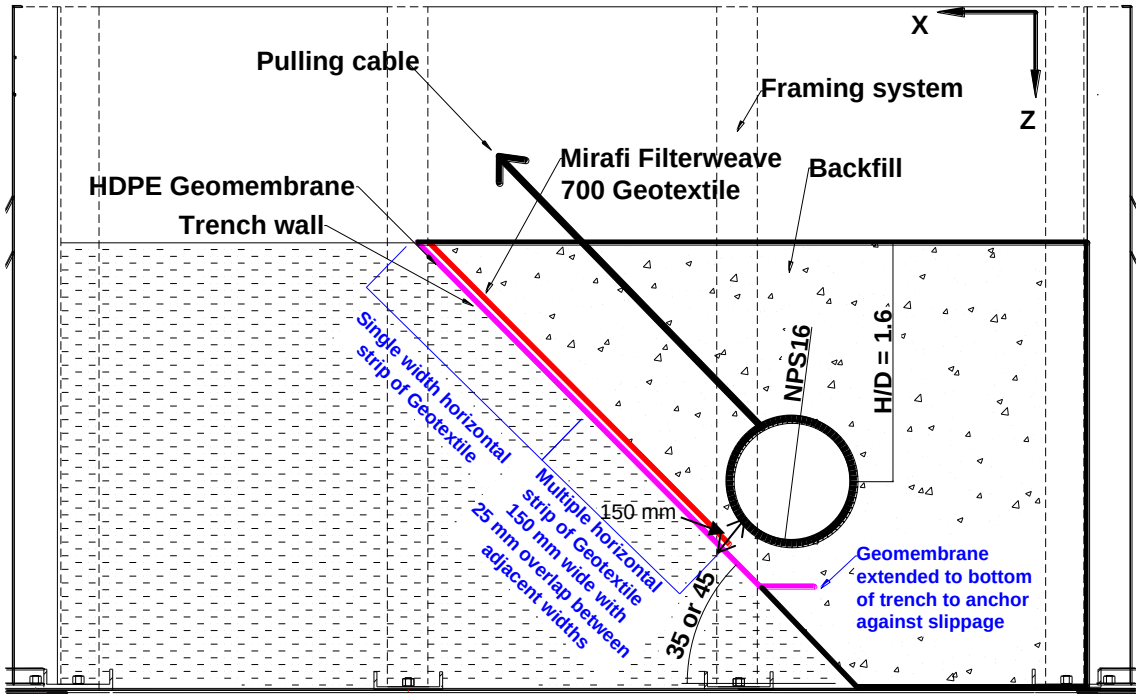

Figure 3.27: Schematic of the geotextile-lined trench wall constructed to study vertical oblique soil restraints for buried pipelines crossing reverse faults.

The geotextile strips after placement on the geomebrane were temporarily held together using small pieces of “painter`s adhesive tape” at discrete intervals to keep the strips in place during backfilling. A photograph of this configuration is shown in **Figure 3.28**. It was expected that the small adhesiveness of the painters tape would be negligible and would not restrain the potential for slippage at the geotextile-geomembrane interface.

As may be noted, the extent of the lower zone with these multiple strips was selected to coincide with the inclined projection of the front of the pipe. It was judged that having the geotextile placed as overlapping strips in this manner would provide more opportunity for slippage of geotextile against the geomembrane than for the condition which would have occurred if one cut geotextile piece were used to cover the whole sloped trench surface.

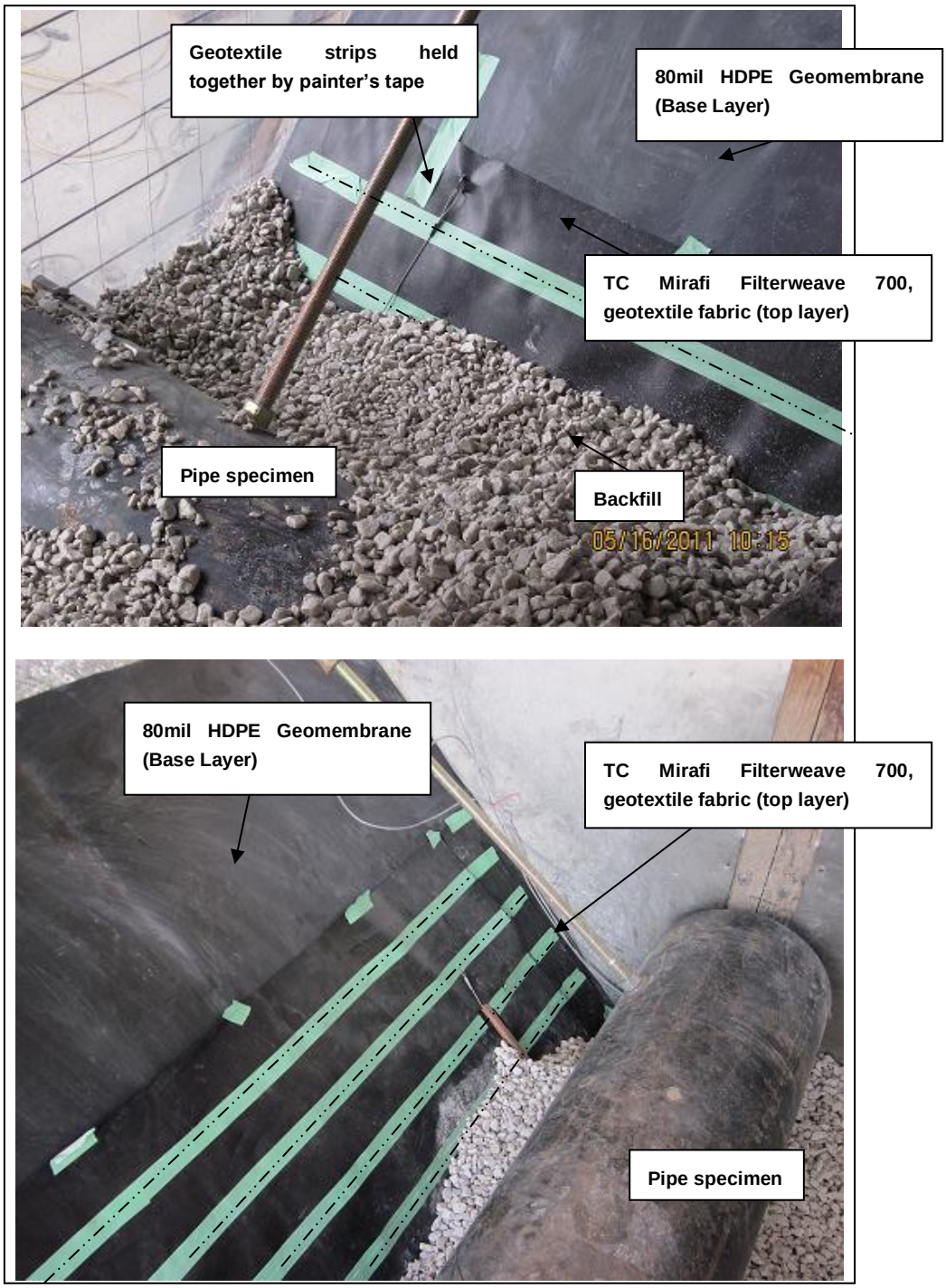

Figure 3.28: Typical configuration of geosynthetic slip surface used in the test program.

3.5 Instrumentation and Data Acquisition

The primary measurements made during the tests included the forces acting on the test pipes and the displacement of pipe specimens relative to the testing chamber. Numerous other measurements were taken to monitor the displacement vector of the pipe during vertical oblique soil restraint tests. The movement of geosynthetic layers was also measured as appropriate.

All measurements from the instrumentation array monitoring the test pipes were recorded at 10 sps (10 samples per second). Signals from the instrumentation array were collected using 16-channel National Instruments, Austin, TX, USA**,** signal conditioning boards. The commercially available software package LabView Version 2, National Instruments Inc., was used for real-time acquisition of data from all the channels. The system was controlled using a dedicated computer system running MS Windows Vista®.

3.5.1 Measurement of Loads (Soil Restraints)

For lateral soil restraint measurements during all horizontal soil restraint tests, a load cell was mounted in-line with each of the two actuators. The load cells were MTS model 661.22, with a maximum load capacity of 225 kN (50,000 lbs). The load cell was operated at an excitation voltage of 10 V and was calibrated over the range of expected loads, which was less than 150 kN. Total lateral soil restraint on the pipe specimens was taken as the sum of the load measured from each load cell.

The additional axial load developed on the pipe during horizontal oblique soil restraint tests was measured with an Interface Model 1020 load cell with a capacity of 25 kN. The load cell is compensated for eccentric loading with side load and eccentric load sensitivities of ±0.1%. The load cell was mounted inside one end of the pipe test specimen. Contact with the wall of

the soil chamber was achieved by connecting a heavy-wall pipe extension from the load cell and using a rounded bearing surface as shown in **Figure 3.29**. The rounded steel bearing cap provides a single point of contact with the testing chamber wall (see **Figure 3.30**). In addition, the space between the end of the pipe and the testing chamber wall was covered with a foam cushion to avoid sand getting into this space. The wall of the testing chamber contacted by the load cell was reinforced with a heavy 12.5 mm (½") thick steel plate that provided a smooth contact surface and allowed axial pipe loads to be distributed between two vertical support members of the testing chamber.

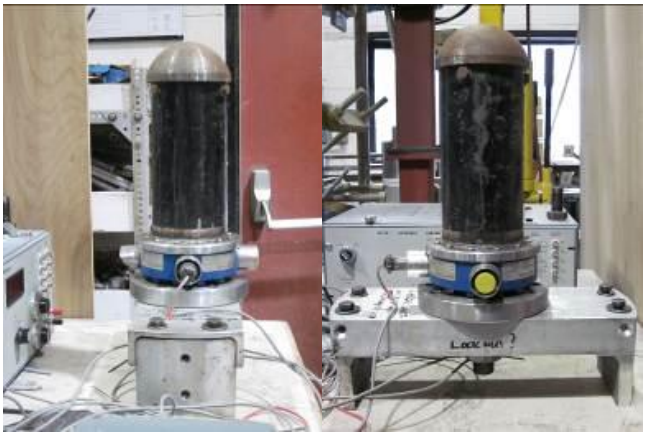

Figure 3.29: Axial load cell installed on internal pipe mount.

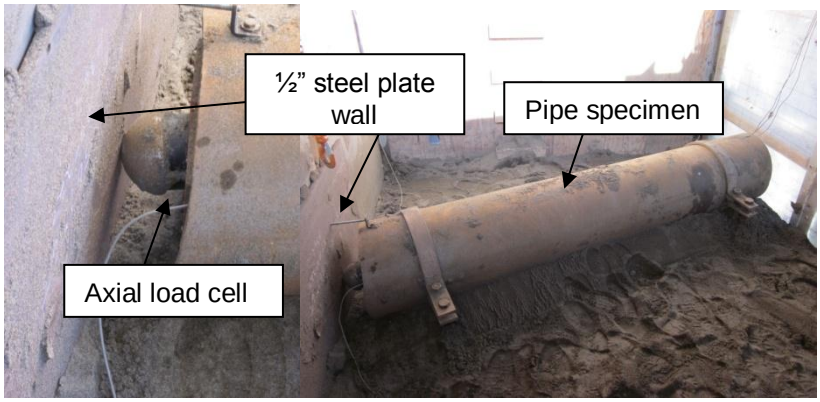

Figure 3.30: Axial load cell bearing on steel plate wall.

During vertical oblique soil restraint tests, each cable that was used to transfer the applied displacement to the test pipe was equipped with a load cell and an inclinometer that provided a means of measuring the applied load and the inclination. A photograph of the load cells and inclinometers arrangement for a typical vertical oblique soil restraint test is shown in **Figure 3.31**.

The actuators were equipped with load cells to measure the applied force to the cables. The load cells used were of MTS make, model 1020, with a maximum load capacity of 113 kN (25,000 lbs). The load cells were operated at an excitation voltage of 10V, and were calibrated over the range of expected loads, which was less than 100 kN.

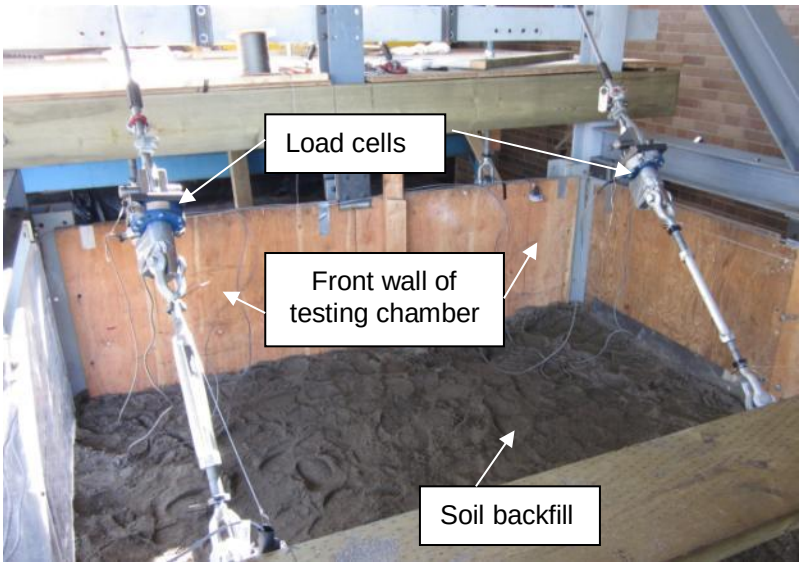

Figure 3.31: Load cell arrangement for the study of vertical oblique soil restraints.

3.5.2 Measurement of Pulling Angle

Two inclinometers and a set of 8 string potentiometers (four per loading cable) were placed for the measurement of the pulling angle during the tests under reverse fault displacement type. The arrangement layout is shown in **Figure**

3.32 and **3.33**. These potentiometers were labeled SP-2 to SP-5 for the left side set and SP-6 to SP-9 for the right side set.

3.5.3 Measurement of Pipe Displacement

Translational pipe displacements relative to the soil test chamber were measured using string potentiometers. For lateral soil restraint tests, 1.6-mm (1/16-in) diameter steel cables were attached to the both ends of the pipe. The cables were passed through small-diameter PVC pipes embedded in the soil from the back end of the pipe to the outside of the testing chamber and attached to string potentiometers mounted at the back of the testing chamber. The arrangement is shown in **Figure 3.5**. For vertical oblique soil restraint tests, the cables from the string potentiometers were attached to the pulling cables as shown in **Figure 3.32** (SP-1).

3.5.4 Measurement of Geotextile Displacement

String potentiometers were used to record displacements of geotextile layers in order to assess the slippage behavior of the layers. For lateral soil restraint tests, very thin extension cables were attached to the top of the geosynthetic fabric layers and attached to string potentiometers mounted on the top of the test chamber. For oblique vertical soil restraint tests, very thin extension cables attached to the mid-length of the geosynthetic layer were attached to the string potentiometers mounted inside protected casings inside the trench base. A photograph that illustrates these instrument locations is shown in **Figure 3.34**. These potentiometers were labeled SP-BL (for left side) and SP-BR (for right side) as shown in **Figure 3.32** (for left side only).

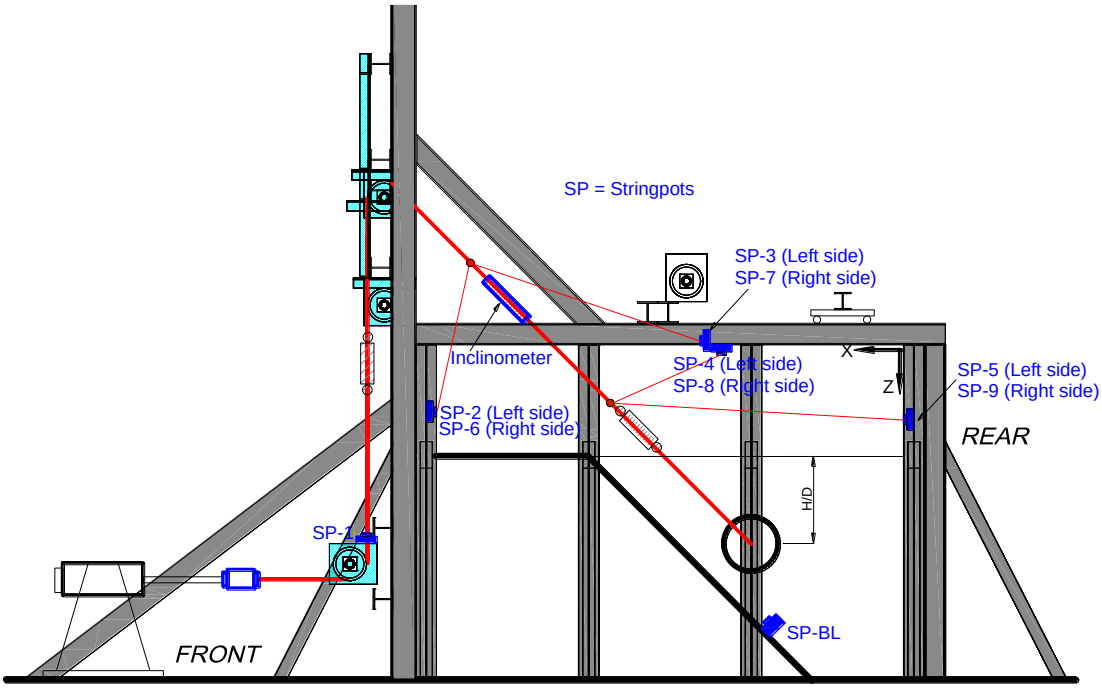

Figure 3.32: String potentiometers (SP) arrangement for the study of vertical oblique soil restraints.

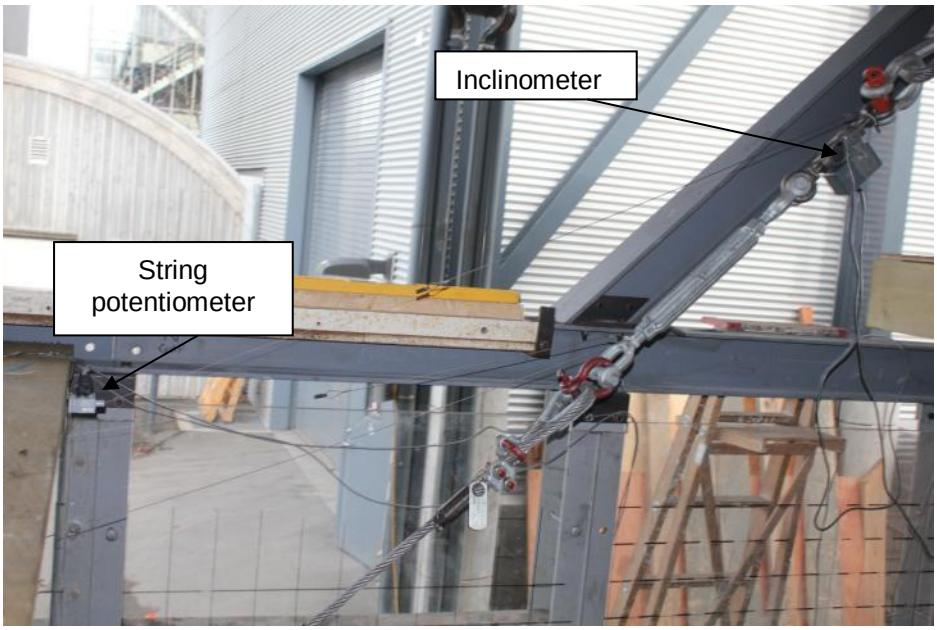

Figure 3.33: Photograph of inclinometers and string potentiometers arrangement for the study of vertical oblique soil restraints.

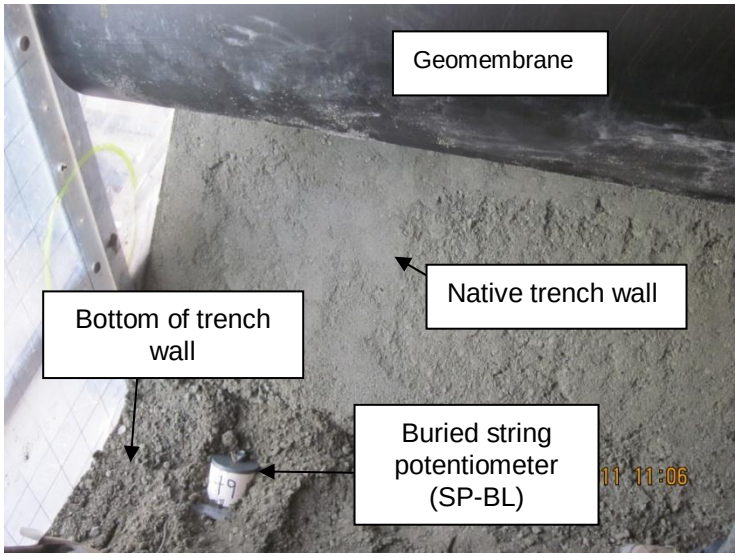

Figure 3.34: Buried string potentiometers to record geotextile displacement.

3.5.5 Measurement of Soil Pressure on Pipe Surface

Soil pressures exerted on the pipe surface were also recorded during the testing to obtain additional information on soil response to pipe displacement. As evidenced in the results presented in **Chapter 4**, many of the data obtained from the pressure transducers were not consistent with their corresponding lateral soil restraint vs. normalized pipe displacement relationship. The measurements from soil pressure cells are dependent on the effects of soil structure interaction and therefore are not reliably for measuring contact pressures (normal stresses) which develop on a soil structure boundary (Talesnik et al. 2008). Therefore, it was decided to use the recorded soil pressures to establish a qualitative assessment of the relative changes in soil pressure and not to reach conclusions in the thesis.

Three total pressure transducers (TPT) were installed on a selected pipe circumference at equidistant locations (45° radial spacing) between the crown

and invert of the pipe to measure normal stresses on the pipe. Bonded semiconductor strain gauge pressure transducers, Type AB/HP manufactured by Honeywell, Freeport, PL, USA were used in this regard. The transducers have a range 0 kPa to 180 kPa.

After cutting holes in the pipe, the transducers were mounted to be flush with the surface of the pipe so that there is minimum opportunity for soil arching or localized disturbance to the pipe-soil interface in the vicinity of the transducer. The holes in the pipe were threaded and transducers were mounted in hollow threaded shafts, which allowed convenient screw-in type attachment. The wires of the pressure transducers were passed through the pipe and connected to the data acquisition system. The diameter of pressure transducers was 19.1 mm (0.75 in) and the diameter of transducer mounted on hollow shaft was 28.6 mm (1-1/8 in).

3.5.6 Measurement of Backfill Density

The density and moisture content of the as-placed backfill sand was measured using a calibrated nuclear densitometer with a sensitivity of ±1 kg/m^3 and ±0.1%. The densitometer readings were further checked with independent density measurements using sand containers placed during compaction. Added information on density measurements are presented in Section 3.4.1 that covers density control aspects.

3.6 Development of the Testing Program

The main aim of this thesis is to determine soil restraint modelling parameters for the seismic design of pipelines crossing active seismic faults. In particular, soil restraint parameters for conditions that arise during the breakout of buried pipelines from their soil embedment on one side of either a strike-slip or a reverse-thrust fault. In this regard, soil restraint-displacement relationships

were measured on segments of pipelines buried in common backfill environments used in practice.

The soil restraint modelling parameters included factors such as the effect of a pipe specimen orientation with respect to a horizontal ground displacement, the effect of using geotextile-lined trenches, and the effect of the position of the pipe with respect to the geotextile-lined trenches. Furthermore, soil restraint modelling parameters for pipe specimens subjected to simulated thrust fault displacement type with dips of 35° and 45° degrees from the horizontal were determined. Load-displacement relationships for a pipe specimen displaced in the vertical direction were also quantified.

A total of 29 tests were performed during the 18-month period between December 2009 and July 2011. Many different configurations were tested, and some tests were performed for configurations that were previously examined to confirm the repeatability and reliability of the test data. Different pipe specimens were buried in backfills made of moist sand, road mulch and crushed limestone material. These geomaterials are commonly employed in pipeline engineering projects around the world. Details of the test pipe configurations are presented in the following paragraphs. The test configurations employed during the 29 tests are also summarized in **Table 3.4**. The following identification code was used to distinguish different tests (see **Figure 3.35**):

D - H/D – Horizontal or Vertical Obliquity – Native Material – Backfill Material – Geotextile – Slope – Spacing - Test Number

Where:

D	=	pipe size expressed as nominal pipe size, NPS;
H/D	=	ratio of depth to pipe centerline and pipe outside diameter;

Horizontal Obliquity	=	Horizontal oblique angle of pipe displacement with respect to the pipe axis alignment (i.e., obliquity of 90° implies pure lateral displacement);
Vertical Obliquity	=	Vertical oblique angle of pipe displacement measured with respect to the horizontal; Native Material (i.e., material outside of the pipe trench)
	=	DS for dry sand; MS for moist sand;
	=	RM for crushed gravel and sand (road mulch);
	=	HB for hard boundary formed by timbers;
Backfill Material (i.e., material in the pipe trench)		
	=	DS for dry sand; MS for moist sand;
	=	RM for road mulch; LM for limestone
Geotextile	=	GY if geotextile trench lining used, otherwise GN
Slope	=	slope of trench wall measured from horizontal
Spacing spring line	=	horizontal distance between the pipe and the trench wall
N	=	test number for test configuration

For example, 18-1.92-45V-MS-MS-GY-45-0.5D-1 naming code represents a test performed with a vertical obliquity of 45 degrees with respect to the horizontal, in moist sand inside and outside the pipe trench with a simulated 45° geotextile-lined trench wall with the pipe 0.5D from the trench wall. It is important to note that the connectivity of these tests to real life is as follows: the loading imparted in horizontal obliquity tests is related to strike-slip fault

scenarios; while those in vertical obliquity tests is corresponding with relative soil-pipe movements under reverse fault conditions.

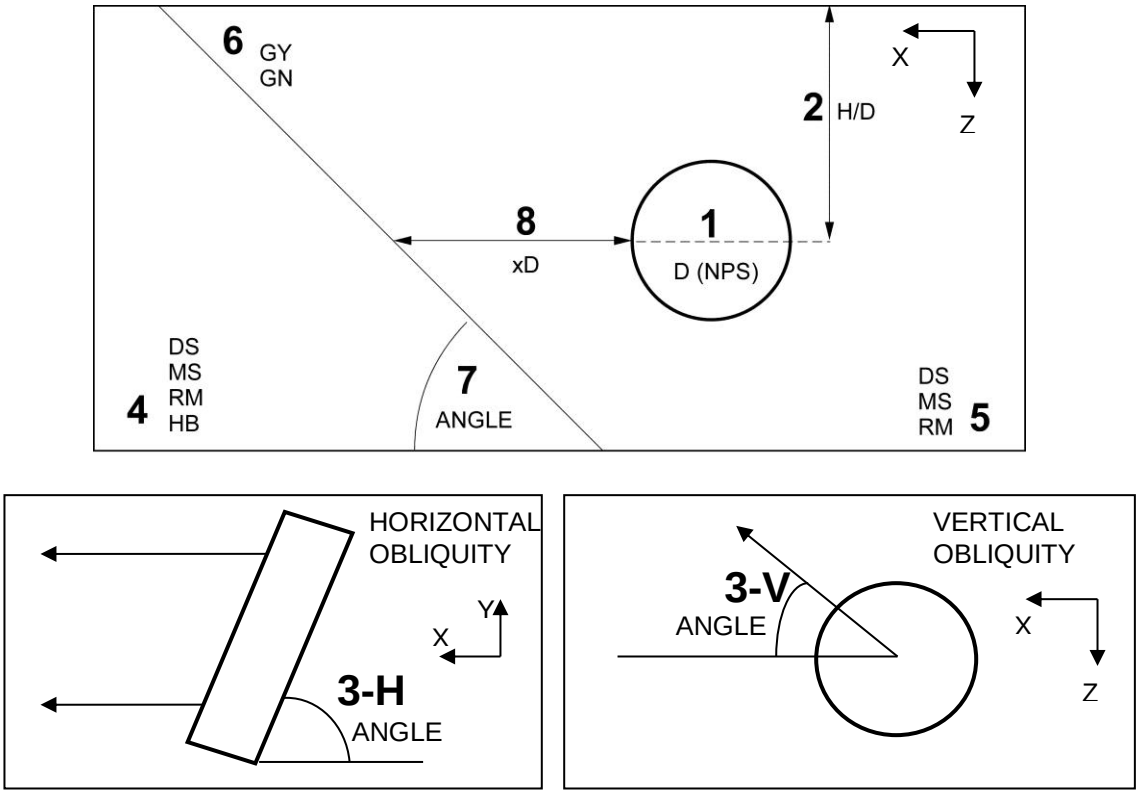

Figure 3.35: Components of test naming convention.

3.6.1 Lateral Soil Restraints

Previous studies on lateral soil restraint for pipeline design are based on pipe specimens buried in sand (Audibert and Nyman 1975; Trautmann and O'Rourke 1983; Hsu et al. 2006; O'Rourke et al. 2008). These studies have found that the maximum soil resistance depends on frictional factors and geometric characteristics which define appropriate failure surfaces. Furthermore, Hsu et al. (2006) and O'Rourke et al. (2008) used and developed analytical approaches to quantify maximum levels of lateral soil restraint and successfully compare those with results from their laboratory

tests. However, sand backfill may not be a feasible option in locations where suitable low-cost sand backfill is not readily available or drainage and erosion issues preclude the use of sand (for example, a real life situation that required the use of alternate materials, led to the present investigation). Thus, it is also important to obtain soil restraint parameters for other backfill soil materials and confirm that the available analytical approaches for estimating lateral soil restraint on pipelines can also be used in geomaterials other than sand usually found in practice.

Therefore, six full-scale tests were carried out in moist sand (MS), in a mixture of sand and gravel (road mulch, RM) and crushed limestone (LM) to determine lateral soil restraint parameters by simulating the lateral breakout of buried pipelines from their soil embedment on one side of a strike-slip fault. Four tests were conducted on a sand-blasted steel pipe specimen with an outside diameter of 457 mm (NPS18) and two tests were performed on a steel pipe specimen with an outside diameter of 406.4 mm (NPS16). All the pipe specimens have 12.7 mm (0.5 in) wall thickness and are oriented perpendicular to the direction of the fault trace.

The backfill soils were uniformly compacted to achieve an average dry density of 1,600 kg/m^3, 1,800 kg/m^3 and 1,700 kg/m^3, for sand, road mulch and crushed limestone, respectively. The densities were chosen under the premise of providing moderately dense conditions to the geomaterials. The lateral soil restraint testing program is summarized in **Table 3.5**. The objective of the tests was to obtain load-displacement data that can be used as a benchmark for comparisons between experiments and existing analytical approaches. In this way, the comparisons will provide the opportunity to evaluate the portability of the available analytical approaches for estimating lateral soil restraints in geomaterials other than sand.

Before each test, the box was emptied to the bottom level of the pipe specimens to remove any possible residual stress in the backfill soils.

Table 3.4: Testing Matrix for the Experimental Work

ID	Pipe Diameter	H/D	Soil Cover (m) [2]	Pipe Length (m)	Backfill Material			Trench wall angle	Distance pipe to trench	Geotextile
					Sand	Sand and gravel	Limestone			
18-1.9-90H-MS-MS-GN-1	NPS18	1.9	0.65	2.40	♦			No Trench	No Trench	No
18-1.9-90H-MS-MS-GN-2	NPS18	1.9	0.65	2.40	♦			No Trench	No Trench	No
16-1.6-90H-MS-MS-GN	NPS16	1.6	0.45	2.48	♦			No Trench	No Trench	No
18-1.9-90H-RM-RM-GN-1	NPS18	1.9	0.65	2.40		♦		No Trench	No Trench	No
18-1.9-90H-RM-RM-GN-2	NPS18	1.9	0.65	2.40		♦		No Trench	No Trench	No
16-1.6-90H-LM-LM-GN	NPS16	1.6	0.45	2.48			♦	No Trench	No Trench	No
18-1.9-90H-HB-MS-GN-45-0.5D-1	NPS18	1.9	0.65	2.40	♦			45	0.5D	No
18-1.9-90H-HB-MS-GY-45-0.5D-2	NPS18	1.9	0.65	2.40	♦			45	0.5D	Yes
18-1.9-90H-HB-MS-GY-45-0.5D-3[1]	NPS18	1.9	0.65	2.40	♦			45	0.5D	Yes
18-1.9-90H-HB-MS-GN-45-1.0D	NPS18	1.9	0.65	2.40	♦			45	1.0D	No
18-1.9-90H-HB-MS-GY-45-1.0D	NPS18	1.9	0.65	2.40	♦			45	1.0D	Yes
18-1.9-90H-HB-MS-GN-45-2.0D	NPS18	1.9	0.65	2.40	♦			45	2.0D	No
18-1.9-90H-HB-MS-GY-45-2.0D	NPS18	1.9	0.65	2.40	♦			45	2.0D	Yes
18-1.9-90H-RM-RM-GY-35-0.5D-1	NPS18	1.9	0.65	2.40		♦		35	0.5D	Yes
18-1.9-90H-RM-RM-GY-35-0.5D-2	NPS18	1.9	0.65	2.40		♦		35	0.5D	Yes
18-1.9-90H-RM-RM-GY-45-0.5D-1	NPS18	1.9	0.65	2.40		♦		45	0.5D	Yes
18-1.9-90H-RM-RM-GY-45-0.5D-2	NPS18	1.9	0.65	2.40		♦		45	0.5D	Yes
18-1.9-75H-MS-MS-GN-1	NPS18	1.9	0.65	2.48	♦			No Trench	No Trench	No
18-1.9-75H-MS-MS-GN-2	NPS18	1.9	0.65	2.48	♦			No Trench	No Trench	No
18-1.9-60H-MS-MS-GN-1	NPS18	1.9	0.65	2.77	♦			No Trench	No Trench	No
18-1.9-60H-MS-MS-GN-2	NPS18	1.9	0.65	2.77	♦			No Trench	No Trench	No
18-1.9-45H-MS-MS-GN-1	NPS18	1.9	0.65	3.39	♦			No Trench	No Trench	No
16-1.6-45V-MS-MS-GN-1	NPS16	1.6	0.45	2.42	♦			No Trench	No Trench	No
16-1.6-45V-MS-MS-GN-2	NPS16	1.6	0.45	2.42	♦			No Trench	No Trench	No
16-1.6-45V-HB-LM-GN	NPS16	1.6	0.45	2.48			♦	45	0.5D	No
16-1.6-45V-HB-LM-GY	NPS16	1.6	0.45	2.48			♦	45	0.5D	Yes
16-1.6-35V-HB-LM-GN	NPS16	1.6	0.45	2.48			♦	45	0.5D	No
16-1.6-35V-HB-LM-GY	NPS16	1.6	0.45	2.48			♦	45	0.5D	Yes
16-1.6-90V-LM-LM-GN	NPS16	1.6	0.45	2.48			♦	No Trench	No Trench	No
16-1.6-90V-MS-MS-GN	NPS16	1.6	0.45	2.48			♦	No Trench	No Trench	No

Notes: [1] Only one geotextile; [2] Soil cover above pipe crown

Table 3.5: List of Conducted Tests for Lateral Soil Restraints

No	Test ID	Backfill	Dry Density (kg/m^3)	Moisture Content (%)	Purpose / Comments
1	18-1.9-90H-MS-MS-GN-1	Sand	1,600	4.0	Provide baseline case for comparison w/published data
2	18-1.9-90H-MS-MS-GN-2	Sand	1,600	4.0	Provide baseline case for comparison w/ published data
3	16-1.6-90H-MS-MS-GN-1	Sand	1,600	4.0	Provide baseline case for comparison w/published data
4	18-1.9-90H-RM-RM-GN-1	Road Mulch	1,800	4.0	Simulate real native soil conditions
5	18-1.9-90H-RM-RM-GN-2	Road Mulch	1,800	4.0	Simulate real native soil conditions – repeatability test
6	16-1.6-90H-LM-LM-GN-1	Crushed Limestone	1,700	4.0	Simulate real native soil conditions

3.6.2 Reduction of Lateral Soil Restraints by Geosynthetic Fabric

The testing program in this thesis is investigated the mobilization of lateral soil restraint on segments of pipelines buried in geotextile-lined trenches. Factors on lateral soil restraint such as the effect of varying a trench slope angle together with the influence of the separation distance between a pipe and the geotextile interface on geotextile contribution to reducing lateral soil restraint were investigated. All the pipe specimens were NPS18 and were oriented perpendicular to the direction of ground displacement. The geosynthetic fabric used for the geotextile interface was TC Mirafi Filterweave 700 woven. The lateral soil restraint reduction testing program is summarized in **Table 3.6**.

Table 3.6: List of Conducted Tests for Reduction of Lateral Soil Restraint by Geotextiles

No.	Test ID	Backfill	Dry Density (kg/m^3)	Purpose / Comments
1	18-1.9-90H-HB-MS-GN-45-0.5D-1	Sand	1,600	Investigate influence of increasing separation on mobilization of geotextile interface and increment of soil resistance due to hard boundary.
2	18-1.9-90H-HB-MS-GY-45-0.5D-2	Sand	1,600	
3	18-1.9-90H-HB-MS-GN-45-1.0D	Sand	1,600	
4	18-1.9-90H-HB-MS-GY-45-1.0D	Sand	1,600	
5	18-1.9-90H-HB-MS-GN-45-2.0D	Sand	1,600	
6	18-1.9-90H-HB-MS-GY-45-2.0D	Sand	1,600	
7	18-1.9-90H-RM-RM-GY-35-0.5D-1	Road Mulch	1,800	Assess instability modes and soil restraint increment response in native trench conditions. Corroborate repeatability.
8	18-1.9-90H-RM-RM-GY-35-0.5D-2	Road Mulch	1,800	
9	18-1.9-90H-RM-RM-GY-45-0.5D-1	Road Mulch	1,800	
10	18-1.9-90H-RM-RM-GY-45-0.5D-2	Road Mulch	1,800	
11	18-1.9-90H-HB-MS-GY-45-0.5D-3 [1]	Sand	1,600	Assess effectiveness of geotextile

Notes: [1] Only one geotextile

3.6.3 Horizontal Oblique Soil Restraints

Five oblique tests to determine coupled horizontal and axial soil restraint resulting from horizontal oblique (oblique on a horizontal plane) ground displacement were performed using three different NPS18 pipe specimens. The pipe specimens were oriented at oblique angles of 75°, 60° and 45 degrees (90° is purely perpendicular) to the direction of ground displacement. A schematic plan view of the specimen placement in the testing chamber is provided in **Figure 3.36**. As previously described in **Section 3.5.1**, one end of the oblique test specimen was fitted with a load cell to measure soil restraint along the pipe axial direction. Horizontal soil restraint was measured by load cells mounted on the two hydraulic actuators. The coupled lateral and axial soil restraint testing program is summarized in **Table 3.7**.

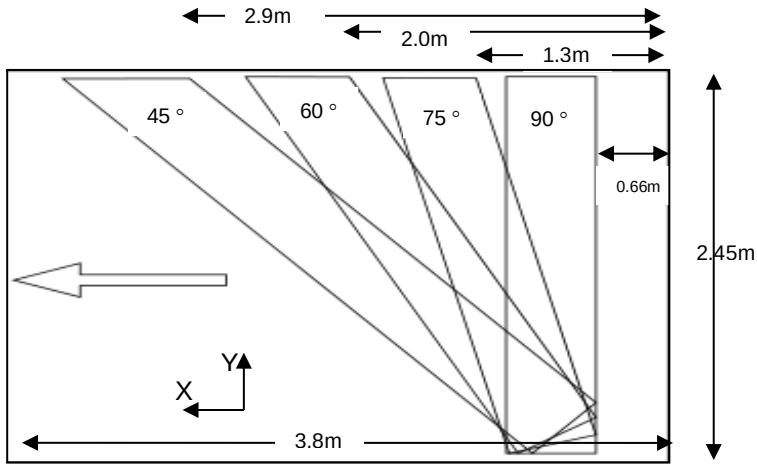

Figure 3.36: Arrangement of horizontal oblique pipe specimens in the testing chamber.

The purpose of these tests was to examine the soil response to oblique ground displacement and to confirm the trends in soil response reported by other researchers from small-scale tests and centrifuge tests (e.g. Hsu et al. 2001, 2006; Phillips et al., 2004; Daiyan et al. 2010).

Table 3.7: List of Conducted Horizontal Oblique Soil Restraint Tests

No.	Test ID	Oblique Angle w.r.t Fault Trace[1]	Backfill	Dry Density (kg/m^3)	Purpose / Comments
1	18-1.9-75H-MS-MS-GN-1	75°	Sand	1,600	Provide corroboration with test by others on coupling effects
2	18-1.9-75H-MS-MS-GN-2	75°	Sand	1,600	Provide corroboration with test by others on coupling effects
3	18-1.9-60H-MS-MS-GN-1	60°	Sand	1,600	Provide corroboration with test by others on coupling effects
4	18-1.9-60H-MS-MS-GN-2	60°	Sand	1,600	Provide corroboration with test by others on coupling effects
5	18-1.9-45H-MS-MS-GN-1	45°	Sand	1,600	Provide corroboration with test by others on coupling effects

Notes: [1] 90° is perpendicular to a fault trace.

3.6.4 Vertical Oblique Soil Restraints

Vertical oblique (oblique on a vertical plane) soil restraint modelling parameters are required for design of pipeline crossing reverse/thrust faults and, therefore, to estimate pipeline segments performance. These data are seldom available in current published technical literature and usually are inferred in practice on the basis of horizontal and vertical soil restraints.

Given the importance of this information for pipeline fault crossing design, a pipe-soil interaction test program was carried out to characterize the pipe-soil interaction behavior of a buried pipeline segment subjected to vertical oblique ground displacement (i.e. those imposed by reverse/thrust faults). All the pipe specimens were NPS16 and were oriented perpendicular to the direction of the fault thrust.

The tests were carried out to determine load-displacement relationships for a pipe buried in a shallow 45° (from horizontal) trench wall backfilled with crushed limestone and sand and displaced at vertical oblique angles of 35° and 45° from horizontal. Similar to the geotextile-lined pipeline trenches subjected to horizontal ground displacement described in **Section 3.6.2**, a geotextile-lined trench wall was constructed to investigate the geotextile contribution to reducing vertical oblique soil restraint. Load-displacement relationships for a pipe specimen displaced in the vertical direction were also investigated. The vertical oblique soil restraint testing program is summarized in **Table 3.8**.

Table 3.8: List of Conducted Vertical Oblique Soil Restraint Tests

No.	Test ID	Oblique Angle w.r.t Horizontal	Backfill	Dry Density (kg/m^3)	Purpose / Comments
1	16-1.6-45V-MS-MS-GN-1	45°	Sand	1,600	Determine soil restraint
2	16-1.6-45V-MS-MS-GN-2	45°	Sand	1,600	Repeatability
3	16-1.6-45V-HB-LM-GN	45°	Crushed Limestone	1,700	Determine soil restraint no geotextile
4	16-1.6-45V-HB-LM-GY	45°	Crushed Limestone	1,700	Determine soil restraint with geotextile
5	16-1.6-35V-HB-LM-GN	35°	Crushed Limestone	1,700	Determine soil restraint no geotextile
6	16-1.6-35V-HB-LM-GY	35°	Crushed Limestone	1,700	Determine soil restraint with geotextile
7	16-1.6-90V-LM-LM-GN	90°	Crushed Limestone	1,700	Determine vertical soil restraint
8	16-1.6-90V-MS-MS-GN	90°	Sand	1,600	Determine vertical soil restraint

3.7 Experimental Limitations and Associated Errors

To investigate the development of soil restraints on segments of pipelines, an ideal testing apparatus would be one that produces uniform levels of state of stress along the pipe specimen. In addition, the apparatus must be able to replicate the loading configurations, likely to exist in the field. A state of stress of this nature can be considered as a representative element of a continuum and the procedures based on nonlinear finite element analysis which incorporates springs that simulate soil restraint boundary conditions are immediately applicable. Thus, the measurements of load-displacement relationships from such ideal testing apparatus provide the desired information for development of models and design approaches.

The development of such equipment is a formidable challenge. In previous soil –pipe interaction experiments conducted at UBC and elsewhere, it has been aimed to come as close as possible to the ideal device. In this way, previous researchers have identified the limitations and associated shortcomings of their tests which were conducted in a controlled environment (Karimian 2006; Hsu et al. 2001, 2006; Daiyan et al. 2010, 2011). Some sources that produce non-uniform state of stresses arise from the difficulty in achieving a uniform level of soil density around the pipe specimen, from the effects of boundary conditions and from the loading system mechanism. These shortcomings are in line with the limitations from any experimental study.

This section presents an evaluation of the likely limitations, shortcoming, and errors during this experimental study. In this way, an identification and appreciation of the importance of these limitations on the load-displacement relationships obtained from the tests of this work can shed light on the applicability of test results to real-scenario field conditions.

3.7.1 Control of Backfill Density

In soils, the mass to volume ratio controls many important engineering parameters such as level of friction angle, dilatancy, and deformation moduli. These parameters, in turn, affect the distribution and uniformity of the stress state in the soil mass during testing. Therefore, the control of backfill density plays an important role in obtaining reliable soil restraint parameters for engineering modeling of pipeline systems. While uniform values of density were obtained in different locations in the backfill soils, the control of backfill density in zones close to the pipe specimen was challenging. This is because of the difficulty in compacting the soil around the pipe to the required values during specimen preparation.

The effect of the density variability along the pipe will be reflected in the slope of the load-displacement relationship obtained from the tests. This effect may be particularly important at initial stages of pipe displacement. However, it will be eventually overcome as the test progresses and the load-displacement relationships will be controlled by the properties of the backfill soil located in front and above of the pipe. Thus, its overall effect is minimal for the purposes of soil-pipe interaction where the pipelines in real-life conditions are usually subjected to large (> 1.0 m) displacement.

As explained in **Section 3.4.1**, the dry density and moisture content of the backfill soils were measured using a nuclear densometer. The density measurements were performed at 4 to 5 random points after the compaction of 0.30 m layers. The average dry soil density in each test varied within less than 5%. Independent tests using sand retrieved from containers buried in the backfill were performed to check validity of the nuclear densometer measurements at the beginning of the testing program. The results were in line with the measurements found with the nuclear densometer.

3.7.2 Boundary Conditions

The development of experiments is crucial for reliable estimation and assessment of pipe-soil interaction parameters. However, some limitations exist in the interpretation of the test results and the applicability of test results for pipeline engineering design. One of the most significant sources of error during experimental testing is related to frictional drag between the soil and the end walls of the testing apparatus.

Available technical literature shows that several methods were employed by different researchers to eliminate or at least minimize the magnitude of the frictional drag during soil-pipe interaction tests. For example, by using 2 layers of polyethylene at the sidewalls, Audibert and Nyman (1977) were able to reduce the sidewall friction to the friction between the polyethylene layers.

Trautmann and O'Rourke (1983) used a glass window on one side of their testing equipment and Formica on the other side to reduce the effect of sidewall friction. Paulin and co-workers (1998) at C-CORE simply used a 3 m wide steel box, without any additional material to reduce sidewall friction. Karimian (2006) used stainless steel sheets attached to plywood panels to reduce the sidewall friction force. In the current study, a procedure similar to that of Karimian (2006) was implemented. A discussion on sidewall friction is presented in **Section 3.7.2.2**.

3.7.2.1 Front and Rear Walls of the Testing Chamber

In tests that simulate the mobilization of lateral and oblique soil restraints, the front and rear walls should be sufficiently far away from the pipe to allow the formation of the active and passive zones freely as shown in **Figure 3-37**. Therefore, the length of the testing chamber was selected on the basis of the active and passive zones formation. The length of the testing chamber for the current study was 3.8 m which is similar to that used by Karimian (2006), but 25% longer than the box used by Paulin et al. (1997) and Popescu et al. (1999), 70% longer than that used by Trautmann and O'Rourke (1983), and close to 2 times of that used by Hsu (2001, 2006).

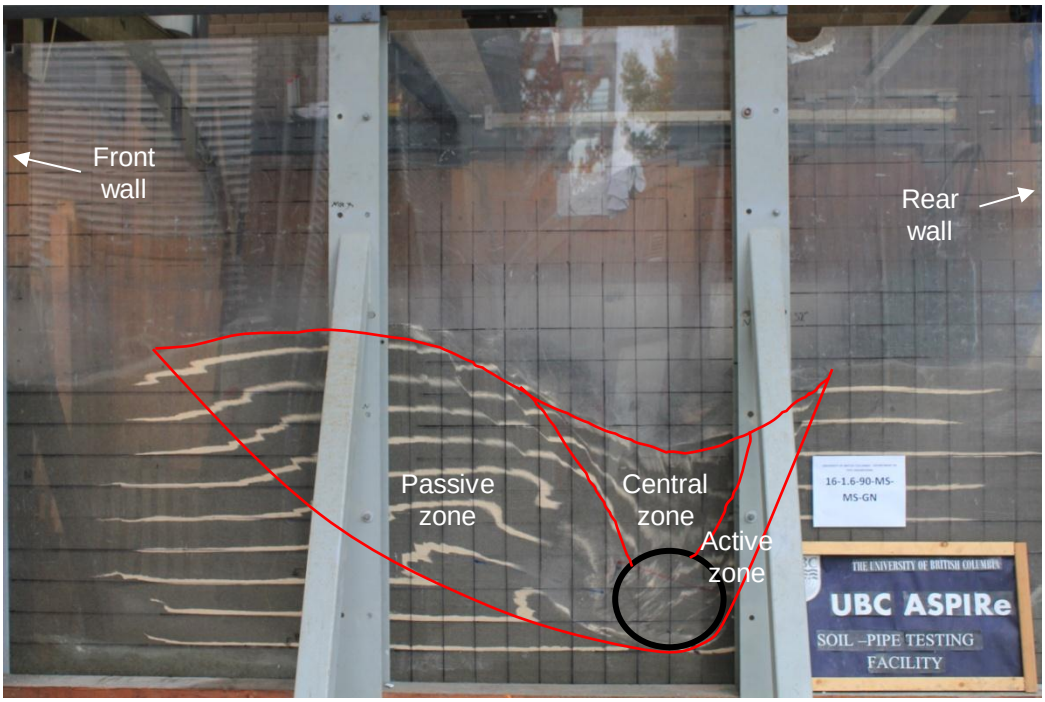

Figure 3.37: Free development of soil failure zones during the testing program.

3.7.2.2 Left and Right Walls of the Testing Chamber

Friction between the end caps of the pipe and the left and right sidewalls of the testing chamber may impede the pipe specimen to move laterally in a uniform and close-to-field conditions manner, and therefore, additional forces may be recorded by the load cells during the soil-pipe interaction tests. To minimize this restraining action, pipe specimen with lengths shorter than the span of the sidewalls (see **Figures 3.5** and **3.7**) and sidewalls close to "frictionless" condition are used. The right side of the wall was covered with 20Ga 304 stainless steel sheets. Similarly, the left sidewall of the testing chamber was made of Plexiglass panels. The Plexiglass panels not only will reduce the frictional to minimum values, but also will provide observational capabilities during the tests as evidenced in **Figure 3.37**.

In order to have a reference value of the side friction provided by the 20Ga 304 stainless steel sheets, Karimian (2006) carried out a failure wedge analysis as shown in **Figure 3-38** with some simplifying assumptions. He found a sidewall friction force of 0.9 kN and concluded that this force is less than 2% of the soil loads on the pipe which were in the order of 50 kN/m and therefore this error can be considered as negligible for the purpose of the study. Ahmadnia (2012) carried out similar calculations for his testing work which was done in the same testing apparatus as that used by Karimian (2006). He reached a similar conclusion.

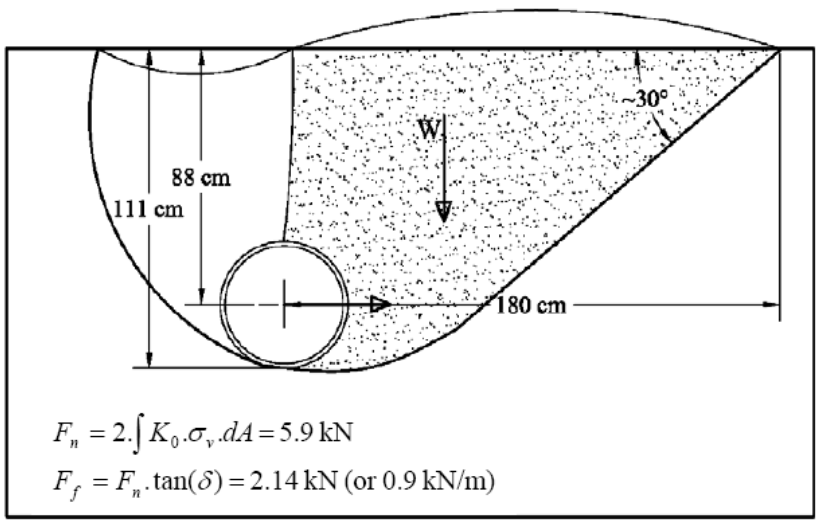

Figure 3.38: Calculation of sidewall friction (from Karimian 2006).

It is important to emphasize that most of the frictional drag condition is minimized by using pipes shorter than the lateral span of the testing chamber. Furthermore, **Figure 3.36** suggests that the sand particles in the space left by the pipe cap and the lateral walls move in line with the movement of the pipe and therefore the failure zones depicted through the plexiglass are adequate for engineering purposes.

3.7.3 Loading System Mechanisms

As described in previous sections, the loading to the pipe specimens was applied by pulling the test pipes laterally, obliquely or upwards; instead of pushing the pipe from the back or below. This type of loading mechanism faces several operational difficulties and requires special considerations to minimize its impacts on the test results. Some common sources of disturbance or errors can be found from:

- Cable slack between the pipe and hydraulic actuators;
- Vibration due to the application of a sudden displacement on the pipe specimen;
- Restriction to horizontal planar movements to the pipe specimens. The pipes should follow the failure surface developed in the backfill soil. Therefore, they should be allowed to move freely in the horizontal and vertical direction.
- Change in the direction of the displacement vector during the tests;
- Friction along the pulling rods or cables.

The coupling system for lateral and oblique soil restraint tests consists of end clamps and a rod connector with shackles at the ends. Each side of these shackles were connected by means of a 1 1/8 inch (28.6 mm) steel cable to the hydraulic actuators. In this way, the buried cable easily moves and is not restricted to horizontal planar movements. The diameter of the cable was selected to maintain very small cable elongations during the tests and therefore the load will be transmitted directly from the pipe to the load cells. For the initial part of the testing program, special care was given to avoid cable slack by carefully controlling the tension on the cables. Later, the cable slack was controlled by a set of turnbuckles which were located as shown in

Figures 3.6 and **3.8**. Cable vibration was minimized by gradually applying to the system a velocity from 0 to 25 mm/s.

For tests that simulate pipelines buried in trapezoidal trenches, the steel cable passed through 0.25 m diameter PVC pipes with the aim of providing minimum soil-cable friction resistance. The PVC pipes acted as ducts embedded in native soil and extended 2.2 m from the trench wall to the front wall of the testing chamber (see **Figure 3.25**). The chosen diameter of the PVC allows the buried cable to move freely in the vertical direction during the lateral loading of the pipe.

The largest cable length in contact with the backfill was about 2 m and corresponds to the case of lateral soil restraint with no trench. ASCE (1984) and PRCI (2004, 2009) indicates that the axial soil load is proportional to the diameter and the length of the buried cable. Following the equations of these guidelines, a friction resistance on the steel cable less than 5% of the peak measured soil restraint values is obtained. Therefore, the soil-pulling cable resistance can be considered negligible for practical purposes.

For vertical oblique tests, special attention was given to maintaining the pulling direction constant throughout each test (see **Section 3.5.2**). This is particularly important for maintaining the assumption of constant thrust angle during a reverse fault rupture.

3.8 Summary of the Chapter

A full-scale testing system was constructed to study the levels of mobilization of soil restraint on buried pipes due to relative ground movements and with different directions. The full-scale testing facility was also adapted to study the effectiveness of geosynthetic-based mitigation measurements in reducing levels of lateral soil restraint. A large testing chamber was specifically designed and constructed for this work to simulate the type of displacements

segments of pipeline systems will be exposed to at strike-slip and reverse fault crossings. The imposition of different types of displacement is achieved by a set of cables that pull the pipe in a predefined direction (e.g. lateral, oblique or upward), rather than pushing it from the back or below. In particular, the testing system was specifically prepared to accommodate testing of buried pipes subjected to horizontal oblique and vertical oblique displacements, and pipes buried in geotextile-lined trapezoidal trenches with different trench backfill soil conditions. Developments for this testing work included:

1. Large soil chamber: A modified soil-pipe interaction testing chamber that enables the application of different pipe displacement directions and allows visual observation of trench configuration, formation of failure wedges, and patterns of deformation and geometric changes in the soil mass. The dimensions of the box (2.45 m x 3.8 m) were selected considering boundary effects during horizontal oblique and vertical oblique pipe displacements.

2. Characterization of backfill materials and interface properties: Uniformly graded, Fraser River sand, a mixture of crushed sand and gravel (road mulch) and crushed limestone were used as backfill materials. The mechanical properties of these materials were characterized through direct shear tests. Furthermore, direct shear tests were performed on interfaces between Fraser River sand and geotextile and road mulch and geotextile layer.

3. Instrumentation: load cells, inclinometers and string potentiometers were used to monitor pulling loads, pulling angle and displacement of pipe and geosynthetic layers. Also a series of pressure transducers was mounted on the pipe surface to record normal stresses on the pipe prior, during, and after pipe displacement.

4. Testing program: A total of 6 horizontal tests and 11 geotextile-lined pipeline trenches tests on steel pipe specimen backfilled with different materials were performed. Also 5 horizontal oblique and 8 vertical oblique tests were conducted on steel pipe specimen buried in different materials.

5. Experimental limitations: These limitations including the effect of sidewall friction, pulling system friction, pulling angle and boundary conditions and associated errors were investigated and discussed in this chapter. Appropriate modifications were made to limit these effects on the recorded data.

Chapter 4: Lateral Soil Restraint on Buried Pipelines

In this chapter, results from tests conducted on shallow pipe buried in sand, crushed sand and gravel mixture (road mulch), and crushed limestone backfills are described. NPS18 (457-mm diameter) and NPS16 (406-mm diameter) pipe specimens were horizontally displaced to simulate the breakout of shallow buried pipelines from their soil embedment on the fixed side of a strike-slip fault. The results of tests performed with pipe buried in geotextile-lined trenches are also presented. A dual layer of TC Mirafi Filterweave 700, woven geotextile fabric was used as a lining material for the trapezoidal trench wall.

The shallow soil-pipe interaction behaviour under relative lateral ground displacement is a function of pipeline configuration (e.g. with trench or no trench), backfill soil properties and level of relative lateral ground displacement. This behaviour is described and presented in terms of three regions observed from the soil restraint vs. pipe displacement results: initial linear and elastic-plastic, full plastic, and hardening region. This is done to point out the different stages of lateral soil restraint mobilization during lateral permanent ground displacement.

Associated geometric changes in the soil mass for these regions, shear rupture surfaces, levels of lateral soil restraint, soil stresses and history of geotextile displacement are described and discussed with the aim of characterizing the soil-pipe interaction behaviour observed from the full-scale tests. In later sections, attempts are made to predict lateral soil restraint assuming full plastic conditions by using a limit equilibrium approach. For no trench conditions, the approach proposed by O'Rourke et al. (2008) is evaluated and verified against test results and a log-spiral shear failure surface. For geotextile-lined pipeline trench conditions, an approach is

proposed and validated through the measurements carried out during the full-scale tests.

4.1 Summary of Test Parameters

Modeling parameters that simulate soil restraint boundary conditions on segments of buried pipelines under different burial depths are usually derived by using normalised soil-pipe restraint properties. The use of normalised soil-pipe restraint properties is well accepted in the pipeline engineering community and is described in engineering pipelines guidelines for seismic design (PRCI 2004, 2009; ASCE 1984). Therefore, test results from this work are presented in terms of normalised values of lateral soil restraint (N_{qh}) and normalised displacement (Y') determined from the equations below:

$$N_{qh} = P / (\gamma \cdot D \cdot H \cdot L) \qquad [4.1]$$

$$Y' = Y / D \qquad [4.2]$$

where, P is the measured load, γ is the dry unit weight of the backfill, D is the pipe diameter, H is the height of soil over the pipe springline, L is the pipe length, and Y is the recorded pipe displacement. The form of the normalized load and displacement shown above follows the relationships presented in previous research about lateral soil restraint (Hansen 1961; Audibert and Nyman 1977; Rowe and Davis 1982; Trautman and O'Rourke 1983; Paulin et al. 1998; PRCI 2004, 2009).

Details related to the testing program and test parameters were shown in **Table 3.4** and **Table 3.5** of **Chapter 3**. Important test characteristics are summarized in **Table 4.1** for the reader's convenience.

Table 4.1: Summary of Parameters for Lateral Soil Restraint Tests[2]

	Fraser River Sand	**Crushed Gravel and Sand (Road Mulch)**
Average Dry Density (kg/m^3)	1,600	1,800
Average moisture (%)	3 to 4	3 to 4
Internal Peak Friction Angle (ϕ'_p)	43°	49°
Dilation Angle (ψ)	12°	16°[1]
Pipe Size	NPS16, NPS18	NPS18
Pipe Length (m)	2.4	2.4
Pipe Grade & Surface	Steel Grade 524A, Sand Blasted Surface	Steel Grade 524A, Sand Blasted Surface
Geosynthetic Material	TC Mirafi Filterweave 700	TC Mirafi Filterweave 700
Interface Friction Angle of Geotextile Layers	21°	21°
Soil-Geotextile Interface Friction Angle	32°±1°	31°±1°
Pulling Rate	2.5 mm/s	2.5 mm/s

Note: [1] Inferred from full-scale test; [2] Crushed limestone properties in **Table 6.1**.

4.2 Results of Lateral Soil Restraint Tests on Pipe Buried in Sand Backfill

In this section, the results of the testing program on lateral soil restraint for soil-pipe systems with no trench conditions are presented and discussed. A series of six tests were conducted utilizing moist Fraser River sand, road mulch, and crushed limestone soil as backfills with dry densities of 1,600 kg/m^3, 1,800 kg/m^3 and 1,700 kg/m^3, respectively. The observed load displacement curves and pressure measurements on the pipe surface during the lateral tests are presented together with visual observations made in

relation to geometric changes in the soil mass, shear rupture surfaces, and levels of lateral soil restraint during the tests.

4.2.1 Normalised Load-Displacement Response on Sand

Normalised lateral soil restraint, $N_{qh} = P / (\gamma \cdot D \cdot H \cdot L)$, vs. pipe displacement, Y', for a NPS16 (406-mm diameter) pipe specimen buried in moist sand with an overburden ratio H/D of 1.6 under lateral displacement, such as that for strike-slip faults, is shown in **Figure 4.1**. Lateral pulling displacement to about 1D was applied to the pipe specimen.

The soil-pipe interaction for Test 16-1.6-90H-MS-MS-GN showed a nonlinear relationship between the mobilised lateral soil restraint and pipe displacement; until the lateral restraint imposed by the soil on the pipe reached its maximum value (it is fully mobilized and overcome).

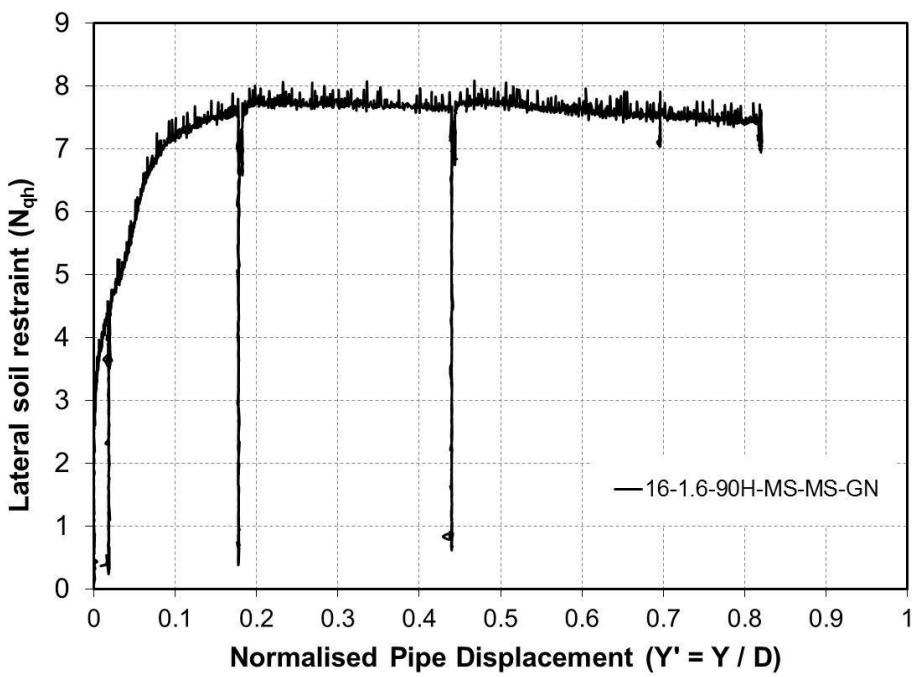

Figure 4.1: Normalised load-displacement relationships for NPS16 pipe specimen with H/D=1.6 buried in moist sand during lateral pulling.

In a lateral pulling test, the condition of maximum normalised lateral restraint, N_{qh}, for test 16-1.6-90H-MS-MS-GN reached a value of about 7.8 or about 34 kN/m at an early stage during the test (Y' = 0.25D). For normalised displacement larger than 0.25D, the value of N_{qh} remained constant.

The effect of unloading and reloading on the soil-pipe interaction response was also investigated for Test 16-1.6-90H-MS-MS-GN. As evidenced from **Figures 4.1**, no effect appears to exist due to unloading and reloading cycles. This is because the pipe specimen did not move after unloading the pulling cables.

Similarly, normalised lateral soil restraint, $N_{qh} = P / (\gamma \cdot D \cdot H \cdot L)$, vs. pipe displacement, Y', for Tests 18-1.9-90H-MS-MS-GN-1 and 18-1.9-90H-MS-MS-GN-2 on NPS18 (457-mm diameter) pipe specimens buried in moist sand with H/D = 1.9 are shown in **Figure 4.2**. These tests show practically identical response in terms of the maximum restraint. This evidences good test repeatability, appropriate specimen preparation and quality control.

A maximum lateral restraint, N_{qh}, of about 7.74 or about 51.2 kN/m was reached for both tests. However, the maximum N_{qh} value for Test 18-1.9-90H-MS-MS-GN-1 was reached at a normalised pipe displacement of 0.08D; while for Test 18-1.9-90H-MS-MS-GN-2 was reached at a much larger normalised pipe displacement of about 0.2D. This load-displacement relationship suggests a moderately brittle condition; the lateral displacement of the pipe at failure was less than 0.2D (given the fact that pipelines crossing active strike-slip faults are subjected to displacements larger than 1D). This characteristic was also seen in tests carried out by other researchers (Audibert and Nyman 1977; Trautman and O'Rourke 1983).

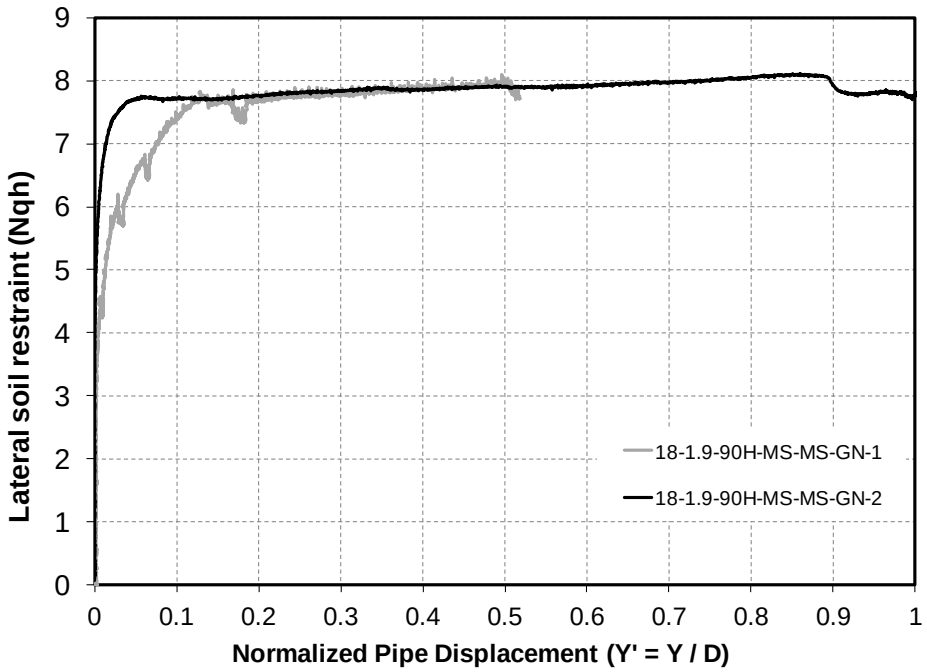

Figure 4.2: Normalised load-displacement relationships for NPS18 pipe specimen with H/D=1.9 buried in moist sand during lateral pulling.

4.2.2 Recorded Contact Pressure for Sand Backfill

Three pressure transducers were mounted on the pipe (see **Section 3.5.5**) to record the variation of soil stress on the face of the pipe. The transducer configuration was oriented on the pipe specimen so that the transducer No. PT-2 is facing the lateral pulling direction (see inset of **Figure 4.3** for transducer identification numbers). The transducers recorded the normal pressure from the soil at the contact point. The values include backfill readings.

It is important to emphasize that the values recorded by the pressure transducers during the lateral pulling tests required significant judgment for their interpretation. The recorded values were highly variable from test to test, which may be related to the different soil density values that existed around the pipe specimens before the tests. In addition, the pressure transducer data

from some tests showed irregularity at a particular pipe position. This is believed to be due to the interface shear that existed between the pressure transducer and the soil during soil-pipe interaction mechanism. The data values, however, can be useful to distinguish in a qualitative manner certain patterns of behavior that were present during the soil-pipe interaction process during the tests, such as the relation between pipe position and the recorded stress values.

The variation of pressure, from pressure transducers PT-1, PT-2 and PT-3, with normalized pipe displacement, Y', recorded during Test 16-1.6-90H-MS-MS-GN is shown in **Figure 4.3**. Among the pressure transducers, PT-1 and PT-2 showed higher stresses than that recorded by PT-3 as the soil was being compressed by the pipe. Maximum pressure of about 60 to 70 kPa occurred at normalised pipe displacements in the range between 0.2D to 0.4D. This pressure-displacement relationship is in agreement with the mobilized lateral soil restraint presented in **Figure 4.1**.

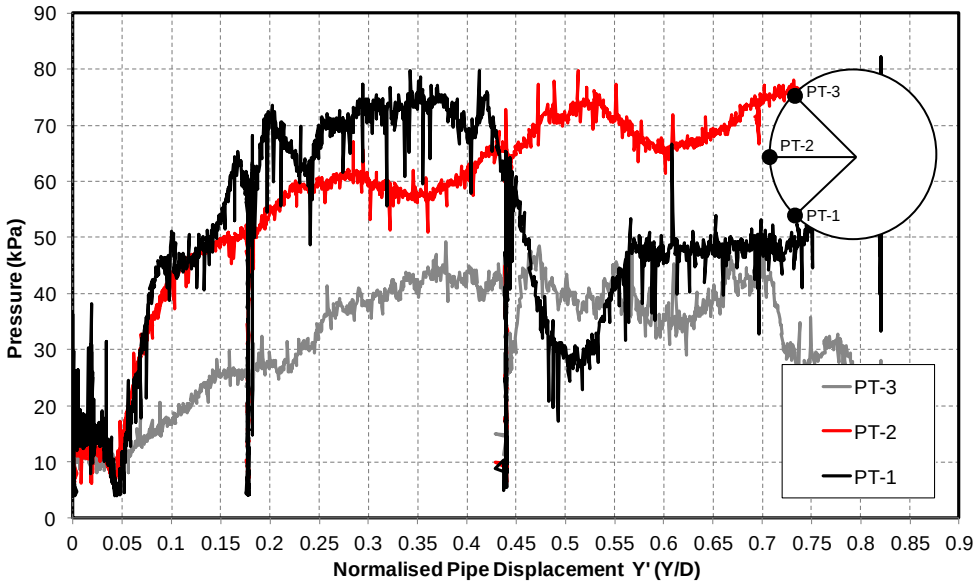

Figure 4.3: Pressure readings as a function of pipe displacement - Test 16-1.6-90H-MS-MS-GN.

After 0.4D, the pressure recorded by PT-1 dropped during Test 16-1.6-90H-MS-MS-GN; while the pressure recorded by PT-2 rose an additional 10 kPa. Pressure dropping implies that the pressure transducers mounted on the pipe were losing contact with the soil; therefore, a compression unloading must have taken place during lateral pulling. This drop of pressure is believed to be associated with an upward pipe displacement that occurred during lateral pulling, as will be described in **Section 4.2.3**.

Previously, **Figure 4.2** showed that during Test 18-1.9-90H-MS-MS-GN-1 the maximum lateral soil restraint was fully mobilized at normalised pipe displacement of around 0.1D to 0.15D. Behaviour observed on the pressure recorded by PT-2 vs. normalised pipe displacement showed that the largest contact pressures were recorded at the same displacement as the peak restraint, as evidenced in **Figure 4.4**.

The maximum pressure recorded by PT-2 reached a maximum value of about 125 kPa at Y' of about 0.1D to 0.15D during Test 18-1.9-90H-MS-MS-GN-1. Thereafter, the pressure fluctuated between 100 to 125 kPa. Furthermore, as in the case for the test on NPS16 pipe, the higher pressures were recorded by PT-1 and PT-2. However, for the case on NPS18 pipe, PT-1 showed a sudden increase of pressure level during the early stages of the test, which reached a value of about 175 kPa at Y' of about 0.05D and then dropped to a relatively constant value of 50 kPa during further lateral pulling.

The above mentioned drop occurred as the pressure recorded by PT-2 increased to its maximum value (100 to 125 kPa). Similarly to the behaviour observed from Test 16-1.6-90H-MS-MS-GN, the drop is believed to be associated with upward pipe displacement occurring after the pipe has overcome the maximum horizontal lateral restraint provided by the soil.

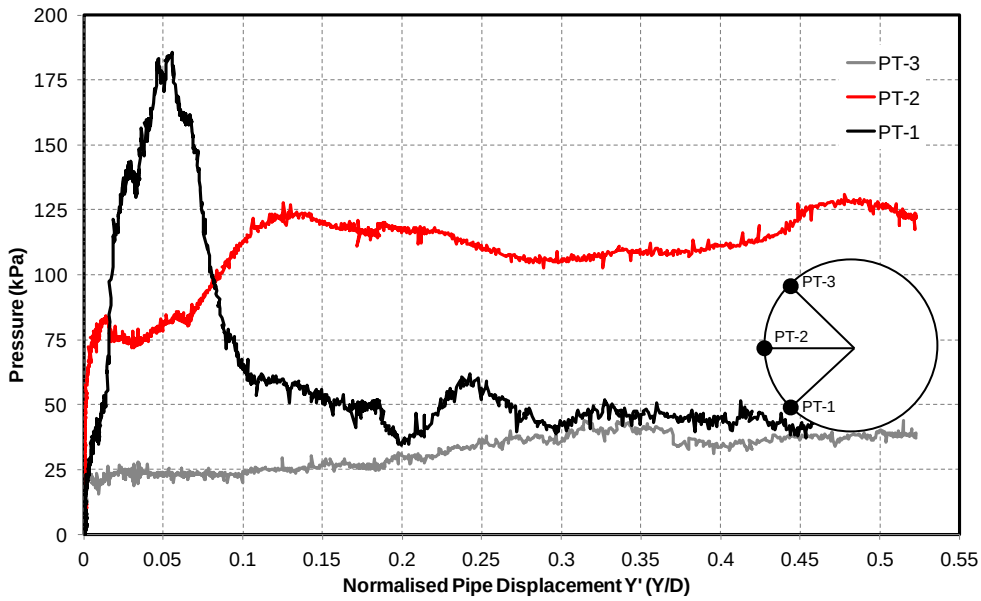

Figure 4.4: Pressure readings as a function of pipe displacement - Test 18-1.9-90H-MS-MS-GN-1.

4.2.3 Observed Backfill Soil Deformation Geometry for Sand

Taking advantage of the large Plexiglas panels installed in the soil testing chamber, experimental observations and measurements were taken for establishing a relation between pipe position and associated soil deformation patterns developed during the tests. Because the observed patterns of backfill soil deformation were similar for both tests (tests on NPS16 or NPS18), only the patterns of soil deformation from test 16-1.6-90H-MS-MS-GN are presented and discussed in the following section.

Different regions observed from the soil restraint vs. pipe displacement results and a log-spiral soil failure surface, developed with the approach of O'Rourke et al. (2008), is also included within the soil deformation patterns observed during test 16-1.6-90H-MS-MS-GN for comparison and discussion purposes.

Details of the regions and the log-spiral failure surface approach are covered in **Section 4.7.1** and **Section 4.7.2**.

Patterns of soil deformation for Test 16-1.6-90H-MS-MS-GN at Y'=0.07D (before peak load), Y'=0.25D (peak load or failure condition) and Y'=0.8D (unbalanced or post failure condition) are illustrated in **Figure 4.5**, **Figure 4.6** and **Figure 4.7**, respectively. Corresponding levels of lateral soil restraint for those pipe displacements and failure conditions can be obtained from **Figure 4.1**. A discussion on failure conditions is presented in **Section 4.7**.

As can be seen from the figures, three zones can be observed from the deformed soil mass: passive zone (A), active zone (C), and a central zone (B). The passive zone A developed in front of the pipe, while the active zone C occurred behind it. The central zone C developed between the active and passive zones. These failure zones are similar to those described by Audibert and Nyman (1977) for lateral tests on pipes buried in sand. Different stages associated with the mobilization of the three zones can be observed from the patterns of soil deformation. These patterns are represented by deformation of the horizontal white layers.

The fact that a log-spiral shape bounded the extension of a passive zone is not surprising for this compression-type mechanism. The log-spiral shape has long been used for the analysis of passive earth forces for retaining walls (Terzaghi, 1943) and has recently been adapted and proposed as an analytical method for evaluating lateral soil restraint on pipelines (O'Rourke et al. 2008).

Figure 4.5 also shows that the active zone (C), which is the narrow and almost vertical zone located behind the pipe, was fully mobilized at small pipe displacements (Y'=0.07D or 32 mm). The central zone (B) occurred just above the pipe specimen and extended up to the sand surface. This central zone is

related with an active wedge that was mobilized due to the loss of lateral confinement that was provided by the active zone (C).

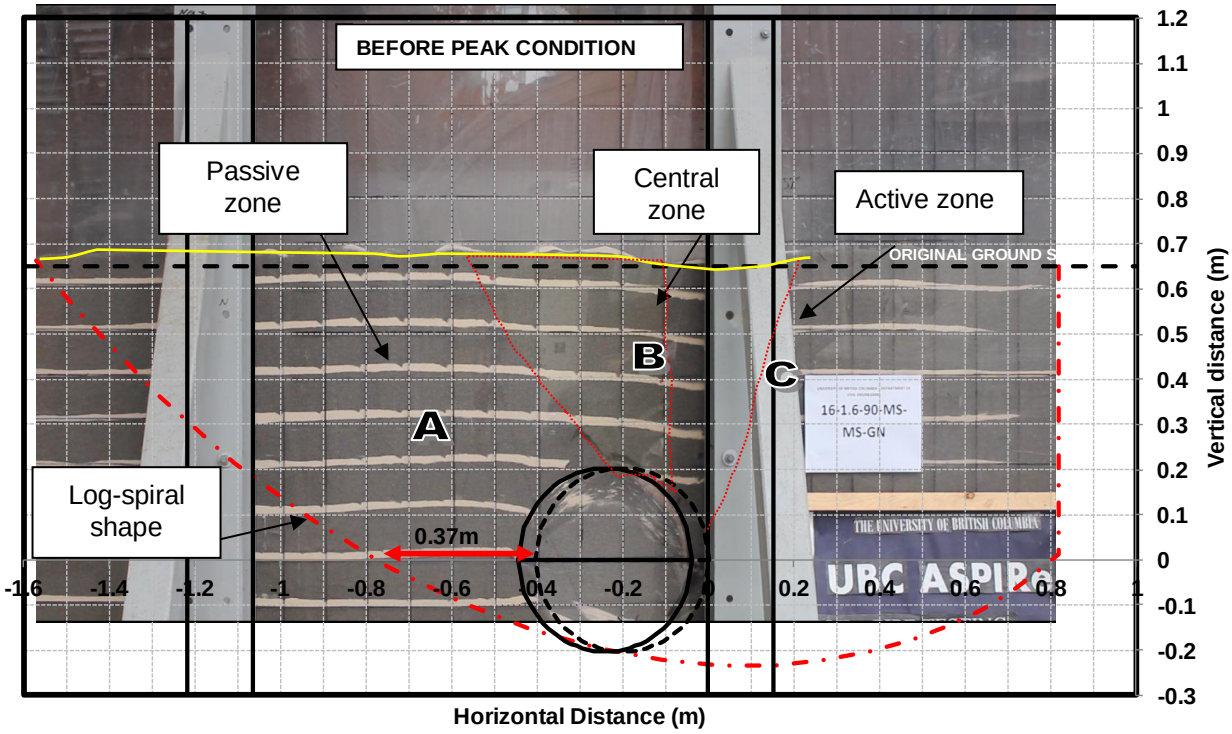

Figure 4.5: Backfill soil deformation during Test 16-1.6-90H-MS-MS-GN – Y'=0.07D.

The patterns of soil deformation at the onset of maximum soil restraint or at a normalized pipe displacement of Y'=0.25D are shown in **Figure 4.6**. The maximum soil restraint (plateau) reached by the soil-pipe system is defined as failure condition in this study. These patterns reinforced the ongoing development of a passive zone which was bounded by a log-spiral shape (note that the log-spiral is traced based on the approach suggested by O'Rourke et al. 2008, see **Section 4.7.2**).

Furthermore, during this failure condition, the shear resistance along the boundaries of the central zone wedge appeared to be also fully mobilized and, thereafter, the wedge started to move downwards with a direction opposing

the pipe displacement. This condition is evidenced by the shear distortions of the white lines observed in the central zone. A similar soil deformation pattern was found during the numerical simulation (see Chapter 7). The downward movement of the central (B) and active (C) zones created a settlement region located above the initial position of the pipe. In addition, the initiation of ongoing upward pipe displacement can be appreciated from **Figure 4.6**.

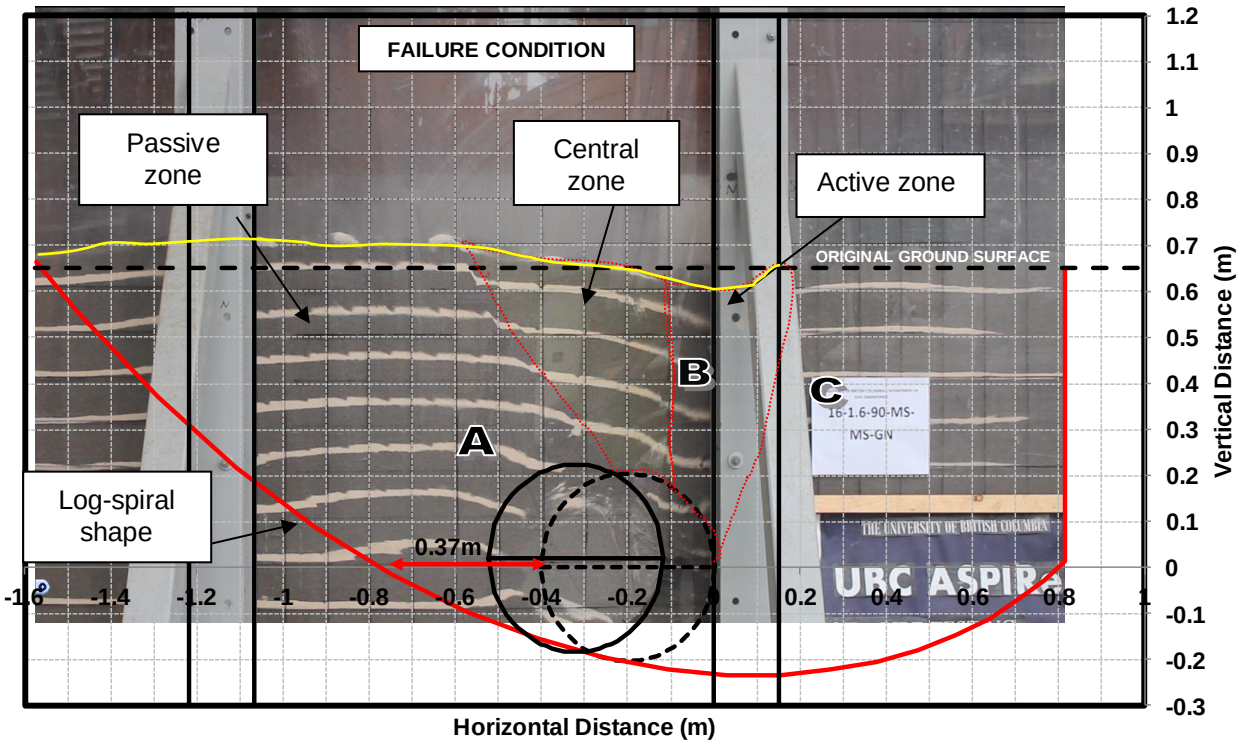

Figure 4.6: Backfill soil deformation during test 16-1.6-90H-MS-MS-GN – Y'=0.25D.

After the maximum lateral soil restraint was overcome during the 16-1.6-90H-MS-MS-GN test by the ongoing imposed lateral pipe displacements (Y' > 0.25D), the passive zone A was no longer in force equilibrium and a stage condition of complete failure was developed for the soil mass in front of the

pipe. This condition and its associated patterns of soil deformation are shown in **Figure 4.7** for Y' = 0.8D.

During the post-failure condition (Y' > 0.25D), additional progressive failure zones (D and E) developed that moved towards the initial position of the pipe and downwards relative to the passive zone (A). At this stage of pipe lateral displacement, the size of passive zone (A) reduced considerable.

Figure 4.7 shows that the pipe kept compressing the soil mass in front of it as evidenced by the highly buckled white layers and the recorded stresses presented in **Figure 4.3**. However, these observed patterns of soil deformation were no longer associated with the initial restraint imposed by the soil, but rather by ongoing movement of the soil mass along a log-spiral failure surface due a post-failure condition.

As seen in **Figure 4.7**, the pipe moved along the passive failure surface represented by a log-spiral shape during the post-failure condition**.** The overall ratio of vertical to horizontal pipe movement observed at the end of the test was about 13° to 14° (0.09 m / 0.37 m). A large settlement or void region was also developed in the initial central (B) and active (C) zones. The pattern of surface movement and settlement for the post-failure condition is shown in **Figure 4.8**.

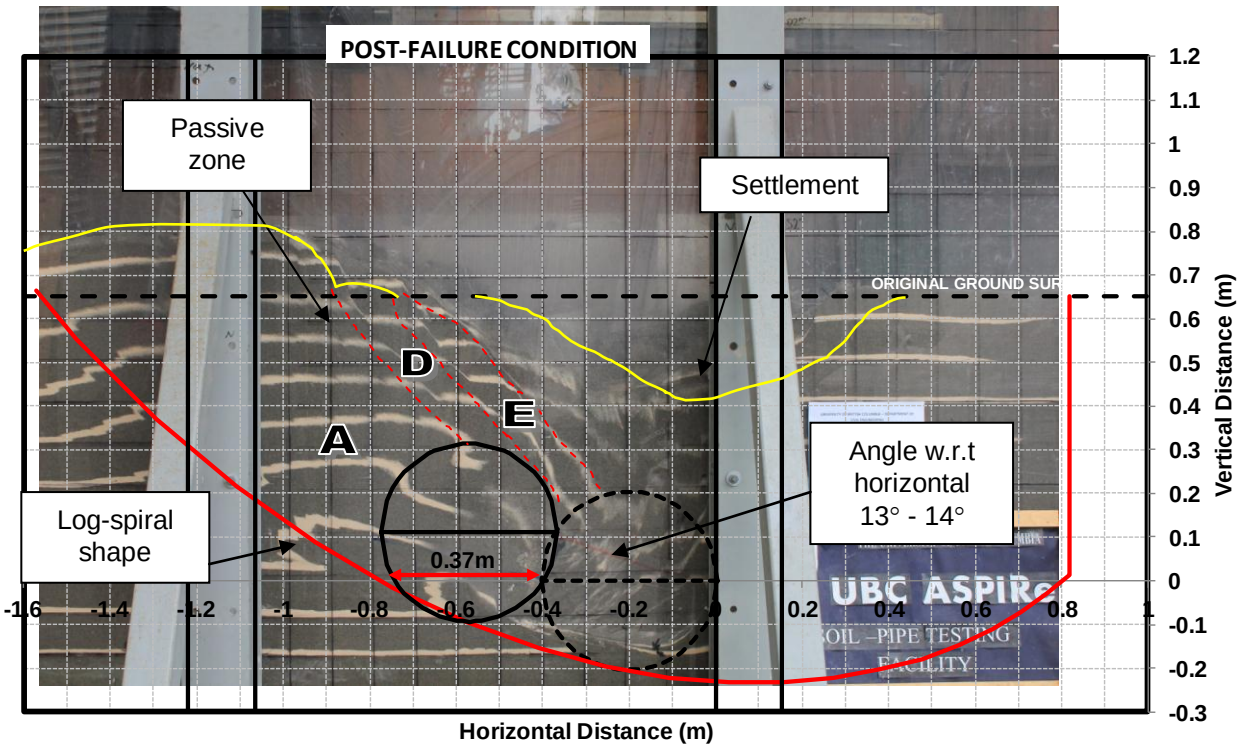

Figure 4.7: Backfill soil deformation during test 16-1.6-90H-MS-MS-GN – Y'=0.8D.

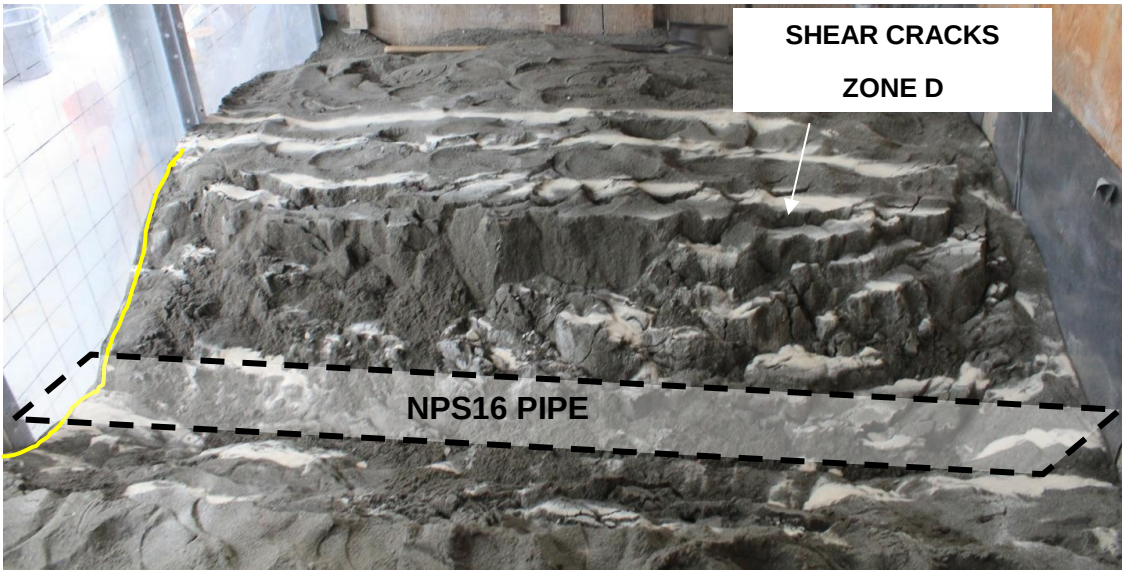

Figure 4.8: Surface deformation of sand backfill Test 16-1.6-90H-MS-MS-GN – Y'=0.8D (looking towards the front of the chamber).

4.3 Results of Lateral Soil Restraint Tests on Pipe Buried in Road Mulch Backfill

4.3.1 Normalised Load-Displacement Response on Road Mulch

Variations of normalised lateral soil restraint as a function of pipe displacement for Tests 18-1.9-90H-RM-RM-GN-1 and 18-1.9-90H-RM-RM-GN-2 under lateral pulling are shown in **Figure 4.9**. The results are for NPS18 pipe specimens buried in road mulch with a cover depth to diameter (H/D) ratio of 1.9. Both tests have similar configurations. Test 18-1.9-90H-RM-RM-GN-2 was carried out to evaluate repeatability. The use of road much as a backfill material simulates cases in which the pipeline is buried in trenches made in native stiff soil, and backfilled with essentially the same material.

As can be seen from **Figure 4.9**, the two lateral tests resulted in fairly similar N_{qh} = P / (γ·D·H·L), vs. normalised pipe displacement Y' relationship. An increase in the levels of lateral soil restraint was observed for the tests during the early stages of pipe displacement; then the rate of increase diminished progressively with further pipe displacement until a relatively constant or maximum lateral soil restraint value was recorded for the rest of the tests.

The maximum lateral soil restraint for Test 18-1.9-90H-RM-RM-GN-2 was N_{qh} = 10.2 (75.8 kN/m), which was slightly less than the about N_{qh} = 11 (82 kN/m) recorded for 18-1.9-90H-RM-RM-GN-1. The maximum lateral soil restraints for both tests were reached at a normalised pipe displacement of about 0.35D to 0.45D. These normalised pipe displacements were larger than those observed for sand (less than 0.25D). This suggests that larger displacements were required to mobilize the higher peak shear resistance of road mulch material (mixture of sand and gravel particles). This condition was also observed in the direct shear soil element test (Appendix A).

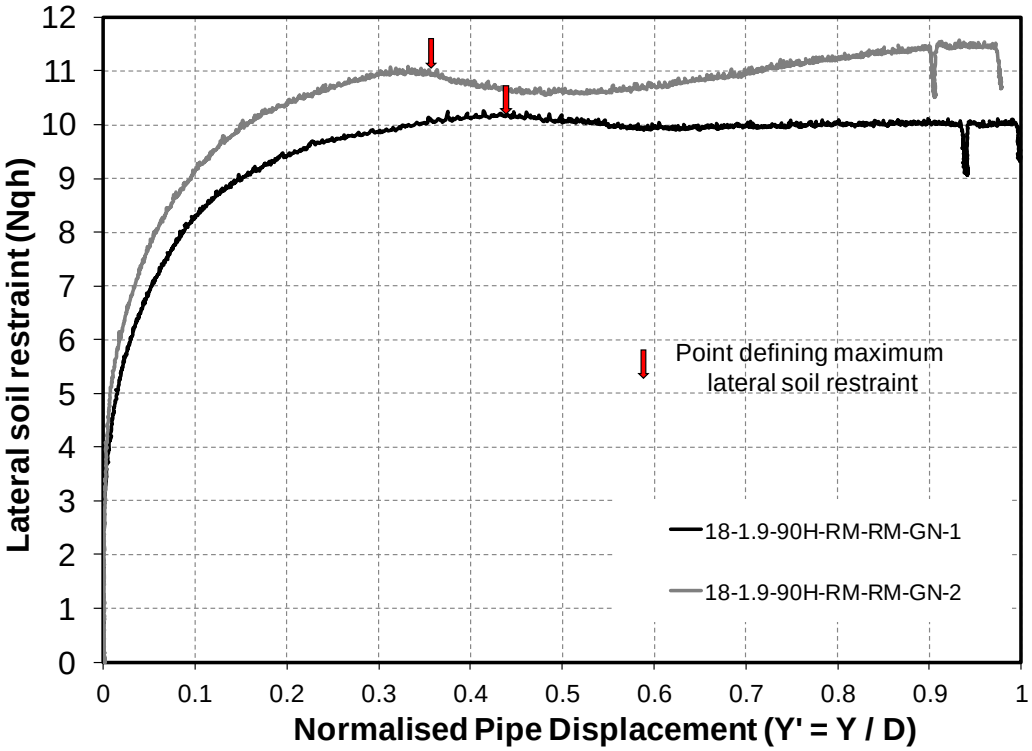

Figure 4.9: Normalised load-displacement relationships for NPS18 pipe specimen with H/D=1.9 buried in road mulch during lateral pulling

4.3.2 Recorded Contact Pressure for Road Mulch Backfill during Lateral Pulling

The variation of pressure, from pressure transducers PT-1, PT-2 and PT-3, with normalized pipe displacement, Y', recorded during Test 18-1.9-90H-RM-RM-GN-1 and 18-1.9-90H-RM-RM-GN-2 is shown in **Figure 4.10** and **Figure 4.11**, respectively. As described previously, these tests were for NPS18 pipe specimens buried in road mulch with a cover depth to diameter (H/D) ratio of 1.9.

Among the pressure transducers, PT-1 and PT-2 showed higher pressure than that recorded by PT-3 for Test 18-1.9-90H-RM-RM-GN-1. In contrast, PT-1 showed the lowest pressure for Test 18-1.9-90H-RM-RM-GN-2. In

general, the pressure measured by the pressure transducer for both tests were very different and showed different behavior. Only the pressure measured by PT-2 for Test 18-1.9-90H-RM-RM-GN-2 seemed to be associated with the lateral soil restraint vs. pipe displacement shown in **Figure 4.11**.

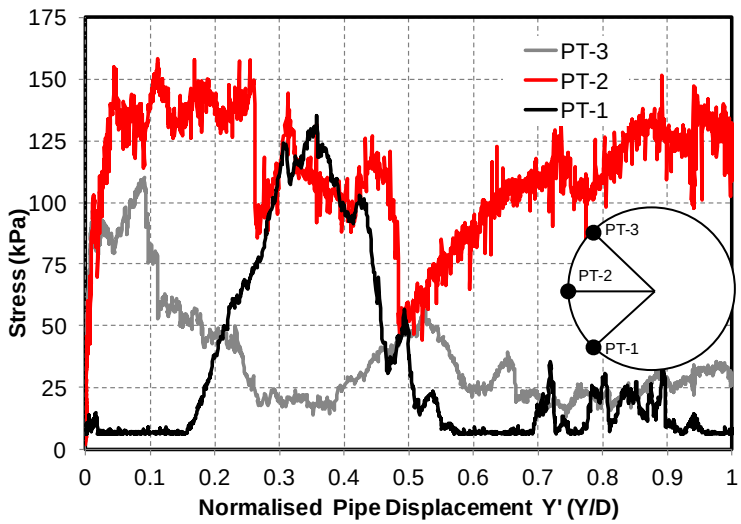

Figure 4.10: Pressure readings as a function of pipe displacement - Test 18-1.8-90H-RM-RM-GN-1.

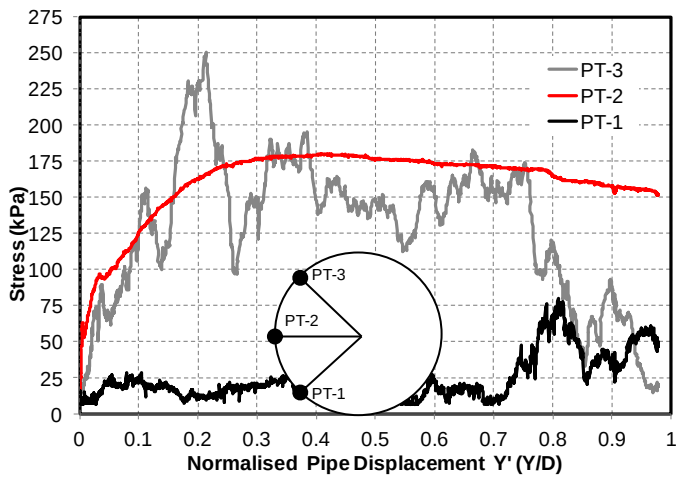

Figure 4.11: Pressure readings as a function of pipe displacement - Test 18-1.8-90H-RM-RM-GN- 2.

4.3.3 Observed Backfill Soil Deformation Geometry on Road Mulch

The patterns of soil deformation observed during Test 18-1.92-90H-RM-RM-GN-1 at a normalised pipe displacement of 0.75D are presented in **Figure 4.12** together with a log-spiral failure surface developed following the procedure described by O'Rourke et al., (2008). Similar to the sand backfill, the active (C) and passive (A) zones of soil deformation were clearly distinguishable. In particular, the passive zone (A) seemed to be appropriately bounded by a log-spiral shape. A settlement or void zone, which occurred above the initial position of the pipe and extended towards the surface of the road mulch backfill, can also be observed.

As the case for sand backfill, it can be seen from **Figure 4.12** that the pipe moved along the trace depicted by a log-spiral failure surface. In particular, the pipe rose about 0.1 m in about 0.35 m of horizontal movement. This ratio of vertical to horizontal pipe movement gives a value of 0.29 or about 16°.

At large levels of pipe displacement (Y' > 0.5D), the limits of the passive zone (A) for road mulch backfill seemed to be larger, more coherent than those observed for the passive zone in sand (see **Figure 4.8**). This is due to the nature of the road mulch skeleton, where the interparticle forces in the gravel and sand matrix created a stronger and denser backfill material that imparted more like a block-type behavior for the soil mass. These characteristics can be further appreciated from the surface deformation that occurred for Test 18-1.9-90H-RM-RM-GN-1 as shown in **Figure 4.13**.

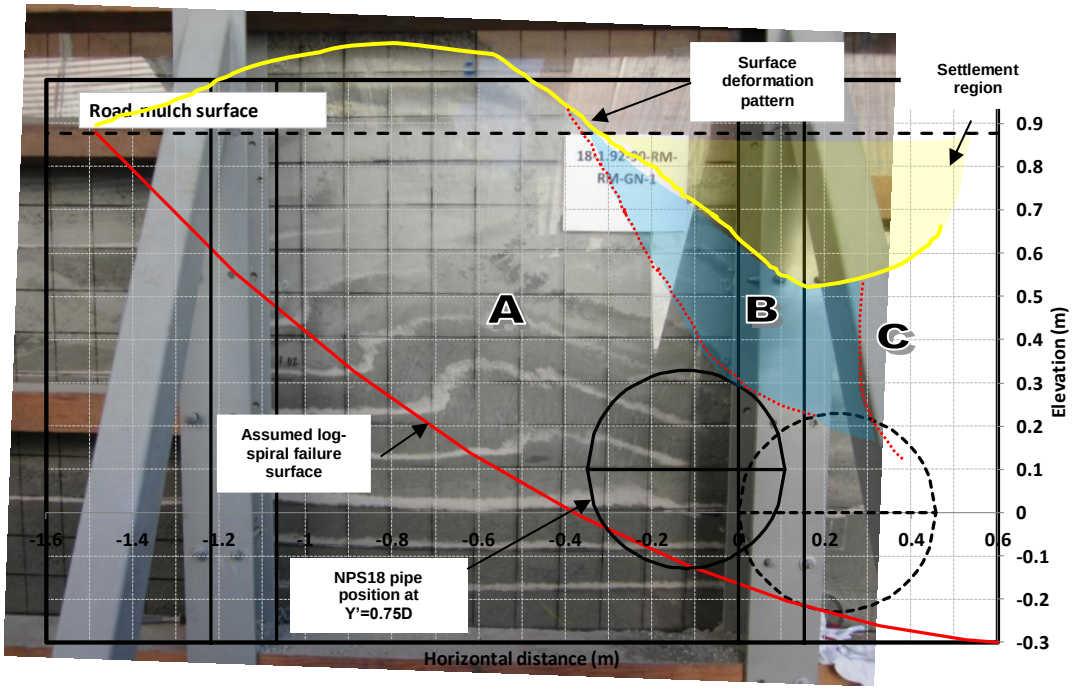

Figure 4.12: Backfill soil deformation during test 18-1.9-90H-RM-RM-GN-1 – Y'=0.75D.

Figure 4.13: Surface deformation of road mulch backfill Test 18-1.9-90H-RM-RM-GN-1 – Y'=0.75D (looking towards the front of the chamber).

4.4 Results of Lateral Soil Restraint Tests on Pipe Buried in Crushed Limestone Backfill

4.4.1 Normalised Load-Displacement Response – Crushed Limestone

Normalised lateral soil restraint, $N_{qh} = P / (\gamma \cdot D \cdot H \cdot L)$, vs. pipe displacement, Y', for NPS16 (406-mm diameter) pipe specimen buried in crushed limestone with an overburden ratio H/D of 1.6 under lateral displacement is shown in **Figure 4.14**. The soil-pipe interaction for Test 16-1.6-90H-LM-LM-GN showed a peak normalised lateral soil restraint N_{qh} of about 12 (53.9 kN/m) at a normalised pipe displacement of around 0.1D; followed by a post-peak drop in lateral soil restraint. A condition of constant lateral soil restraint of N_{qh} 10 for the pipe specimen was achieved after Y' = 0.3D. The presence of a peak followed by a drop suggests a more dilatant behavior for the crushed limestone under lateral pulling than those recorded for tests on sand and road mulch backfills. Under the premise claimed by O'Rourke et al. (2008) that the backfill dilation angle is related to the vertical to horizontal ratio of pipe displacement, the ratio observed from the test on crushed limestone should also be higher than those observed from the test on the other backfill materials. This condition will be verified in **Section 4.7.1.3**.

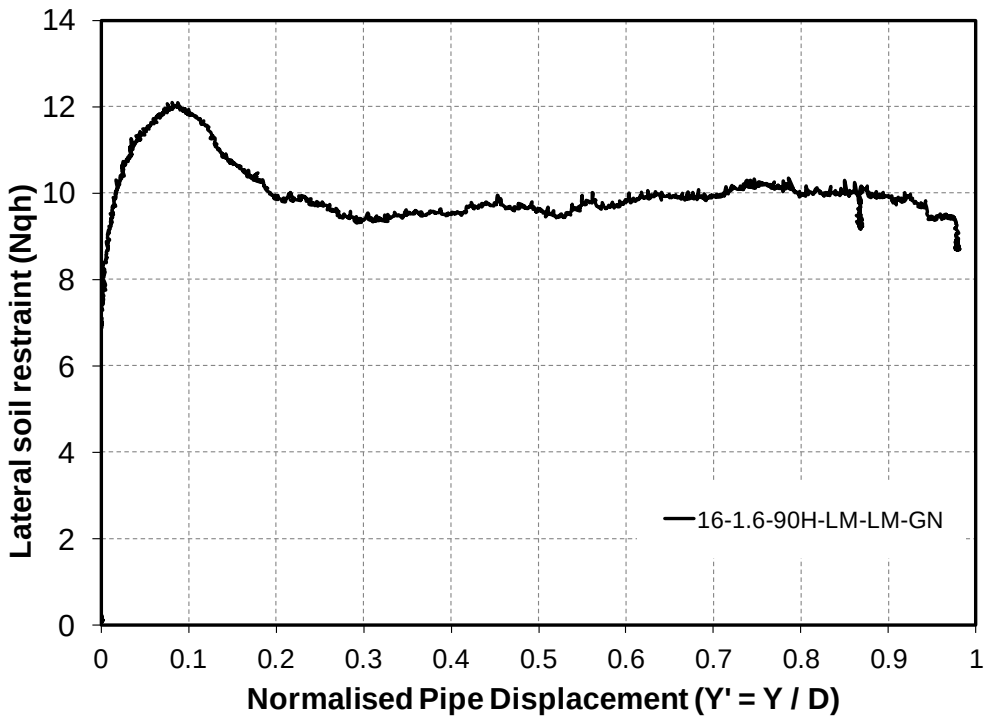

Figure 4.14: Normalised load-displacement relationships for NPS16 pipe specimen with H/D=1.6 buried in limestone during lateral pulling

4.4.2 Recorded Contact Pressure for Crushed Limestone Backfill during Lateral Pulling

The variation of stresses, from pressure transducers PT-1, PT-2 and PT-3, with normalized pipe displacement, Y', recorded during Test 16-1.6-90H-LM-LM-GN on NPS16 pipe buried in crushed limestone is shown in **Figure 4.15**. For this test, the higher stresses were recorded by the pressure transducers PT-2 and PT-3 during the compression of the crushed limestone imposed by the change in lateral pipe position. PT-1 recorded constant values that were equal to the initial stress level before the test. The maximum lateral stress, recorded by PT-2, rose and fell between 100 to 150 kPa and occurred during normalised pipe displacements in the range between 0.03D to 0.1D. These levels of maximum stress are in agreement with the maximum mobilized

lateral soil restraint (N_{qh} = 12) presented in **Figure 4.14**. After 0.4D, the stress recorded by PT-2 dropped to a value of around 75 kPa until a normalised pipe displacement of 0.4D. Thereafter, the stress kept dropping to a value close to 25 kPa. This behavior does not match the constant lateral restraint observed in **Figure 4.14**. This inconsistency may be due in part to the particle size of crushed limestone (D_{50} of about 15 mm) which is comparable with the diameter of the pressure transducer of 19.1 mm. The particle arrangement in the vicinity of the pressure transducers, therefore, could cause particle arching around the transducer or induce contact separation from the pressure transducer-limestone interface.

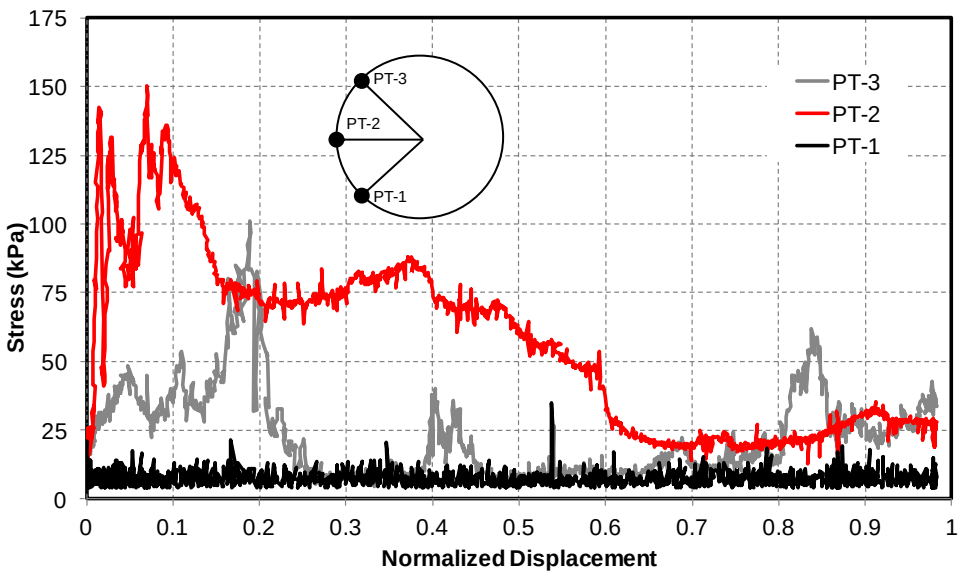

Figure 4.15: Pressure readings as a function of pipe displacement - Test 16-1.6-90H-LM-LM-GN.

4.4.3 Observed Backfill Soil Deformation Geometry for Crushed Limestone

The surface deformation patterns observed from Test 16-1.6-90H-LM-LM-GN at Y'=0.1D or at maximum soil restraint are shown in **Figure 4.16**. As expected, levels of surface deformation were too small to be directly observed, because the soil mass was still in equilibrium with the applied pulling load. Once this equilibrium was overcome, large levels of plastic and irrecoverable deformation were observed in the surface of the crushed limestone. These conditions can be observed from **Figure 4.17** and **Figure 4.18** at Y'=0.94D.

It is interesting to note that because of the size and the uniformly graded particle distribution of the crushed limestone, the particles flowed more easily after the maximum soil restraint was achieved. This was particularly evident in the soil zone above the pipe. Similarly to the observed patterns of deformation for tests on sand and road mulch backfills in the passive zone (A), the failure surface for the passive zone of the crushed limestone test can be bounded by a log-spiral shape, as shown in **Figure 4.18**.

Figure 4.16: Surface deformation of crushed limestone backfill - Test 16-1.6-90H-LM-LM-GN – Y'=0.1D.

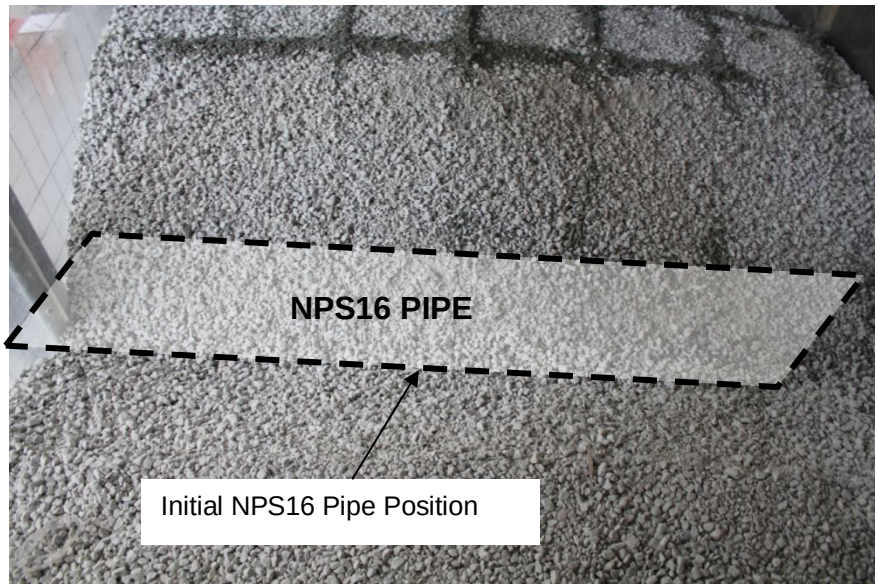

Figure 4.17: Surface deformation of crushed limestone backfill - Test 16-1.6-90H-LM-LM-GN – Y'=0.94D.

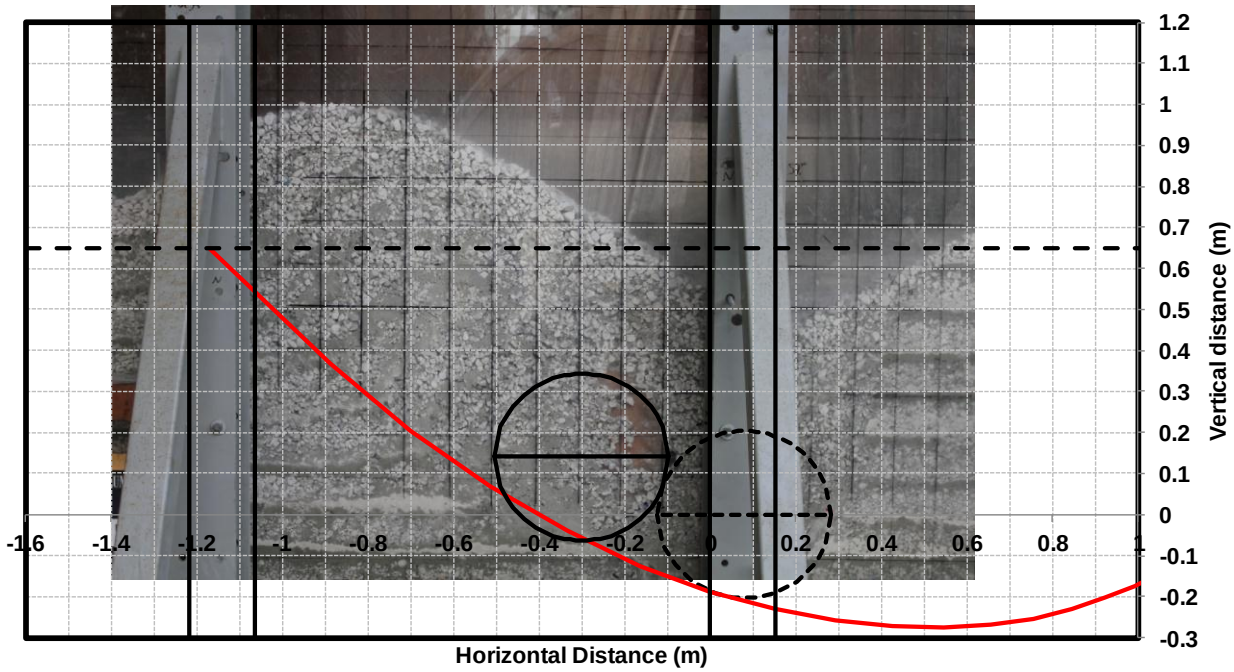

Figure 4.18: Backfill soil deformation during Test 16-1.6-90H-LM-LM-GN – Y'=0.94D.

4.5 Results of Tests on Reduction of Lateral Soil Restraint by Geosynthetic Fabrics - Sand Backfill

Karimian (2006) hypothesized that reduced levels of lateral soil restraint might occur if the distance between a pipe specimen and a boundary with a hard trench is increased, thus, minimizing the confinement of soil between the pipe and the hard trench. A goal of the testing program of this work is to assess the impact on soil restraint behavior under geotextile-lined trench configurations from a change in the distance between the pipe and the trench wall.

A series of six test configurations were conducted utilizing a trench with a hard boundary, with and without two layers of geotextile fabric, moist sand trench backfill with a dry density of 1,600 kg/m^3, and a space between the pipe and the hard boundary of 0.5D, 1.0D and 2.0D as illustrated in **Figure 4.19**. The primary purpose of these tests is to identify the spacing necessary to mobilize sliding between the layers of geotextile fabric, and therefore, achieve the expected reduction of soil restraint in geotextile-lined pipe trenches. In this same line of thinking, one additional test was conducted with a space between the pipe and the hard boundary of 0.5D, but with only one geotextile, to compare its result with that with two geotextiles.

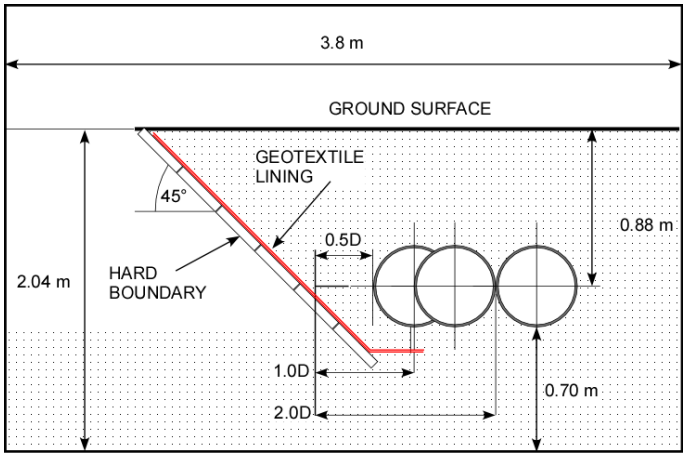

Figure 4.19: Schematic of hard boundary test arrangement.

4.5.1 Normalised Load-Displacement Response for Geotextile-Lined Pipeline Trench - Sand Backfill

The development of soil restraint as a function of relative lateral pipe displacement for test configurations with a trench wall-pipe distance (S) of 0.5D and without and with geofabric lining, 18-1.9-90H-HB-MS-GN-45-0.5D-1 and 18-1.9-90H-HB-MS-GY-45-0.5D-2, respectively, is shown in **Figure 4.20**. From the results of these tests in can be observed that the lateral soil restraint increased with pipe displacement until a constant lateral soil restraint was reached (a plateau) at normalized pipe displacements that ranged from 0.1D to about 0.3D to 0.4D. Further pipe displacements beyond 0.3D produced a continuous and significantly nonlinear increase of lateral soil restraint on the pipe. This later behavior suggests the development of additional soil deformation mechanisms due to the proximity of the pipe with respect to the rigid trench wall.

From the data plotted in **Figure 4.20**, it can be seen that for tests without and with geotextile fabric the lateral soil restraint at the plateau level was only reduced by about 15% due to the application of the geotextile-lining. Similar limited benefit observed for mitigation configurations based on geotextile-lined trenches and the development of an increase in lateral soil restraint at large pipe displacements were also observed by Karimian et al. (2006).

Further tests were conducted to investigate the effect of the trench wall on the mechanical behavior during soil-pipe interaction. Tests 18-1.9-90H-HB-MS-GN-45-1D-1 and 18-1.9-90H-HB-MS-GY-45-1D-2 were carried out with a trench wall-pipe distance (S) of 1D and without and with geotextile lining, respectively. The results of these tests are presented in **Figure 4.21**. It can be observed that soil-pipe response from these tests were very similar, reaching levels of lateral soil restraint N_{qh} of about 7.6 (50 kN/m). It is important to note that this level of lateral soil restraint is similar to those recorded for tests on pipe specimen buried in moist sand without trench wall (18-1.9-90H-MS-MS-GN-1 &

18-1.9-90H-MS-MS-GN-2). This suggests that the trench wall did not influence the development and the mobilisation of maximum level of lateral soil restraint under small lateral pipe displacements during the tests with wall-pipe distance (S) of 1D.

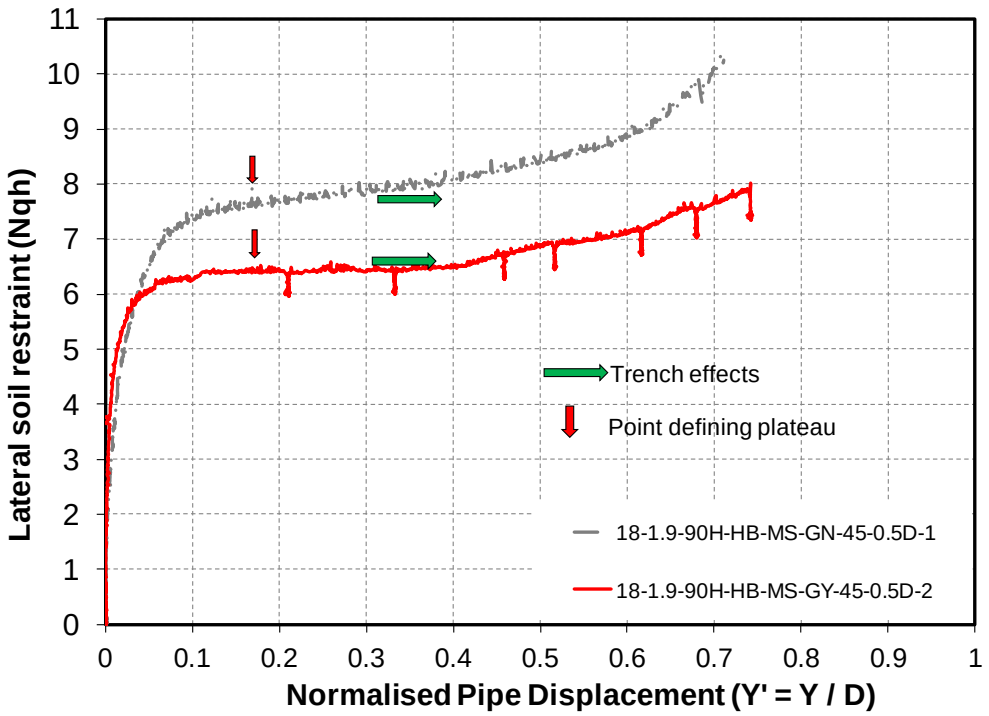

Figure 4.20: Lateral soil restraint in sloped trench walls with moist sand backfill and with (GY) and without (GN) geotextile lining.

From the data plotted in **Figure 4.21** it can be seen that for tests with wall-pipe distance (S) of 1D the nonlinear increase of lateral soil restraint, due to trench wall effects, occurred after the pipe reached Y' of about 0.6D. This level of pipe displacement is about twice the pipe displacement required for the onset of lateral restraint increase after the plateau observed in the test with a trench wall-pipe distance (S) of 0.5D (18-1.9-90H-HB-MS-GY-45-0.5D-2).

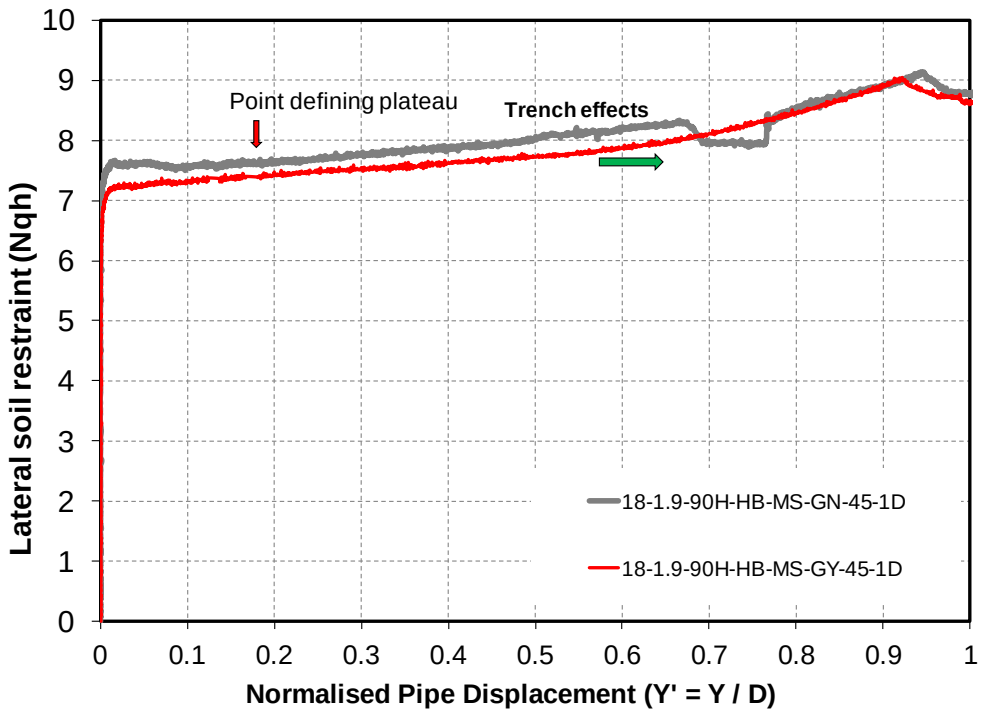

Figure 4.21: Lateral soil restraints in sloped trench walls with S=1D with moist sand backfill and with (GY) and without (GN) geotextile lining.

Results for tests 18-1.92-90H-HB-MS-GN-45-2.0D and 18-1.9-90H-HB-MS-GY-45-2.0D, which were carried out with a trench wall-pipe distance (S) of 2D, are presented in **Figure 4.22**. The maximum lateral soil restraints for both tests were also similar, with an N_{qh} of about 7.7 (51 kN/m). Furthermore, the results from tests with S of 2D are also similar to the results from tests carried out with no trench (18-1.9-90H-MS-MS-GN) or with an S of 1D for lateral pipe displacements less than 0.6D (18-1.9-90H-HB-MS-GY-1D) reported previously (i.e. no further increase of lateral soil restraint due to trench wall effects). This suggests that the maximum lateral soil restraint for the tests with wall-pipe distance (S) of 2D was entirely controlled by the mechanical behavior of the backfill rather than a behavior governed by the interface properties of the trench wall.

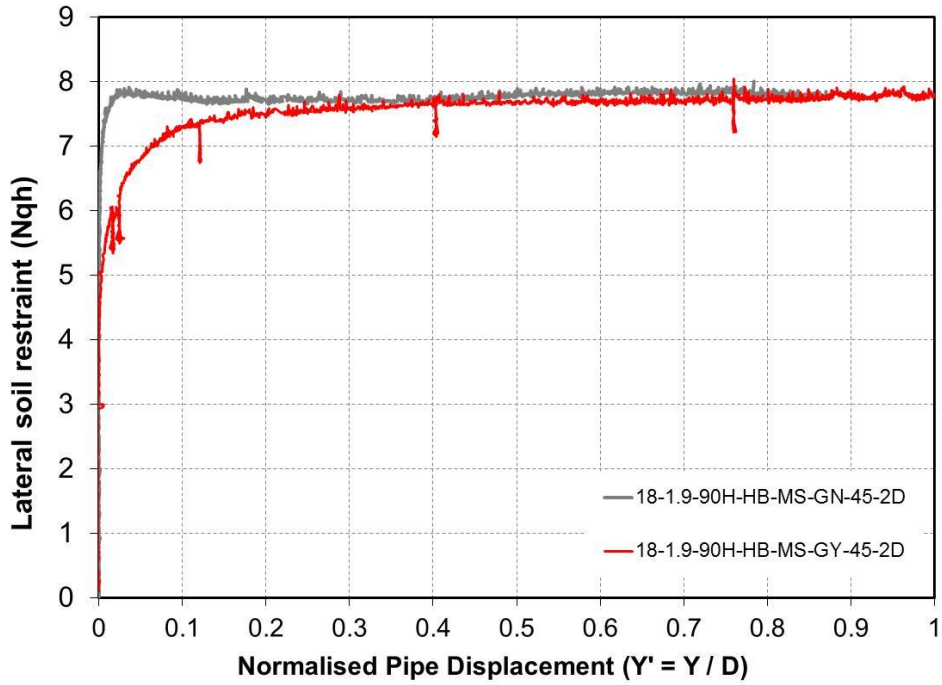

Figure 4.22: Lateral soil restraints in sloped trench walls with S=2D with moist sand backfill and with (GY) and without (GN) geotextile lining.

From the results plotted in **Figure 4.20**, **Figure 4.21** and **Figure 4.22**, there is clearly a relationship between the variation of soil restraint with displacement and the proximity of the pipe to the trench wall (i.e., trench wall-pipe distance, S). Furthermore, the effect of the proximity of the pipe to the trench wall on the soil restraint seems to be realized only when pipe is at distances less than 1D from the trench wall.

An additional test was carried out with a trench wall-pipe distance, S, of 0.5D but with only one geotextile (18-1.9-90H-HB-MS-GY-45-0.5D-3). The result of this test is presented in **Figure 4.23** along with the result for lateral soil restraint obtained from a similar test but with two layers of geotextile (18-1.9-90H-HB-MS-GY-45-0.5D-2). By comparing the levels of lateral soil restraint at the plateau portion of the load vs. pipe displacement from both tests, it can be deduced that both the responses are similar. This suggests that the benefit of

using two layers of geotextile fabric to reduce levels of lateral soil restraint is minimal. This observation suggests that the level of lateral soil restraint at the plateau portion should be controlled by the backfill soil-geotextile interface properties and not by the geotextile-geotextile properties. This condition will be evaluated and verified in subsequent sections.

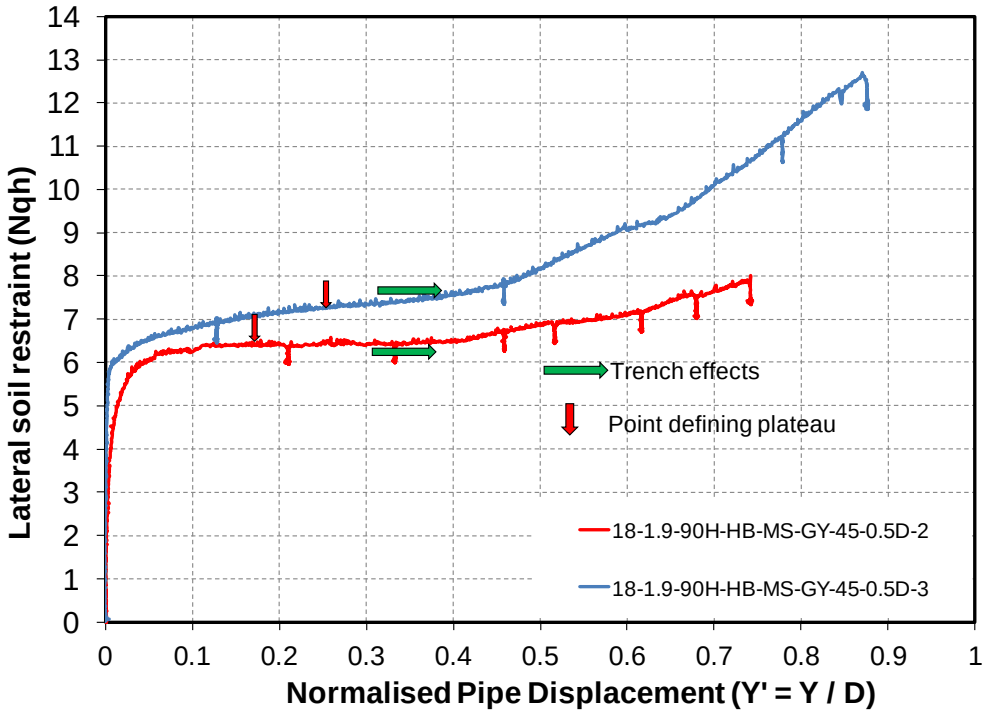

Figure 4.23: Lateral soil restraints in sloped trench walls with moist sand backfill and with geotextile lining.

In addition, the results from both tests indicate that the trench effects occurred at approximately similar levels of lateral pipe displacement (around Y'=0.3D). However, the rate of increase of lateral soil restraint, after Y' 0.3D, was higher for the test with only one geotextile than it was for the test with two geotextiles. This characteristic suggests that there may be a relative benefit in placing two geotextiles. However, the overall behavior indicates that regardless of the use of 2 geotextiles, 1 geotextile or no geotextile for lining the trench wall, a continuous increase in the levels of lateral soil restraint develops for pipelines

buried in trenches with a trench wall-pipe distance, S, of 0.5D, which is the most common distance use in the field. This increase can be effectively eliminated by simply placing the pipe at a distance larger than 1D from the trench wall.

4.5.2 Recorded Contact Pressure for Geotextile-Lined Pipeline Trenches - Sand Backfill

Three pressure transducers were also mounted on the pipe to record the variation of soil pressure during tests that involve rigid and native (hard soil conditions) trench wall. The transducer configuration is similar to that used for plain cases (no trench). The values recorded by the pressure transducers during the tests with trench conditions are more variable than those presented in **Section 4.2** to **4.4**. This is because a uniform density along the pipe was even more difficult to achieve due to space considerations imposed by the trench wall. Therefore, many of the data obtained from the pressure transducers were not consistent with their corresponding lateral soil restraint vs. normalized pipe displacement relationship. The data presented in **Figure 4.24** for the test on NPS18 with a trench wall distance-to-pipe ratio of 0.5D and lined with two layers of geotextile (18-1.9-90H-HB-MS-GY-45-0.5D-2) is an example of this situation.

As shown in **Figure 4.24**, a rapid increase in the pressure recorded by PT-2, which was the one aligned with the lateral pulling direction, occurred during the test. The maximum value of stress was 170 kPa and occurred at a normalised pipe displacement of about 0.2D. This point seems to coincide with the maximum lateral soil restraint at the plateau level shown in **Figure 4.23**. However, the overall response shape is different. PT-2 recorded a drop in the pressure to a value of 100 kPa until a Y' of 0.35D, instead of the increasing response observed from the load vs. displacement relationship. The pressure recorded by PT-1 and PT-3 were essentially constant and less than 20 kPa. Therefore, the pressure vs. normalised pipe displacement

behavior presented in **Figure 4.24** shows no apparent similarity with the lateral soil restraint results from **Figure 4.23**.

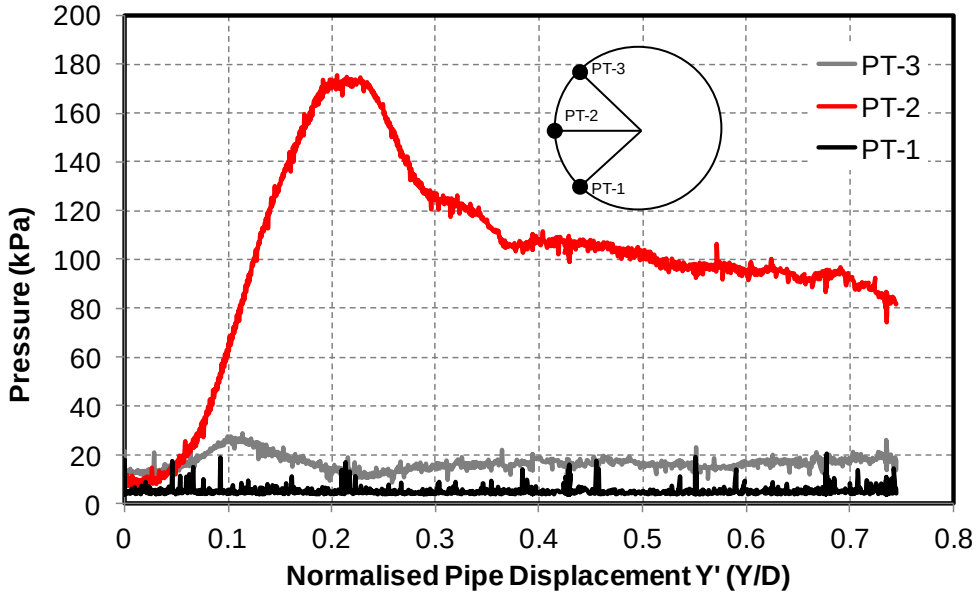

Figure 4.24: Pressure readings as a function of pipe displacement - Test 18-1.9-90H-HB-MS-GY-45-0.5D-2.

The variation of soil pressure recorded by PT-1, PT-2 and PT-3 during Test 18-1.9-90H-HB-MS-GY-45-0.5D-3 can be observed in **Figure 4.25**. This test was carried out with a trench wall distance-to-pipe ratio of 0.5D and lined with only one layer of geotextile. A displacement of about 0.2D was required to reach the maximum level of soil pressure during the test. The observed pattern of behaviour recorded by PT-2 appears to be similar to the lateral soil restraint behaviour observed in **Figure 4.23**.

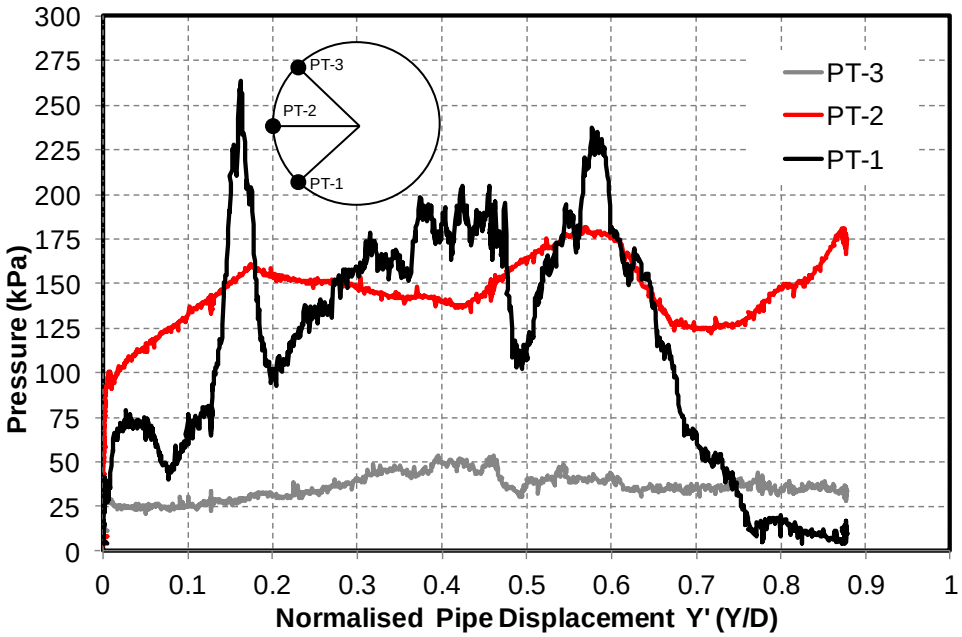

Figure 4.25: Pressure readings as a function of pipe displacement - Test 18-1.9-90H-HB-MS-GY-45-0.5D-3

4.5.3 Observed Sand Backfill Deformation Geometry for Geotextile-Lined Pipeline Trench – Sand Backfill

Patterns of soil deformation for Test 18-1.9-90H-HB-MS-GY-45-0.5D-2 at Y'=0.05D are illustrated in **Figure 4.26**. At this pipe displacement, the level of lateral soil restraint reached its maximum value (N_{qh} of about 6.4), and therefore, corresponded to a failure condition, as can be verified by the load vs. displacement response shown in **Figure 4.23**. As can be seen from the **Figure 4.26**, a passive wedge (A) bounded by the trench wall was developed in front of the pipe, together with a central zone (B), and an active zone (C, not directly observed from **Figure 4.26**) during the lateral pulling test.

As already deduced from the load vs. pipe displacement relationships for tests with or without trench wall, the trench wall alters the soil-pipe interaction response. This is due to the formation of a failure surface different than the

log-spiral shape, which bounds the passive zone for tests without a trench wall.

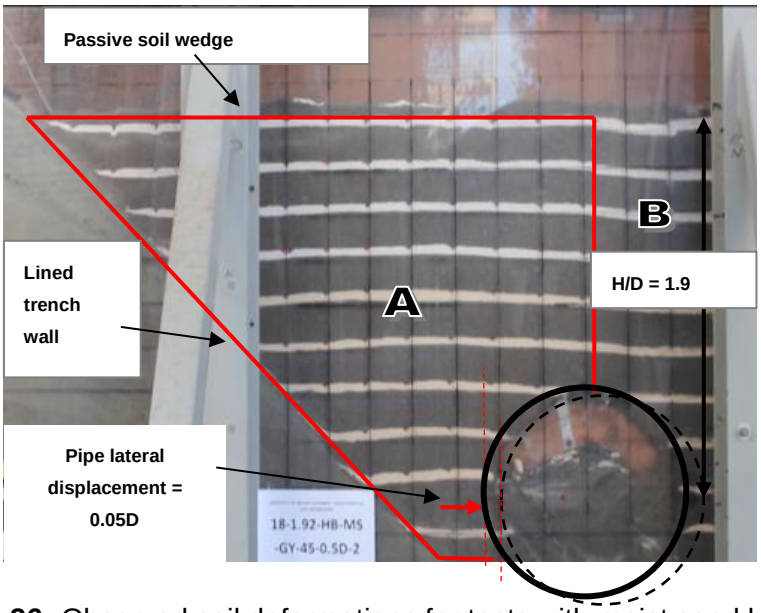

Figure 4.26: Observed soil deformations for tests with moist sand backfill at Y'=0.05D. Note that grid on Plexiglas is 0.1 x 0.1 m.

Patterns of soil deformation for the same test (18-1.9-90H-HB-MS-GY-45-0.5D-2), but at Y'=0.45D are illustrated in **Figure 4.27**. At this pipe displacement, the level of lateral soil restraint N_{qh} was 6.8 and corresponded to the risen portion of the load vs. pipe displacement relationship due to the trench effects, as can be seen from **Figure 4.23**.

As shown in **Figure 4.27**, the pipe was very close to the lined hard boundary and followed a lateral path of movement with an inclination of 30 to 35 degrees from the horizontal, or a change in pipe elevation of 0.26D at about Y'= 0.45D of lateral displacement. This was clearly very different to the 10 to 15 degrees observed during the test with no trench (18-1.9-90-MS-MS-GN). The change in pipe elevation with respect to horizontal pipe displacement for Test 18-1.9-90-HB-MS-GY-45-0.5D-2 appears to result from the interaction

between the imposed lateral displacements and the 45° boundary condition of the sloped trench wall.

Additional zones of soil failure developed during Test 18-1.9-90-HB-MS-GY-45-0.5D-2 at Y'=0.45D. They can be observed in **Figure 4.27**. The shape of the already developed passive zone (A) changed into a nearly narrow zone. Passive zone A rested on and displaced along the inclined wall of the trench. At this level of lateral pipe displacement, an active shear zone (E), next to the passive zone (A), was fully mobilized and moved towards the initial position of the pipe and downwards relative to the passive zone (A). A large settlement region was also developed in the initial central (B) and active (C) zones. Clearly, this behavior no longer conforms to the initial passive wedge or the associated displacement that was intended to be produced by providing a low-slip interface with two layers of geotextile fabric.

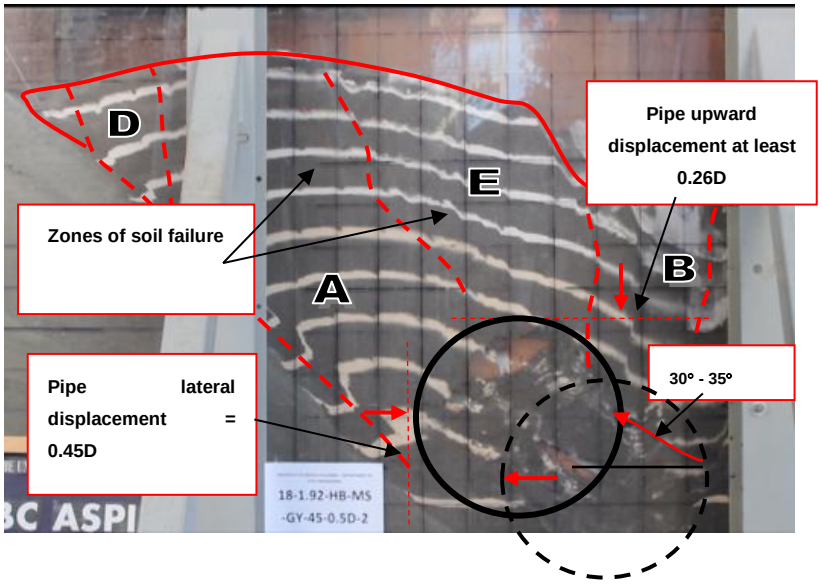

Figure 4.27: Observed soil deformations for tests with moist sand backfill at Y'=0.45D. Note that grid on plexiglass is 0.1 x 0.1 m.

The effect of a trench wall on the lateral response of buried pipelines can be further evidenced by observing the patterns of soil deformation for a test with a trench wall-pipe distance, S, of 2D (Test 18-1.9-90H-HB-MS-GY-45-2D) as presented in **Figure 4.28**. A log-spiral shape depicted by following the procedure proposed by O'Rourke et al. (2008) is also presented in this figure. The load vs. lateral pipe displacement for Test 18-1.9-90H-HB-MS-GY-45-2D is presented in **Figure 4.22.** This relationship shows a mobilization of lateral soil restraint until a maximum N_{qh} value of 7.7 is reached that remains constant for the rest of the test. As expected, this behavior is associated with the fact that the log-spiral failure surface does not intersect the trench wall, as seen in **Figure 4.28**. Thus, the lateral soil restraint is governed only by the properties of the backfill soil.

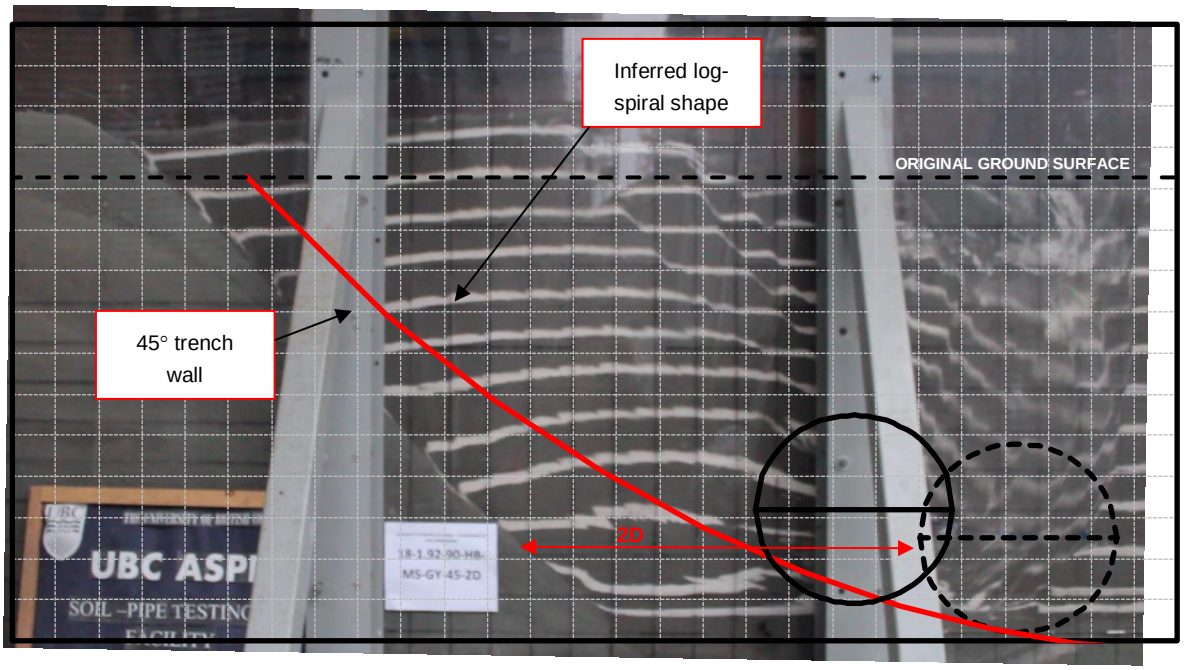

Figure 4.28: Patterns of soil deformation and inferred log-spiral failure surface developed for trench wall-pipe distance S = 2D (grid 0.1 x 0.1 m).

4.5.4 Recorded Movement of Upper Geotextile - Sand Backfill

String potentiometers were used to measure displacements of each geosynthetic fabric layer. Only data from the tests with a trench wall-pipe distance, S, of 0.5D and 2D were available due to problems that occurred during the test at 1.0D spacing. The displacement of the outer fabric layer (geotextile in contact with backfill sand) for the tests are plotted in **Figure 4.29**. The dashed line in **Figure 4.29** represents a hypothetical case of geotextile displacement for pure sliding of a rigid block along the geotextile interface.

From **Figure 4.29**, it can be seen that relative displacement between the geotextiles occurred at very small levels of lateral pipe displacement for the test with a trench wall-pipe distance, S, of 0.5D. By relating the pipe displacement with the corresponding mobilized lateral soil restraint from **Figure 4.23**, it can be concluded that geotextile slippage occurred before the soil restraint on the pipe has reached a plateau. The variation in geotextile displacement for very small levels of lateral pipe displacement was in close agreement with what would be expected if the mass of backfill sand were sliding up the trench wall as a single unit (i.e. follows the dashed line inclination). At larger levels of pipe displacement, the rate of movement of the geotextile decreased to an average of approximately 40%. This suggests deviation from block-like displacement. A reason for this behavior is the development of an additional shear failure surface that produces relative displacement between the backfill soil and the geotextile or relative displacement through the backfill alone at this stage of the test.

By contrast, geotextile slippage for the test with a trench wall-pipe distance, S, of 2D occurred at a normalised lateral pipe displacement Y' of about 0.1D. It is interesting to note that this level of normalised pipe displacement corresponds to the maximum lateral soil restraint N_{qh} of 7.7 reached for Test 18-1.9-90H-HB-MS-GY-45-2D (see **Figure 4.22**). This behavior implies that the geotextile

layer slipped after the failure of the corresponding passive zone (A), as evidenced by the patterns of soil deformation from **Figure 4.28**.

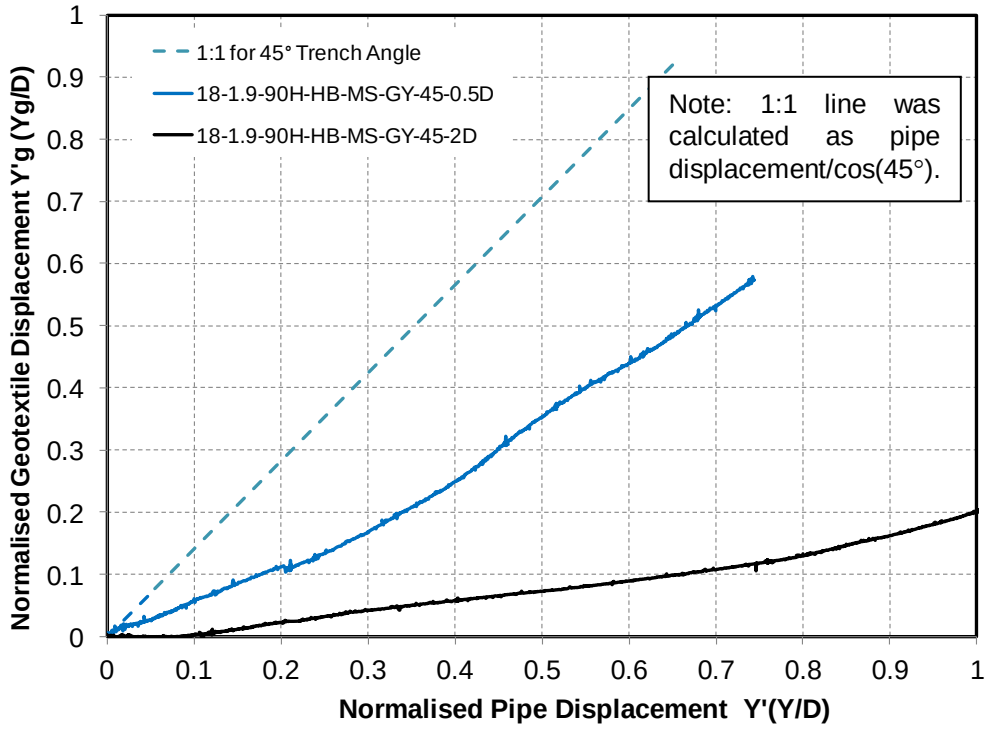

Figure 4.29: Displacement of upper geotextile for moist sand and hard trench boundary tests.

4.6 Results of Tests on Reduction of Lateral Soil Restraint by Geosynthetic Fabric - Road Mulch Backfill

The results from tests on a stronger backfill material (mixture of sand and gravel or road mulch) are presented in this section. The tests were carried out with a lined trench wall with a slope of 45 degrees and 35 degrees from the horizontal. The trench wall was constructed from the same backfill material, but to a higher density, to represent native soil conditions usually encountered in the field. Each test was repeated for quality control of the soil-pipe interaction response. The failures zones developed during the tests are similar

to those from tests on sand. Therefore, the observed deformation geometry for road mulch backfill are not discussed in this section.

4.6.1 Normalised Load-Displacement Response for Geotextile-Lined Pipeline Trench - Road Mulch Backfill

The development of lateral soil restraint as a function of relative lateral pipe displacement for test configurations in road mulch with a trench wall-pipe distance (S) of 0.5D and with a lined trench wall with a slope of 45 degrees and 35 degrees from the horizontal, 18-1.9-90H-RM-RM-GY-45-0.5D and 18-1.9-90H-RM-RM-GY-35-0.5D, respectively, is shown in **Figure 4.30**. The results from the corresponding repeated tests and the results from test without a trench are also included for discussion purposes.

The results from **Figure 4.30** display a response similar to tests with moist sand where there is an increase of lateral soil restraint after reaching a plateau. However, the effectiveness of geofabrics in reducing the lateral load imposed on the pipe is more noticeable. A reduction of about 33% and 45% of lateral soil restraint was reached for the cases of geotextile-line trench walls of 45° and 35° at normalised pipe displacements (Y') of less than 0.2D, respectively. As soil-pipe interaction continued, the reduction of lateral load diminished and as the shape of the load-displacement suggests, the lateral soil restraint can even be higher than those obtained from the plain case (no trench) of Tests 18-1.9-90H-RM-RM-GN-1 & 2 (N_{qh} greater than 11).

From the results of the tests with sand and gravel backfill, even though slippage at the geotextile interface occurred during the tests, the use of dual-geotextile lined trench configurations did not provide the benefit that was expected from this mitigation option. Even though the restraint was significantly reduced, indicating greater benefit than those observed with the moist sand tests, this reduction began to disappear as the pipe approached the trench wall (Y' $\geq$ 0.3D).

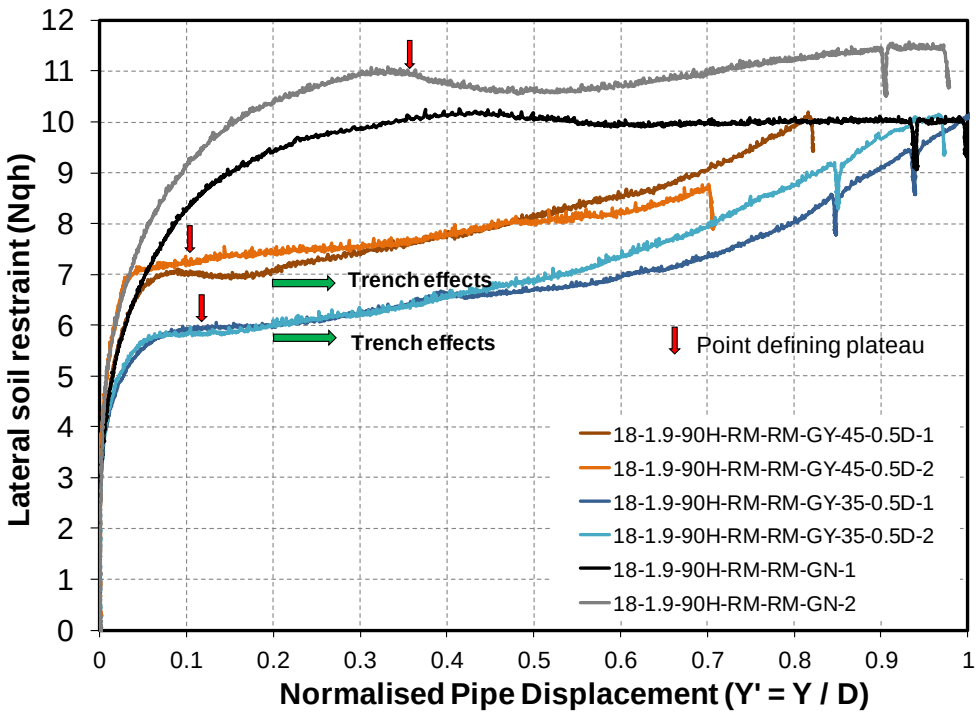

Figure 4.30: Lateral soil restraints in sloped trench walls with sand and gravel backfill.

4.6.2 Recorded Movement of Upper Geotextile - Road Mulch Backfill

Displacements of geotextile fabric layers for the tests conducted with a lined trench and road mulch are summarized in **Figure 4.31**. As with the hard trench boundary tests, the dashed lines showing the displacement of a layer of geotextile if the soil and the geotextile slide as a block along the trench wall are also provided in **Figure 4.31**.

Similarly as for the case with sand backfill, the ideal block-like displacement occurred only at very small levels of lateral pipe displacement. For larger levels of pipe displacement, the displacement of the outer geotextile layer for the 35° tests was approximately 43% of the displacement corresponding to block-like displacement of the pipe and surrounding road mulch. The ratio of

the rate of displacement between the pipe and outer geotextile layer was approximately constant for the range of displacement applied in the 35° tests. The displacement of the outer geotextile layer for the 45° tests was approximately 15% to 25% of the displacement corresponding to block-like displacement of the pipe and surrounding road mulch.

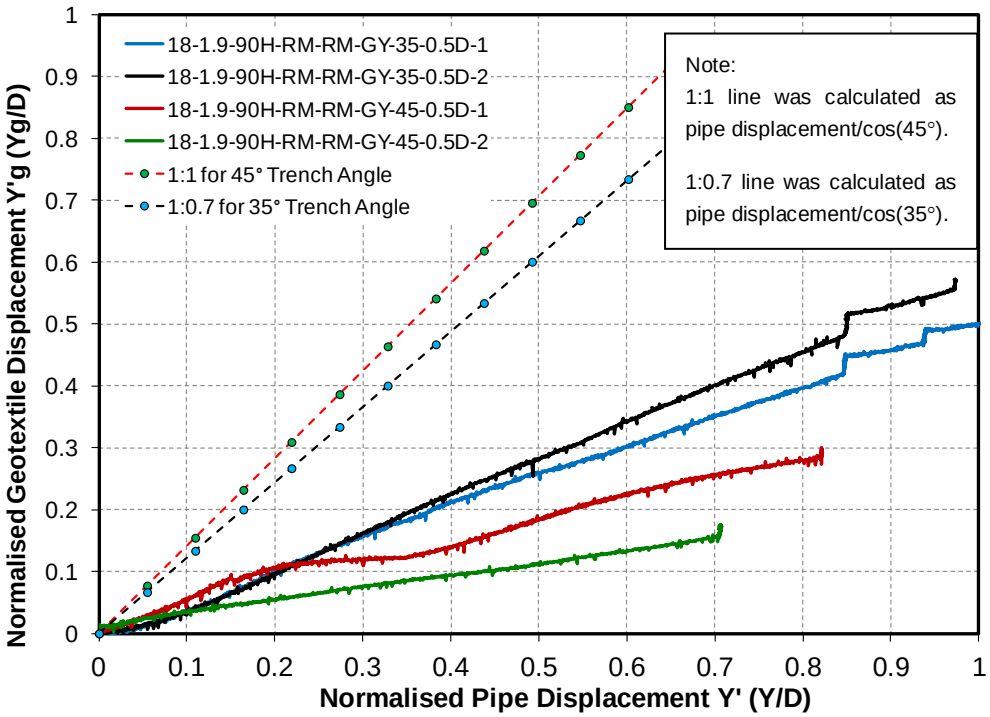

Figure 4.31: Displacement of geotextile fabric for road mulch tests.

4.7 Evaluation of Test Results

4.7.1 General Comments on Maximum Lateral Soil Restraint

The already presented test results, demonstrate that the lateral soil restraints are dependent on the pipe configuration (e.g. with trench or no trench), backfill soil properties (peak friction angle and dilation angle) and for some cases at small displacements whether the inclined trench wall is lined with a geotextile. The results have also shown that the mobilization of soil restraint depends on levels of relative lateral displacement between the buried pipeline and its surrounding soil. To this end, some very important regions can be identified from the test results that can describe the observed soil-pipe interaction behavior under lateral displacement.

A typical lateral soil restraint-normalised pipe displacement relationship for a pipeline configuration without a trench wall obtained from the experimental portion of this work is shown in **Figure 4.32**. For a pipeline configuration with a trench wall, a typical lateral soil restraint, N_{qh}, vs. normalised pipe displacement, Y', relationship is shown in **Figure 4.33**. From these figures it can be observe that, in general, the curves consist of an initial linear and transition region (Region 1); and a plastic region (Region 2) associated with a maximum lateral soil restraint. In addition, the lateral soil restraint-pipe displacement relationship for a pipeline configuration with a trench wall shows a hardening region (Region 3) due to the trench wall-soil-pipe interaction, in which no maximum lateral soil restraint appears to exist.

The linear portion of Region 1 occurs very early during the test and is associated with very small lateral pipe displacements. The plastic or plateau portion of Region 2 is associated with failure or collapse of the backfill soil mass as evidenced from the observed backfill soil deformations presented in **Section 4.2** to **Section 4.5**. In Region 2, the lateral soil restraint reaches its maximum value; it increases very little or stays constant while the pipe

displacement increases considerably. The transition portion from linear to mainly plastic behavior of Region 1 represents a condition of progressive mobilization of stresses for different levels of shear strain along a narrow zone of shear deformation that extends from the bottom of the pipe up to the backfill surface. The shape of this narrow zone of shear deformation appears to be associated with a log-spiral for cases with no trench, and a plane for cases of pipelines buried in trenches (wall trench-pipe distance less or equal to 0.5D).

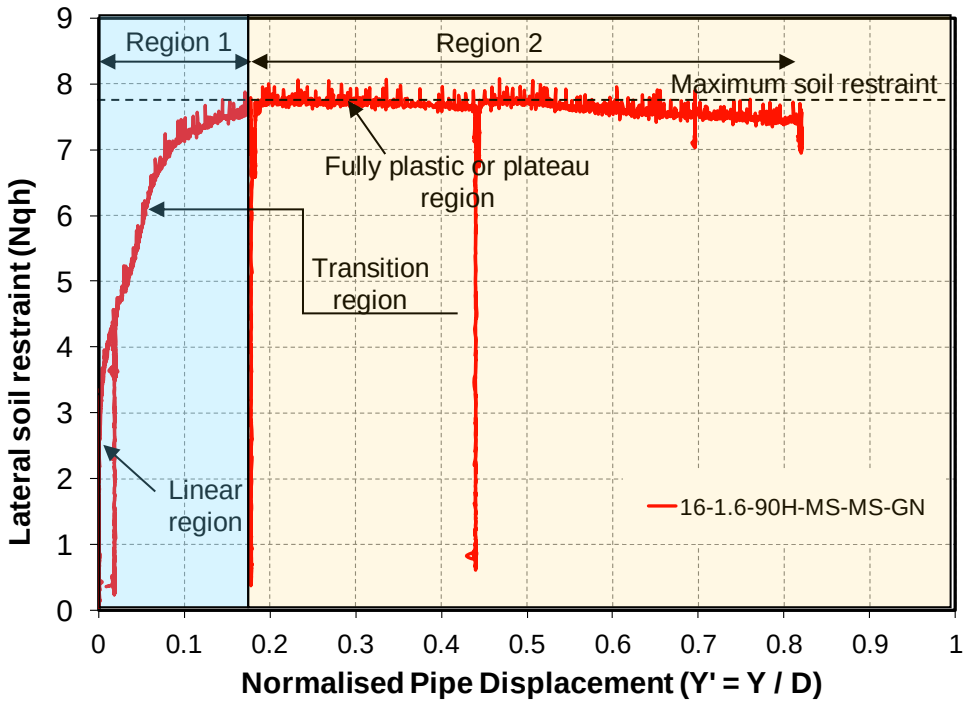

Figure 4.32: General normalised load-displacement relationship for pipelines crossing strike-slip faults without a trench boundary.

In tectonically active regions, pipelines are usually subjected to large lateral ground displacements (larger than 1 m). The sources of these ground displacements are from strike-slip surface faulting, triggered landslides, or lateral spreading. It can be inferred that these severe lateral ground displacements will fully mobilize the maximum lateral soil restraint and will place the soil-pipe interaction behavior into the plastic or eventually into the

Region 3 (hardening region) of the lateral soil restraint-pipe displacement relationship.

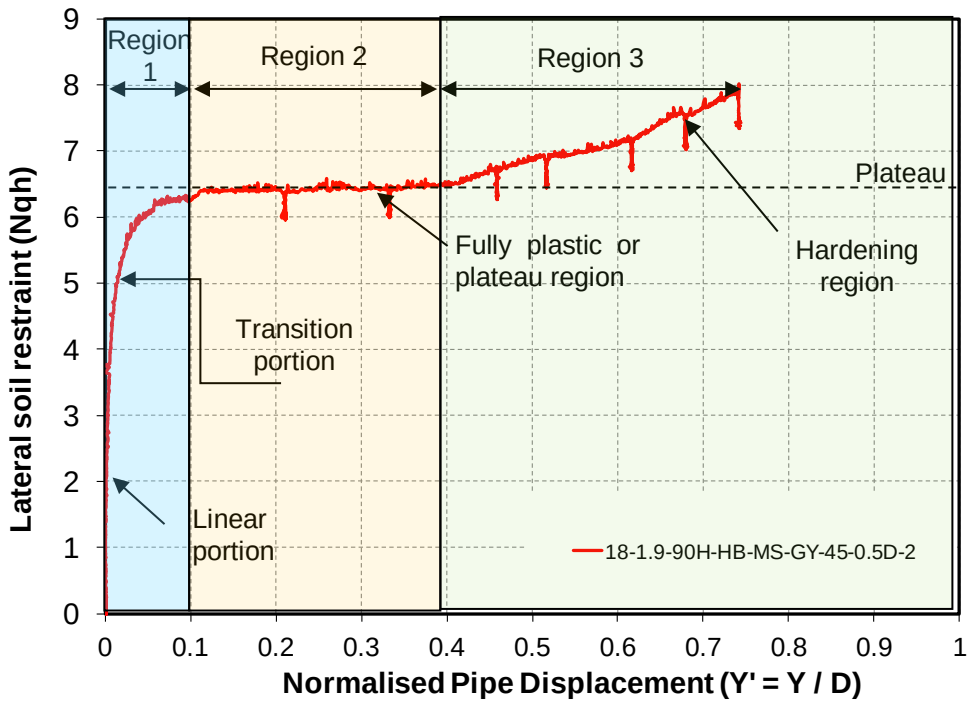

Figure 4.33: General normalised load-displacement relationship for pipelines crossing strike-slip faults with a trench boundary.

Therefore, one of the main considerations related to the earthquake performance of buried pipelines is the estimation of this maximum level of lateral soil restraint developed during large potential permanent ground movements crossing the pipeline alignment. The reason for this is that the main focus has to be on a design that meets performance expectations of the pipeline under this maximum soil restraint rather than soil design. For the latter, the designer has to limit soil deformations in the field to maintain the soil-structure system in the elastic or elastic-plastic region and, therefore, control that the imposed stress paths will not touch the failure envelopes.

For the purpose of determining the maximum level of lateral soil restraint associated with the Region 2 (plastic region), an appropriate portion of the backfill soil should be idealized as a perfectly plastic medium with no changes in its geometry so that to represent a condition in which levels of lateral pipe displacement can increase without limit while the maximum lateral soil restraint is held constant, as observed in the tests. This condition is the basis for approaches based on limit equilibrium analysis or plastic limit analysis.

Limit equilibrium analysis deals with the determination of a failure or collapse load (i.e. a load that will cause failure or collapse of a soil mass). Solutions for limit equilibrium analysis are often obtained by simple statics on a rigid body bounded by an assumed failure surface of various simple shapes (e.g. plane, circular, log-spiral) and by using Coulomb's failure criterion for cohesionless soils.

Some of the earliest use of the limit equilibrium method can be credited to Coulomb himself, who not only proposed his widely applied failure criterion in 1773, but also established the concept of limiting equilibrium to a continuum in order to predict soil pressures on a retaining wall. Also, in 1857, by studying the limiting equilibrium of an infinite body, Rankine developed the earth pressure theory still used in soil mechanics.

During the 20th Century, Fellenius (1926) and Terzaghi (1943), among many others, showed the benefits, simplicity and practicality of the limit equilibrium method to solve many problems that deal with ultimate failure of a soil mass such as soil stability problems, bearing capacity and earth pressures. However, the method has frequently been criticized because of the perfect plasticity assumption from the Coulomb's failure criterion. Soils are not linearly elastic or perfectly plastic for the entire range of soil deformation of common engineering interest. Actual soil behavior is very complicated and it shows a different variety of behavior when subjected to different stress paths. In fact, the development of mathematical models that successfully describe the

complex behavior of soils is far from complete. Thus, idealizations under a given application are very common in engineering practice. This is of special relation to the limit equilibrium method, in which good predictions are often obtained of soil behavior near ultimate strength conditions based on the perfect plasticity assumption.

Plastic limit analysis, on the other hand, is an improved method for estimating collapse loads. It is based on the framework of perfect plasticity, but introduces the stress-strain relations of soils in an idealized manner. This idealization is called normality or flow rule and establishes the limit theorems on which limit analysis is based (Chen and Liu 1990). Before the improvement of computer speed and development of appropriate and flexible computer codes, this approach appeared to be rigorous and became competitive with those of limit equilibrium approach. Nowadays, however, the use of this approach has been replaced in practice by the use of finite element or finite differences methods implemented in commercially available computer software.

Maximum levels of lateral soil restraint for Region 2 can also be obtained from charts included in current available engineering guidelines (e.g. ASCE, PRCI), which are based on results from experimental studies. These guidelines also describe procedures for determining pipeline performance when pipelines are subjected to seismic-induced loading conditions. Typical analyses from the guidelines use finite element methods in which the pipeline is treated as a pressurized beam-type element with soil restraint boundary conditions that are modeled by nonlinear discrete springs in three orthogonal directions (axial, lateral and vertical). The soil springs for each orthogonal loading axis are represented with a multi-linear or hyperbolic force versus displacement function, which is defined by the maximum soil restraint per unit length and its associated relative pipe displacement.

Because the levels of demand imposed on the backfill soil by lateral pipe displacements are large, it is prudent to assume that the backfill soil behavior is controlled entirely by plastic flow (it reaches its ultimate strength condition). Thus, the underlain assumptions of perfect plasticity and rigid body in the limit equilibrium approach should be appropriate for estimating maximum levels of lateral soil restraint in the Region 2 of the normalised lateral soil restraint vs. pipe displacement relationship for soil-pipe interaction analysis. The appropriateness of using a simple limit equilibrium approach to predict maximum levels of lateral soil restraint for the Region 2 for cases with and without trenches will now be verified in the following sections.

4.7.2 Estimation of Maximum Lateral Soil Restraint for Cases with no Trench

Lateral soil loads arising due to abrupt ground movement, like those imposed by landslides and lateral strike-slip faults, are among the most commonly studied cases of soil-structure interaction for pipelines. The research findings on this subject have been based upon a relatively large number of laboratory, numerical and field experimental investigations on pipe response in buried soils and also studies on related structures (piles, anchor plates, strip footings). Charts and theoretical procedures to estimate maximum loads on pipelines during relative lateral soil movements are available and often based on frictional properties (peak friction angle and dilation angle) of the soil and assumed failure mechanisms (Hansen 1961; Oveson 1964; Audibert and Nyman 1977; Trautmann and O'Rourke 1983; O'Rourke et al. 2008).

One of the most recent recommended approaches is that proposed by O'Rourke et al. (2008). This approach assumes a log-spiral failure surface that bounds the passive zone in front of the pipe. The log-spiral has the form:

$$r = r_o e^{\theta tan\emptyset'\mathrm{p}} \qquad [4.3\text{-A}]$$

In which r_o is a reference radius, r is the radius at any angle, θ, and ϕ'_p is the peak effective friction angle of the backfill soil. The log-spiral failure surface and the force components of O'Rourke et al. (2008) approach are depicted in **Figure 4.34**. The following parameters are used in the approach:

P_H = horizontal soil force

W_S = weight of soil mass (shaded in **Figure 4.34**)

W_P = pipe weight (including contents)

L_H = moment arm between horizontal soil force and center of rotation

L_S = moment arm between soil mass and center of rotation

L_P = moment arm between pipe weight and center of rotation

β = angle between horizontal and r_1

ϕ'_p = peak effective internal friction angle

θ = angle between r_0 and r

ψ = soil dilation angle

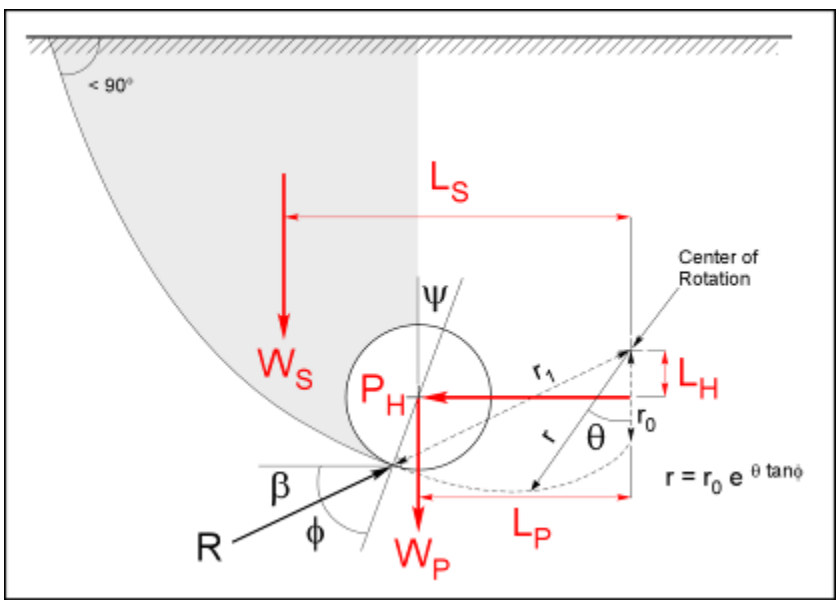

Figure 4.34: Assumed forces for estimating lateral soil restraint using a log-spiral failure surface (based upon O'Rourke et al. 2008).

It is important to note that the O'Rourke et al. (2008) approach is different from the other methods because the approach incorporates the dilation angle (ψ). O'Rourke et al. (2008) claim that at maximum lateral soil restraint, the pipe displaces at an angle with respect to the horizontal similar to that of the backfill soil dilation angle, ψ. They further indicate that the point of tangency between the log-spiral failure surface and the pipe should be oriented at ψ, as shown in **Figure 4.34**. This tangency point and the angle β, define the orientation of the trajectory along which the center of rotation of the log-spiral failure surface is located.

The lateral soil restraint (P_H) is found by satisfying moment equilibrium about the center of rotation and shown in **Equation 4.3-B**. The value of P_H is determined by the location for the center of rotation that results in the minimum value of P_H.

$$P_H = \frac{W_S L_s + W_p L_p}{L_H} \qquad [4.3\text{-B}]$$

The approach proposed by O'Rourke et al. (2008) is based on full-scale 2-D soil-pipe tests on moist sand (4% - 5% water content). These were carried out in a testing apparatus of 1.82 m deep and 2.44 m in length and width. During the tests, measurements were performed for the pipe movement.

4.7.2.1 Prediction of Lateral Soil Restraint for Tests in Sand

For Fraser River sand (FRS) backfill with dry density of about 1,600 kg/m^3 (D_r=75%) and moisture content of 4%, the peak effective internal friction angle (ϕ'_p) from triaxial and direct shear tests varies from 42° to 46° (**Section 3.3.1.1**). For this work a ϕ'_p of 43° and a ϕ_{cv} of 33° were used in the prediction efforts of the maximum lateral soil restraint for the Region 2 of the normalised lateral soil restraint vs. pipe displacement relationship. The dilation angle (ψ)

for FRS was calculated from the relationship proposed by Bolton (1986) as shown in **Equation 4.4**. Based on this, the dilation angle of the FRS is 12°.

$$\psi = \phi'_p - \phi_{cv} \qquad [4.4]$$

Using these soil parameters in the log-spiral model proposed by O'Rourke et al. (2008) for an NPS16 pipe specimen buried with an overburden ratio H/D of 1.6, the normalized lateral soil restraint, P_H, was computed to be 8.0. This P_H value is similar to the N_{qh} of 7.8 recorded during Test 16-1.6-90H-MS-MS-GN. The log-spiral shape used for the calculations of maximum soil restraint is shown in **Figure 4.35**.

The O'Rourke et al. (2008) approach is based on the assumption that a pipe starts to develop a vertical component of motion once the maximum lateral soil restraint is mobilized in dilatant soil. O'Rourke et al. (2008) claim that the ratio of vertical to horizontal pipe movement is approximately equal to the tangent of the backfill dilation angle (tan ψ). This claim can be evaluated using the pipe movement trace depicted in **Figure 4.35**, which is the same as **Figure 4.7** and repeated here for convenience.

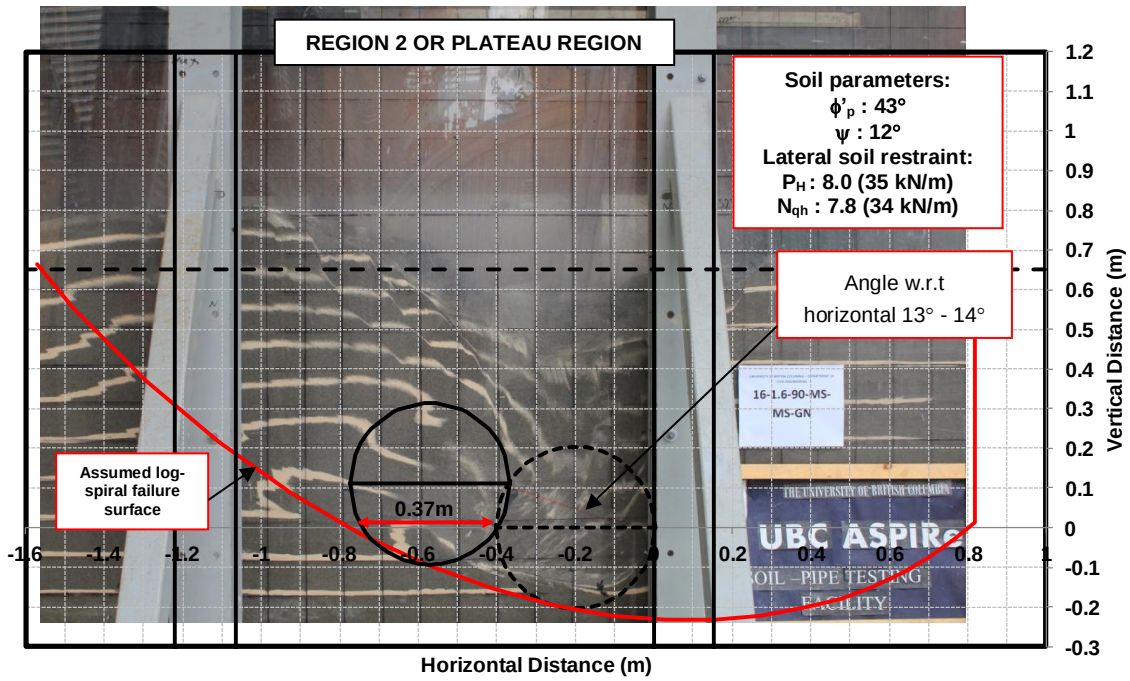

Figure 4.35: Pipe displacement trace and log-spiral failure surface from O'Rourke et al. (2008)'s approach for test 16-1.6-90H-MS-MS-GN.

From **Figure 4.35**, the argument of O'Rourke et al. (2008) appears to be reasonable for practical purposes. Even though small vertical pipe displacement was observed during the progressive failure condition (see **Section 4.2.3**), the more prominent pipe rising was observed after the failure condition or after the maximum lateral soil restraint was reached. The overall ratio of vertical to horizontal movement observed at the end of the test was about 13° to 14° (0.09 m / 0.37 m), which is in accordance with the dilation angle of 12° used for the sand mass with a dry density of 1,600 kg/m^3.

Similarly, for an NPS18 pipe specimen buried with an overburden ratio H/D of 1.9, the normalized lateral soil restraint, P_H, was computed to be 7.8. Again, this P_H value is similar to the N_{qh} of 7.8 recorded during Test 18-1.9-90H-MS-MS-GN. Altering the assumed friction and dilation angle by ±1° changes the normalized lateral soil restraint, P_H, by approximately ±0.35.

Other sources of recommended maximum lateral restraint for pipe specimen buried with an overburden ratio H/D of 1.9 in sand include the following for an internal peak friction angle (ϕ'_p) of 43°:

- Yimsiri et al. (2004) (recommended in PRCI landslide guidelines): 8.7;
- O'Rourke et al. (2008): approximately 8.0;
- Hsu et al. (2006): 7.3 interpolated from plotted results for H/D of 1 and 2 and internal peak friction angle of 42°; and
- Karimian (2006): approximately 8.0 for an H/D = 1.92.

4.7.2.2 Prediction of Lateral Soil Restraint for Tests in Road Mulch

Similarly as the case for sand backfill, an estimation of the lateral soil restraint for a pipe specimen buried in road mulch using the approach proposed by O'Rourke et al. (2008) is presented in this section. Based on the results shown in **Figure 4.10**, the normalized lateral soil restraints estimated from tests in road mulch are N_{qh} = 10.2 to 11.1.

A peak internal friction angle (ϕ'_p) of 49° measured from a 0.3 x 0.3 m direct shear test for the road mulch was used in the calculations (**Section 3.3.1.2**). By measuring the ratio of vertical to horizontal pipe movement reached at the end of the test, a dilation angle of 16° was inferred for the road mulch material. After using these soil parameters in the log-spiral model presented in **Section 4.7.2**; and carrying out the moment equilibrium from **Equation 4.4**, the normalized lateral soil restraint factor P_H was computed to be 11.3.

The above prediction is very similar to the maximum lateral soil restraint values recorded during the corresponding tests. The log-spiral failure surface associated with the computed P_H of 11.3 is overlaid on the soil failure patterns observed at a Y' of 0.75D during Test 18-1.92-90-RM-RM-GN-1 in **Figure**

4.36. It can be inferred from this figure that a log-spiral shape captures very well the failure surface that occurred in the soil mass.

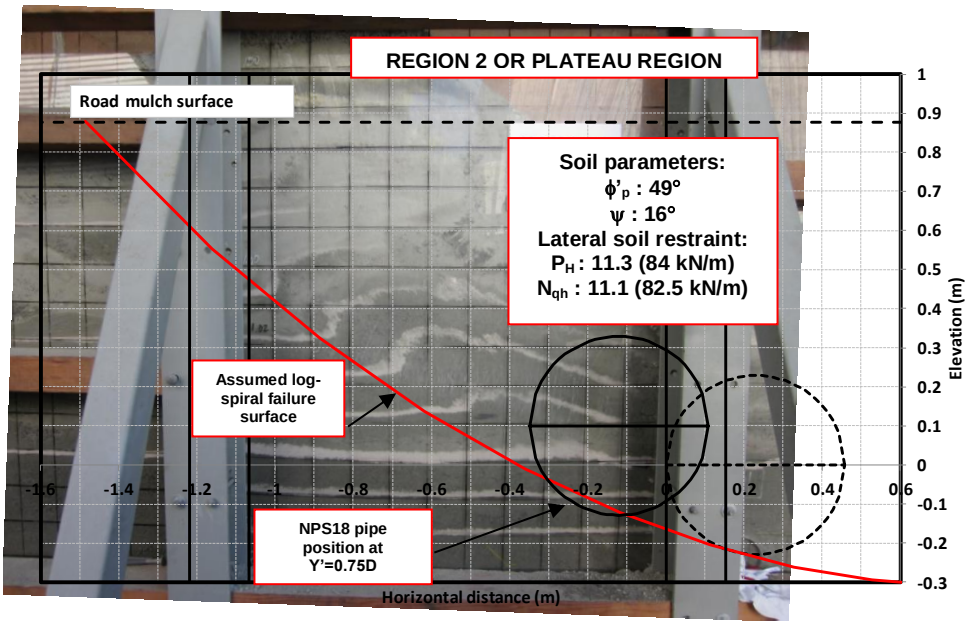

Figure 4.36: Log-spiral failure surface from O'Rourke et al. (2008) approach and soil deformation for Test 18-1.9-90H-RM-RM-GN-1.

4.7.2.3 Prediction of Lateral Soil Restraint for Tests in Crushed Limestone

As shown in **Figure 4.13**, the normalised lateral soil restraint, N_{qh}, measured during the test in crushed limestone is around 12. Similarly as in the case for road mulch tests, the dilation angle was inferred from the measurements performed along the trace depicted by the pen markers attached to the pipe specimen and the observed pipe position before and after the test.

The observational measurements indicate that the pipe rose 0.12 m in 0.38 m of horizontal displacement. This ratio results in a dilation angle of about 18°. The peak internal friction angle measured from a 0.3 x 0.3 m direct shear test is 54°. Based on these parameters, the normalized horizontal load factor (P_H) is computed to be 24.8 using the log-spiral model presented in **Section 4.7.2**.

The log-spiral failure surface is plotted in **Figure 4.37**. This figure also shows the corresponding patterns of soil deformation observed at a Y' of 0.94D (Region 2) during Test 16-1.6-90H-LM-LM-GN. It can be observed that the calculated P_H value over predicts the failure mechanism occurring in the soil mass and does not agree with the N_{qh} obtained from the experimental test. A difference of about two times between these values was computed.

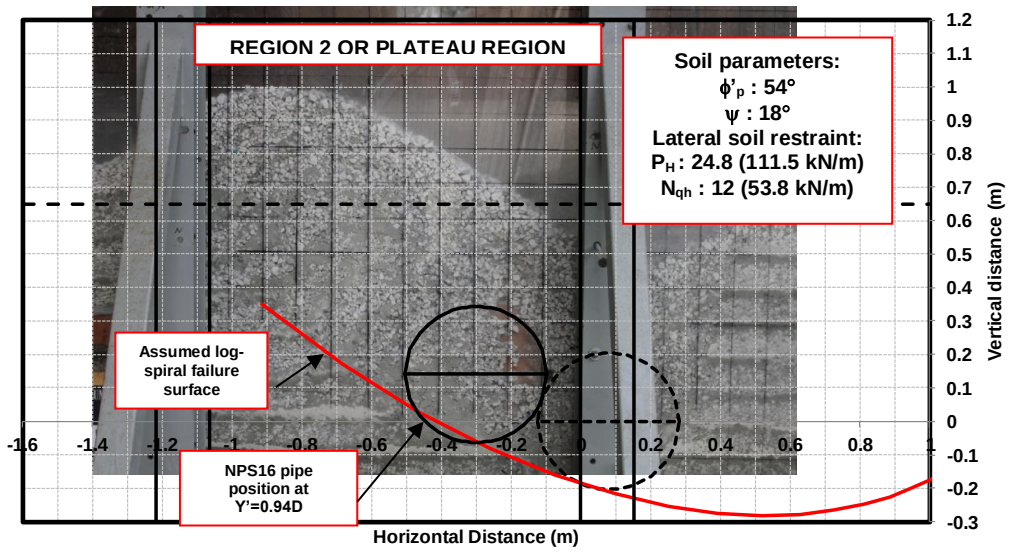

Figure 4.37: Log-spiral failure surface from O'Rourke et al. (2008)'s approach and soil deformation for Test 16-1.6-90H-LM-LM-GN – peak friction angle 54°.

The successful estimation of lateral soil restraint using the log-spiral shape from the approach suggested by O'Rourke et al. (2008) for cases of pipe specimens buried in granular soils such as sand and road mulch, supports the claim that the log-spiral failure shape should also predict the lateral soil restraint measured from the test on crushed limestone (at least close to the measured value). Therefore, the reason for the inconsistency must be related with the soil parameters used in the log-spiral approach.

By assuming that the dilation angle is correct, the only parameter left to consideration is the peak friction angle for the crushed limestone. A trial and error process was carried out to infer the peak friction angle that correctly associates the log-spiral failure shape with the measured N_{qh} of 12. The results from such process indicates a peak internal friction angle of 46° and a normalised lateral soil restraint factor (P_H) of 11.6; which is in agreement with the N_{qh} recorded during Test 16-1.6-90H-LM-LM-GN. The above suggests that the shear resistance results obtained from the direct shear (DS) test on crushed limestone (friction angle of 54°) is misleading. The log-spiral failure surface associated with the P_H of 11.6 is shown in **Figure 4.38**.

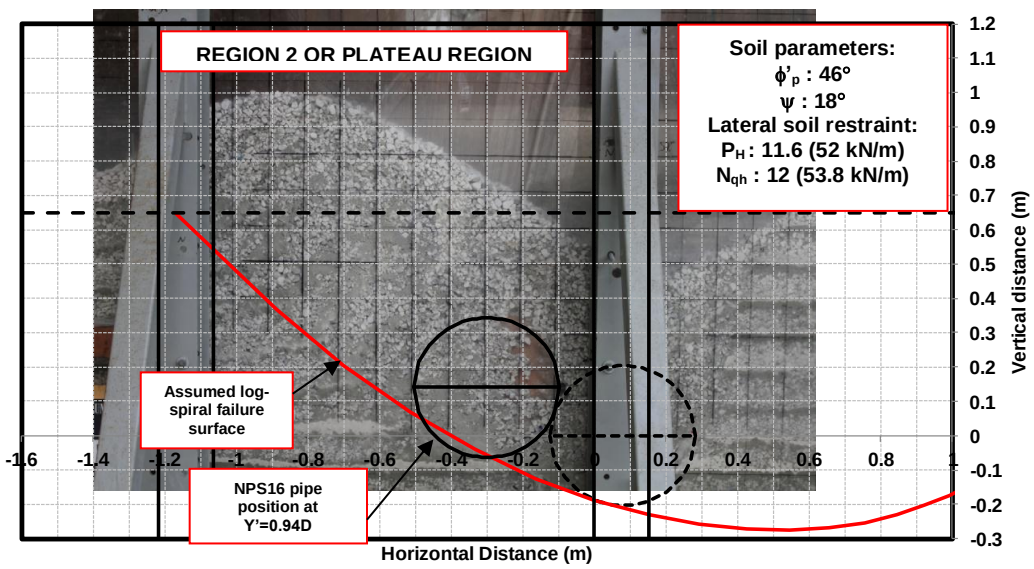

Figure 4.38: Log-spiral failure surface from O'Rourke et al. (2008)'s approach and soil deformation for Test 16-1.6-90H-LM-LM-GN – peak friction angle 46°.

4.7.2.4 Summary of Predictions of Lateral Soil Restraint for Cases with No Trench

A summary of the predicted values for maximum lateral soil restraint tests for the Region 2 of the normalised lateral soil restraint vs. pipe displacement relationship for plain cases (no trench) is presented in **Table 4.2**. The table

also shows diameter of the pipe specimen, peak friction and dilation angle and type of soil backfill (e.g. Fraser River sand, road mulch or crushed limestone). In general a favorable agreement is observed between the values predicted with the O'Rourke et al. (2008) approach and the values measured during the full-scale tests.

Table 4.2: Summary of Predicted Values for Maximum Lateral Soil Restraint (Region 2)

Backfill	**H/D**	**Pipe specimen**	**Peak friction angle (ϕ'_p) degrees**	**Dilation angle (ψ) degrees**	**Predicted normalised soil restraint (P_H)**	**Measured normalised soil restraint (N_{qh})**
Moist Sand	1.6	NPS16	43	12	8.0	7.8
Moist Sand	1.9	NPS18	43	12	7.8	7.8
Crushed Gravel and Sand (Road Mulch)	1.9	NPS18	49	16	11.3	10.2 to 11.1
Crushed Limestone	1.6	NPS16	46	18	11.6	12

4.7.3 Estimation of Lateral Soil Restraint for Cases with Trench Wall

For pipelines located in tectonically active regions, sources of large ground displacements include surface faulting, triggered landslides, and lateral spreading. These large ground displacements can impose large levels of demand that may greatly exceed established pipeline acceptance criteria. When confronted with this technical challenge, one of the first mitigation options is to reduce soil restraint on the buried pipeline and therefore increase the displacement capacity. For example, the installation of pipelines in a trapezoidal trench with loose to moderately dense sand backfill is one of the common mitigation measures undertaken to reduce soil loads in situations of abrupt ground movement such as pipeline fault crossings. The use of a trapezoidal trench with sand backfill, however, may not be a feasible option in locations where suitable low-cost sand backfill is not readily available or drainage and erosion issues preclude the use of sand.

Another recommended mitigation option given by design guidelines (e.g. PRCI, 2004, 2009) is the use of geosynthetic fabric on sloped trench walls. This recommendation is based upon the premise that slippage in the form of a contiguous soil blocks would be promoted due to the low frictional properties prevalent at the geosynthetic fabric interfaces. However, the effectiveness of this technique is currently poorly understood, and little guidance is available to permit more complete specifications on geosynthetic installation requirements and define methods for quantifying reductions in soil restraint.

The work previously undertaken at UBC on this topic suggests that the behavior of geotextile-lined pipeline trenches subjected to permanent lateral ground deformation does not seem to reduce soil loads on pipeline to the extent it was intended (Karimian et al. 2006). Development of local shearing of sand between the front of pipe and trench wall was the inferred reason for the low effectiveness of the geotextile interface in reducing soil loads.

Karimian et al. (2006), based on their test results, proposed an equation to quantify the observed lateral soil restraint based on the assumption that the observed behaviour can be predicted using the limit equilibrium method on a passive wedge. The formulation depends on the weight of the passive wedge, geotextile interface friction angle and the backfill soil friction angle. The basis for this formulation is depicted in **Figure 4.39**. Karimian et al. (2006) indicated that the proposed equation is not able to estimate the horizontal soil resistance for dual-geotextile lined trench configurations. They pointed out the hypothesis that relative movement of the pipe within the backfill is the main reason for this inability.

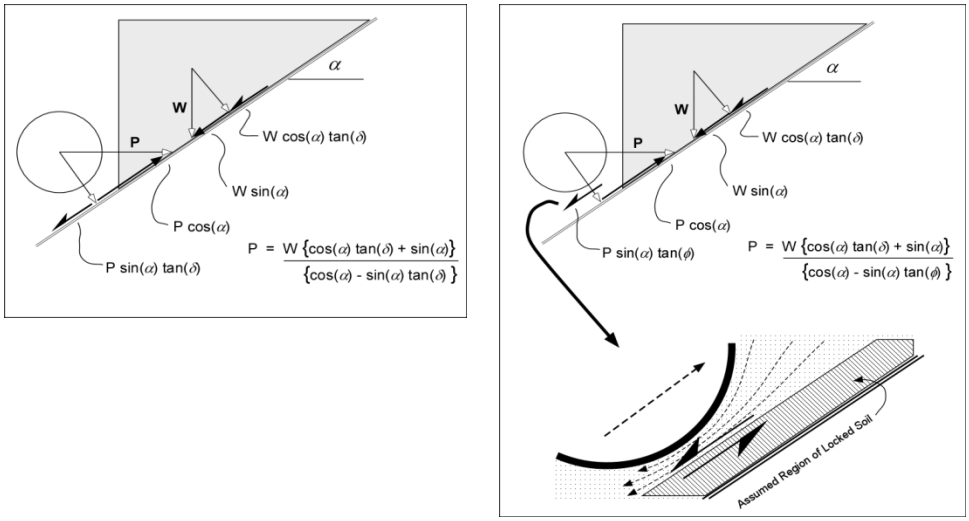

Figure 4.39: Sliding block mechanisms for geotextile-lined trench wall after Karimian et al. (2006) (a) sliding only at geotextile interface (left); (b) sliding at geotextile interface and shear failure through soil between pipe and trench wall (right).

Load-displacement relationships obtained from full-scale testing of buried pipelines in geotextile-lined trenches in this research suggest that the level of lateral soil restraint does not reach a limiting value for Region 2 (as in the case of no trench conditions); instead, it increases with pipe displacement once the pipe approaches the sloped trench wall (see Region 3 of **Figure 4.33**). This

behaviour occurred in spite of the slippage observed between the geotextile layers. Similar behavior was observed by Karimian et al. (2006) on the basis of a limited number of geotextile-lined pipeline trench tests in dry and moist sand. This points out the fact that an equation that gives only one value of lateral soil restraint, and that is not associated to pipeline displacement, is not appropriate to represent the complex behavior observed for pipelines buried in geotextile-lined trenches (Monroy et al. 2012).

4.7.3.1 Comments on Test Results for Geotextile-Lined Pipeline Trenches

Patterns of soil deformation for Test 18-1.9-90H-HB-MS-GY-45-0.5D-2 at Y'=0.05D (Region 2 of the normalised lateral soil restraint vs. pipe displacement relationship) and Y'=0.45D (Region 3) are illustrated in **Figure 4.40.a** and **4.40.b**, respectively. They were already discussed in **Section 4.5.3** and are repeated here for convenience. Patterns of soil deformation at Y'=0.05D were associated with an N_{qh} of 6.4. Patterns of soil deformation at Y'=0.45D were associated with a level of lateral soil restraint N_{qh} of 6.8. This N_{qh} value corresponded to the risen portion of the load vs. pipe displacement relationship due to the trench effects (Region 3 or hardening region), as can be seen from **Figure 4.33 or 4.23**.

As seen in **Figure 4.40**, clearly the N_{qh} values at Y'=0.05D and at Y'=0.45D are associated with two very different patterns of soil deformation and modes of instability. At Y'=0.05D (Region 2 or plateau region) most of the appreciable shear deformation appears to be occurring along the edges of a passive wedge configuration, while the soil mass in front of the pipe and inside the wedge showed no significant shear deformation.

By contrast, at Y'=0.45D or for the hardening region the soil mass inside the wedge showed significant shear deformation (**Figure 4.40.b**) which occurred after the pipe started to move upward with an inclination of about 30° to 35°

from the horizontal. This vector may have developed due to the interaction between the imposed lateral displacement and the 45° boundary condition of the sloped trench wall. This mode of instability appears to represent a soil response governed by shearing through the backfill soil as the pipe moves upward and shearing of a compressed soil mass due to the proximity of the pipe to the trench wall. This mode also shows the development of several different active zones of soil failure.

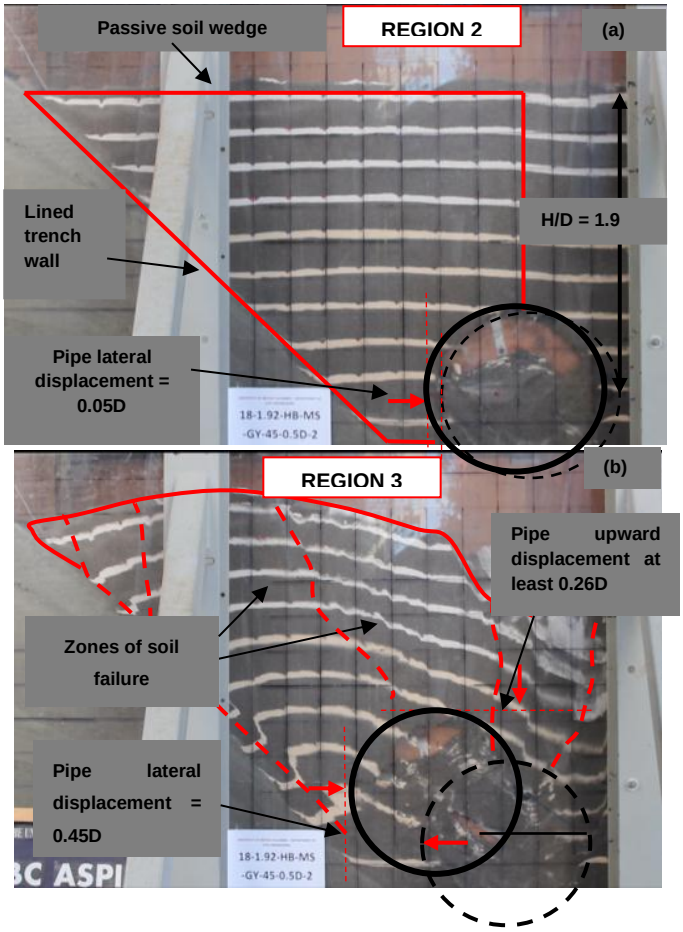

Figure 4.40: Observed patterns of soil deformation for Test 18-1.9-90H-HB-MS-GY-45-0.5D-2: (a) Y'=0.05D, and (b) Y'=0.45D.

Because the limit equilibrium approach is based on the condition that changes in geometry of a body (a passive wedge for this case) during perfect plastic

conditions are insignificant, this approach can only be applied to the stage of the test observed at Y'=0.05D, as the shape of the passive wedge is for practical reasons intact. Therefore, the use of the limit equilibrium approach is only applicable to the Region 2 of the normalised lateral soil restraint vs. pipe displacement relationship for cases with trench wall; and cannot be used for the Region 3 or hardening region as indicated by Karimian et al. (2006).

Under the above frame of reference, two modes of instability need to be incorporated in a predictive equation for geotextile-lined pipeline trenches under lateral displacements. The first instability mode can be represented and quantified by a limit equilibrium approach with a front passive wedge whose frictional resistance along the trench wall is fully mobilized (perfectly plastic condition). The second mode of instability represents a soil response predominantly and likely governed by shearing of a compressed soil mass between the pipe and trench wall. Predictive equations to capture these modes of instability are explored in **Section 4.1.1.2**.

PRCI (2004, 2009) guidelines identify the use of two layers of geosynthetic fabric as a means to reduce lateral soil restraint under the premise that a low-friction failure surface will be developed along the sloped trench wall and a passive wedge of soil, as indicated in **Figure 4.40**, will slide up the trench wall. The validity of this premise will now be evaluated based on the data presented in **Figure 4.41**, which shows the development of N_{qh} and the measured displacement of the outer geotextile as a function of test duration (time).

The N_{qh} level required to overcome the geotextile friction can be obtained by identifying the time above which the outer geotextile slides. From **Figure 4.41**, this time is 40 s. However, the response of the soil-pipe system has not reached the plateau in terms of N_{qh}, but rather, it is still in a process of additional soil restraint development. The results presented in **Figure 4.42** for Tests 18-1.9-90H-RM-RM-GY-35-0.5D-1 and 18-1.9-90H-RM-RM-GY-35-0.5D-2 also showed a similar response.

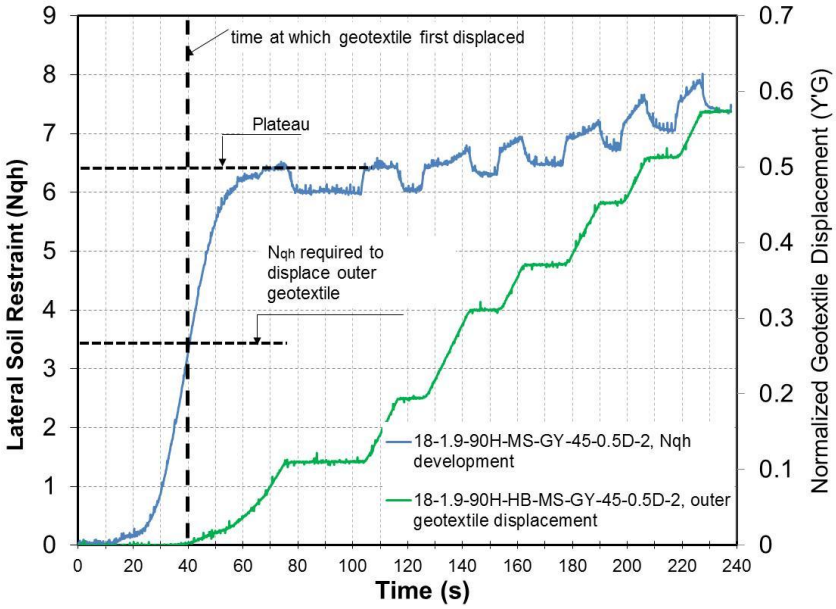

Figure 4.41: Evolution of lateral soil restraint and geotextile displacement as a function of time for Test 18-1.9-90H-HB-MS-GY-45-0.5D-2.

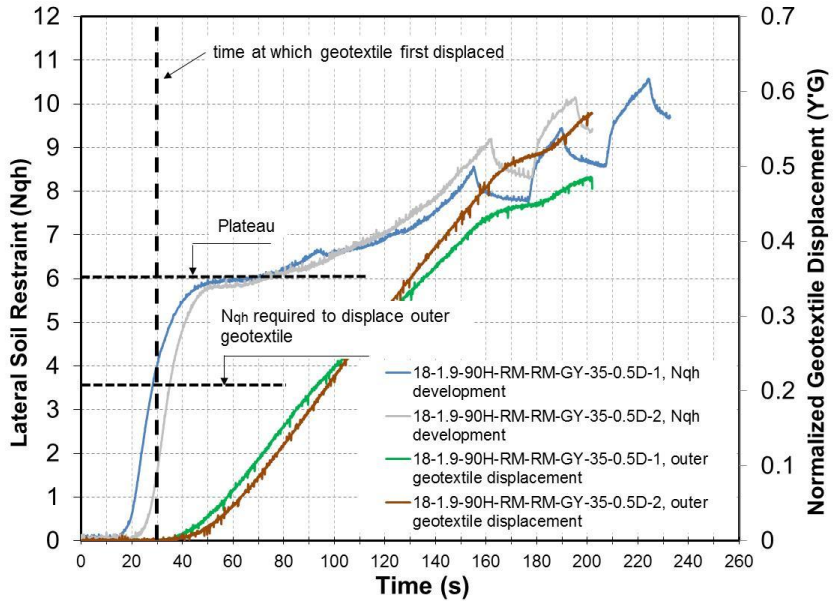

Figure 4.42: Evolution of lateral soil restraint and geotextile displacement as a function of time for Test 18-1.9-90H-RM-RM-GY-35-0.5D.

It is reasonable to state that the horizontal resistance beyond what is necessary to induce slippage at the inner-outer geotextile interface results from the need to overcome additional energy induced by the deforming soil mass such as:

1. Work due to deformations internally occurring within the soil (in overcoming both internal soil friction as well as shear-induced dilative response of soil).
2. Work required to overcome friction at the outer geotextile-soil interface.
3. Work dissipated during relative movements between soil and pipe.
4. Work required for movements against gravity.
5. Work required to overcome the limitations in the test chamber in simulating ideal two-dimensional conditions.

The degree of contribution of the above factors to the observed increase in soil restraint over what is necessary to initiate sliding of the outer geotextile is likely affected by the test configuration, the amount of pipe movement, and other factors. For example, with increasing pipe displacements, it is possible that the work mechanisms noted in items 1 through 3 above would contribute more to the observed increase of pipe-soil restraint over that corresponding to the work required to overcome friction at the inner-outer geotextile interface. In recognition of these factors, numerical modelling seems to be necessary to investigate in depth the above mechanisms. This will be presented in **Chapter 7**.

4.7.3.2 Proposed Simplified Mechanism to Predict Lateral Soil Restraint in Geotextile-Lined Pipeline Trenches

An analytical study was conducted to try to estimate N_{qh} values associated with the different regions of the normalised lateral soil restraint vs. pipe displacement relationship recorded during the tests. For example, the N_{qh}

associated with Region 2 and required to overcome the shear resistance along the trench wall was calculated by determining the lateral force required by the soil-pipe system to be in limit equilibrium. A free body diagram on a wedge configuration was used for this purpose (**Figure 4.43**). Sliding resistance along the trench wall was evaluated for inner-outer geotextile interface ($\phi_{interface}$=21°) and for outer geotextile-soil interface ($\phi_{interface}$ =32°). The equilibrium equation is shown in **Equation 4.5**.

$$F_y = W \cdot \frac{(\sin\theta + \tan\phi_{interface} \cdot \mathrm{Cos}\theta)}{(\cos\theta - \tan\phi_{interface} \cdot \mathrm{Sin}\theta)} \qquad [4.5]$$

where, W is the weight of the front passive wedge, $\phi_{interface}$ is the interface friction angle along trench wall and θ is the inclination of trench wall from the horizontal plane.

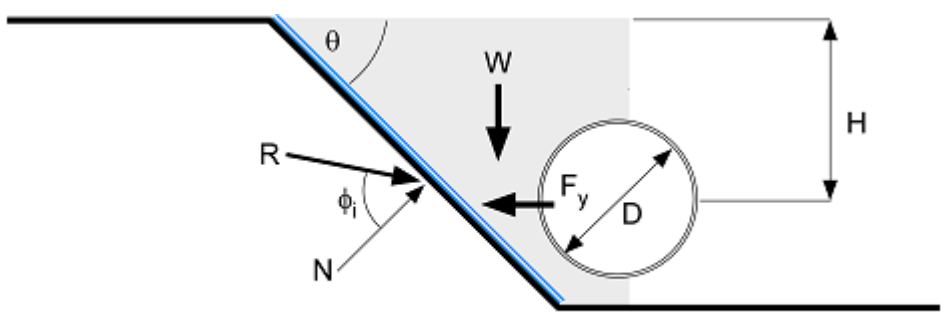

Figure 4.43: Sliding block mechanism for quantifying F_y for pipeline systems with geotextile-lined trench walls. $\phi_i = \phi_{interface}$.

A comparison between levels of lateral soil restraint (N_{qh}) estimated from **Equation 4.5** and from the test data is shown in **Figure 4.44**. The computed load from **Equation 4.5**, using the interface friction angle between the geotextile fabric, reasonably predicted the N_{qh} required to slide the outer

geotextile (**Table 4.3**). Likewise, when the interface friction angle between the soil and the outer geotextile fabric was used for $\phi_{interface}$ in **Equation 4.5**, it matched satisfactorily with the N_{qh} associated with the plateau of Region 2 recorded during the tests.

As can be observed from **Figure 4.44** and, the computed lateral soil restraint from **Equation 4.5** using the interface friction angle between the geotextile fabric layers ($\phi_{interface}$ = 21°) substantially under predicts the plateau load observed during the tests.

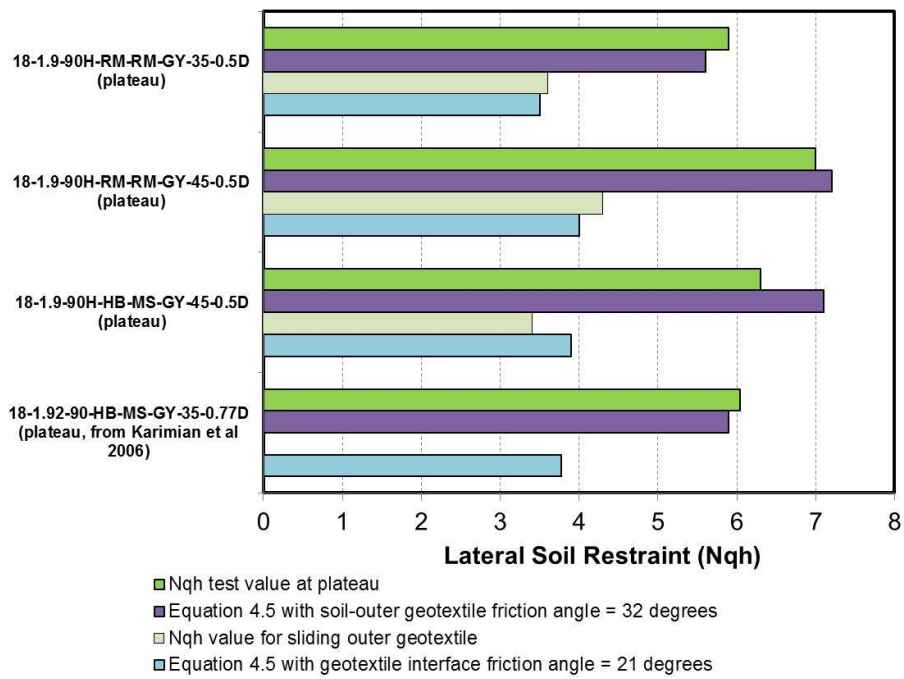

Figure 4.44: Comparison between lateral soil restraint from tests and soil restraint from **Equation 4.5** for different interface friction angles**.**

Table 4.3: Measured Versus Calculated Lateral Soil Restraint for Geotextile-Geotextile Interface Conditions

Test ID	Passive Wedge Weight (kN/m)	N_{qh} Measured[1]	N_{qh} Predicted using $\phi_{interface}$ = 21° (Equation 4.5)
18-1.92-90-HB-MS-GY-35-0.77D	17.5	NA	3.7
18-1.92-90-HB-MS-GY-45-0.5D	12.5	3.4	3.9
18-1.92-90-RM-RM-GY-35-0.5D	18.5	3.6	3.5
18-1.92-90-RM-RM-GY-45-0.5D	14.1	4.3	4.0

(1) N_{qh} determined from lateral soil restraint vs. time plot

Given the similarity in the shape of the load-displacement response observed in the tests, the development of a simple predictive tool was investigated. This led to **Equation 4.6** and **Equation 4.7** which predicts levels of lateral soil restraint (N_{qh}) as a function of normalized pipe displacement Y' for geotextile-lined pipeline trenches for the three regions of the normalised lateral soil restraint vs. pipe displacement relationship observed during the tests.

$$N_{qh} = N_y + K(Y' - 0.3D)^n \quad \text{if } Y' > 0.3D \qquad [4.6]$$

$$N_y = \frac{Y'}{\left(\frac{0.05 \cdot Y_p'}{F_y} + \frac{0.95 \cdot Y'}{F_y}\right)} \quad \text{if } Y' \leq 0.3D \qquad [4.7]$$

where Y_p' is the normalized pipe displacement at F_y (assumed Y_p'=0.1D). K and n are constants equal to 7.0 and 1.65, respectively, and were determined from fitting the data of the tests to a power law. Because the N_{qh} level for Y'

>0.3D (Region 3 or hardening region) can be eliminated by simply increasing the pipe-trench wall distance, S, to values larger than 1D, it was judged reasonable and practical to follow the curve fitting approach, given the confidence regarding the quality of data and the scale of the tests.

The constants 0.05 and 0.95 in **Equation 4.7** were obtained from fitting the data with Y'< 0.1D (Region 1) from the tests to a rectangular hyperbola.

Comparisons between the normalised soil restraint vs. normalised pipe displacement predicted by **Equations 4.6** and **4.7** and data from Karimian et al. (2006) and data from the tests of this work are shown in **Figure 4.45**. Remarkably similarity is observed. A comparison between predicted F_y with $\phi_{interface}$=32° versus measured normalised lateral soil restraint, N_{qh}, at the plateau is shown in **Table 4.4**. Again, a very good prediction is observed.

Table 4.4: Measured versus Calculated Lined Trench Lateral Soil Restraint

TEST ID	N_{qh} Measured		N_{qh} Predicted using $\phi_{interface}$ = 32±1°	
	Plateau	Post-plateau [1]	Plateau (F_y)	Post-plateau (N_{qh})[1]
18-1.92-90-HB-MS-GY-35-0.77D	6.0	7.2	5.9	6.6
18-1.92-90-HB-MS-GY-45-0.5D	6.4	6.9	7.1	7.9
18-1.92-90-RM-RM-GY-35-0.5D	5.9	6.8	5.6	6.3
18-1.92-90-RM-RM-GY-45-0.5D	7.0	8.1	7.2	8.0

[1] Post-plateau (Region 3) reference soil restraint calculated at Y'=0.5D.

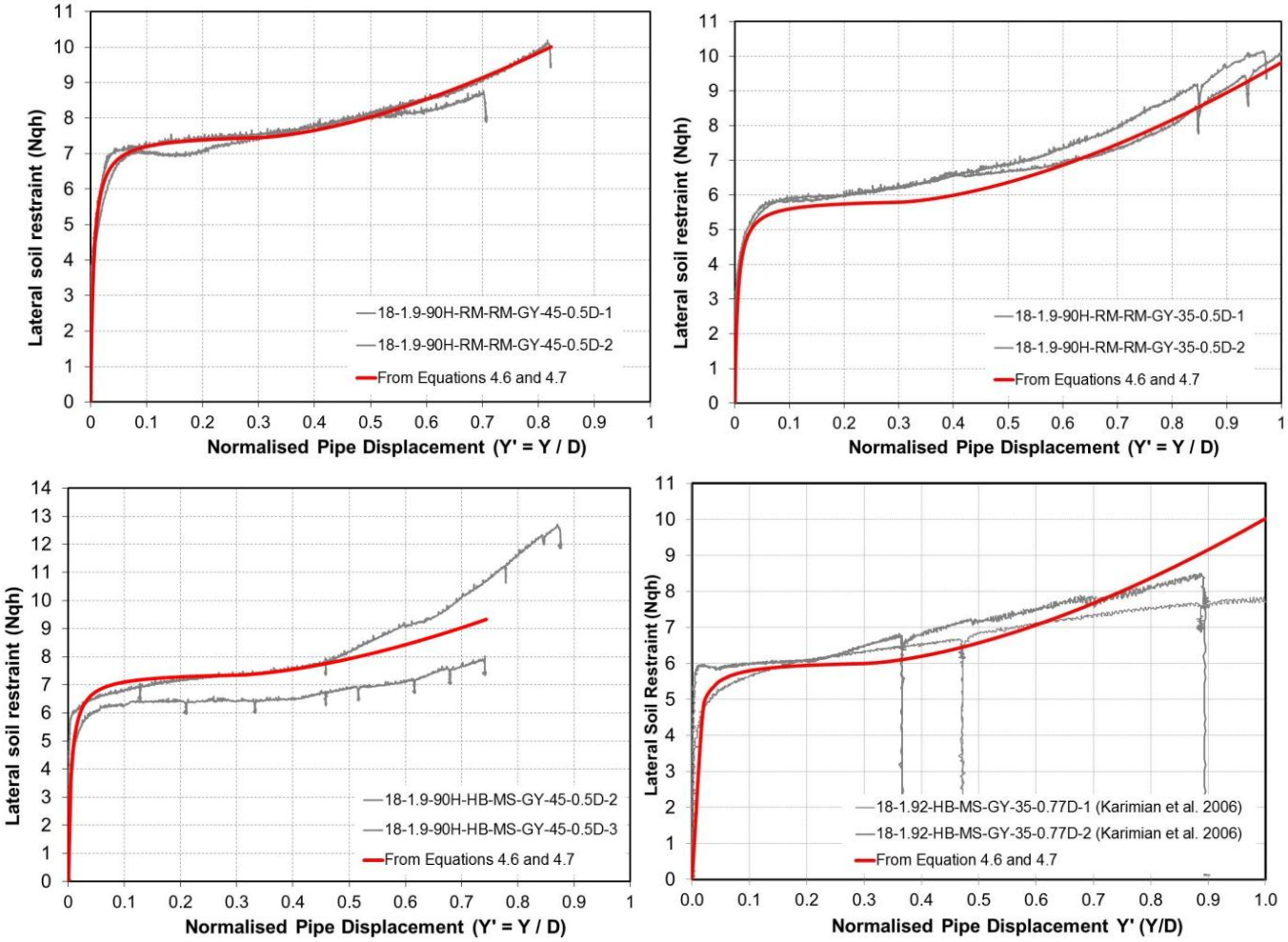

Figure 4.45: Lateral soil restraint-displacement from **Equation 4.6** and **4.7** vs. tests results.

4.8 Summary of the Chapter

The mobilization of levels of lateral soil restraint on shallow buried steel pipes due to simulated breakout of buried pipelines from their soil embedment on the fixed side of a strike-slip fault was investigated through 2D full-scale horizontal pulling tests, conducted using a large soil testing chamber at UBC. The pipeline configurations simulated in this research program included: pipe placed in dense moist sand, road mulch and crushed limestone backfills. The testing program also included pipe specimens buried in a trench excavated in dense coarse-grained “native” soil, backfilled with moist dense sand or the same strong native soil (road mulch). The effectiveness of a dual-layer geosynthetic fabric along a trench wall to provide a preferential failure surface was also investigated during the testing work.

In addition to the measurement of lateral soil restraints, pipe displacement and the soil pressure on the pipe surface, changes in the soil mass geometry and traces of variation of pipe position during the tests were evaluated and related to recorded levels of lateral soil restraint.

The direct observations of patterns of soil failure, pipe position and their relation with levels of soil restraint were critical for an appropriate understanding of the mechanisms that developed during the complex soil-pipe interaction process. Furthermore, three regions of the observed normalised lateral soil restraint vs. pipe displacement relationship were identified to establish a frame of reference for discussion purposes.

Monitoring of the movement of geosynthetic fabrics lining the trench surface, in combination with the observations on changes in the soil mass geometry and pipe position during different pulling stages, provided useful information to understand the basic failure mechanisms and were instrumental for the development of an equation that successfully predicts lateral soil restraint vs. pipe displacement relations for geotextile-lined pipeline trenches conditions.

Based upon the test results presented and the evaluation of them in the previous sections, the following conclusions can be drawn for pipelines buried in plain conditions (i.e. no trench):

1. The maximum normalised lateral soil restraint N_{qh} of about 7.8 (Region 2) developed in the tests in uniform moist dense sand for H/D = 1.9 with no trench is similar to the values reported by other investigators (e.g. O'Rourke et al. 2008; Hsu et al. 2006; Karimian 2006); except for Yimsiri et al. (2004) that reported a value of 8.7.
2. The maximum lateral soil restraint (Region 2) on pipelines buried in coarse-grained geomaterials can be predicted with sufficient engineering accuracy by the log-spiral failure surface determined using the methodology described in O'Rourke et al. (2008).

The data from 2-D tests to evaluate the effectiveness of lining pipe trenches with two layers of geotextile as means to reduce lateral soil restraint on shallow buried pipelines support the following conclusions:

1. A sloped trench side-wall lined with two layers of geotextile plays a role in the variation of soil restraint with pipe displacement only when the pipe-trench wall distance was less than half a pipe diameter (0.5D). If the pipe was more than one diameter from the trench wall, the lateral soil restraint was controlled by the shear resistance of the backfill.

2. The test results indicated that the lateral soil restraint associated with the Region 2 of the normalised lateral soil restraint vs. pipe displacement relationship for cases with a trench wall was not constant with lateral pipe displacement but rather it increased to values larger than those observed from cases with no trenches.

3. The Region 2 (plateau or plastic region) and Region 3 (hardening region) of the normalised lateral soil restraint vs. pipe displacement

relationship are associated with two distinct modes of instability of the backfill soil mass. One mode of instability is associated with Region 2 and showed that most of the appreciable shear deformation occurred along the edges of a passive wedge configuration, while the soil mass in front of the pipe and inside the wedge showed no significant shear deformation.

4. The second mode of instability is associated with the Region 3 of the normalised lateral soil restraint vs. pipe displacement relationship. In this mode the soil mass inside the soil wedge showed significant shear deformation. This mode occurred after the pipe started to move upward with an inclination of about 30° to 35° from the horizontal. This mode of instability appears to represent a soil response governed by shearing through the backfill soil as the pipe moves upward and by shearing of a compressed soil mass due to the proximity of the pipe to the trench wall.

3. A simple mechanical model based on limit-equilibrium and a power law, whose parameters were obtained from the full-scale test results, was proposed to quantify the levels of lateral soil restraint from the two failure modes, respectively. The predictions from the proposed analytical approach were in very good agreement with the results from the tests carried out herein and those reported by Karimian et al. (2006).

4. Lining sloped pipeline trench side-walls with two layers of geotextile fabric as a means of reducing lateral soil restraint for pipeline crossing should be discouraged or its use limited to conditions governed by small relative soil-pipe displacements that may arise from thermal expansion, subsidence, or slope creep.

Chapter 5: Horizontal Oblique Soil Restraint on Pipelines

Current state of practice (ASCE 1984; PRCI 2004, 2009) for fault crossing design or similar geohazards assumes that soil restraints act independently (e.g., lateral and axial soil restraints react only to components of displacement in the lateral and axial directions, respectively). Some recent works suggest that axial-lateral coupling effects occur during oblique or three dimensional soil-pipe relative movements (Hsu et al. 2006; Phillips et al. 2004; Daiyan et al. 2010, 2011). Hsu et al. suggest that axial and lateral soil restraint vary as the cosine and sine of the oblique angle, respectively. In contrast, Phillips et al. 2004 and Daiyan et al. 2010, 2011, claim that a significant increase in axial soil restraint exists as the oblique angle decreases from 90° (purely lateral) during coupling. To date, very little has been done to understand and validate these coupling effects under axial and lateral conditions. It is clear that there is a great need for such validation if coupling effects are to be included, for example, in the design of pipeline systems crossing faults.

This chapter describes the results from large-scale horizontal oblique tests on a steel pipe specimen buried in moist sand. As described in **Chapter 3**, the test program consisted of five tests using NPS18 (457-mm) diameter steel pipe with different lengths. The pipe specimen was oriented at oblique angles (β values) of 75°, 60° and 45° degrees to the direction of a strike-slip fault trace or of a main ground displacement and then was horizontally displaced to simulate the breakout of buried pipelines from their soil embedment on the fixed side of a strike-slip fault (Note: β = 90° is pure horizontal lateral ground movements perpendicular to the alignment of the pipeline). The pipes had about 640 mm of soil cover above the crown (H/D=1.9).

Horizontal oblique test measurements included pipe displacement along the direction of the actuators, load in the actuators, and axial reaction load

between the pipe specimen and the soil test chamber wall. These measurements were processed to provide soil restraint versus pipe displacement responses in the axial direction and the lateral direction perpendicular to the pipe axis.

While other researchers have only reported oblique displacement, resolving the components of displacement to parallel the direction of the load of interest has the advantage of allowing direct comparison with purely axial and lateral soil restraint tests. Comparisons of horizontal oblique soil restraints measured in this test program with recommended relationships by Hsu et al. (2006), Phillips et al. (2004) and Daiyan et al. (2010, 2011) are also provided in this chapter in order to discuss and assess the trends in maximum horizontal oblique soil restraint response reported by these researchers and the current work.

5.1 Summary of Test Parameters

Test results are presented in terms of normalized oblique displacement (Y'= Y / D) as per **Equation (4.2)**; where D is the pipe diameter and Y is the recorded oblique pipe displacement. Details related to the testing program and test parameters were shown in **Table 3.4** and **Table 3.7** of **Chapter 3** and repeated here in **Table 5.1** for the reader's convenience. Important test characteristics are summarized in **Table 5.2**.

Table 5.1: List of Conducted Horizontal Oblique Soil Restraint Tests

No.	Test ID	Oblique angle w.r.t ground movement[1]	Backfill	Average backfill dry density (kg/m^3)
1	18-1.9-75H-MS-MS-GN-1	75°	Sand	1,600
2	18-1.9-75H-MS-MS-GN-2	75°	Sand	1,600
3	18-1.9-60H-MS-MS-GN-1	60°	Sand	1,600
4	18-1.9-60H-MS-MS-GN-2	60°	Sand	1,600
5	18-1.9-45H-MS-MS-GN-1	45°	Sand	1,600

Notes: [1] 90° is perpendicular to direction of ground movement induced by a strike-slip fault trace or other geohazard.

Table 5.2: Summary of Parameters for Horizontal Oblique Soil Restraint Tests

	Fraser River Sand
Average Dry Density (kg/m^3)	1600
Average moisture (%)	3 to 4
Internal Peak Friction Angle (ϕ_p)	43°
Soil Dilation Angle (ψ)	12°
Pipe Diameter (D)	NPS18
Pipe Length (L)	75° oblique angle = 2.48 m 60° oblique angle = 2.77 m 45° oblique angle = 3.39 m
Pipe Grade & Surface	Steel Grade 524A, Sand Blasted Surface
Soil-Steel Pipe Interface Friction Angle	Peak = 36°; Constant volume friction = 31°
Pulling Rate	2.5 mm/s
Direction of Pulling Rate	Parallel to direction of ground movement induced by a strike-slip fault trace or other geohazard

5.2 Framework for Interpreting Horizontal Oblique Tests

Horizontal oblique pipe-soil interaction is defined in this work as the combined effect of axial and lateral soil restraints that acts on pipeline segments subjected to relative oblique ground displacements on a horizontal plane. A general layout showing a typical horizontal oblique test arrangement is shown in **Figure 5.1**. This figure shows a typical pipe position and orientation before the test on the fixed side of a strike-slip fault, definition of horizontal oblique angle (β), and direction of recorded oblique (F) and axial (A) reaction forces. It is worthwhile mentioning that the pulling direction for simulating pipe breakout from soil embedment was kept constant. A photograph showing an expanded view of the load cell used to measure the axial (A) reaction force is also included in **Figure 5.1**.

As described in **Section 3.6.1**, horizontal oblique test measurements included pipe displacement along the direction of the actuators, load in the actuators and axial reaction load between the pipe specimen and the soil test chamber wall. These measurements were processed to provide soil restraint-displacement responses in the axial direction and the lateral direction perpendicular to the pipe axis. In addition, a cushion foam between the end of the pipe specimen and the steel plate on the inside of the soil test chamber was included to keep this space free of sand and therefore avoid the development of restraining forces during pipe axial movement.

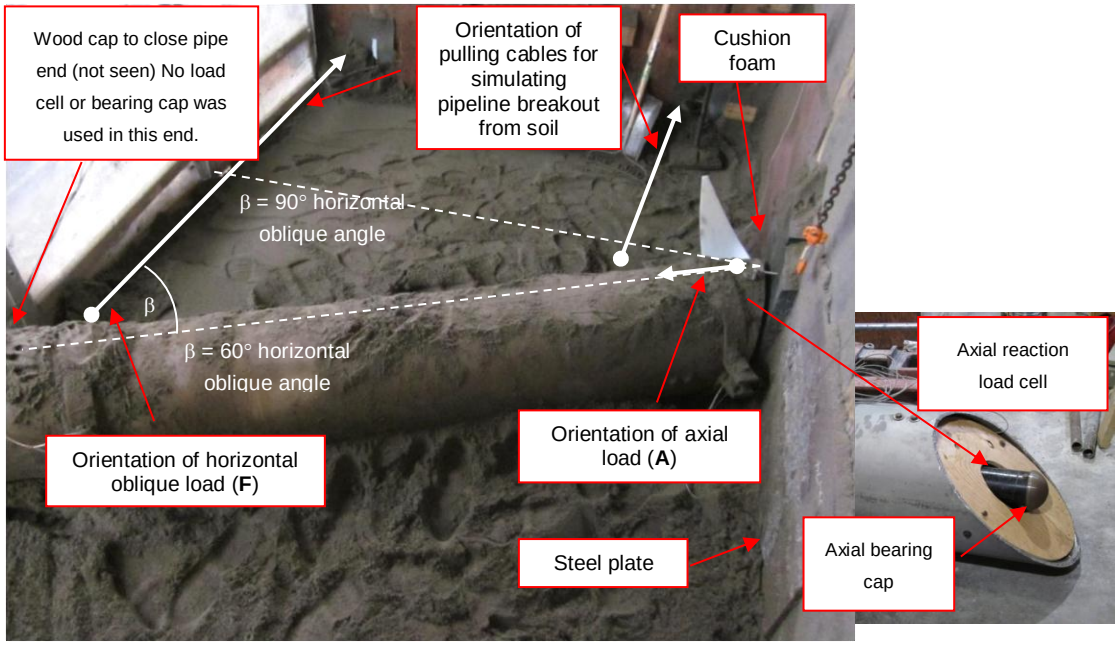

Figure 5.1: Photograph insets show general arrangement and direction of oblique (F) and axial (A) reaction forces.

The free-body diagram representing the loads acting on horizontal oblique test specimens is illustrated in **Figure 5.2**. In this figure, the effect of sliding friction between the axial bearing cap and the steel plate on the inside of the soil test chamber wall is accounted for by the factor f. From the diagram the lateral soil restraint (P_H) and axial soil restraint (T) were obtained as follows:

$$P_H = F \cdot \cos(\theta) - A\,[\,\sin(\theta)\cdot\cos(\theta) + f\cdot\cos^2(\theta)] \qquad [5.1]$$

$$T = F \cdot \sin(\theta) - A\,[1 + f\cdot\sin(\theta)\cdot\cos(\theta) + \sin^2(\theta)] \qquad [5.2]$$

Where F is the measured oblique load, A is the measured axial reaction load, $\theta = 90° - \beta$, β is the horizontal oblique angle, and f is the sliding friction factor.

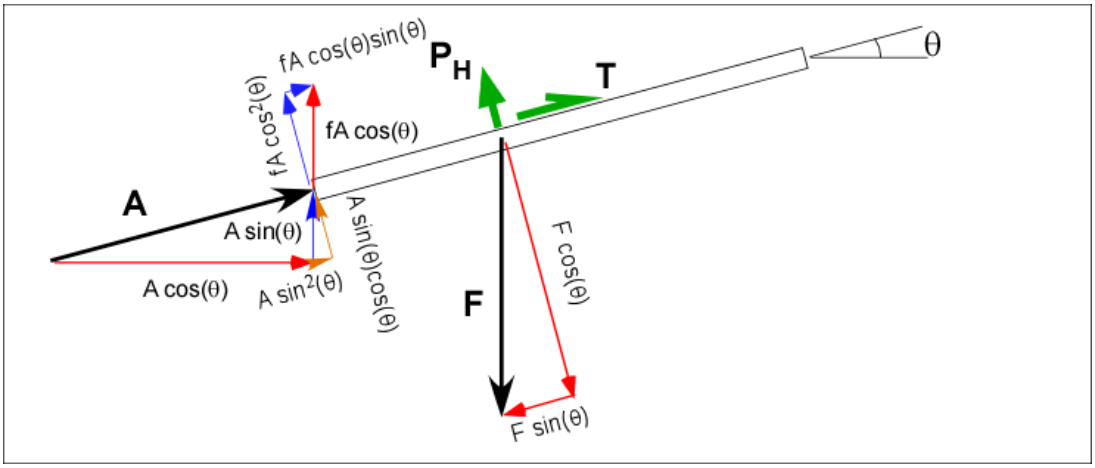

Figure 5.2: Forces acting on horizontal oblique pipe test specimens.

In a similar way, oblique displacement or displacement parallel to F can be resolved in components of displacement parallel to the direction of lateral soil restraint, P_H, or axial soil restraint, T, as follows:

$$Y_P = Y \cdot \cos(\theta) \qquad [5.3]$$

$$Y_T = Y \cdot \sin(\theta) \qquad [5.4]$$

Where Y_P is ground displacement parallel to the lateral soil restraint, P_H, and Y_T is ground displacement parallel to the axial soil restraint, T.

Finally, test results are presented in terms of normalized values of lateral soil restraint, N_{qh}, normalized axial soil restraint, T_a, and normalized displacement, Y' determined from the equations below:

$$N_{qh} = P_H / (\gamma \cdot D \cdot H \cdot L) \qquad [5.5]$$

$$T_a = T / (\gamma \cdot D \cdot H \cdot L) \quad [5.6]$$

$$Y' = Y_P / D \text{ or } Y_T / D \quad [5.7]$$

Where P_H is the calculated lateral load, T is the calculated axial load, γ is the dry unit weight of the backfill, D is the pipe diameter, H is the height of soil over the pipe springline, L is the pipe length, and Y is the recorded pipe displacement. The form of the normalized load and displacement shown above follows the relationships presented in **Chapter 4** about lateral soil restraint.

5.3 Results of Horizontal Oblique Tests – β = 75 degrees

5.3.1 Soil Restraint-Displacement Response

The change in oblique, F, and axial reaction, A, load for the pipe specimen under oblique displacement with β = 75° is shown in **Figure 5.3**. Both, the oblique and axial load cell measurement recorded continuous nonlinear load increase behaviour during the test until a maximum condition was reached. However, an additional increase of load was observed after normalized oblique pipe displacement Y' = 0.4D. This increase is believed to be associated with constraints provided by both the lateral and frontal walls of the testing chamber as the pipe specimen displaces towards them, rather than an increase due to soil resistance. As seen in **Chapter 4** for lateral tests (β = 90°), the value of soil restraint is considered constant after the maximum soil resistance is fully mobilised. Therefore, only the values before Y' = 0.4D were considered meaningful for this work.

From **Figure 5.3**, it is interesting to note that the axial load cell started recording values after the pipe had experienced oblique loads in the order of 30 kN/m to 35 kN/m. This behaviour is associated with the overcome of pipe-soil friction along the length of the pipe shaft. The load cell started to record load values only after the pipe has moved along its axis or after the pipe-soil friction has been overcome. Also as expected, the movement of the pipe in its axial direction depends on the level of the oblique load, F, as evidenced by the curve traces depicted in **Figure 5.3**.

The variation of normalized lateral soil restraint, N_{qh}, and normalized axial soil restraint, T_a, with normalized pipe displacement Y'_P, and Y'_T, respectively, obtained from **Equations 5.5** through **5.7** is shown in **Figure 5.4**. This figure also shows the lateral soil restraint vs. normalized pipe displacement, Y', for Tests 18-1.9-90H-MS-MS-GN-1 and 18-1.9-90H-MS-MS-GN-2 on NPS18 (457-mm diameter) pipe specimens buried in moist sand with H/D = 1.9.

The computation of normalized axial and lateral soil restraints was performed with an assumed sliding friction factor of 10%. Changing the assumed sliding friction factor to 5% or 20% changes the magnitude of the computed normalized axial and horizontal soil restraints by less than 5% from the values for a 10% sliding friction. The effect of the sliding friction factor on the computed normalized axial and lateral soil restraints can be further observed in **Figure 5.5**.

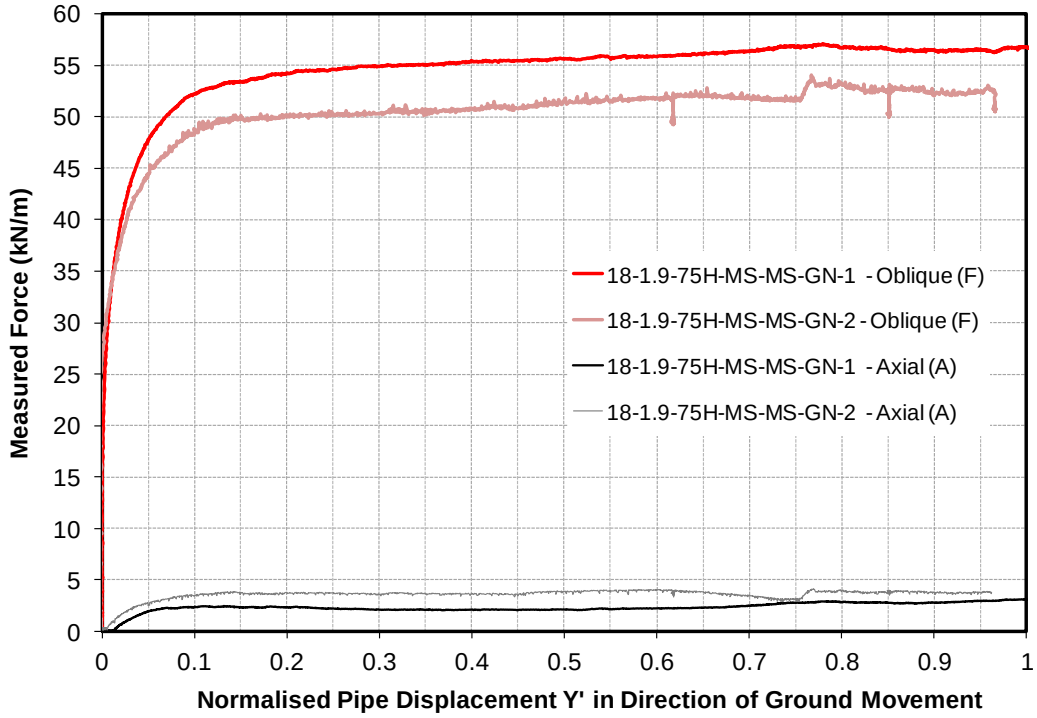

Figure 5.3: Load-displacement relationships measured for β = 75° with H/D=1.9 buried in moist sand during horizontal oblique pulling.

Values for normalized lateral soil restraint, N_{qh}, were selected as those that correspond to the oblique displacement at which the onset of the maximum normalized axial soil restraint was reached. Values normalized for axial soil restraint were selected at the points identified in **Figure 5.4**. As seen in this figure, maximum levels of normalized lateral soil restraint, N_{qh}, vary between 7.0 and 7.85 (46 kN/m to 52 kN/m). These values are similar to those recorded for lateral tests in sand with NPS18 (see **Section 4.2.1**). It is interesting to note that the maximum levels of lateral soil restraint, N_{qh}, occurred at normalized pipe displacement Y'_P, of 0.1D to 0.2D. This range of normalized lateral pipe displacements is similar to that observed for lateral tests in sand with NPS16 and NPS18. Maximum levels of normalized axial soil restraint, T_a, vary between 1.2 and 1.8 (8 kN/m to 12 kN/m).

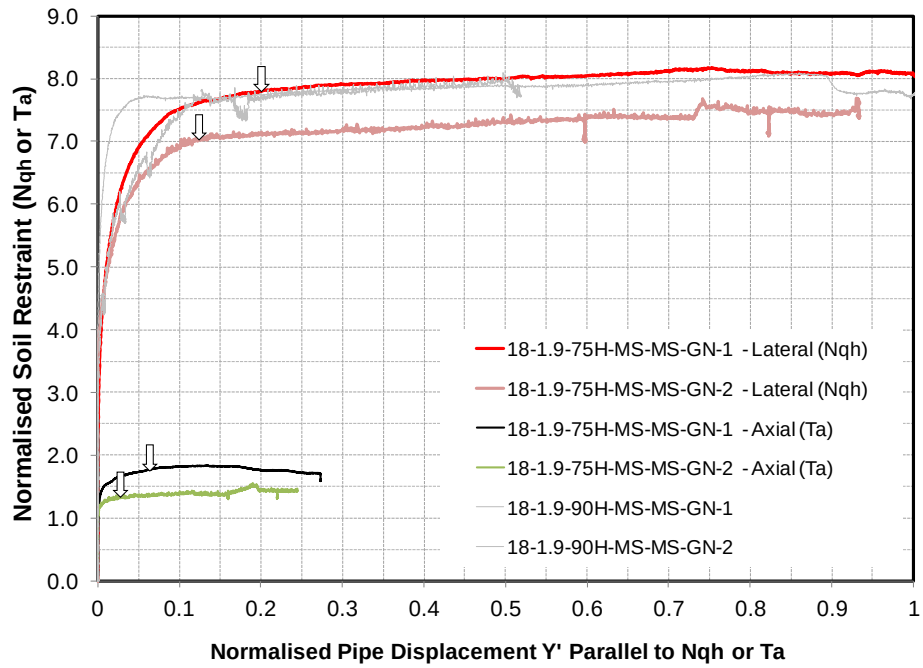

Figure 5.4: Axial and lateral soil restraint-displacement relationships for β = 75° with H/D=1.9 buried in moist sand during horizontal oblique pulling.

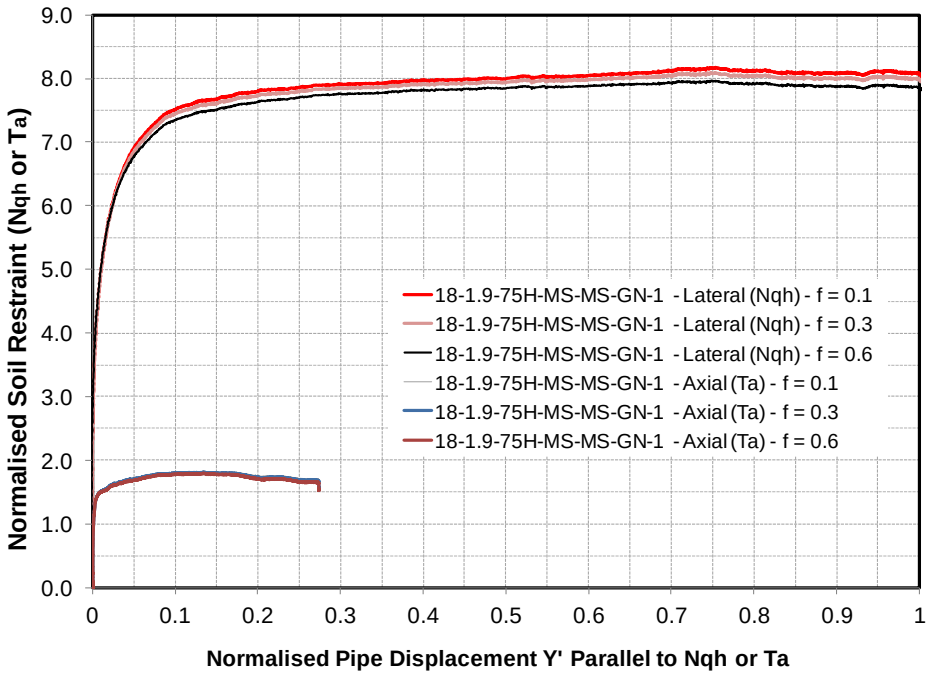

Figure 5.5: Effect of the sliding friction factor on the computed axial and lateral soil restraint values.

5.4 Results of Horizontal Oblique Tests – β = 60 degrees

5.4.1 Load-Displacement Response

The variation in oblique, F, and axial reaction, A, load for the pipe specimen under oblique displacement with β = 60° is shown in **Figure 5.6**. Both, the oblique and axial load cell measurement recorded continuous nonlinear load increase behaviour. However, similar to the case of oblique displacement with β = 75° some increase in load is believed to be associated with constraints provided by the size of the box, rather than an increase due to soil resistance. After evaluating the data and the pipe specimen kinematics, only the values before Y' = 0.2 to 0.3D were considered meaningful for this work.

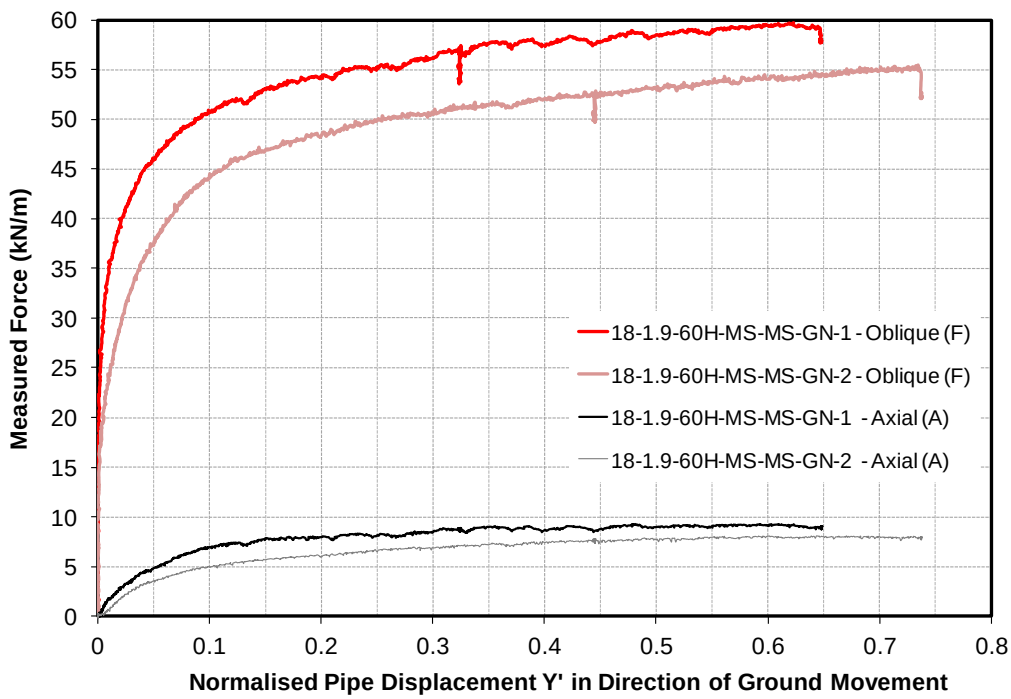

Figure 5.6: Load-displacement relationships measured for β = 60° with H/D=1.9 buried in moist sand during horizontal oblique pulling.

Similar to the case of β = 75°, the computation of axial and lateral soil restraints was performed with an assumed sliding friction factor of 10%. The variation of lateral soil restraint, N_{qh}, and axial soil restraint, T_a, with normalized pipe displacement Y'_P, and Y'_T, respectively, obtained from **Equations 5.5** through **5.7** is shown in **Figure 5.7**. This figure also shows the lateral soil restraint vs. normalized pipe displacement, Y', for Tests 18-1.9-90H-MS-MS-GN-1 and 18-1.9-90H-MS-MS-GN-2 on NPS18 (457-mm diameter) pipe specimens buried in moist sand with H/D = 1.9.

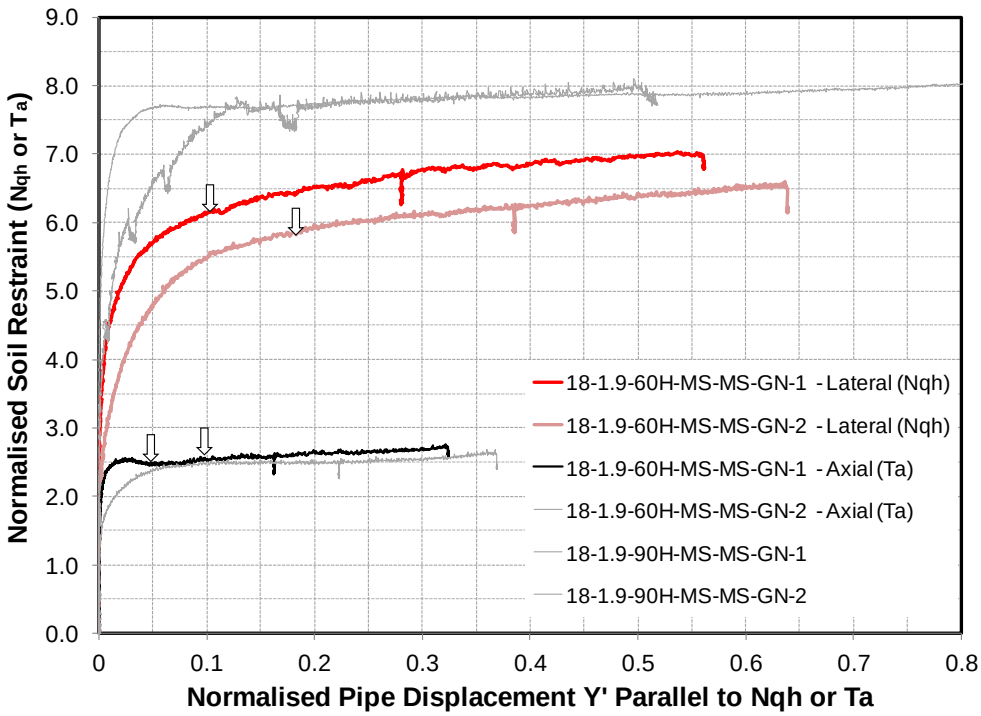

Figure 5.7: Axial and lateral soil restraint-displacement relationships for β = 60° with H/D=1.9 buried in moist sand during horizontal oblique pulling.

Values for normalized lateral soil restraint, N_{qh}, were selected as those that correspond to the oblique displacement at which the onset of the maximum normalized axial soil restraint was reached. Values for normalized axial soil restraint were selected at the points identified in **Figure 5.7**. As seen in this

figure, maximum levels of normalized lateral soil restraint, N_{qh}, vary between 5.7 and 6.3 (38 kN/m to 42 kN/m). These values are about 25% lower than those recorded for lateral tests in sand with NPS18. It is interesting to note that the maximum levels of normalized lateral soil restraint, N_{qh}, also occurred at the same range of normalized pipe displacement as that observed for lateral tests in sand with NPS16 and NPS18 (0.1D to 0.2D). Maximum levels of normalized axial soil restraint, T_a, vary between 2.4 to 2.6 (16 kN/m to 17 kN/m) and occur at Y'_T of 0.05D to 0.1D.

5.5 Results of Horizontal Oblique Tests – β = 45 degrees

5.5.1 Load-Displacement Response

The change in oblique, F, and axial reaction, A, load for the pipe specimen under oblique displacement with β = 45° is shown in **Figure 5.8**. Both, the oblique and axial load cell measurement recorded continuous nonlinear load increase behaviour. This noticeably persistent increase in load is believed to be associated with constraints provided by the lateral walls of the testing chamber, similar to those from oblique displacement with β = 60° and 75°. In light of the above concerns, the values from this test required more engineering judgment for meaningful interpretation.

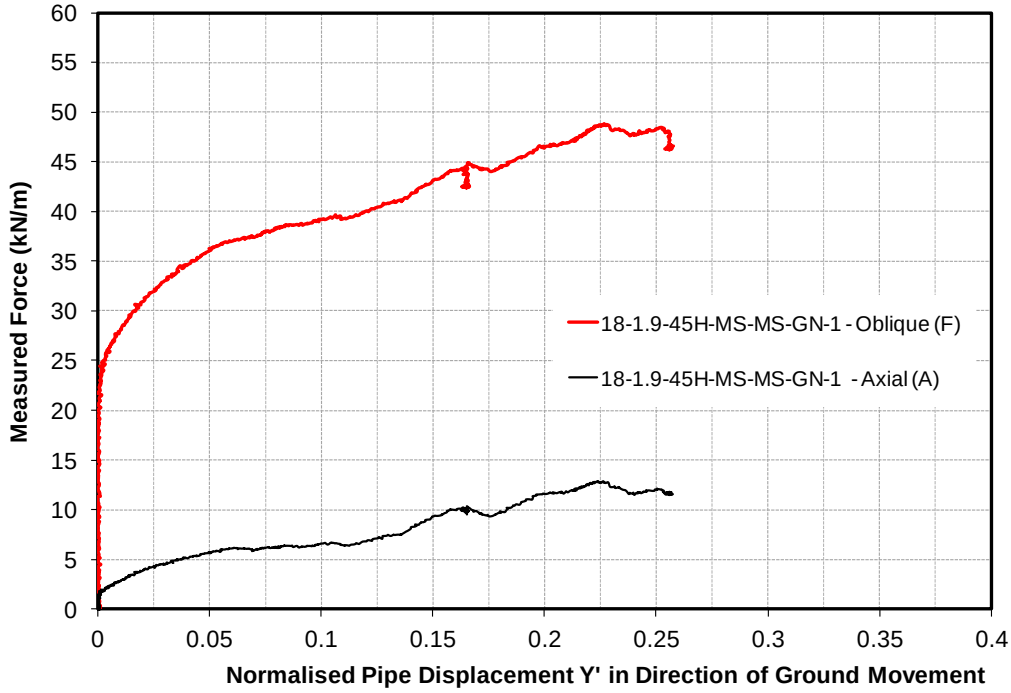

Figure 5.8: Load-displacement relationships measured for β = 45° with H/D=1.9 buried in moist sand during horizontal oblique pulling.

The variation of normalized lateral soil restraint, N_{qh}, and normalized axial soil restraint, T_a, with normalized pipe displacement Y'_P, and Y'_T, respectively, obtained from **Equations 5.5** through **5.7** is shown in **Figure 5.9**. The computation of axial and lateral soil restraints was performed with an assumed sliding friction factor of 10%. Lateral soil restraint vs. normalized pipe displacement, Y', for Tests 18-1.9-90H-MS-MS-GN-1 and 18-1.9-90H-MS-MS-GN-2 on NPS18 (457-mm diameter) pipe specimens buried in moist sand with H/D = 1.9 are also shown in **Figure 5.9**.

As seen in **Figure 5.9**, the maximum level of normalized lateral soil restraint, N_{qh}, is about 3.6 (24 kN/m) and occurs at a normalized ground displacement parallel to the lateral soil restraint Y'_P of 0.08D. The maximum level of normalized lateral soil restraint, N_{qh}, is about 50% lower than those recorded

for lateral tests in sand with NPS18 (around 7.7). The maximum level of axial soil restraint, T_a, is 2.6 (17.5 kN/m) and occurs also at Y'_T of 0.08D.

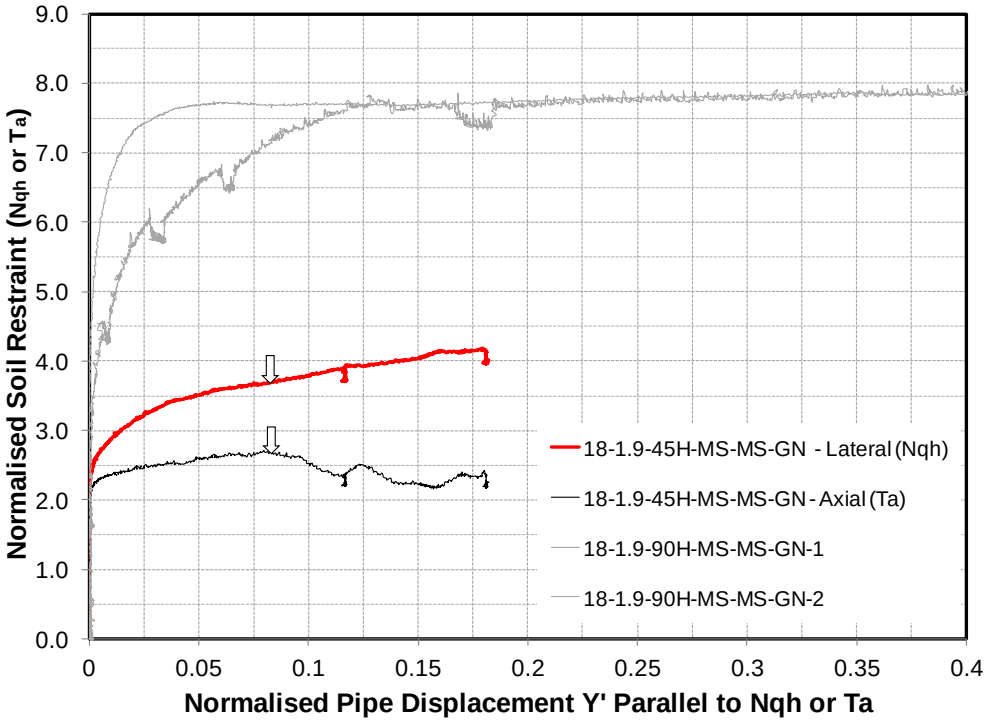

Figure 5.9: Axial and lateral soil restraint-displacement relationships for β = 45° with H/D=1.9 buried in moist sand during horizontal oblique pulling.

5.6 Discussion on Horizontal Oblique Pipe-Soil Interaction

The soil-pipe interaction relationships for oblique loading in the existing literature arises from those reported by Hsu et al. (2001, 2006) and investigators at C-CORE (Phillips et al. 2004; Daiyan et al. 2010, 2011). These interaction relationships are based on the values of maximum lateral and axial soil restraint and were developed upon a limited number of small-scale test, centrifuge tests and finite element modeling, where sand was used as the surrounding soil. The interaction envelops proposed by these

investigators are shown in **Figure 5.10**. Furthermore, Ha et al. (2008) presented results from four centrifuge tests for two oblique loading (β of 85° and 63.5°) on HDPE pipes. However, no lateral-axial interaction relationship was evaluated.

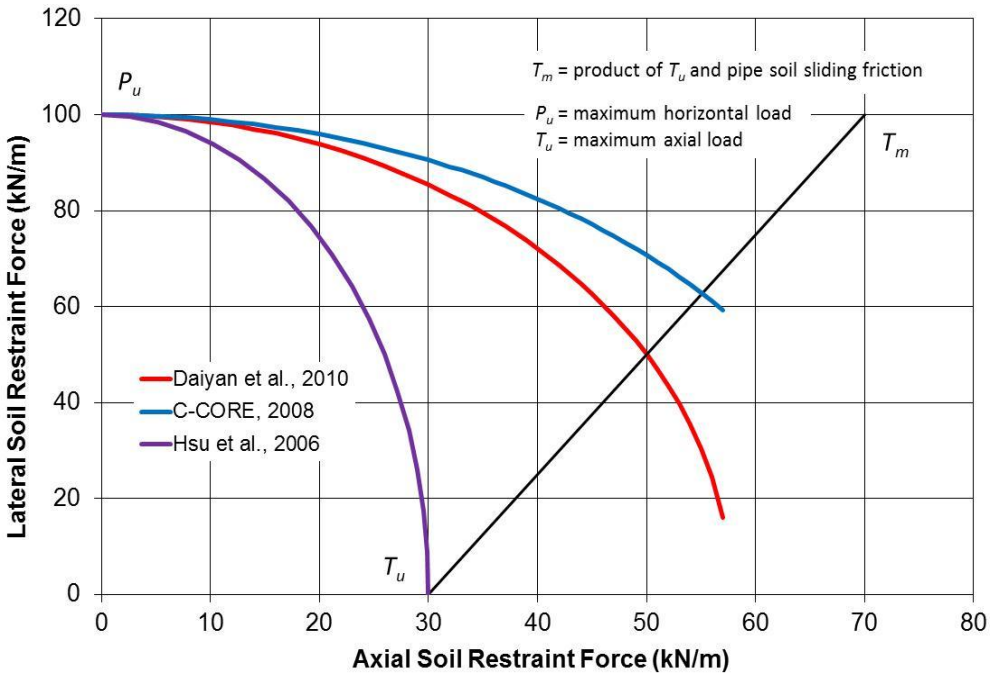

Figure 5.10: Axial-lateral soil restraint interaction envelopes proposed by Hsu et al (2006); C-CORE (2008) and Daiyan et al. (2010, 2011).

Based upon observed trends in small-scale test results with the oblique direction of horizontal ground displacement relative to the pipeline axis (0° being purely axial and 90° being purely lateral), Hsu et al. (2001, 2006) argued that the relation between axial and lateral soil restraint during relative oblique displacements is a function of the cosine and sine of the oblique angle, respectively. Their tests were based on pipe specimens with outside diameters of 152.4 mm, 228.6 mm, and 304.8 mm buried in loose and dense

sand which were subjected to relative displacements at oblique angles from 0° to 90°.

Investigations by Phillips et al. (2004) and Daiyan et al. (2010, 2011), however, showed that the interaction between axial and lateral soil restraint during relative oblique displacements do not fit in the pattern of cosine and sine of oblique angle relationship for oblique soil-pipe interaction. The reason for this disagreement was not addressed by Phillips et al. (2004) and Daiyan et al. (2010, 2011). Nevertheless, it can be hypothesized that the disagreement is due to the different loading equipment used for their tests.

Phillips et al. (2004) and Daiyan et al. (2010, 2011) claimed that the value of axial soil restraint during axial-lateral soil restraint coupling is more than the pure axial condition; with a factor of even 2.5 for oblique angles less than 40°. The observed higher axial soil restraint by Phillips et al. (2004) and Daiyan et al. (2010, 2011) is attributed to an increase in normal or lateral pressure due to the lateral component of oblique relative displacement. They also observed large increments of axial soil restraint for oblique angles of even 1° (pipe misalignment) during their numerical simulation. However, this condition required oblique displacements larger than 1D.

Based on results from centrifuge tests and numerical modelling, they proposed a two-dimensional interaction envelope by using the axial and lateral soil restraint values as axes. This interaction envelope can be characterised by a combination of a linear and nonlinear relationship (see **Figure 5.10**). The linear relationship is associated with soil failure along the pipe axis (pipe circumference) and the nonlinear relationship is related to failure occurring in the soil mass. The transition between linear and nonlinear relationship was found to occur at an oblique angle of approximately 40°. The interaction envelopes proposed by Phillips et al. (2004) and Daiyan et al. (2010, 2011) are as follows:

$$N^2_{qh} + 2 \cdot N_t^2 = N^2_{qh(90)} \text{ Phillips et al. (2004)} \quad [5.5]$$

$$N^2_{qh} + 3 \cdot N_t^2 = N^2_{qh(90)} \text{ Daiyan et al. (2010, 2011)} \quad [5.6]$$

where $N_{qh(90)}$ is the ultimate lateral soil restraint during pure lateral pipe–soil relative movement. The parameters N_{qh} and N_t are lateral and axial soil restraint, respectively, and specify completely the interaction state during horizontal oblique relative displacement. The linear part of **Equation 5.5** and **5.6** connects the point associated with the pure axial condition to a point with horizontal coordinate of (δN_{qh}) and vertical coordinate of (N_{qh}); where δ is the soil-pipe interface friction coefficient.

Numerical sensitivity analyses carried out by Daiyan et al. (2010, 2011), in which parameters such as peak soil friction angle, H/D ratio and soil-pipe friction angle were changed, showed that the interaction envelopes proposed by Phillips et al. (2004) and Daiyan et al. (2010, 2011) possess a unique surface in N_{qh} and N_t space.

A comparison between the horizontal oblique soil restraints from this testing program to the interaction envelopes for oblique soil restraints proposed by other researchers will now be examined. To do so, it is necessary to have the values of maximum soil restraint under direct axial (β = 0 deg) and lateral loading (β = 90 deg) events to serve as “anchor points” on a normalized axial and normalized lateral restraint plot similar to that shown in **Figure 5.10**. Axial tests were not included in this testing work. Therefore, peak axial soil restraint values were determined using the knowledge available from already published information. This process of determining the axial soil restraint considering the current literature will be discussed in the following paragraphs in a context comparable to the H/D of 1.9 tests carried out in this research. Lateral soil restraint values from this work can be found in **Section 4.7.2** of **Chapter 4**.

As described in **Section 2.1.2** of **Chapter 2**, the ASCE (1984) "Guidelines for the Seismic Design of Oil and Gas Pipeline Systems", the American Lifeline Alliance (2001) "Guidelines for the Design of Buried Steel Pipe", and the PRCI (2004) "Guidelines for the Seismic Design and Assessment of Natural Gas and Liquid Hydrocarbon Pipelines" recommend the following equation for calculating values of axial soil restraint per unit length:

$$F_a = \pi \cdot D \cdot (\sigma'_n)_{av} \cdot \tan(\delta) \qquad [2.5]$$

where:

$$(\sigma'_n)_{av} = \left(\frac{1+Ko}{2}\right) \cdot \gamma \cdot H \qquad [2.5\text{-A}]$$

$(\sigma'_n)_{av}$ is the average normal soil stress on the pipe in at rest conditions; H is the height of the soil over the pipe springline; D is the nominal diameter of the pipe; δ is the soil-pipe interface friction angle; K_0 is the coefficient of lateral earth pressure at rest, taken as 1-sinϕ; and γ is the soil density. **Equation 2.5** can be expressed in terms of the normalized axial soil restraint

$$T_a = F_a / (\gamma \cdot D \cdot H) \qquad [2.6]$$

Equation 2.6 leads to a F_a of 10 kN/m or a T_a value of about 1.5 for the pipe-soil interaction parameters used in this work (i.e. pipe specimen buried in sand with H/D=1.9, soil peak friction angle of 43° and soil-pipe interface friction angle of 36°, see **Table 5.2**).

Hsu et al. (2006) reported a maximum normalized axial soil restraint, T_a, of about 1.1 for a pipe specimen (diameter of 228.6 mm) buried in sand with peak friction angle of 42°, soil-pipe interface friction angle of 26° and for H/D = 2. As indicated by Hsu et al. (2006), this value is close to that obtained from

Equation 2.6. However, the axial displacement to failure reported by Hsu et al. (2006) is much larger than the usual range of about 3 mm expected for dense sand (PRCI, 2004). They reported an axial displacement of around 0.2D. A similar large lateral displacement to failure was reported by Hsu et al. (2006). These findings by Hsu et al. appear anomalous, and it is possibly due to substantial interference of the loading system with the soil stresses around the pipe specimen.

In addition, Hsu et al. (2006) reported a normalized lateral soil restraint displacement N_{qh} of about 7.5 for H/D = 2 on dense Da-Du riverbed sand with density of 17.2 kN/m^3 (relative density of 94%) and peak friction angle of 42°. Hsu et al. (2006) did not report lateral pipe displacement values associated with the above N_{qh} value. However, the lateral displacement associated with the maximum lateral soil load for H/D = 1 was about 0.25D. This value of lateral displacement is much larger than the maximum range of ultimate displacement for lateral movement of pipe in sand of 0.1D to 0.15D suggested by PRCI (2004) or the range recommended by Trautmann (1983) and Audibert and Nyman (1977) of 0.03D to 0.045D for H/D of 1.

The result of full-scale axial tests performed by Karimian (2006) and Wijewickreme et al. (2009) on steel pipe (diameter of 457 mm) in dense Fraser River sand with peak friction angle of 43°, soil-pipe interface friction angle of 36° and H/D ratio of 2.5 is provided in **Figure 5.11**. As illustrated in this figure, the axial response of the pipeline in dense sand exhibits a high peak load, T, of approximately 27 kN/m with a residual axial load, T, determined as the load during a subsequent loading cycle, of approximately 17 kN/m. These are equivalent to a normalized maximum axial soil restraint, T_a, of about 3.3 and a normalized residual axial soil restraint, T_a, of about 2.0.

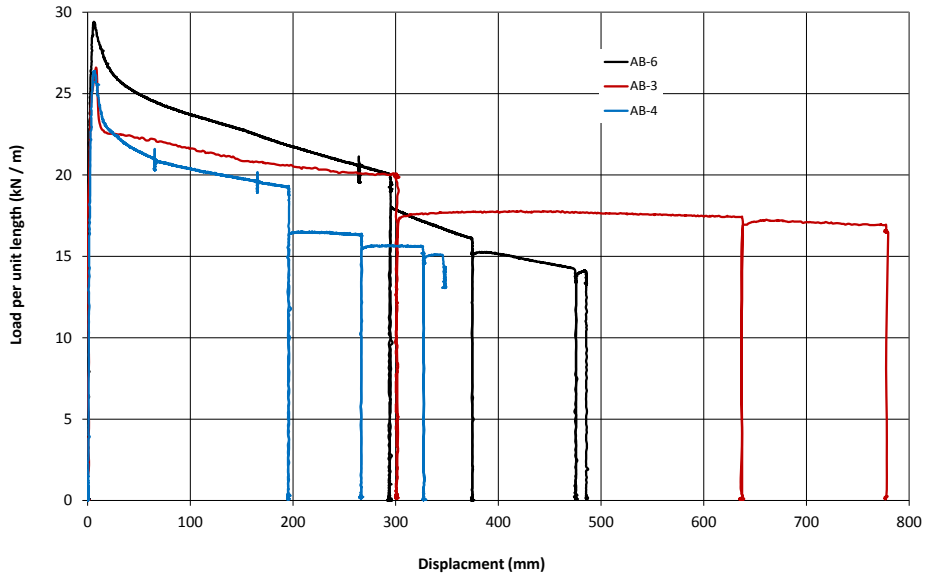

Figure 5.11: Axial load-displacement response from Karimian (2006) (H/D = 2.5, NPS18, dry density = 16 kN/m^3; Fraser River sand).

As noted in Wijewickreme et al. (2009), the range of axial values measured during full-scale tests (**Figure 5.11**) is considerably higher than the value calculated following the recommended equation from PRCI (2004) or ASCE (1984). The difference is attributed by Wijewickreme et al. (2009) to increased normal soil force on the pipeline from shear-induced soil dilation. Disturbance of the pipe soil interface from continued axial displacement or cycling of the axial displacement reduces the axial soil load to a value more consistent with the computed value.

Because the test bed used in the oblique tests was prepared in the same manner as for the dense moist sand tests reported in Wijewickreme et al. (2009), their results were scaled to H/D of 1.9 to account for differences in pipe diameter and burial depth. Therefore, the purely axial load is taken to be the value from prior test results, but scaled by the *H/D* ratios in accordance with the effect of *H* on axial load. Accordingly, peak axial load, T, is taken to be approximately 21 kN/m or T_a, of 3.3.

Daiyan et al. (2010, 2011), based on their results from centrifuge tests, reported a maximum normalized axial soil restraint, T_a, of about 2.0 for a pipe specimen buried in sand with peak friction angle of 43°, unit weight of 16 kN/m^3, soil-pipe interface friction angle of 24°and H/D = 2. Daiyan et al. (2010, 2011) acknowledged that both the purely horizontal soil restraint and purely axial soil loads measured in their centrifuge tests for H/D = 2 on dense sand were approximately two times higher than what they should have been if **Equation 2.6** is applied. The high horizontal soil load was attributed to the high weight of the pipe loading system.

Similar to the case of the extremely large pipe displacement value required to reach maximum axial soil restraint in small-scale tests reported by Hsu et al. (2006), axial load-displacement response in the Daiyan et al. (2010, 2011) centrifuge tests showed a pipe displacement value of 14 mm at model scale (0.34D at prototype scale), against values less than approximately 5 mm to 10 mm (less than 0.05D) that are typically observed in full-scale pipe tests (NOVA, 1995; Karimian, 2006). Daiyan et al. (2010, 2011) considered their centrifuge tests as valid because their 3D numerical simulation resulted in comparable peak load values when the weight of the pipe and loading mechanism were incorporated in the simulation. However, the large pipe displacements to failure were not reproduced in their numerical work.

A simulation without the additional weight from the loading mechanism was carried out by Daiyan et al. (2011) to further verify their numerical model. They found N_{qh} of about 9.7 and normalized axial soil restraint, T_a, of about 1.1 for a pipe specimen buried in sand with H/D = 2, soil peak friction angle of 45° and soil-pipe interface friction angle of 24°. Their maximum normalized value for axial soil loads is very similar to the value T_a of 0.92 calculated following **Equation 2.5**. Similarly, the computed N_{qh} value is similar to those reported in the literature for H/D = 2 and the one obtained in this work.

A summary of the peak axial soil restraint values existing in the current technical literature and described previously is shown in **Table 5.3**. A comparison between the normalized axial soil restraint values reported in the literature and those obtained from **Equation 2.5** is shown in **Table 5.4**.

As noted in both tables, the pure axial restraint soil values present a large range. Wijewickreme et al. (2009) values are about 2 to 3 times higher than those reported by Hsu et al. (2006), Dayian et al. (2011) and those calculated from the equation recommended by PRCI (2004). Therefore, interaction envelopes will be constructed based on both peak and residual axial soil restraint values from Wijewickreme et al. (2009) and the peak axial soil restraint value from PRCI (2004). The latter one is considered representative for the normalized values reported by Hsu et al. (2006) and Dayian et al. (2011). An N_{qh} of 7.7 will be used for the maximum lateral soil restraint. The results of all the horizontal oblique tests carried out in this work are summarized in **Table 5.5**.

Table 5.3: Normalized Axial Soil Restraint Values Available in the Literature

Source	Soil Backfill	Peak friction angle	Soil-pipe friction angle	H/D	Peak Axial Soil Restraint T_a	Residual Axial Soil Restraint T_a
Hsu et al., (2006)	Dense sand	42°	26°	2.0	1.1	1.1
Wijewickreme et al., (2009)[1]	Dense sand	43°	36°	1.9	3.3	2.0
Dayian et al (2011)[2]	Dense sand	43°-45°	24°	2.0	1.1	1.1

[1] Values scaled from test data with H/D=2.5
[2] Values read from Figure 18 (Dayian et al. 2011) based on numerical modelling without weight of loading system

Table 5.4: Normalized Axial Soil Restraint Values Predicted by PRCI (2004)[1] and ASCE (1984)[1]

Source	Peak T_a from test	Residual T_a from test	Peak T_a from PRCI (2004)	Residual T_a from PRCI (2004)
Hsu et al., (2006)	1.1	1.1	1.0	1.0
Wijewickreme et al., (2009)	3.3	2.0	1.5	1.5
Dayian et al (2011)	1.1	1.1	0.92	0.92

[1] Values based on soil and soil-pipe parameters reported in **Table 5.3**

Table 5.5: Maximum Horizontal Oblique Soil Restraint Values from This Work

Test	Lateral Soil Restraint N_{qh}	Axial Soil Restraint T_a
18-1.9-75H-MS-MS-GN-1	7.78	1.71
18-1.9-75H-MS-MS-GN-2	7.07	1.33
18-1.9-60H-MS-MS-GN-1	6.43	2.55
18-1.9-60H-MS-MS-GN-2	5.86	2.48
18-1.9-45H-MS-MS-GN-1	3.62	2.64

A comparison of oblique soil restraints measured in the current testing program and recommended relationships by Hsu et al. (2006) is provided in **Figure 5.12**. As can be observed from **Figure 5.12**, the trend in the variation of maximum horizontal and axial load roughly approximates the variation in the interaction relationships proposed by Hsu et al. (2006) when the peak axial soil restraint from Wijewickreme et al. (2009) is used as the x-axis "anchor point" on a normalized axial and normalized lateral restraint plot. However, the test values for 60° and 75° from this work are somewhat higher than those recommend by Hsu et al. (2006) for oblique angles greater than 45°.

For other values of axial soil restraint (i.e., if residual from Wijewickreme et al. (2009) and peak from PRCI (2004)) were used as anchor points, the interaction relationships built upon the concept proposed by Hsu et al. (2006) would not agree with the oblique soil restraint values measured in this work.

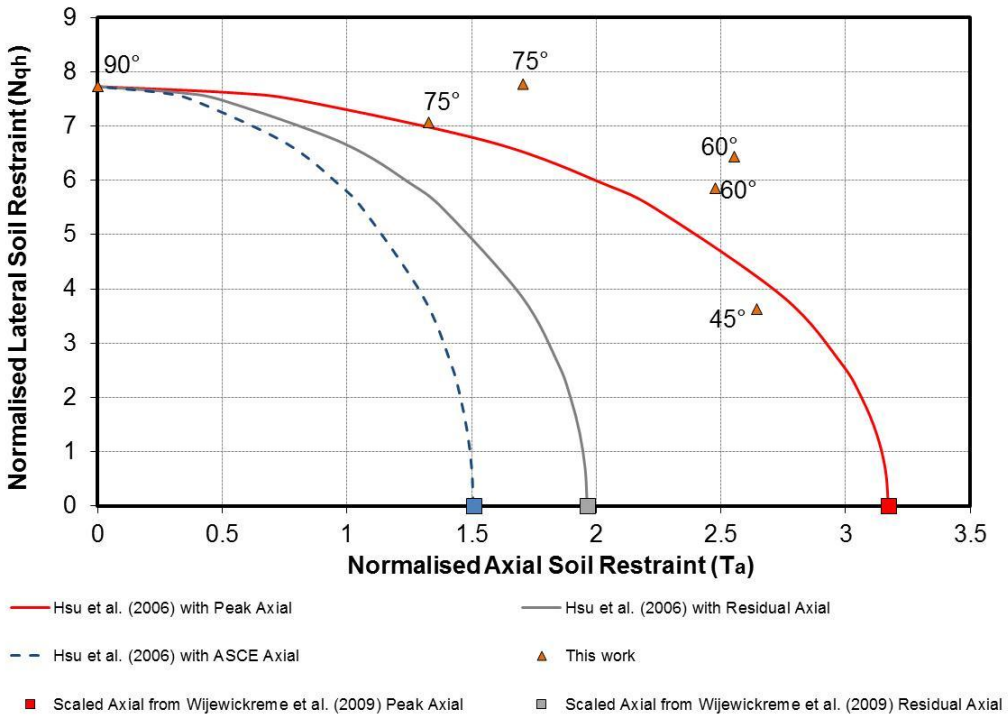

Figure 5.12: Horizontal oblique test results compared to Hsu et al. (2006) interaction relationship.

In a similar manner, the results of the current tests are compared with the recommended relationships of Phillips et al. (2004) and Daiyan et al. (2011) in **Figure 5.13**. Except for the data for a horizontal oblique angle of 45°, there is a close agreement between the nonlinear relationship, related to failure occurring in the soil mass proposed, by Phillips et al. (2004) and Daiyan et al. (2011), to the data for horizontal oblique angles of 60° and 75° from this research. As may be noted, this agreement is not sensitive to the selected anchor point value of the pure axial soil restraint in plotting the Phillips et al. relationships.

The discrepancy at the horizontal oblique angle of 45°appears to be due to the selection of axial soil restraint for the interaction envelopes. For example, if the peak and residual axial soil restraint values from Wijewickreme et al.

(2009) are used as anchor points to construct the interaction envelopes, the results for an horizontal oblique angle of 45° from this work does not support the large increase in axial restraint under oblique conditions that are required for the Phillips et al. (2004) and Daiyan et al. (2011) recommendations. On the other hand, if the axial soil restraint value from PRCI (2004) is used, then the trend in the variation of maximum horizontal and axial soil restraint roughly approximates the variation in the interaction relationships proposed by C-CORE investigators - in particular, the relationship proposed by Phillips et al. (2004).

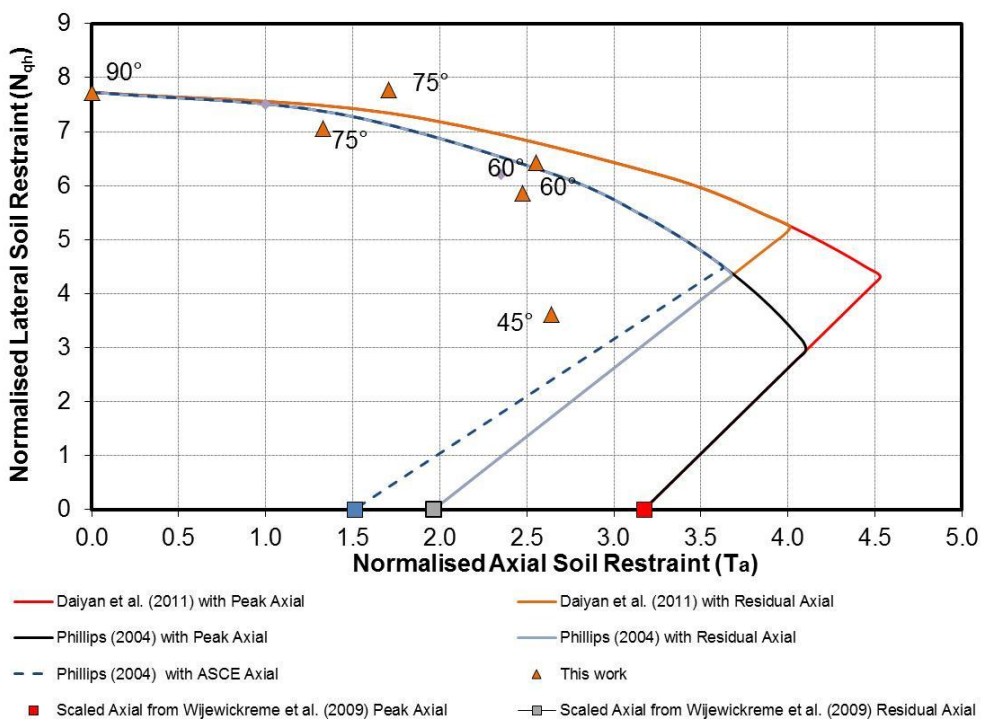

Figure 5.13: Horizontal oblique test results compared to Phillips et al. (2004) and Daiyan et al. (2011) interaction relationships.

The above comparison highlights the importance of the pure axial soil restraint value (i.e., x-axis anchor point value) in comparing among the available oblique soil restraint envelopes by different researchers, regardless of the agreement in results for oblique angles β less than 45°. If a much lower purely

axial load is used as the anchor point for the horizontal axis, the observed horizontal and axial soil restraint coupling from the present work would be much greater than that given by the relationship proposed by Hsu et al. (2006). Conversely, the use of a lower value for the case of pure axial loading measure would lead to a decrease in the difference in the data from the present work and the recommendations of Phillips et al. (2004) and Daiyan et al. (2011). In essence, the horizontal oblique states measured from the present study are not sufficient to affirm or refute the recommended relationship of Hsu et al. (2006) or Daiyan et al. (2011) due to the impact of the pure axial soil restraint value on the horizontal oblique relationships.

Numerical results presented in Daiyan et al. (2011) indicate little variation in maximum axial soil restraints for oblique angles between approximately 2° and 50°. Full-scale testing at oblique angles less than 45°, in order to capture soil failure along the pipe axis, is not practical in the soil test chamber at UBC. Testing specimens at the same scale used in this research work at smaller oblique angles would require the length of the test chamber to be increased substantially. Alternatively, tests at smaller β values would be feasible if the scale of the test specimen could be reduced with a commensurate reduction in the width of the test chamber.

5.7 Summary of the Chapter

A series of horizontal oblique tests were conducted on several pipe specimens buried in moist sand to characterize axial and lateral soil-pipe interaction coupling effects during relative oblique ground displacements. In addition to the measurement of horizontal oblique loads and pipe displacements during the tests, a load cell arrangement was designed and constructed inside the pipe specimens to continuously measure axial reaction loads. Monitoring of both axial reaction and horizontal oblique loads allowed the successful quantification of coupled axial and lateral soil restraints that arise during oblique or three dimensional soil-pipe relative movements. The axial-lateral coupling effects measured during the full-scale tests of this work provided limited clarification on whether or not soil restraints should be considered independent for fault crossing designs.

Some of the key findings/assessments are summarized below:

1. The results from horizontal oblique tests showed a proportional decrease in lateral soil restraint as the oblique angles reduced from 90° (pure lateral) to 60°. Conversely, the axial soil restraint increased as the oblique angles changed from 90° to 60°.

2. The recorded horizontal oblique pipe displacement was also resolved in components of axial and lateral pipe displacements. Resolving the displacements in components parallel to the direction of the load of interest has the advantage of allowing direct comparison with the displacements associated with purely axial and lateral maximum soil restraint data. The results showed that the pipe displacements required to mobilise peak soil restraint in the axial direction and the

lateral direction (perpendicular to the pipe axis) were in line with the pipe displacement ranges specified by PRCI (2004, 2009).

3. The comparisons highlighted the importance of the pure axial soil restraint in the evaluation of the available oblique soil restraint envelops. The current literature shows a large range for values of pure axial restraint soil. For example, Wijewickreme et al. (2009) values observed in pipes buried in dense soils are about 2 to 3 times higher than those reported by Hsu et al. (2006), Dayian et al. (2010, 2011), and those calculated from the equation recommended by PRCI (2004).

4. A selection of the lower end of pure axial soil restraint value led to the coupled horizontal and axial soil restraint from the present work being much greater than that given by the relationship proposed by Hsu et al. (2006). Conversely, there would be a decrease in the difference in the data from the present work and the recommendations of Phillips et al. (2004) and Daiyan et al. (2010, 2011) if the lower end of pure axial soil restraint value is used in the existing relationships. Therefore, the horizontal oblique states measured from the present study are not sufficient to affirm or refute the recommended relationship of Hsu et al. (2006) or Daiyan et al. (2010, 2011). Further studies on axial soil restraint for pipes buried in dense sand are necessary.

5. There is some uncertainty on the values measured in the test at an oblique angle of 45°. However, the results for the 45° oblique angle appear to be more critical to judging how the data from this work compare with Phillips et al. (2004) and Daiyan et al. (2010, 2011).

6. Full-scale testing at oblique angles less than 45°, in order to capture soil failure along the pipe axis, is not practical in the soil test chamber at UBC. Testing specimens at the same scale used in this research work at smaller oblique angles would require the length of the test

chamber to be increased substantially. Alternatively, the scale of the test specimen could be reduced with a commensurate reduction in the width of the test chamber.

Chapter 6: Vertical Oblique Soil Restraint on Pipelines

The design of reverse/thrust fault crossings requires pipe-soil restraint properties to estimate the performance of pipeline segments. Experimental data to obtain these properties are seldom available in current published technical literature, and usually, they are inferred in practice on the basis of horizontal and vertical soil restraints. This involves a large degree of extrapolation tempered with conservative engineering judgment.

In this chapter, the results from a series of vertical oblique soil restraint tests conducted to obtain parameters supporting the design of reverse fault crossings for onshore pipelines are described. Five tests were carried out using a NPS16 (406-mm) diameter steel pipe buried in uniformly graded crushed limestone; three other tests were conducted on pipe specimens buried in moist Fraser River sand backfill to provide a comparison and baseline case for the limestone backfill material. The pipes had about 450 mm of soil cover above the crown (H/D = 1.6) of pipe. A selected number of tests included a typical trench wall sloped at an angle of 45° degrees from the horizontal that was constructed inside the soil testing chamber, and lined with geosynthetic in an effort to study the effectiveness of the geosynthetic to reduce vertical oblique soil restraints on buried pipes.

Relative vertical oblique displacements at angles of 35° and 45° degrees from the horizontal were applied to a pipe specimen to simulate the oblique angle breakout of buried pipelines from their soil embedment on the footwall side of reverse/thrust faults. Two inclinometers and a set of 8 string potentiometers (four per loading cable) were utilized in order to record and also to verify that loads were applied along the required inclinations during the testing process.

Geometric changes in the soil mass, shear rupture surfaces, levels of vertical oblique soil restraint, and patterns of geotextile displacement are described and discussed with the aim of characterizing the soil-pipe interaction behaviour observed from the large-scale tests.

6.1 Summary of Test Parameters

As indicated in **Section 3.7.4**, a total of six (6) tests were conducted to characterize the mechanical soil-pipe behavior under vertical oblique ground displacements induced by thrust or reverse faults. In addition, two tests were conducted to determine soil-pipe interaction behaviour under vertical upward displacements.

The tests were undertaken with moist sand or uniformly graded limestone trench fill materials, using different trench configurations with or without the presence of geotextile interfaces between trench backfill and sloping trench surface. The description of the materials, placement procedures and techniques related to the testing are detailed in **Chapter 3**. A summary of the main test parameters are described in **Table 6.1**.

The observed vertical oblique soil restraint-pipe displacement responses for the six model tests will be described in the following sub-sections on a test-by-test basis. The results from tests on pipe buried in moist sand backfill were conducted to provide a comparison and baseline case for the limestone backfill material. The list of conducted tests is described in **Chapter 3** and repeated in **Table 6.2** for the reader's convenience. All the tests were conducted on NPS16 steel pipe specimens.

Table 6.1: Summary of Parameters for Vertical Oblique Soil Restraint Tests

	Fraser River Sand	Crushed Limestone
Average Dry Density (kg/m^3)	1600	1700
Average moisture (%)	3 to 4	Approx. less than <4%
Internal Peak Friction Angle	43°	46°[1]
Dilation Angle	12°	18°[1]
Pipe Size	NPS16	NPS16
Pipe Length (m)	2.42	2.48
Pipe Grade & Surface	Steel Grade 524A, Sand Blasted Surface	Steel Grade 524A
Geosynthetic Material	-	TC Mirafi Filterweave 700 & GSE HDE 080A000 (80mil HDPE)
Soil-Geotextile Interface Friction Angle	-	ND
Pulling Rate	2.5 mm/s	2.5 mm/s

Note: [1] Inferred from lateral large-scale test; ND = Not determined

For all tests, the total load per unit length on the pipe was determined by adding the load measured from each load cell and then dividing it by the length of the pipe specimen. Symmetry of the pulling system was verified by controlling the difference in recorded readings from each load cell to be less than 5%.

Test results from this work are presented in terms of normalized values of vertical oblique soil restraint, N_{vo}, vertical soil restraint, N_{qv}, and normalized displacement, Y' determined from the equations below:

$$N_{vo} = P_{vo} / (\gamma \cdot D \cdot H \cdot L) \qquad [6.1]$$

$$N_{qv} = P_{qv} / (\gamma \cdot D \cdot H \cdot L) \qquad [6.2]$$

$$Y' = Y / D \qquad [4.2]$$

where P_{vo} is the measured vertical oblique load (with respect to horizontal), P_{qv} is the measured vertical upward load, γ is the dry unit weight of the backfill, D is the pipe diameter, H is the height of soil over the pipe springline, L is the pipe length, and Y is the recorded pipe displacement. The form of the normalized load and displacement shown above follows the relationships presented in **Chapter 4** about lateral soil restraint.

Table 6.2: List of Vertical Oblique Soil Restraint Tests

No.	Test ID	Pulling oblique angle (θ) w.r.t horizontal	Backfill	Average backfill dry density (kg/m^3)	Purpose / Comments
1	16-1.6-45V-MS-MS-GN-1	45°	Sand	1,600	Determine soil restraint
2	16-1.6-45V-MS-MS-GN-2	45°	Sand	1,600	Repeatability
3	16-1.6-45V-HB-LM-GN	45°	Crushed Limestone	1,700	Determine soil restraint no geotextile
4	16-1.6-45V-HB-LM-GY	45°	Crushed Limestone	1,700	Determine soil restraint with geotextile
5	16-1.6-35V-HB-LM-GN	35°	Crushed Limestone	1,700	Determine soil restraint no geotextile
6	16-1.6-35V-HB-LM-GY	35°	Crushed Limestone	1,700	Determine soil restraint with geotextile
7	16-1.6-90V-LM-LM-GN	90°	Crushed Limestone	1,700	Determine vertical soil restraint
8	16-1.6-90V-MS-MS-GN	90°	Sand	1,600	Determine vertical soil restraint

6.2 Results of Vertical Oblique Soil Restraint Tests Using Sand Backfill (θ = 45°)

6.2.1 Normalized Soil Restraint-Displacement Response: Sand Backfill - θ = 45°

Variations of normalized vertical oblique soil restraint vs. normalized vertical oblique pipe displacement, Y'= Y/D, for Tests 16-1.6-45V-MS-MS-GN-1 and 16-1.6-45V-MS-MS-GN-2 on a NPS16 (406-mm diameter) pipe specimen buried in moist sand with an overburden ratio H/D of 1.6 are shown in **Figure 6.1**. Vertical oblique pulling displacement with an angle, θ, of 45° from the horizontal to about 1.1D to 1.3D were applied to the pipe specimens to simulate the type of ground displacement at a reverse fault. The tests showed similar characteristic response. Therefore, the soil restraint vs. pipe displacement relationships suggest good test repeatability, appropriate specimen preparation and quality control.

The soil-pipe interaction for Tests 16-1.6-45V-MS-MS-GN-1 and 16-1.6-45V-MS-MS-GN-2 showed a continuous increase of soil restraint during the test until an average peak normalized vertical oblique resistance, N_{vo}, of about 3.2 (14 kN/m) was mobilized at an average normalized displacement, Y', of about 0.12D. After the peak soil restraint was reached, a decrease of loading with a fairly constant rate was observed during the rest of the tests. A minimum average normalized soil restraint, N_{vo}, of 2.2 (9.5 kN/m) was measured at a 45° vertical oblique normalized pipe displacement, Y', of 1D.

As evidenced from the normalized soil restraint vs. normalized pipe displacement curve shown in **Figure 6.1** for Test 16-1.6-45V-MS-MS-GN-1, an anomaly occurred between 0.25D to 0.3D of normalized vertical oblique pipe displacement, after the pipe had overcome the maximum vertical oblique soil resistance. One of the pulling cables inadvertently rubbed against a wooden plank on the working platform leading to this transient anomaly.

Except for the transient portion, the test is considered satisfactory as evidenced by comparing the test result from this test to the one from Test 16-1.6-45V-MS-MS-GN-2.

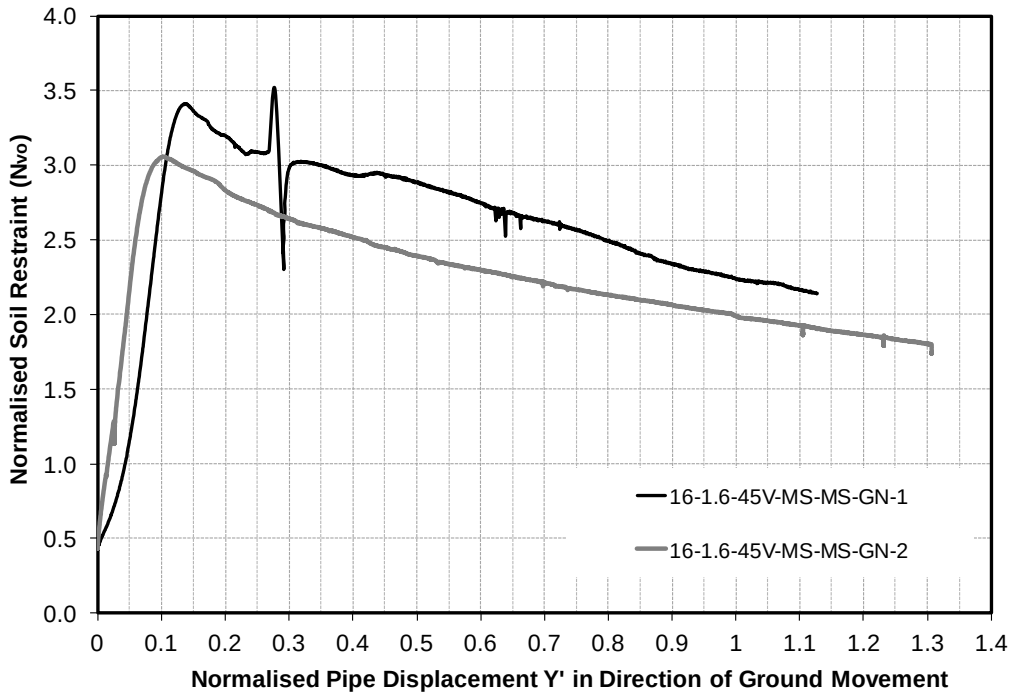

Figure 6.1: Normalized Load-displacement relationships for NPS16 pipe specimen with H/D=1.6 buried in moist sand during vertical oblique displacement (θ = 45°).

6.2.2 Recorded Soil Restraint Angle: Sand Backfill - θ = 45°

Two inclinometers and a set of 8 string potentiometers (four per loading cable) were placed on the soil testing chamber (see **Section 3.5.2**) to record the variation of load angle during the tests. The string potentiometers were placed on the front and rear walls and also on the top of the soil testing chamber. The ends of the thin cables from the string potentiometers were attached to reference points along each pulling cable (left and right side) with the aim of

calculating their spatial change in position continuously during the tests. The spatial change in position was calculated from the recorded change in length of the thin cables and a computer algorithm that was specifically developed for this purpose. The location of the string potentiometers and the reference points are depicted in **Figure 3.32** of **Chapter 3**. The position of the left and right side is shown in **Figure 3.7**.

The spatial changes in position of two reference points located along the left pulling cable and calculated from the recordings of the string potentiometers during Test 16-1.6-45V-MS-MS-GN-2 are shown in **Figure 6.2.a**. The initial position of the NPS16 pipe and the backfill ground surface before the test is also depicted in **Figure 6.2**. The coordinates follow the convention shown in **Figure 3.32**. As seen in **Figure 6.2.a**, the trajectories of the reference points were along a 45° line during the test. This indicates that the displacement from a constant dip thrust angle of 45° from the horizontal was successfully simulated during the test. Similarly, the spatial changes of the two reference points located along the right pulling cable showed a 45° line trajectory, as evidenced in **Figure 6.2.b**. The average readings from the inclinometers located at each pulling cable showed a nearly constant angle of 45°, thus meeting the test requirements as seen in **Figure 6.3**.

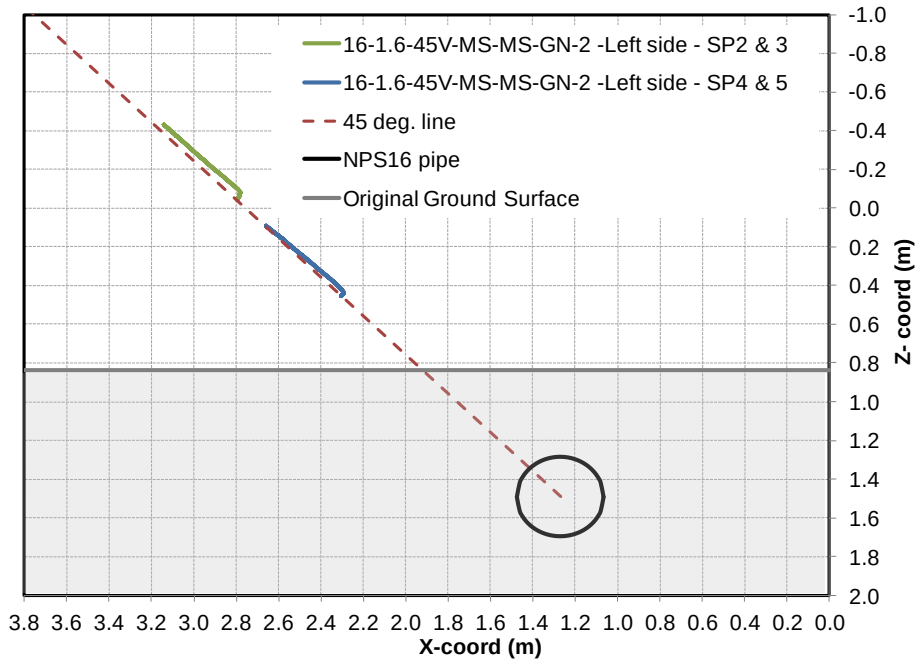

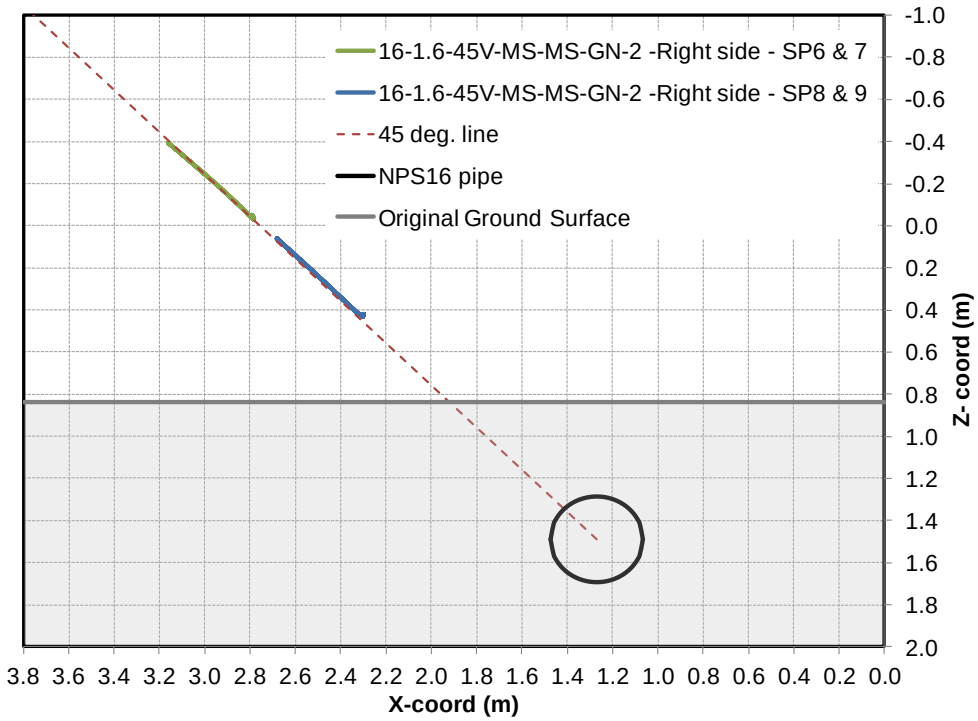

Figure 6.2: Reference points trajectory during Test 16-1.6-45V-MS-MS-GN-2 - vertical oblique pulling (θ = 45°) a) upper graph: left side of pulling cable; b) lower graph: right side of pulling cable.

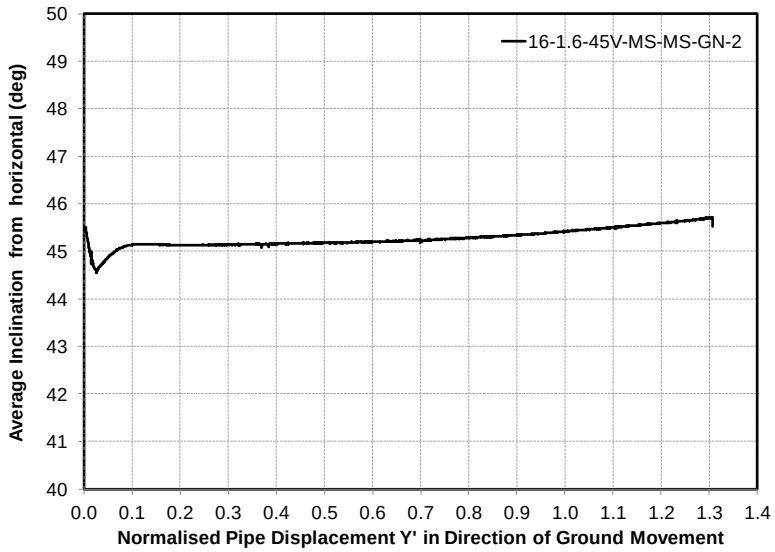

Figure 6.3: Average pulling angle during Test 16-1.6-45V-MS-MS-GN-2 from inclinometers.

6.2.3 Observed Soil Deformation Geometry: Sand Backfill - θ = 45°

Patterns of movements (geometric changes in the soil mass) for Test 16-1.6-45V-MS-MS-GN-1 and Test 16-1.6-45V-MS-MS-GN-2 were essentially the same. Therefore, soil deformations from only Test 16-1.6-45V-MS-MS-GN-1 are shown. Geometric changes in the soil mass for this test at normalized vertical oblique pipe displacements oriented at 45° from the horizontal of 0, 0.25D, 0.57D, and 0.73D are illustrated in **Figure 6.4.a**, **6.4.b**, **6.4.c** and **6.4.d**, respectively. Except for the position before the test, the patterns of soil movements correspond to conditions after failure or peak vertical oblique soil restraint. The corresponding levels of vertical oblique soil restraint for those pipe displacements and conditions can be obtained from **Figure 6.1**.

As seen in the figures, a clearly planar failure surface oriented at roughly 45° from the horizontal and located in front of the pipe developed during the failure condition (**Figure 6.4.b**). Similar to the cases observed during lateral soil

restraint tests, large changes in the soil mass were observed after this failure condition. As test progressed, other failure surfaces developed in the soil mass. However, these failure surfaces were related to active conditions imposed by movements of the soil mass towards void zones. As notable from the figures, the decrease in vertical oblique soil restraint observed in **Figure 6.1** appears to be directly related to the overburden reduction as the pipe moved towards the surface.

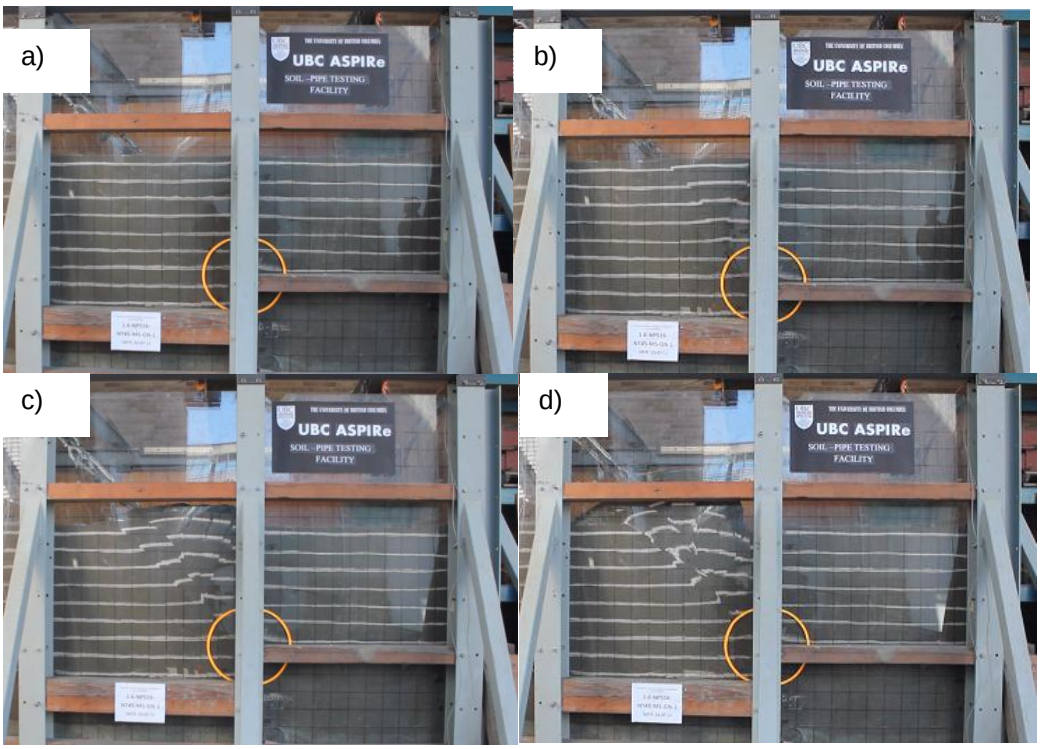

Figure 6.4: Backfill soil deformation during Test 16-1.6-45V-MS-MS-GN-1 – a) Y'=0; b) Y'=0.25D; c) Y'=0.57D; d) Y'=0.73D.

6.3 Results of Vertical Oblique Soil Restraint Tests on Crushed Limestone Backfill (θ = 45°)

6.3.1 Normalized Load-Displacement Response: Crushed Limestone Backfill - θ = 45°

Variations of normalized vertical oblique soil restraint, N_{vo}, vs. normalized vertical oblique pipe displacement, Y'= Y/D, for Tests 16-1.6-45V-HB-LM-GN and 16-1.6-45V-HB-LM-GY on a NPS16 (406-mm diameter) pipe specimen buried in uniformly crushed limestone with an overburden ratio H/D of 1.6 and with a hard trench wall are shown in **Figure 6.5**. Vertical oblique pulling displacement with an angle, θ, of 45° from the horizontal to about 1.25D were applied to the pipe specimens. As summarized in **Table 6.2**, Tests 16-1.6-45V-HB-LM-GN and 16-1.6-45V-HB-LM-GY were carried out without and with geosynthetic-lined trench wall, respectively. The trench wall was sloped at 45° from the horizontal.

As seen in **Figure 6.5**, a continuous and similar rise of soil restraint occurred during the initial part of both tests until a normalized vertical oblique soil restraint, N_{vo}, of about 2.0 (9 kN/m) was reached; then a relatively softer behaviour was observed for the test with no geosynthetic. However, both tests showed a continuous decrease in soil restraint after the peak value was attained.

The peak normalized vertical oblique soil restraint, N_{vo}, for Test 16-1.6-45V-HB-LM-GN was about 2.9 (13.1 kN/m) and occurred at a normalized vertical oblique displacement, Y', of 0.15D. The lowest recorded vertical oblique soil restraint, N_{vo}, value was 1.4 (6.4 kN/m) at a normalized vertical oblique displacement, Y', of 1.2D. For Test 16-1.6-45V-HB-LM-GY, the normalized vertical oblique soil restraint vs. pipe displacement showed a peak vertical oblique soil restraint, N_{vo}, of about 2.8 (12.5 kN/m) at a normalized vertical oblique displacement of 0.1D. A normalized vertical oblique soil restraint, N_{vo},

of about 1.5 (6.6 kN/m) at a vertical oblique displacement of 1.2D was recorded for Test 16-1.6-45V-HB-LM-GY.

Comparison of the results between tests that involved the use of the geosynthetic slip surface with the one that did not suggest that the soil-pipe interaction behaviour under simulated reverse fault action is similar, and that the benefit from the presence of a geosynthetic slip surface is relatively minimal.

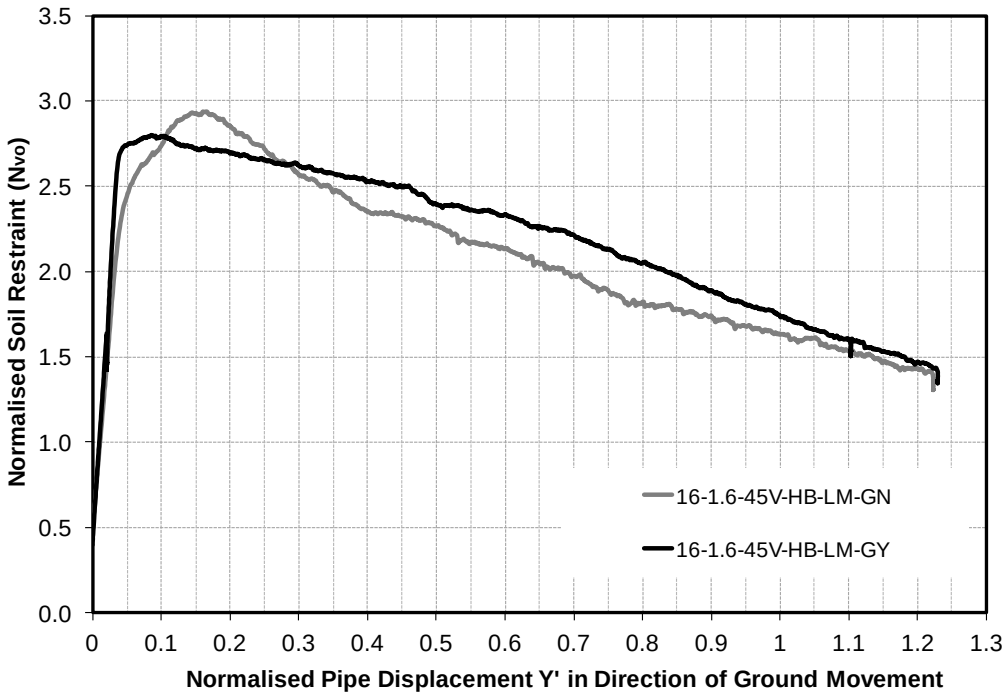

Figure 6.5: Normalized load-displacement relationships for NPS16 buried in crushed limestone with hard trench wall during vertical oblique displacement (θ = 45°).

6.3.2 Recorded Soil Restraint Angle: Crushed Limestone Backfill - θ = 45°

The spatial changes in position of each pair of control points located along the left and right pulling cables and calculated from the recordings of the string potentiometers during Test 16-1.6-45V-HB-LM-GN are shown in **Figure 6.6**. The initial position of the NPS16 pipe and the backfill ground surface before the test is also depicted in the figure. Similar to the case of sand backfill, the trajectories of the reference points were along a 45° line during the test as seen in **Figure 6.6**. Therefore a constant dip thrust angle of 45° from the horizontal was successfully simulated during the test. As seen in **Figure 6.7**, the average readings from the inclinometers located at each pulling cable showed a nearly constant angle of 45° during the test.

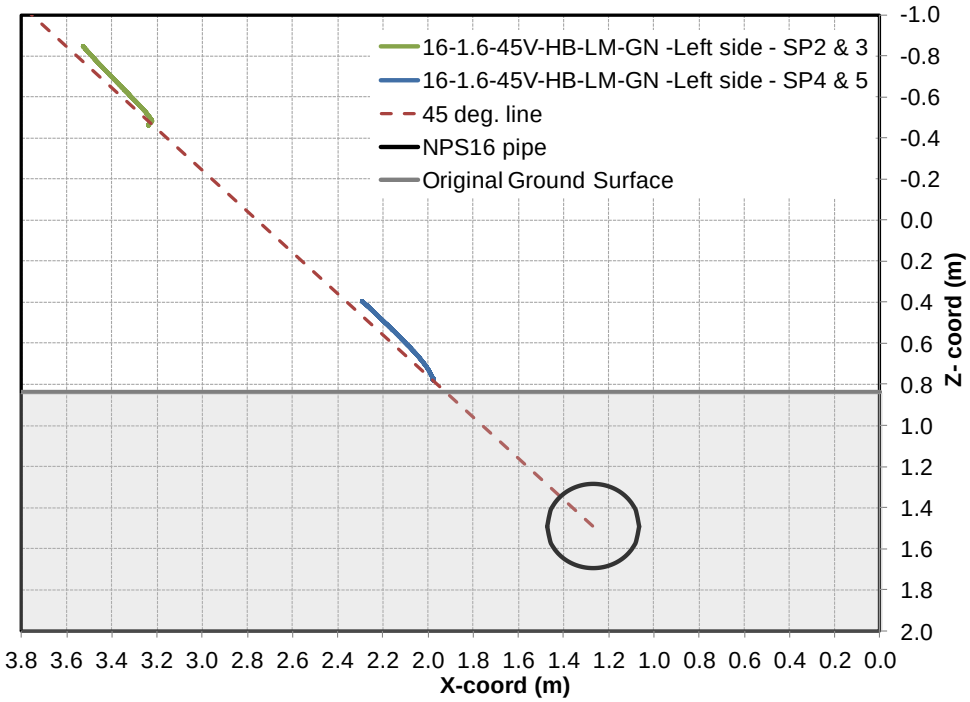

Figure 6.6.a: Reference points trajectory during Test 16-1.6-45V-HB-LM-GN - vertical oblique pulling (θ = 45°) - Left side of pulling cable.

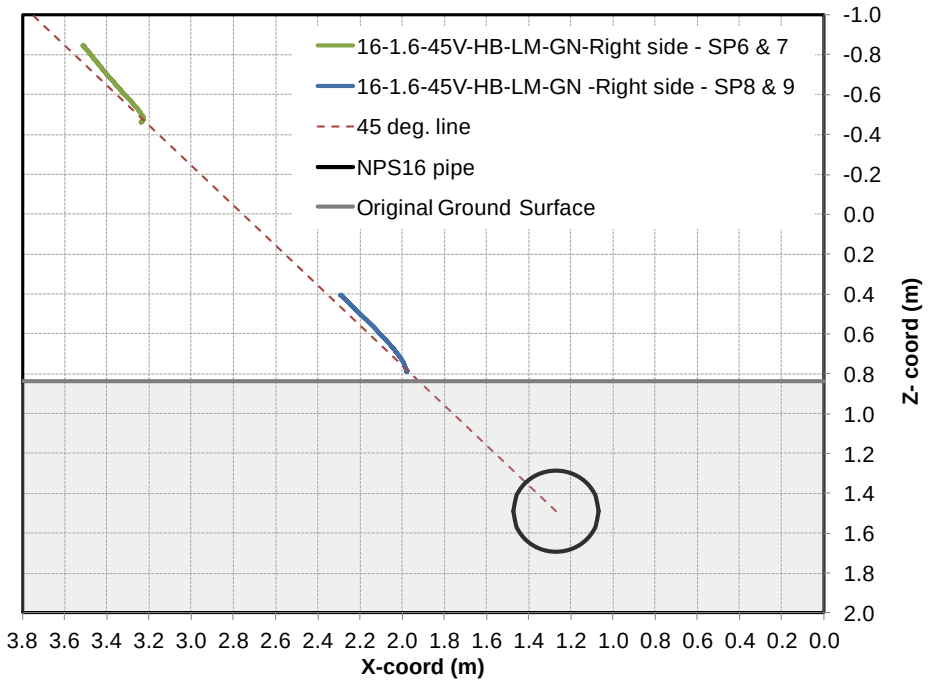

Figure 6.6.b: Reference points trajectory during Test 16-1.6-45V-HB-LM-GN - vertical oblique pulling (θ = 45°) - Right side of pulling cable.

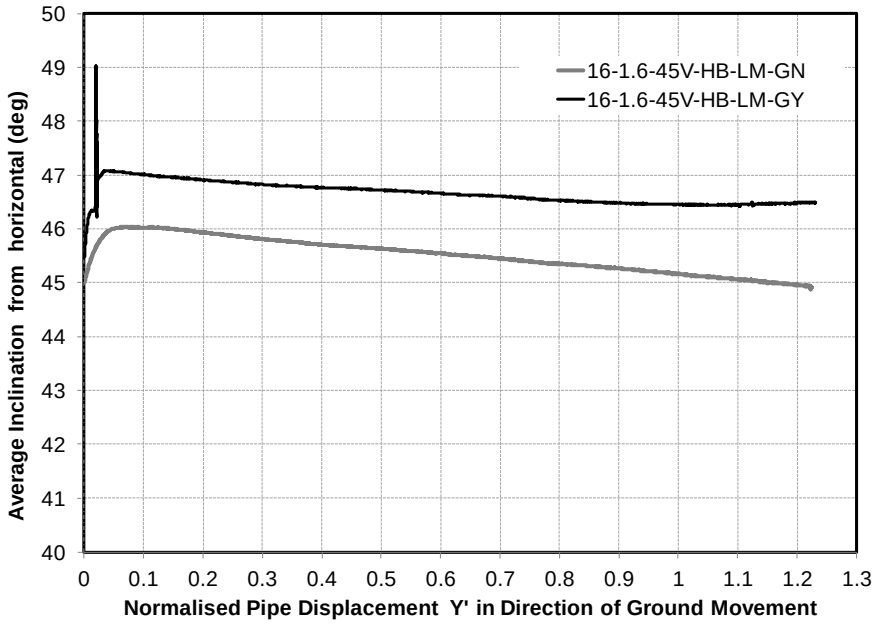

Figure 6.7: Average pulling angle during Tests 16-1.6-45V-HB-LM-GN & 16-1.6-45V-HB-LM-GY from inclinometers.

6.3.3 Observed Soil Deformation Geometry: Crushed Limestone Backfill - θ = 45°

Test 16-1.6-45V-HB-LM-GN and Test 16-1.6-45V-HB-LM-GY indicated similar patterns of geometric changes in the soil mass. Therefore, soil deformations from only Test 16-1.6-45V-HB-LM-GY are shown. Geometric changes in the soil mass for this test at normalized vertical oblique pipe displacements oriented at 45° from the horizontal of 0, 0.25D, 0.65D, and 1.23D are illustrated in **Figure 6.8.a**, **6.8.b**, **6.8.c** and **6.8.d**, respectively. Except for the position before the test, the patterns of geometric changes correspond to conditions after failure or peak soil restraint. Levels of lateral soil restraint associated with those pipe displacements and conditions can be obtained from **Figure 6.5**.

Similar to the case of sand backfill, a planar failure surface oriented at roughly 45° from the horizontal and located between the front of the pipe and the trench wall (inclined at 45°) appeared to be developed during the failure condition (**Figure 6.8.b**). Large movements in the soil mass behind and above the pipe specimen were observed after this failure condition as crushed limestone particles flowed towards void zones. It is interesting to note the nearly vertical wall formed behind the pipe during the test which evidence a high shear resistance associated with the compacted crushed limestone. Again, the decrease in soil restraint observed in **Figure 6.5** appears to be directly related to the overburden reduction as the pipe moved towards the surface.

As evidenced in Figure 6.8, a wood cap was placed on the left end of the pipe (the end observed through the Plexiglas). This was done to observe the change in pipe position as the test progresses. The wood cap was not in contact with the Plexiglas to avoid frictional resistance or pipe end effects. While a few gravel particles got trapped between the end cap and the Plexiglas, this condition occurred after the peak soil restraint was reached.

The trapped gravel particles produced no appreciable additional soil resistance to pipe movement as most of the resistance was produced by the material located in front of the pipe and not by some frictional resistance developed at the end of pipe. Additional comments on boundary effects are described in Section 3.7.2.

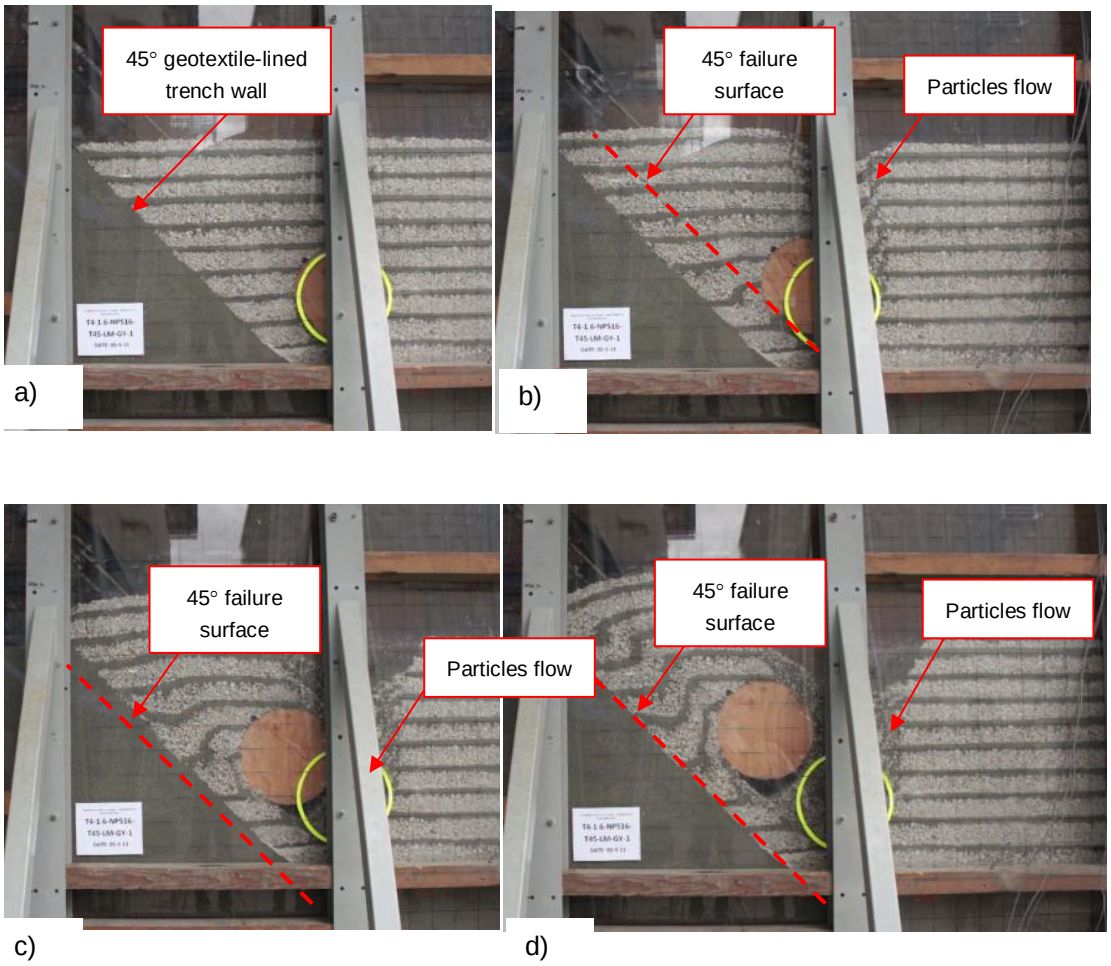

Figure 6.8: Backfill soil deformation during Test 16-1.6-45V-HB-LM-GY – a) Y'=0; b) Y'=0.25D; c) Y'=0.65D; d) Y'=1.23D.

End-of-test measurements of geosynthetic displacement for Test 16-1.6-45V-HB-LM-GY showed an estimated total geosynthetic slip of about 210 mm. The pattern of geosynthetic displacement is displayed in **Figure 6.9**. As seen in

this figure, only the geosynthetic strips located essentially above the location of the springline of the pipe (i.e., geotextile Strips 3, 4, and 5) were subjected to slippage. The geotextile strips 1 and 2, located below the spring line, exhibited minimal to no slippage against the geomembrane.

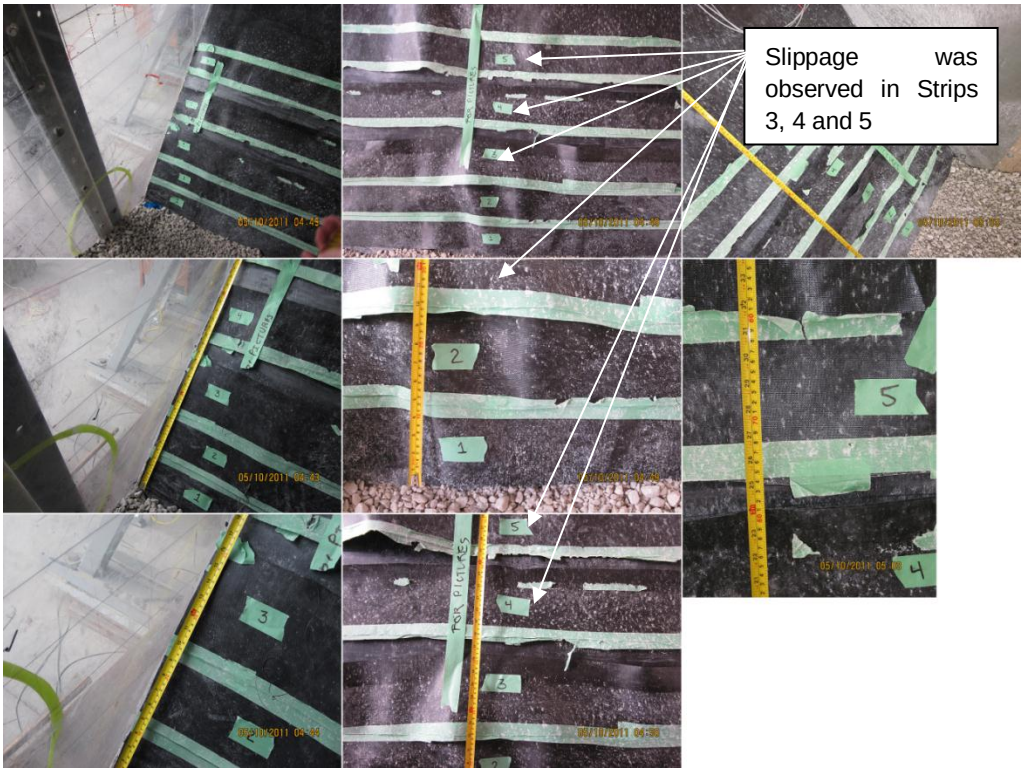

Figure 6.9: Photos of geotextile slip surface at the end of Test 16-1.6-45V-HB-LM-GY.

6.4 Results of Vertical Oblique Soil Restraint Tests in Crushed Limestone Backfill (θ = 35°)

6.4.1 Normalized Load-Displacement Response: Crushed Limestone Backfill - θ = 35°

Changes in normalized vertical oblique soil restraint, N_{vo}, vs. normalized vertical oblique pipe displacement, Y'= Y/D, for Tests 16-1.6-35V-HB-LM-GN

and 16-1.6-35V-HB-LM-GY on a NPS16 (406-mm diameter) pipe specimen buried in uniformly crushed limestone with an overburden ratio H/D of 1.6 and with a hard trench wall are shown in **Figure 6.10**. Vertical oblique pulling displacement with an angle, θ, of 35° from the horizontal to about 1.25D were applied to the pipe specimens. Tests 16-1.6-35V-HB-LM-GN and 16-1.6-35V-HB-LM-GY were carried out without and with geosynthetic-lined trench wall, respectively. The trench wall was sloped at 45° from the horizontal.

As seen in **Figure 6.10**, and similar to the case of 45° vertical oblique displacement, a continuous and similar increase in soil restraint occurred during the initial part of both tests until a normalized vertical oblique soil restraint, N_{vo}, of about 2.9 (13 kN/m) was reached; then a softer behaviour was observed for the test with geosynthetic. This softer behaviour is contrary to the one observed for tests with 45° vertical oblique displacements (i.e. the softer behaviour was observed for the test with no geosynthetic. See **Figure 6.5**). Therefore, this behaviour appears to be related to test to test variability rather than to the presence of geosyntethic.

The peak normalized vertical oblique soil restraint, N_{vo}, for Test 16-1.6-35V-HB-LM-GN was about 3.8 (17 kN/m) and occurred at a normalized vertical oblique displacement of 0.18D. The lowest recorded vertical oblique soil restraint, N_{vo}, value was 1.9 (8.5 kN/m) at a normalized vertical oblique displacement of 1.23D. For Test 16-1.6-35V-HB-LM-GY, the normalized vertical oblique soil restraint vs. pipe displacement showed a peak N_{vo} of about 3.4 (15.2 kN/m) at a normalized vertical oblique displacement of 0.16D. A normalized vertical oblique soil restraint of about 2.0 (9.2 kN/m) at a normalized vertical oblique displacement of 1.23D was recorded for Test 16-1.6-35V-HB-LM-GY.

Similar to the case of 45° vertical oblique displacement, a comparison of the results between the tests with and without geosynthetic slip surface suggest that the benefit from the presence of a geosynthetic slip surface is not

significant especially from practical applicability point of view. A reduction of about 14% for peak conditions was observed from the test results. However, this benefit was diminished at large pipe displacements.

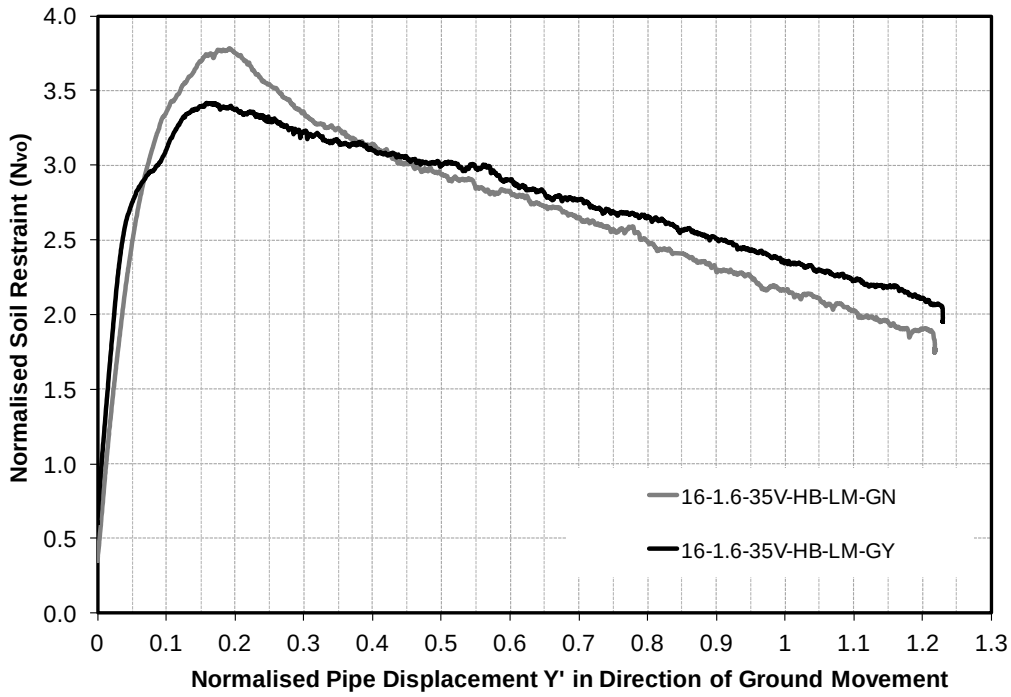

Figure 6.10: Normalized load-displacement relationships for NPS16 buried in crushed limestone with hard trench wall during vertical oblique displacement (θ = 35°).

6.4.2 Recorded Soil Restraint Angle: Crushed Limestone Backfill - θ = 35°

The history of spatial position of each pair of control points located along the left and right pulling cables and calculated from the recordings of the string potentiometers during Test 16-1.6-35V-HB-LM-GY are shown in **Figure 6.11**. Similar to the case of sand and crushed limestone (θ = 45°) backfill, the trajectories of the reference points were along a 35° line during the test.

Therefore a constant dip thrust angle of 35° from the horizontal was successfully simulated during the test.

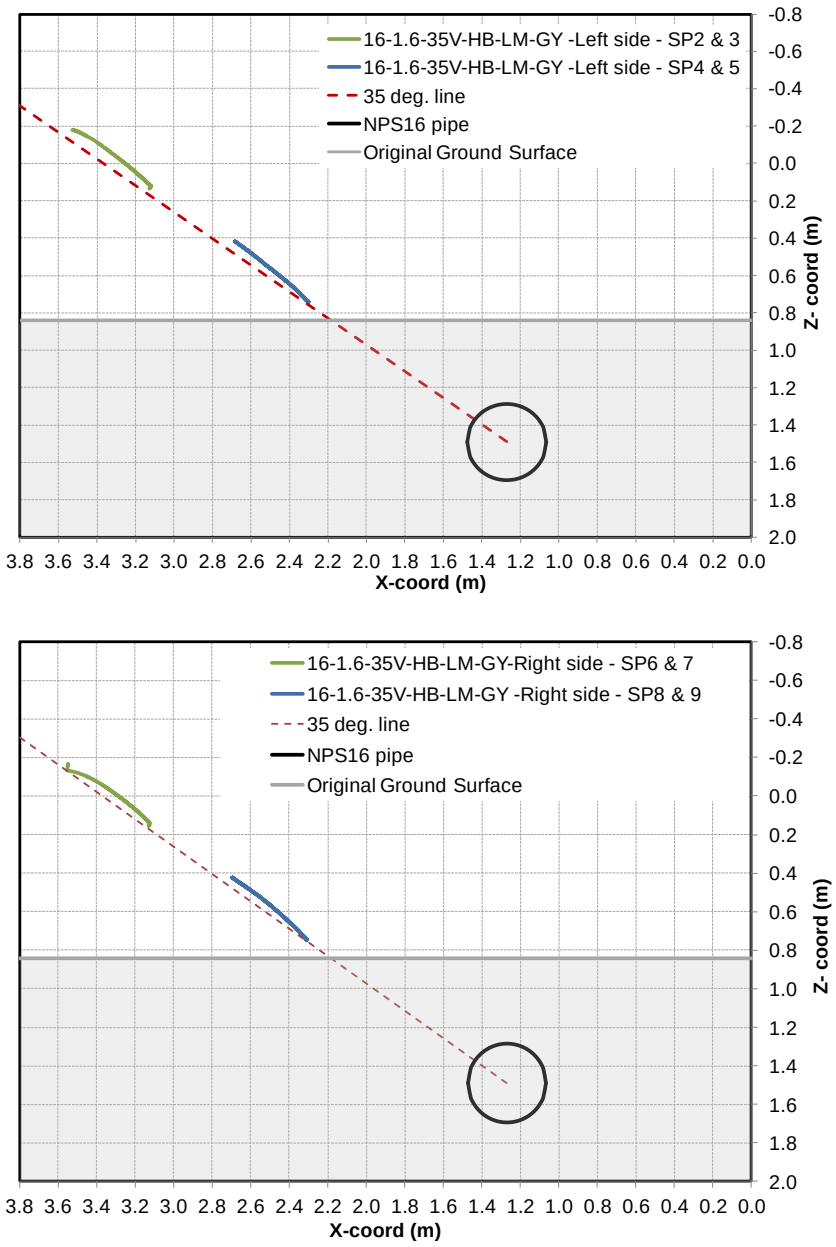

Figure 6.11: Reference points trajectory during Test 16-1.6-35V-HB-LM-GY - vertical oblique pulling (θ = 35°) a) Left side of pulling cable; b) Right side of pulling cable.

The average reading from the inclinometers located at each pulling cable during Test 16-1.6-35V-HB-LM-GN is shown in **Figure 6.12**. The readings from Test 16-1.6-35V-HB-LM-GY were not recorded during the test due to a malfunction of the data acquisition system. As seen in **Figure 6.12**, the average reading from the inclinometers during Test 16-1.6-35V-HB-LM-GN showed a nearly constant angle of 35° during the test.

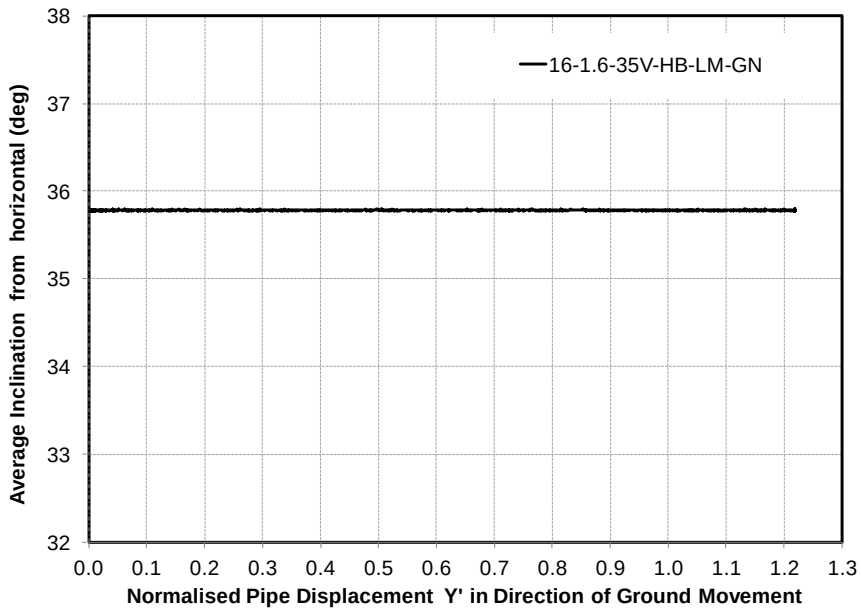

Figure 6.12: Average pulling angle during Tests 16-1.6-35V-HB-LM-GN from inclinometers.

6.4.3 Observed Backfill Soil Deformation Geometry: Crushed Limestone Backfill - θ = 35°

Test 16-1.6-35V-HB-LM-GN and Test 16-1.6-35V-HB-LM-GY showed similar patterns of geometric changes in the soil mass. Therefore, soil deformations from only Test 16-1.6-35V-HB-LM-GY are shown. Geometric changes in the soil mass for this test at normalized vertical oblique pipe displacements oriented at 35° from the horizontal of 0, 0.34D, 0.72D, and 1.23D are illustrated in **Figure 6.13.a**, **6.13.b**, **6.13.c** and **6.13.d**, respectively. Levels of

lateral soil restraint associated with those pipe displacements and conditions can be obtained from **Figure 6.10**.

Similar to the case of crushed limestone with 45° vertical oblique displacements, a planar failure surface oriented at roughly 35° from the horizontal and located between the front of the pipe and the 45° trench wall appeared to be developed during the failure condition (**Figure 6.13.b**). Large movements in the soil mass behind and above the pipe specimen were observed after this failure condition as crushed limestone particles flowed towards void zones.

Measurements of geotextile displacement at the end of Test 16-1.6-35V-HB-LM-GY showed an estimated total geotextile slip of about 40 to 70 mm. The pattern of geosynthetic displacement is displayed in **Figure 6.14**, and it shows that movement of geosynthetic occurred essentially upwards from a position that coincided with the location of the springline of the pipe. This observation is similar to that noted earlier for the test conducted for the case for $\theta = 45°$.

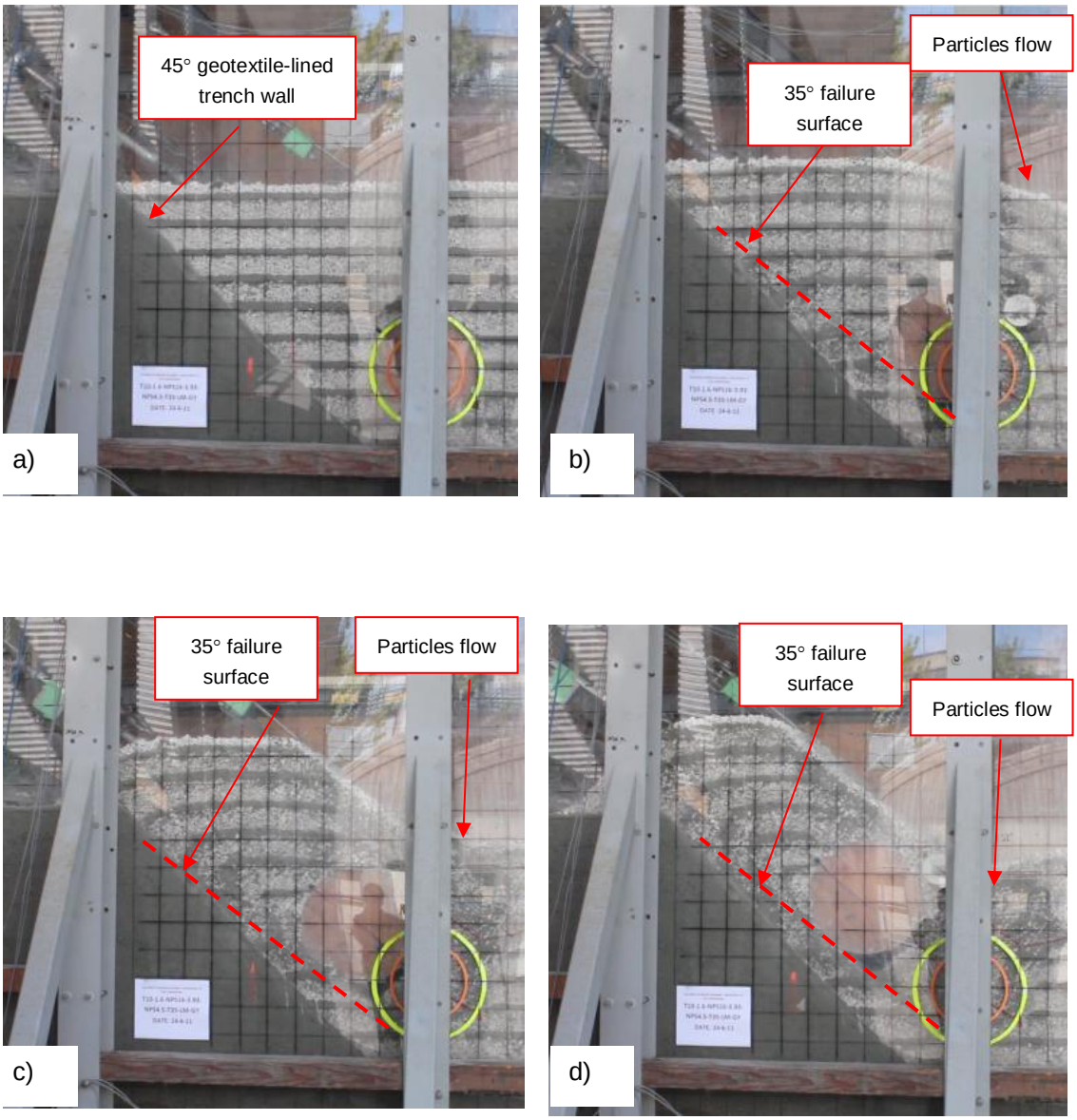

Figure 6.13: Backfill soil deformation during Test 16-1.6-35V-HB-LM-GY – a) Y'=0; b) Y'=0.34D; c) Y'=0.72D; d) Y'=1.23D.

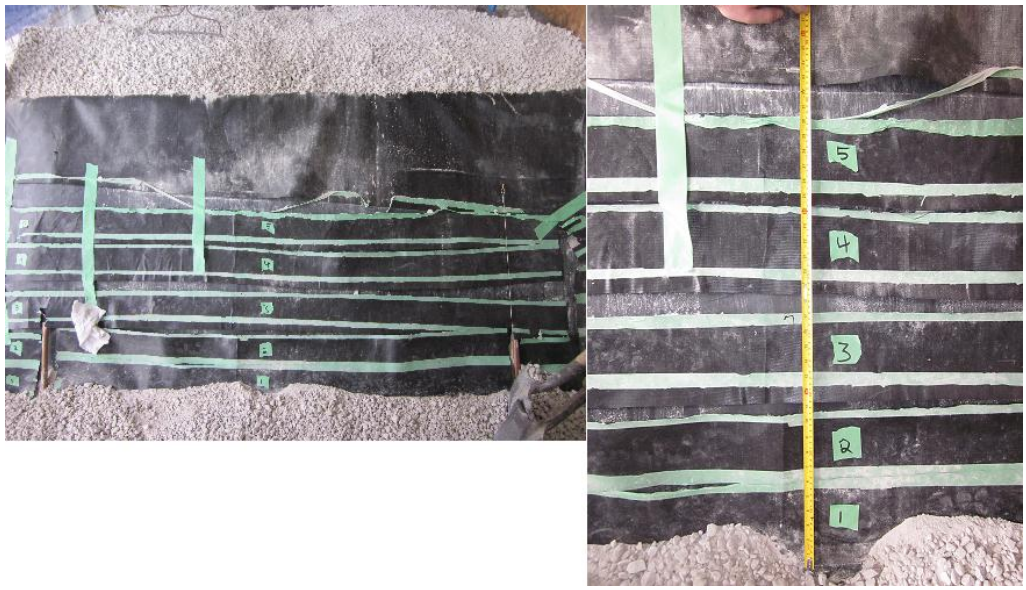

Figure 6.14: Photos of geotextile slip surface at the end of Test 16-1.6-35V-HB-LM-GY.

6.5 Results of Vertical Soil Restraint Tests Using Sand or Crushed Limestone Backfill (θ = 90°)

6.5.1 Normalized Load-Displacement Response: Sand or Crushed Limestone Backfill (θ = 90°)

Variations of normalized vertical soil restraint, N_{qv}, vs. vertical pipe displacement, Y'= Y/D, for Tests 16-1.6-90V-LM-LM-GN and 16-1.6-90V-MS-MS-GN on a NPS16 (406-mm diameter) pipe specimen buried in uniformly crushed limestone and moist Fraser River sand, respectively, are shown in **Figure 6.15**. Vertical pulling displacement with an angle, θ, of 90° from the horizontal to about 1.25D were applied to the pipe specimens buried with an overburden ratio H/D of 1.6. No trench wall or geotextiles were considered in these tests. The following characteristics of the results can be noted from the figure.

1. Both tests under vertical pulling resulted in similar N_{qv} vs. Y' behaviour i.e. a continuous raise of vertical soil restraint during the initial part of the test until the peak vertical soil restraints for the backfill materials were fully mobilized. Then, a reduction of vertical restraint occurred, very sharply initially and then moderately until the end of the tests.

2. The peak normalized vertical soil restraint, N_{qv}, for test on crushed limestone (Test 16-1.6-90V-LM-LM-GN) was about 2.3 (10.2 kN/m) and occurred at a normalized vertical displacement of 0.1D. This value is 16% higher than the one recorded for the test on sand backfill (Test 16-1.6-90V-MS-MS-GN), which showed a peak vertical soil restraint, N_{qv}, of about 2.0 (8.8 kN/m) at a normalized vertical displacement of 0.06D.

3. The results from vertical pulling tests on uniformly graded crushed limestone and moist Fraser River sand backfills suggest that the characteristic soil-pipe interaction behaviour under vertical displacement is relatively similar. They both showed brittle behaviour.

4. Difference in the levels of peak vertical soil restraint for both materials (difference of 16%) can be attributed to the frictional properties of each material.

5. The rates of change in vertical soil restraint with pipe displacements after peak may be related with the particle size distribution of each backfill material. The fact that crushed limestone particles can flow more easily (due to the lack of suction from moisture, if compared to moist Fraser River sand) and therefore less soil mass exists above the pipe may explain the lower vertical soil restraint noted for crushed limestone backfill at large vertical pipe displacements than the corresponding one observed in sand.

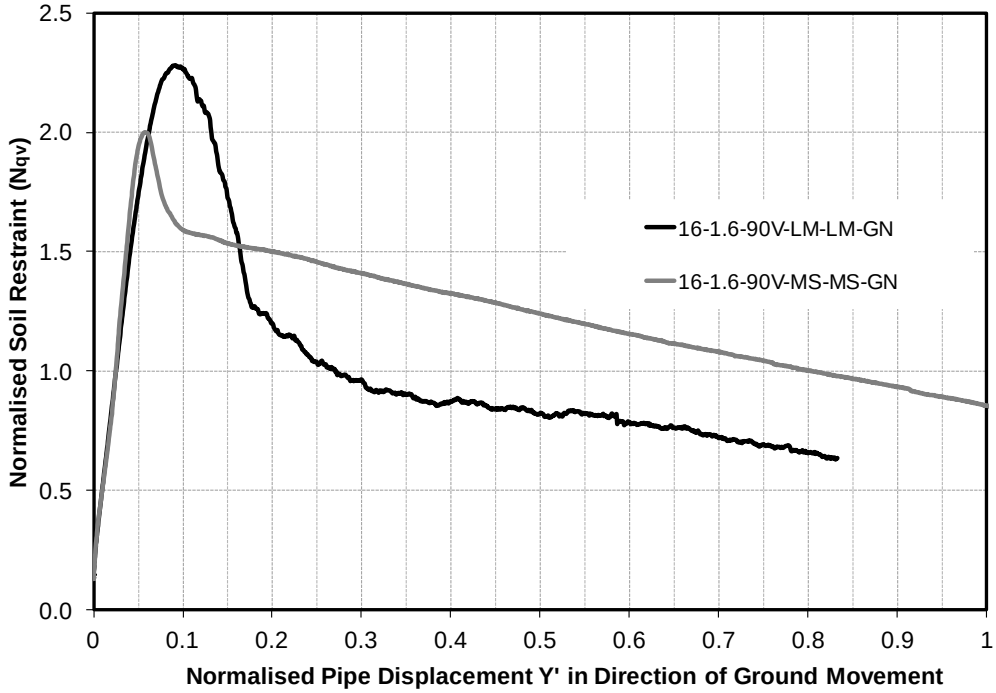

Figure 6.15: Normalised load-displacement relationships for NPS16 pipe specimen buried in crushed limestone and sand during vertical displacement (θ = 90°).

6.5.2 Observed Backfill Soil Deformation Geometry: Sand and Crushed Limestone Backfill (θ = 90°)

Geometric changes in the soil mass for Test 16-1.6-90V-LM-LM-GN (crushed limestone backfill) at normalized vertical pipe displacements (oriented at 90° from the horizontal) of 0, 0.22D, and 0.83D (end of test) are illustrated in **Figure 6.16.a**, **6.16.b**, and **6.16.c**, respectively. Both lateral and plan view are illustrated in these figures. Except for the position before the test, the patterns of geometric changes correspond to conditions after failure or peak soil restraint. Levels of lateral soil restraint associated with those pipe displacements and conditions can be obtained from **Figure 6.15**.

As seen in **Figure 6.16**, an inclined wedge with slip planes oriented at roughly 75° from the horizontal appeared to have developed during the failure condition (**Figure 6.16.b**). Large movements in the soil mass above the pipe specimen were observed after this failure condition as crushed limestone particles flowed towards the void zone formed below the pipe. As in the cases of vertical oblique soil restraint, the decrease in vertical soil restraint observed in **Figure 6.15** appears to be directly related to the overburden reduction as the pipe moved towards the surface.

Patterns of geometric changes in the soil mass for Test 16-1.6-90V-MS-MS-GN (Fraser River sand) are shown in **Figure 6.17**. As seen in this figure, a slightly different slip surface developed during the test on sand compared to the one from crushed limestone. A nearly vertical slip surface that extended about 0.4 m above the pipe springline was observed during the test. At the end of this slip surface, another slip surface with an average inclination of 55° from the horizontal developed and extended towards the ground surface. It is interesting to note that a void space was formed below the pipe during pulling and it remained stable almost throughout the test duration (see **Figure 6.17.b** for a visual understanding). It is possible that this condition rose due to an apparent “cohesion” formed by the moist nature of the sand backfill used in the tests. Similar condition was observed by Karimian (2006) during lateral soil-pipe interaction tests on moist Fraser River sand. He observed heights of free standing soil at the back of the pipe that covered the total soil overburden on the pipe.

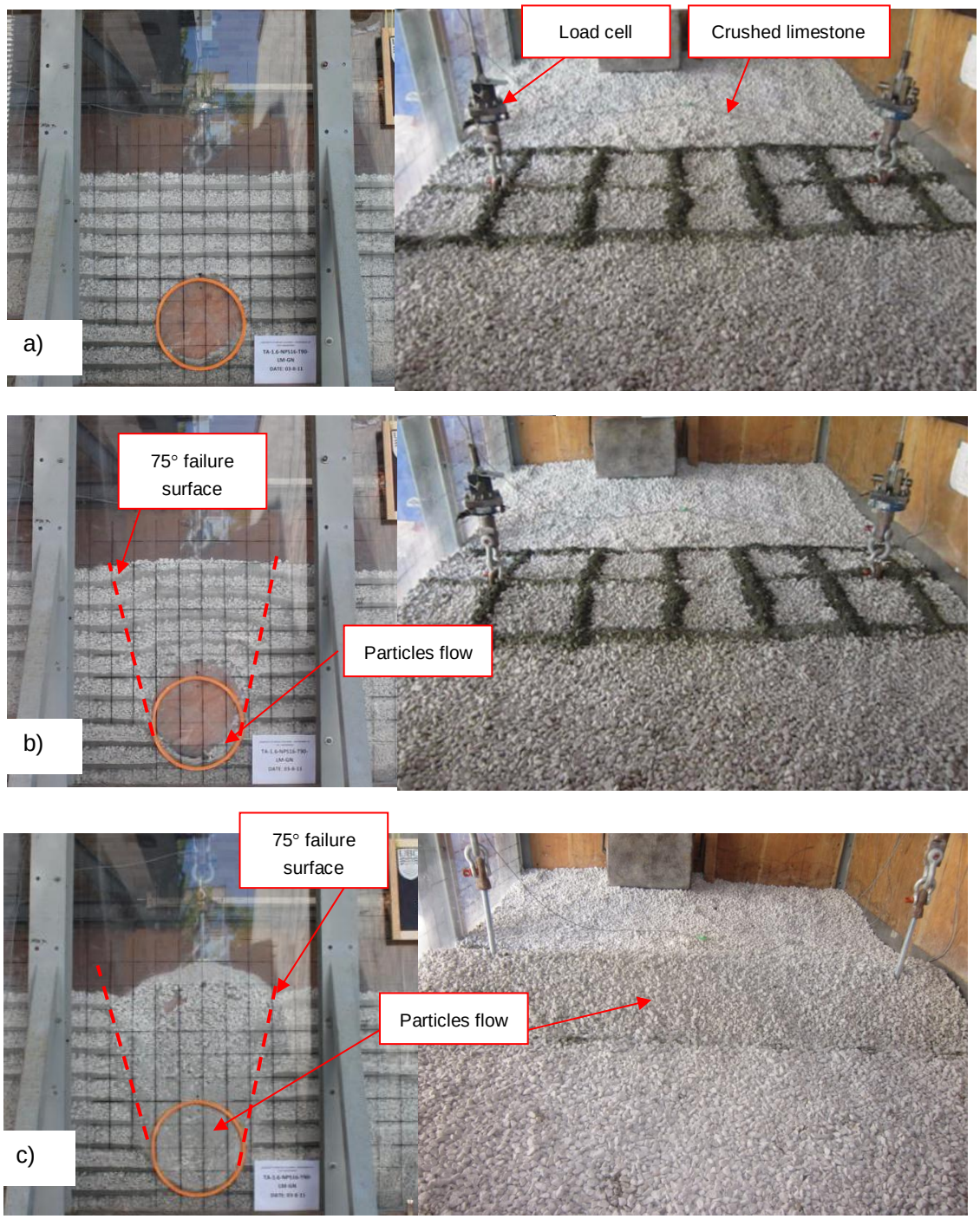

Figure 6.16: Backfill soil deformation during Test 16-1.6-90V-LM-LM-GN – a) Y'=0; b) Y'=0.22D; c) Y'=0.83D.

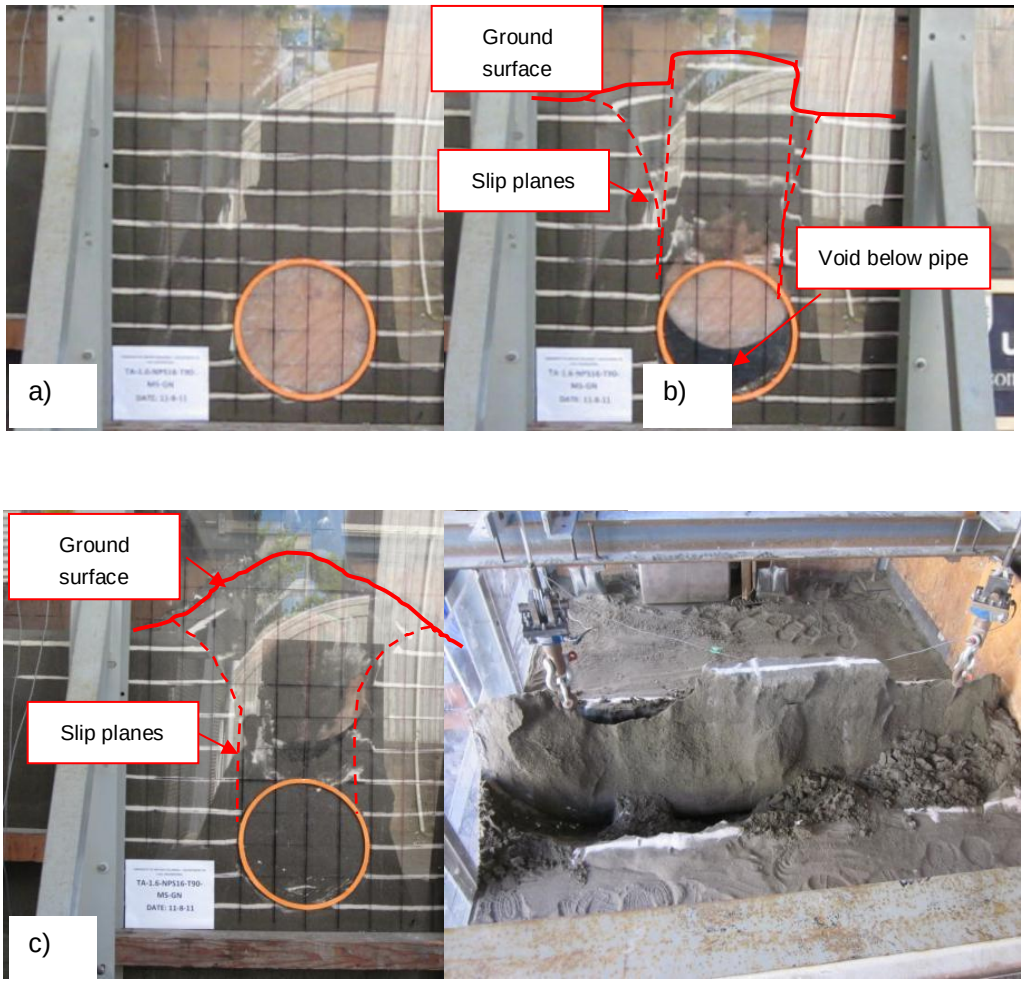

Figure 6.17: Backfill soil deformation during Test 16-1.6-90V-MS-MS-GN – a) Y'=0; b) Y'=0.38D; c) End-of-test condition.

6.6 Summary of Soil Restraint Tests

The results of all the vertical oblique and pure vertical soil restraint tests are summarized in **Table 6.3**. For tests conducted using the same type of backfill soil, the normalized soil restraint, N_{vo}, as characterised by P_{vo} / ($\gamma \cdot D \cdot H \cdot L$), depends on the nature of the inclination of the simulated thrust/reverse fault angle. Tests with pipe specimen displaced at a 35° angle from the horizontal

resulted in vertical oblique soil restraint being higher than the vertical oblique soil restraint from tests with pipe specimen displaced at a 45° for identical specimens (i.e. similar H/D, pipe diameter and soil backfill, or trench wall condition). Tests with vertical relative soil displacement showed the lowest values.

Table 6.3: Summary of Vertical Oblique Soil Restraint Test Results (H/D=1.6)

No.	Test ID	Geotextile	Oblique angle (θ) w.r.t horizontal	Backfill	Peak Normalized Soil Restraint	Pipe Displacement at Peak (Y')
1	16-1.6-45V-MS-MS-GN-1	No	45°	Sand	3.4	0.13
2	16-1.6-45V-MS-MS-GN-2	No	45°	Sand	3.1	0.10
3	16-1.6-45V-HB-LM-GN	No	45°	Crushed Limestone	2.9	0.15
4	16-1.6-45V-HB-LM-GY	Yes	45°	Crushed Limestone	2.8	0.10
5	16-1.6-35V-HB-LM-GN	No	35°	Crushed Limestone	3.8	0.18
6	16-1.6-35V-HB-LM-GY	Yes	35°	Crushed Limestone	3.4	0.16
7	16-1.6-90V-LM-LM-GN	No	90°	Crushed Limestone	2.3	0.10
8	16-1.6-90V-MS-MS-GN	No	90°	Sand	2.0	0.06

A comparison of the measured peak vertical oblique soil restraint for trench wall conditions with and without geotextile is also shown in **Table 6.3**. Under pipe displacements with 35° and 45° angles from the horizontal, the peak vertical oblique soil restraints for these trench wall conditions were very similar. Therefore, the benefit from the presence of a geosynthetic slip surface is minimal. This important observation provides an opportunity to examine the value of using the geotextile from a cost-benefit point of view in real-life applications.

Except for the vertical oblique tests with an inclination of 45° from the horizontal, the soil restraint on a pipe buried in uniformly graded crushed limestone was higher than the soil restraint on a pipe buried in moist sand. As seen in **Table 6.3** a difference of 16% was observed between the vertical soil restraint in crushed limestone and sand. A similar pattern of response was observed for lateral soil restraints. As reported in **Chapter 4**, the maximum lateral soil restraint in crushed limestone was 25% to 50% higher than their counterpart in moist sand. The discrepancy for the vertical oblique tests with an inclination of 45° from the horizontal appears to be related to the use of the sloping trench wall, which altered the development of the failure surface.

6.7 Summary of the Chapter

A series of vertical oblique tests were conducted on a pipe specimen buried in moist Fraser River sand and uniformly graded crushed limestone to characterize soil restraints during simulated oblique angle breakout of buried pipelines from their soil embedment on the footwall side of reverse/thrust faults. The test program included different trench configurations with or without the presence of geotextile interfaces between trench backfill and a pipe trench surface inclined at 45° to the horizontal. Tests were also conducted to understand soil-pipe interaction during vertical pipe movement. The pipe specimen had about 450 mm of soil cover above the crown (H/D = 1.6) in all the tests.

In addition to the measurement of vertical oblique loads and pipe displacements during the tests, two inclinometers and a set of 8 string potentiometers were installed on the pulling cables of the soil testing chamber to record and control the inclination of the simulated reverse fault actions.

Uniform reverse/thrust angles of 35° and 45° degrees with respect to the horizontal were successfully simulated and achieved during the tests.

Currently, the design of pipeline segments crossing active reverse/trust fault environments are inferred on the basis of pure horizontal and vertical soil restraints; as such, the results from this work can provide valuable and improved understanding of soil-pipe behaviour for developing appropriate design parameters and for adequately assessing pipeline integrity for specific design conditions.

Some of the key findings/assessments are summarized below:

1. The vertical oblique soil restraint-displacement relationships indicated a generally continuous increase in soil restraint during the test, reaching a peak value at relatively small pipe displacements (i.e., 0.1D to 0.18D). After the peak soil restraint was reached, a fairly constant rate of decrease in soil resistance with increasing pipe displacements was noted and was attributed to decreasing overburden as the pipe displaced. The testing work conducted under displacement-controlled loading provided a unique opportunity to observe and quantify this post-peak response – which is a valuable piece of information in the development of more realistic “soil springs” for numerical simulations.

2. Soil restraints depend on the inclination of the pipe movement with respect to the soil mass. Peak soil restraint values diminish as the inclination of the angle of breakout of buried pipelines increases with respect to the horizontal. For example, the vertical oblique soil restraint derived from tests conducted with pipe displacement at a 35° angle from the horizontal was about 31% higher than that resulted from tests conducted where the pipe specimen was displaced at a 45° angle from the horizontal.

3. The results from vertical oblique soil restraint for trench walls lined with and without geotextile indicated that the peak vertical oblique soil restraints for the two configurations are similar. The maximum soil resistance was reduced only by about 12% due to geotextile lining of the

trench indicating that the benefit derived from the introduction of a geosynthetic slip surface is minimal. This important observation provides an opportunity to examine the value of using the geotextile from a cost-benefit point of view in real-life applications.

4. The vertical oblique soil restraint for tests with 35° vertical oblique displacement without geosynthetic showed a softer behaviour than for the test with geosynthetic. This softer behaviour is contrary to the one observed for tests with 45° vertical oblique displacements in which the softer behaviour was observed for the test with no geosynthetic fabric. Therefore, this behaviour appears to be related to test to test variability rather than to the presence of geosyntethic.

5. The vertical soil restraint on a pipe buried in uniformly graded crushed limestone was 16% higher than the soil restraint on a pipe buried in moist sand. A similar pattern of response was observed for lateral soil restraints. This characteristic was not observed for the vertical oblique tests with an inclination of 45° from the horizontal. The discrepancy may be related to the use of the sloping trench wall, which altered the development of the failure surface.

6. The differences in the levels of peak vertical soil restraint observed between tests conducted with uniformly graded crushed limestone and those with Fraser River sand can be attributed to the frictional properties of each material. The rates of change in vertical soil restraint with pipe displacements after peak appears to be related with the particle size distribution of each backfill material. The fact that crushed limestone particles can flow more easily may explain the lower vertical soil restraint noted for crushed limestone backfill at large vertical pipe displacements than the corresponding one observed in sand.

Chapter 7: Numerical Simulation of Lateral Soil Restraint

Chapter 4 presented both the measured lateral soil restraint vs. normalised pipe displacement and analytical approaches to evaluate conditions of ultimate failure or collapse of a backfill soil mass in an effort to predict maximum levels of lateral soil restraint using the limit equilibrium approach. This chapter presents the approach, procedures and results of 2D numerical simulations of the stages prior to ultimate failure or collapse of a backfill soil mass, i.e. initial linear and transition region (Region 1) and ultimate state of the soil by plastic flow (Region 2). The aim of this chapter is to better understand the mobilisation of soil restraint during the progressive breakout of buried pipelines from their soil embedment before the ultimate failure condition under lateral pipe displacements for cases with and without trench wall. Numerical estimations of maximum levels of normalised lateral soil restraint are also presented.

The soil-pipe interaction problem was modelled assuming plane strain conditions and was carried out with the help of the parameters derived from direct shear and triaxial laboratory element testing carried out by Karimian (2006). No simple shear element tests were conducted in this thesis due to the difficulty in performing those tests at the stress levels that exist at the current soil-pipe problem (<20kPa).

The numerical simulations of the soil-pipe interaction were achieved by laterally displacing the buried pipe with a constant rate of movement using the commercially available computer program FLAC – Fast Lagrangian Analysis of Continua - Version 7.0 (Itasca 2012). Fraser River sand, crushed gravel and sand mixture and crushed limestone soil backfills were used in the numerical model.

7.1 Numerical Simulation Procedure

The numerical simulation of the mobilisation of lateral soil restraint during the progressive failure stage is a stress-deformation problem. The solution requires that equilibrium and compatibility be satisfied for the boundary and initial conditions and at all nodes at all times of the soil-pipe interaction problem, using appropriate constitutive models. In this study, these conditions will be satisfied by using finite difference techniques already implemented in the geotechnically-oriented computer code FLAC 7.0.

The numerical procedure applied in FLAC considers that for each element in the geometric domain, stresses and forces are used in the equation of motion to obtain new velocities and displacements. With these new values, the constitutive equation or stress-strain relationship is then used to predict a new set of stresses. This is the basis of the explicit calculation method. The procedure is depicted in **Figure 7.1**.

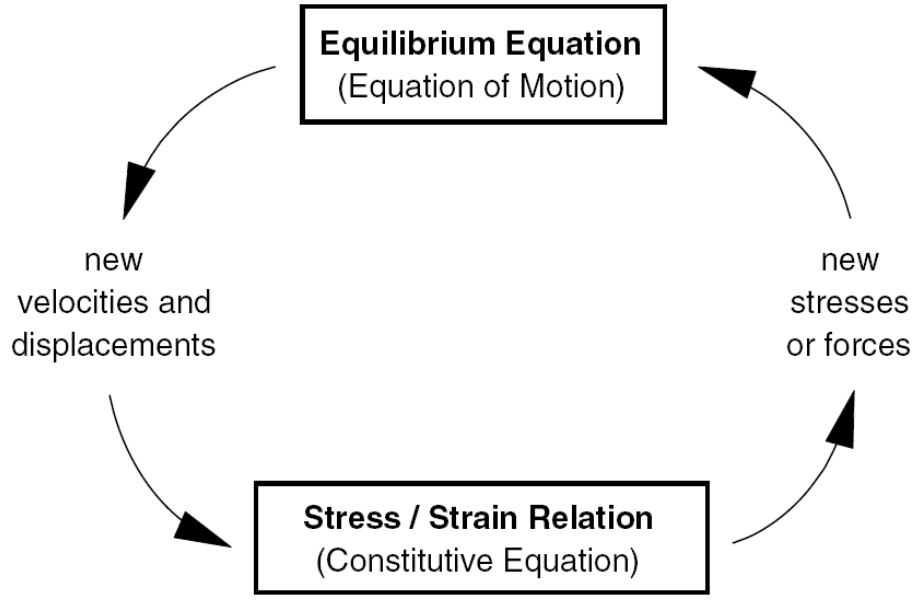

Figure 7.1: Basic explicit calculation cycle used by FLAC (Itasca 2012).

During the computation of the new set of stresses by FLAC, the input velocities are assumed unaffected by the new set of stresses. The achievement of this condition requires the use of very small time steps to avoid the exchange of physical information from one element to another during that period. By maintaining the computational front ahead of the physical front, stresses can be computed from strains in an element without requiring an iteration process even for nonlinear constitutive laws (Itasca, 2012). After several calculation cycles, changes in stresses and strains propagate across elements in a similar way as they would propagate physically.

Based on the above considerations for stresses computation by FLAC, a steady rate of displacement equal to $1x10^{-8}$ to $2x10^{-8}$ m per step was applied to the pipe model specimen to numerically represent the soil-pipe interaction during strike-slip fault crossings.

The soil-pipe interaction problem was modelled assuming plane strain conditions, i.e. no deformations are allowed in the out-of-plane direction, while the stress acting perpendicular to the plane of strain is considered one of the principal stresses. Plane strain conditions are routinely employed to model many geotechnical engineering problems.

The steel pipe was modeled through a set of beam elements having weight and stiffness selected to match the actual steel pipe test specimen. The numerical simulation also includes interfaces to characterise the contact between the steel pipe and the soil and the contact between geotextile-geotextile and geotextile-backfill soil for cases that consider a trench wall.

7.1.1 Constitutive Models for Soil Backfills

All methods for stress and deformation analysis of structures require a stress-strain relation to simulate the response of the structure to loading. A rigorous

simulation of a problem that involves soil-pipe interaction would require constitutive models for both the soil backfill and the pipe. However, by comparing the stiffness of the soil to that of the steel pipe specimen, it can be assumed that the pipe behaves like a rigid body. Thus, only constitutive models for the soil backfill were employed for the numerical simulation.

Soil constitutive models based on the incremental elastic-plastic theory are routinely employed to estimate soil behaviour to loading. These models generally assume that the total strain increment can be decomposed into elastic and plastic strain increments (Hill 1950; Desai and Christian 1977). In addition, regions of elastic and plastic behavior are assumed separated by a boundary called a yield surface, yield locus or loading surface. The zone in which only elastic response is exhibited is called the elastic region, whereas the zone in which the stress states are outside the current boundary of the elastic region inducing plastic deformations frames the plastic region.

A classical elastic-plastic model includes yield surface, flow rule, hardening rule and hardening parameter. Yield surfaces are defined exclusively in stress space, and define the size of the elastic region. The evolution of the yield surface is limited by the failure surface, which defines the ultimate state that soil can achieve under loading and controlled by a failure criterion, e.g. Mohr-Coulomb, extended Tresca, Drucker and Prager, or Lade and Duncan.

The flow rule determines the direction of plastic shear and volumetric strain increments and can be associated (i.e. yield surface = plastic potential) or non-associated. The hardening rule specifies the manner in which the elastic region evolves as yielding takes place. Two possible hardening conditions are: isotropic (i.e. proportional expansion of yield surface in all directions) and kinematic (i.e. moving of the yield surface without change in orientation, size or shape of the elastic region). A combination of these two types is also possible and is called mixed hardening. Finally, the hardening parameter is a

scalar quantity used to record the plastic deformation history developed during the loading process.

Most of the available soil constitutive models found in the technical literature can be categorized into two types: Mohr-Coulomb (and its modifications) model types and Critical-State model types (Puebla 1999). In this work, the Mohr-Coulomb types were employed.

Soils are complex materials with nonlinear, inelastic and stress level dependent response (Byrne et al. 1987). However, most of these complexities can be captured by relatively simple stress-strain hyperbolic relationships (Kondner and Zelaski 1963; Duncan et al. 1980; Beaty and Byrne 1998; Puebla 1999). Some analysis based on simplified models such as those based on linear elastic-plastic constitutive models are also appropriate.

Two soil constitutive models already built in FLAC and based on the incremental elastic-plastic theory were selected for evaluating the soil-pipe interaction behavior from simple to complex: a linear elastic-plastic soil response represented by the Mohr-Coulomb model and a hyperbolic shear stress-strain relationship through the Cap -Yield (CYSOIL) model. General information for both constitutive models is presented in the following sections.

7.1.1.1 Linear Elastic-Plastic Mohr-Coulomb Model

The Mohr-Coulomb material model in FLAC 7.0 shows a linear elastic-perfectly plastic behavior. The elastic behavior occurs when the stress state is within the yield surface, whereas the plastic behaviour starts when the soil stress state is on the yield surface which is defined by the Mohr-Coulomb failure criterion.

The Mohr-Coulomb model implemented in FLAC 7.0 has a non-associated flow rule and it requires any of two stiffness parameters from shear modulus, G, Poisson's ratio, ν, Young's modulus, E, and bulk modulus, B to describe

the elastic behaviour of the soil material. The plastic behavior is characterized by strength parameters such as the peak friction angle, ϕ, and dilation angle, ψ, to determine the failure criterion and volume change of the material.

Young's Modulus, E, and Poisson's ratio, ν, are not constants for a soil, but rather they depend on stress level. Young's Modulus, E, is often directly determined from the deviator stress versus axial strain curve obtained from the standard triaxial laboratory test. Typically the tangent Young's modulus decreases with increasing deviator stress and becomes zero at the peak of the stress-strain relationship. Therefore, terms such as tangent and secant modulus are used to specify Young's modulus.

The value of tangent modulus, i.e. the slope of a straight line drawn tangent to a particular point of the stress-strain relationship, will vary with the point selected. The tangent modulus at the initial point of the stress-strain curve from a drained triaxial test is often called initial Young modulus, E_i. The secant modulus is the slope of a straight line connecting two separate points of the stress-strain relationship. The tangent or Young modulus is usually determined following the approach proposed by Duncan et al. (1980). Researchers have found that E_i is about 1/3 to ¼ of the maximum elastic modulus E_{max} (Byrne et al. 1987).

Values for Poisson's ratio, ν, vary in the range of 0.1 to 0.4. Hardin and Drnevich (1972) concluded that the elastic Poisson's ratio, ν, for sand varies between 0 to 0.2, recommending a value of 0.12. Other investigations using advanced techniques (i.e., local strain measurements with special internal high-resolution instrumentation) have confirmed that the value of Poisson's ratio ranges from 0.1 to 0.2 for all type of geomaterials at low strain levels, increasing to larger values as failure states are approached (Burland 1989; Tatsuoka and Shibuya 1992; Lehane and Cosgrove 2000; Mayne 2007). Byrne et al. (1987) also showed that ν varies between 0.1 to 0.5 for small strain levels and strains at failure for a sand mass, respectively. In this

research, a constant Poisson's ratio of 0.2 is assumed for all the simulated cases.

Even though, the Young's Modulus, E, and Poisson's ratio, ν, are the most commonly used parameters for deformation analysis of sand masses, the shear modulus, G, and the bulk modulus, B, are more fundamental parameters because they separate distortional and volumetric components of strain. Therefore, they are more desirable to use (Itasca 2012; Byrne et al. 1987). In this study, the elastic component of response is assumed to be isotropic and specified by a shear modulus, G, and bulk modulus, B, that are stress level dependent. G can be expressed as:

$$G = k_G{}^{e} * P_a * (\frac{p'}{P_a})^{ne} \qquad [7.1]$$

Where k_G is the shear modulus number which depends on the density of the soil; p' is the mean normal effective stress; P_a is a reference pressure in a chosen unit (e.g. 100 kPa); and ne is an elastic exponent that varies between 0.4 and 0.6.

Byrne et al. (1987) showed that k_G is about 1/3 of the $k_G{}^e$ (the elastic shear modulus number, e stands for elastic). Available current technical literature shows that typical values of $k_G{}^e$ for sand varies from about 500 for loose sand to 2000 for dense sand. $k_G{}^e$ can also be related to K_{2max} (Seed and Idriss 1970) as follows:

$$k_G{}^e = 21.7 \cdot (K_{2max}) \qquad [7.2]$$

where K_{2max} is a function of $(N_1)_{60}$, the penetration value corrected by energy and an effective overburden stress of 1 atm, or relative density. Seed et al. (1986) suggested the following relation for K_{2max}:

$$K_{2max} = 20 \cdot (N_1)_{60}^{1/3} \qquad [7.3]$$

The elastic bulk modulus, B, can be directly measured by using high quality measurements of volumetric response during unloading. However, there is little data for this direct measurement. Alternatively, the elastic bulk modulus B can be obtained indirectly from the elastic shear modulus G as a function of Poisson's ratio, ν, as follows:

$$B = \alpha_B \cdot G \qquad [7.4]$$

Where $\alpha_B = \left(\frac{2(1+\nu)}{3(1-2\nu)}\right)$ $\alpha_B = \left(\frac{2(1+\nu)}{3(1\text{-}2\nu)}\right)$ depends on the elastic Poisson's ratio, ν. For ν in the range of 0.0 to 0.2, α_B varies between 2/3 to 4/3 and can be approximated as unity.

Among the three soil backfills used in this work (i.e. Fraser River sand (FRS), road mulch and crushed limestone), only Fraser River sand has triaxial test and direct shear test data available.

Shear strength parameters and initial Young modulus (E_i) for FRS were presented in **Section 3.3.1.1**. These parameters were characterised by Karimian (2006) and Wijewickreme et al. (2009) for their numerical simulations of the mobilization of axial and lateral soil restraints on steel pipes. The peak shear strength parameters for FRS were based on triaxial and direct shear tests; while constant volume shear strength for FRS were obtained from Uthayakuma (1996) and Sivathayalan (2000).

In this study, values similar to those used by Karimian (2006) and Wijewickreme et al. (2009) were used for the plane strain numerical simulations (ϕ'_p of 43°, ϕ'_{cv} of 33°). A dilation angle (ψ) of 12° was used based on the relationship proposed by Bolton (1986) and presented in **Equation 4.4**. These values were also used in the calculations of the maximum level of

lateral soil restraint on a pipe specimen buried on FRS by a limit equilibrium approach, as shown in **Section 4.7.2.1**.

Likewise, the calculated initial Young's moduli for different tests are shown in **Figure 7.2** along with power law equations to calculate initial Young modulus as a function of confining stress of the form:

$$E_i = k_E * P_a * \left(\frac{\sigma_3'}{P_a}\right)^n \qquad [7.5]$$

Where k_E is the Young's modulus number; n is the Young's modulus exponent; σ_3' is the effective confining stress; and P_a reference pressure (100 kPa).

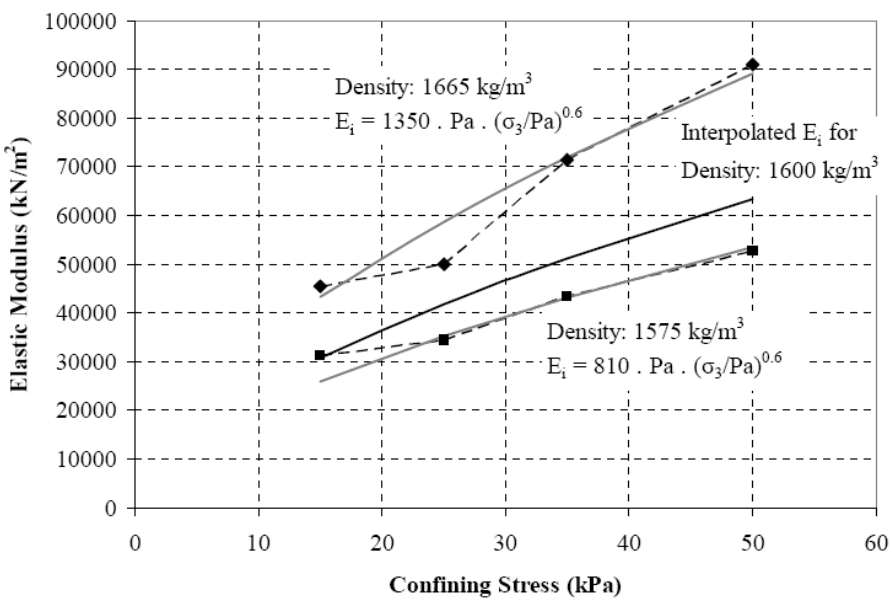

Figure 7.2: Initial Youngs modulus for Fraser River sand from triaxial test results (after Karimian 2006).

From **Figure 7.2** a Young's modulus number k_E equal to 1000 can be interpolated for Fraser River sand with dry density of 1,600 kg/m^3 (D_r = 75%). By using a Poisson's ratio, ν, of 0.2, a k_G of about 415 is obtained for Fraser

River sand. This value is in line with a k_G of 411 calculated from **Equation [7.3]** and reduced by 1/3 (Byrne et al. 1987) (K_{2max} = 57 for relative density of 75% which would correspond to approximately a $(N_1)_{60}$ of 23).

No triaxial testing data is available for the road mulch or crushed limestone backfill materials; therefore, available published typical ranges of initial elastic modulus and Poisson's ratio for loose and dense sandy and gravelly material were used as a reference for selecting values that would match the measured lateral soil restraint vs. pipe displacement relationships for these backfill materials.

The literature shows that representative values of K_{2max} for sand are generally in the range of 30 for very loose sand to 75 for very dense sand. Values of K_{2max} for relatively dense gravels are generally in the range of 80 to 180 (Seed et al. 1986). In addition, values of k_G^e for gravels are generally greater than those for sand by factors ranging from 1.35 to 2.5. Therefore, a value of 1.7 and 2.0 was used in this study for the road mulch and crushed limestone backfill materials, respectively.

The summary of the Mohr-Coulomb model parameters used for the numerical simulation of development of lateral soil restraint is presented in **Table 7.1**.

Table 7.1: Mohr-Coulomb Model Parameters Used in the Numerical Simulation for No Trench Cases

Material	Dry Density (kg/m^3)	D_r (%)	k_G	n	ϕ'_p (degrees)	ψ (degrees)
Fraser River Sand	1,600	75	415	0.6	43	12
Road Mulch	1,800	-	705	0.6	49	16
Crushed Limestone	1,700	-	830	0.6	46	18

Note: $k_G = 1/3 \cdot k_G^e$; Poisson's ratio (ν) = 0.2

7.1.1.2 Cap -Yield (CYSOIL) Model

The CYSOIL model built in FLAC 7.0 is a strain-hardening constitutive model characterized by a frictional and cohesive Mohr-Coulomb failure surface and an elliptic volumetric cap. The model offers the flexibility of adding user-defined hardening or softening stress-strain relationships for simulating soil behavior. In particular three types of hardening law can be specified for the model: a cap-hardening law, a friction-hardening law, and a compaction/dilation law.

The hardening law allows capturing the volumetric power law behavior observed in isotropic compaction tests. The friction-hardening law reproduce the hyperbolic stress-strain relationship behavior observed in drained triaxial tests. The compaction/dilation law models the irrecoverable volumetric strain

taking place as a result of soil shearing. General characteristics and formulations of the model are presented in the **Appendix D**.

As described in **Section 7.1.1**, the stress-strain curve for granular materials is usually approximated by a hyperbola (e.g. Kondner and Zelaski 1963; Duncan et al. 1980; Matsuoka and Nakai 1977; Beaty and Byrne 1998; Puebla 1999). The CYSOIL constitutive model is supplemented by a friction, strain hardening table to capture this hyperbolic behavior. In particular, CYSOIL adopts a hyperbolic incremental law similar to the one implemented in the UBCSAND model (Byrne et al. 2003):

$$d(\sin\varphi_m) = \frac{G^p}{p'} d(\gamma^p) \qquad [7\text{-}6]$$

Where p' is effective pressure, and the plastic shear modulus, G^p, is given by

$$G^p = \beta \cdot G^e (1\text{-} \frac{\sin\varphi_m}{\sin\varphi_f} R_f)^2 \varphi_m \leq \varphi_f \qquad [7\text{-}7]$$

In the previous equation, G^e is the elastic tangent shear modulus, ϕ'_p is the peak friction angle, ϕ'_m is the mobilized friction angle, R_f (the failure ratio) is a constant smaller than 1, and β is a calibration factor.

The elastic tangent shear modulus is a function of p', and we have

$$G^e = k_G{}^e \cdot P_a (\frac{p'}{P_a})^m \qquad [7\text{-}8]$$

Where $k_G{}^e$ is the elastic shear modulus number; m is the shear modulus exponent; and P_a is the atmospheric pressure.

The model properties in the CYSOIL model for Fraser River sand backfill were calibrated in two steps during the numerical simulation. First, an initial

estimate of the drained triaxial test response obtained by Karimian (2006) was carried out to obtain a first estimate of property values. The Karimian (2006) test with confining pressure of 25 kPa and dry density of 1576 kg/m^3 was chosen for the calibration. The result of such calibration is shown in **Figure 7.3**. Second, the property values were improved by matching the results obtained from the numerical simulation to the full-scale tests.

Similar to the Mohr-Coulomb model case, a Young's modulus number k_E equal to 1000 can be interpolated for Fraser River sand with dry density of 1,600 kg/m^3 from **Figure 7.2**. k_G^e was calculated by multiplying k_G by 3 (Byrne et al. 1987). Therefore, a k_G^e value of 1230 will be used in the numerical simulations involving Fraser River sand. Fitting the predicted values to the observed soil response will be done through the parameter β.

The final parameters used in the numerical simulation of the breakout of buried pipelines from their soil embedment for Fraser River sand, road mulch and crushed limestone are shown in **Table 7.2**.

Table 7.2: Cysoil Model Parameters Used in the Numerical Simulation

Material	Dry Density (kg/m^3)	β	k_G^e	n	R_f	ϕ'_p (degrees)	ψ (degrees)
Fraser River Sand	1,600	0.2	1230	0.6	0.98	43	12
Road Mulch	1,800	0.2	2091	0.6	0.98	49	16
Crushed Limestone	1,700	0.2	2460	0.6	0.98	46	18

Note:
Poisson's ratio (ν) = 0.2

7.1.1.3 Discussion

As can be noted in **Figure 7.3**, the simulated response of the drained triaxial test result shows a very good agreement with that experimentally obtained by Karimian (2006) on Fraser River sand with confining pressure of 25 kPa and dry density of 1576 kg/m^3. The parameters used in the CYSOIL model are k_G^e of 1230, β of 0.33, ν of 0.2, R_f of 0.98, ϕ'_p of 43° and ψ of 12°. This comparison evidences the ability of the CYSOIL model to fit to any one curve when the appropriate constitutive parameters of the model are described and the parameters reflect the measured behaviour. However, it is important to notice the difference between capturing characteristic behavior and matching a measured response.

The good agreement shown in **Figure 7.3** would not be of much help for the development of the lateral soil restraint simulation from the full-scale models. In the full-scale models, the problem is of a plane strain type, rather than an

axisymmetric one. In addition, the relative density is particularly difficult to estimate in the vicinity of the pipe specimen (see **Section 3.4**). Therefore, refining the fit to any single curve is not as important as capturing the fundamental characteristics of the soil-pipe interaction response.

The use of triaxial test data in a plane strain problem also led to the question of whether or not these results could be used as input parameters for the current plane strain field problem. Previous research on numerical modeling of soil-pipe interaction used results from triaxial and direct shear tests (Dayian et al. 2011; Wijewickreme et al. 2009; Yimsiri et al. 2004; Guo and Stolle 2005) with adequate results. Lee (1970) concluded that the shear strength and stiffness determined by triaxial tests are not significantly different (usually lower) than those determined by plane strain tests. Therefore, it was considered appropriate to use soil parameters determined from the available triaxial test in the numerical simulations.

As stated in previous sections, the mobilization of soil restraint during the transition from initial linear state to the ultimate state observed in the full-scale tests was captured in the numerical simulation through the parameter β (equal to 0.2, see **Table 7.2**). This was considered appropriate due to the difficulty of measuring and estimating the soil density around and in particular below the pipeline springline.

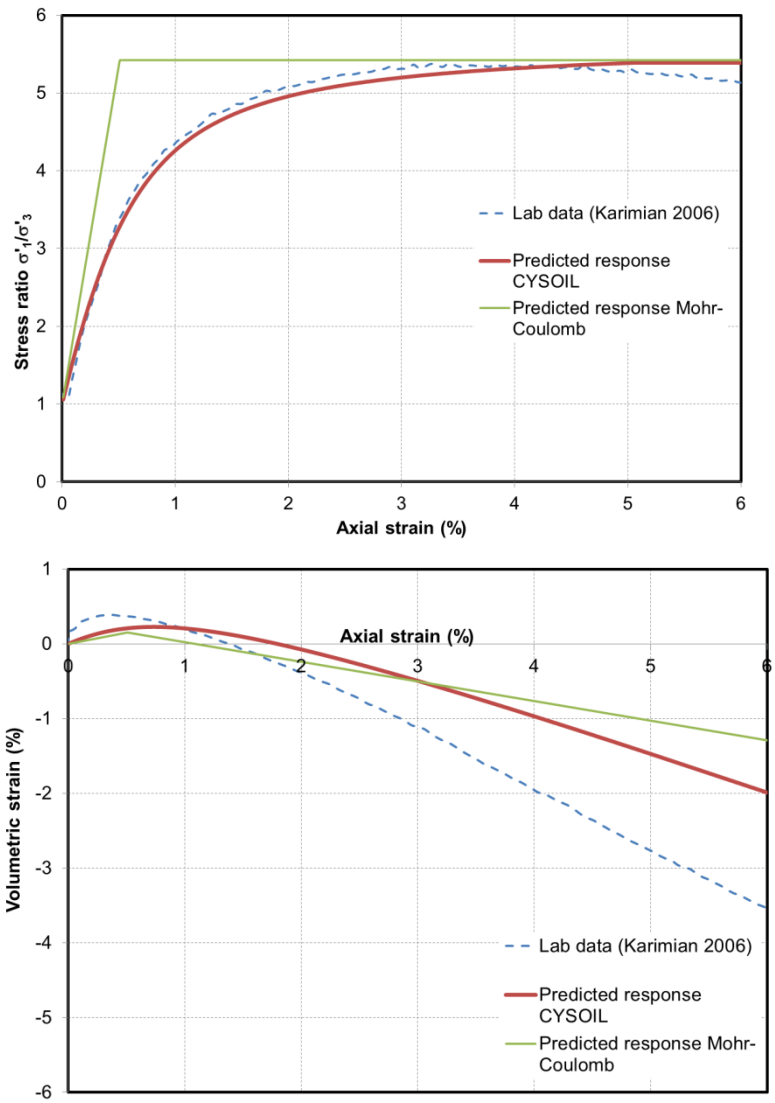

Figure 7.3: Comparison between measured and simulated response of Fraser River sand tested in drained triaxial compression. Data from Karimian (2006). Dry density = 1576 kg/m^3 (D_r=69%) and confining stress of 25 kPa.

In an effort to evaluate the use of the above value, a numerical simulation was carried for the NPS18 pipe with an H/D=1.9 and a parameter β of 0.33 (similar to the one used in the one element test, see **Figure 7.3**). A reduced soil density of 1,400 kg/m^3 was used for the grid elements around the pipe, while

keeping the soil density of 1,600 kg/m^3 for the other elements. The result of such simulation is shown in **Figure 7.7** together with the result from the simulation with parameters from **Table 7.2**.

As evidenced in **Figure 7.7**, the mobilisation of normalized lateral restraint with pipe displacement predicted by the model with β of 0.33 and reduced soil density is similar to the result from simulation with parameters from **Table 7.2**. However, the result from the latter agrees better with the results from the full-scale tests. Therefore, it was considered appropriate to do all the simulations with those parameters.

7.2 Numerical Simulation of Lateral Soil Restraint on Pipelines

7.2.1 Numerical Simulation for Cases with no Trench

7.2.1.1 Mesh Configuration

The dimension and boundary conditions of the model were selected similar to those of the testing chamber and the pipe specimen dimensions used for the full-scale tests. As described in **Chapter 3**, the length and width of the testing chamber are 3.8 m and 2.45 m respectively. The height of the model varies depending on burial soil depth.

The geometric domain for modelling the soil-pipe interaction behaviour was discretized into uniform and fine grid elements. Because the overall response of the soil-pipe system depends on boundary conditions, loading characteristics and mechanical properties of each element comprising the grid; the discretization was selected so that the numerical results are not grid-sensitive. Criteria such as convergence, analysis time and accuracy were considered for selecting the appropriate discretization. After examining several mesh configurations for convergence and minimum analyses time, those

mesh configurations as shown in **Figure 7.4** and **Figure 7.5** for NPS16 and NPS18, respectively, were selected to simulate the full-scale test conditions.

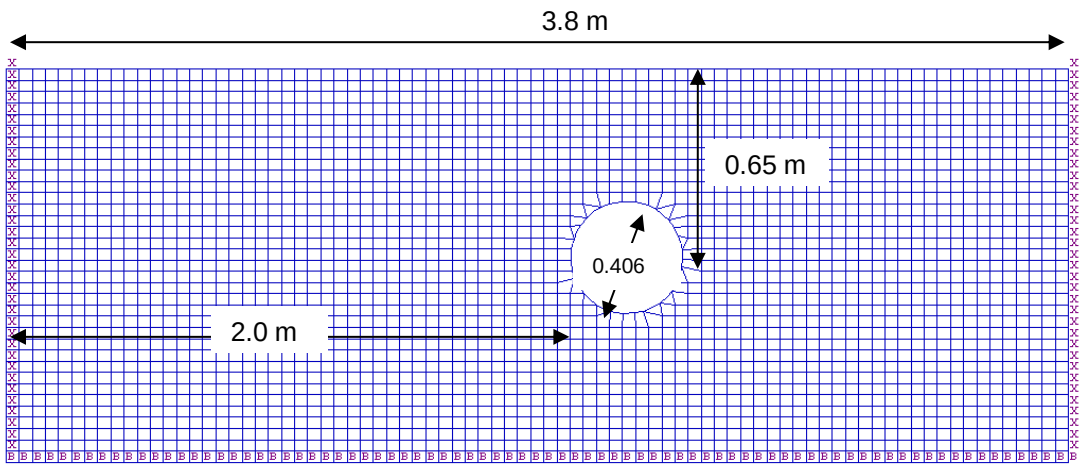

Figure 7.4: Grid configuration for simulating tests with NPS16.

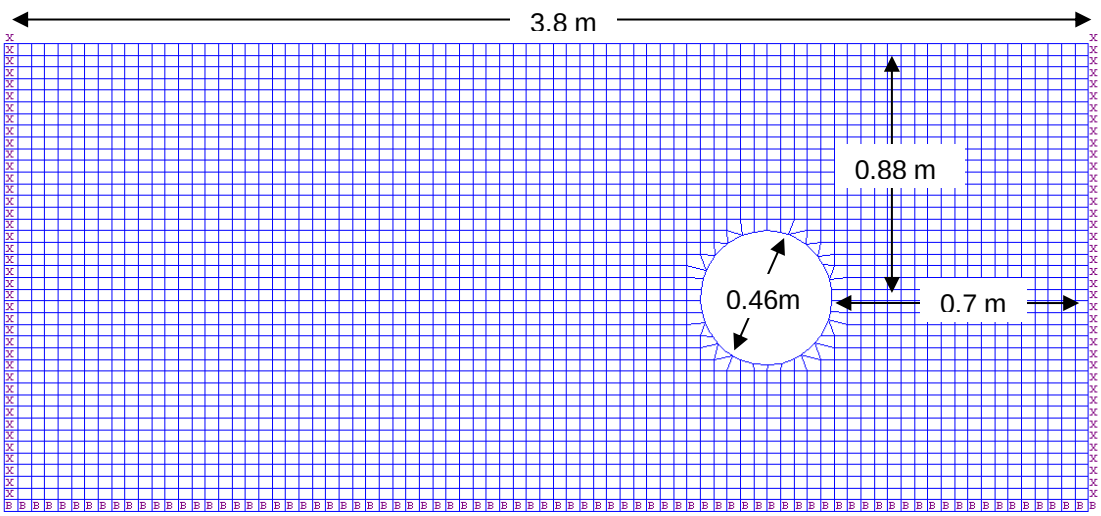

Figure 7.5: Grid configuration for simulating tests with NPS18.

The number of elements in the model for simulating lateral tests with NPS16 and NPS18 pipe specimens was equal to 2835 and 3240, respectively. 44 beam elements were used to model both NPS16 and NPS18 pipe specimens.

Weight and stiffness of the beam elements were selected to match the actual pipe test specimen. When compared to the stiffness of the soil, the pipe behaved like a rigid body. Soil nodes along the lateral boundaries were restrained against lateral movement, but were allowed to move vertically.

7.2.1.2 Simulation of Soil-Pipe Interface

Unbonded interface elements were used to model the interface between pipe and soil. These interface elements with Coulomb shear-strength criterion allows for slippage when shear force between soil and pipe exceeds F_{smax} as per **Equation [7.9]**.

$$F_{smax} = c \cdot L + F_n \cdot \tan(\phi_{interface}) \qquad [7.9]$$

Where c = cohesion (in stress units) along the interface; L = effective contact length along pipe; $\phi_{interface}$ = interface friction angle; and F_n = normal force per unit length on the interface.

In the current model, no cohesion is considered, thus F_{smax} is only a function of interface friction and normal stress. Interface friction angle between dense sand and sand-blasted steel was obtained from Karimian (2006). Peak and constant volume friction angle at pipe-sand interface are 36° and 31° respectively. Karimian (2006) found that the effect of interface friction angle variations (e.g. from 36° to 31°) on the values of lateral soil restraint during soil-pipe interaction is negligible. This coincides with the findings from Yimsiri et al. 2004. Therefore, a 36° friction angle was selected as input parameter for the numerical simulation in this study. Similar to the interface friction angle, Karimian (2006) showed that variation of dilation angle value from 0° to 10° results in less than 1% increase in the levels of maximum lateral soil restraint on pipelines. Thus, in the current model, dilation at the interface is defined by a constant dilation angle, ψ, of 3°.

7.2.1.3 Stress State Prior to Pulling

To simulate the stress state condition in the soil chamber prior to pulling the pipe, the soil weight was applied in three steps during the numerical simulation. At first, the soil up to the level of the pipe invert with the pipe on top of it was modeled. A first iteration was carried out to reach equilibrium. Then, the weight of soil backfill from the pipe invert level to the level corresponding to the top of the pipe was applied and an analysis was conducted to achieve equilibrium. Finally, the weight of soil backfill to the desired overburden ratio (1.6 or 1.9) was applied to the model. At this stage, the analysis was continued to achieve full equilibrium before displacing the pipe. The contours of computed horizontal and vertical stresses prior to pulling the pipe are shown in **Figure 7.6**.

7.2.1.4 Results of Numerical Simulation on Sand Backfill

The normalised lateral soil restraints, $N_{qh} = P / (\gamma \cdot D \cdot H \cdot L)$, versus normalised pipe displacement, $Y' = Y / D$, predicted by the Mohr-Coulomb and CYSOIL constitutive models on NPS18 (457-mm diameter) pipe specimen buried in moist sand with H/D = 1.9 are shown in **Figure 7.7**. The corresponding parameters used for the constitutive models are shown in **Table 7.1** and **Table 7.2**. The results of Tests 18-1.9-90H-MS-MS-GN-1, and 18-1.9-90H-MS-MS-GN-2 are also overlain in the same figure. In addition, the measured response from Test 18-1.9-90H-MS-MS-GY-45-2D performed with a trench wall-pipe distance (S) of 2D was also included. Note that the trench wall has no effect on the soil-pipe interaction response if S > 1D.

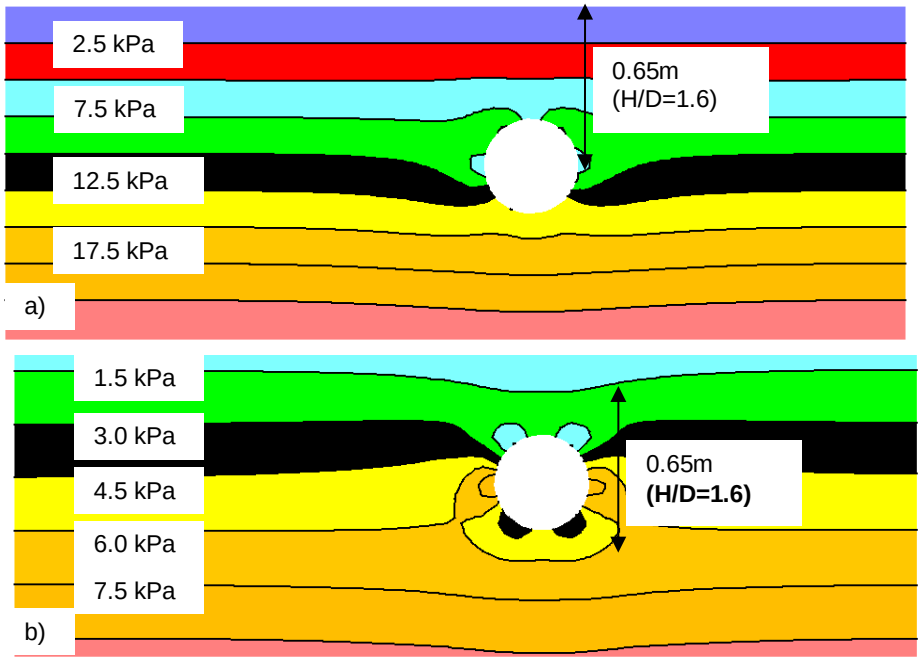

Figure 7.6: Vertical (a) and horizontal (b) stresses (kPa) prior to lateral pulling for Test 16-1.6-90H-MS-MS-GN.

As can be observed from Figure 7.7, initially both predicted curves were similar because the state of stress in all elements was still within the elastic region. After yielding of some elements, the normalised soil restraint-pipe displacement curves started to deviate from each other. This stage corresponded to the elastic-plastic transition region identified in Section 4.7.1. Here, the predicted curves were less stiff than those recorded during the experimental testing. However, a reasonable agreement in terms of characteristic behaviour can be noted.

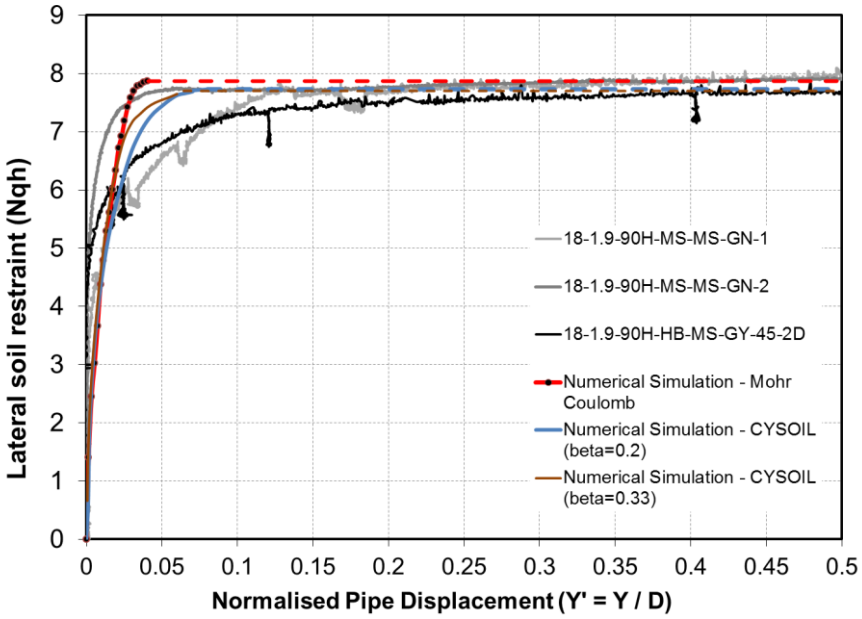

Figure 7.7: Simulation of Tests 18-1.9-90H-MS-MS-GN-1 and 18-1.9-90H-MS-MS-GN-2 using bilinear Mohr-Coulomb and CYSOIL models.

For the Mohr-Coulomb model, yielding started at an N_{qh} of about 2.5 and reached a maximum normalised lateral soil restraint N_{qh} of about 7.8. This load was quite close to those recorded during the full-scale testing (N_{qh} = 7.74). As for the CYSOIL model, yielding also started at an N_{qh} of about 2.5 and then showed a nonlinear behaviour until it reached a maximum normalised lateral soil restraint N_{qh} of about 7.7.

A comparison between the simulated and the observed normalised lateral soil restraint, N_{qh}, vs. normalised pipe displacement, Y', responses indicates that in general using the CYSOIL model yields results that are in better agreement with results from full-scale tests that those obtained using a bilinear elastic model. This result was expected, as the CYSOIL model incorporates the nonlinearity of the soil. Also, this is in accord with the findings from Karimian (2006) that the Mohr-Coulomb model predicts stiffer results than a model based on a hyperbolic relation.

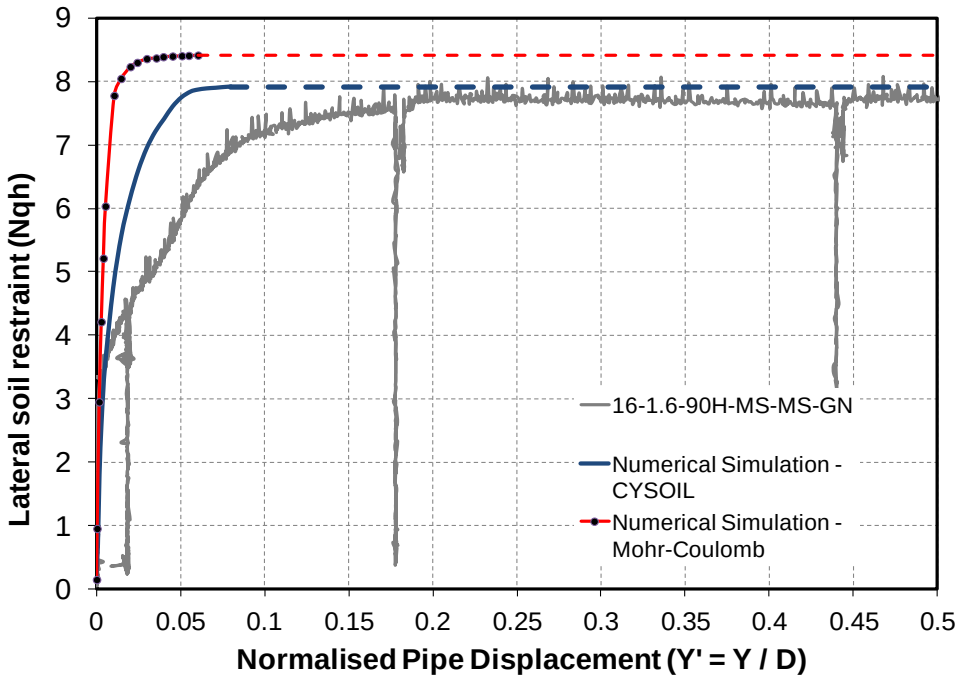

Figure 7.8: Simulation of Test 16-1.6-90H-MS-MS-GN using bilinear Mohr-Coulomb and CYSOIL models.

A comparison between the predicted and measured normalised lateral soil restraints, $N_{qh} = P / (\gamma \cdot D \cdot H \cdot L)$, versus normalised pipe displacement, Y' = Y / D, curves for an NPS16 (406-mm diameter) pipe specimen buried in moist sand with H/D = 1.6 under lateral displacement to simulate pipeline breakout from its soil embedment is shown in **Figure 7.8**. The similarity in characteristic behavior pattern for both NPS18 and NPS16 pipe specimens may be noted. It is interesting to note that the numerical simulation predicted normalised pipe displacement, Y', to failure 25 to 35% lower than those recorded from the full-scale tests. However, differences less than 3% were reported for the maximum lateral soil restraint values.

Patterns of soil backfill deformation, maximum shear strain and displacement fields at failure condition (Y'=0.07D) from the CYSOIL model numerical simulation corresponding to Test 16-1.6-90H-MS-MS-GN are illustrated in **Figure 7.9**. The magnitude and direction of displacement vector at each node

is represented by an arrow. As shown in **Figure 7.9**, the higher values of the maximum shear strain by the CYSOIL model were seen to be in fair agreement with the position of the log-spiral failure surface described in **Section 4.2.3** and observed from the full-scale test (see **Figure 4.7**).

Further, it can be seen that the magnitude of the displacement vector was relatively constant along the slip flow in the shearing zone of the log-spiral mechanism from the bottom of the pipe to the free boundary surface. The displacement field also agreed quite well with the sizes of three zones distinguished from the deformed soil mass during the experimental testing as described in **Section 4.2.3**: passive zone (A), active zone (C), and central zone (B). The pipe vertical displacement observed during the tests was also captured by the numerical simulation.

The corresponding distribution of mobilised friction and dilation angle predicted by the CYSOIL model at Y'=0.07D (failure condition) for Test 16-1.6-90H-MS-MS-GN are shown in **Figure 7.10**. From this figure, it can be seen that the friction and dilation angles were fully mobilized along the slip flow in the shearing zone of the log-spiral mechanism and as expected they coincided with the zones of maximum shear strain (**Figure 7.9**).

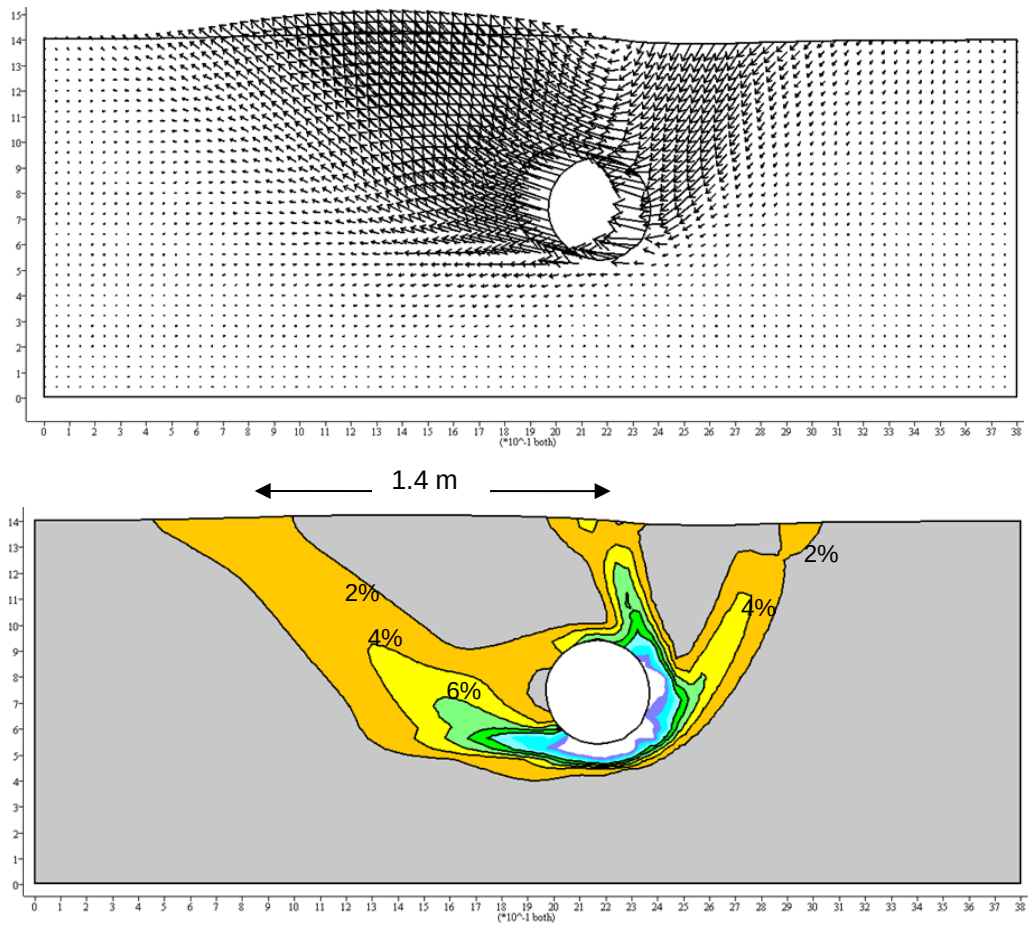

Figure 7.9: Displacement and maximum shear strain field predicted by the CYSOIL model at Y'=0.07D (failure condition) for Test 16-1.6-90H-MS-MS-GN.

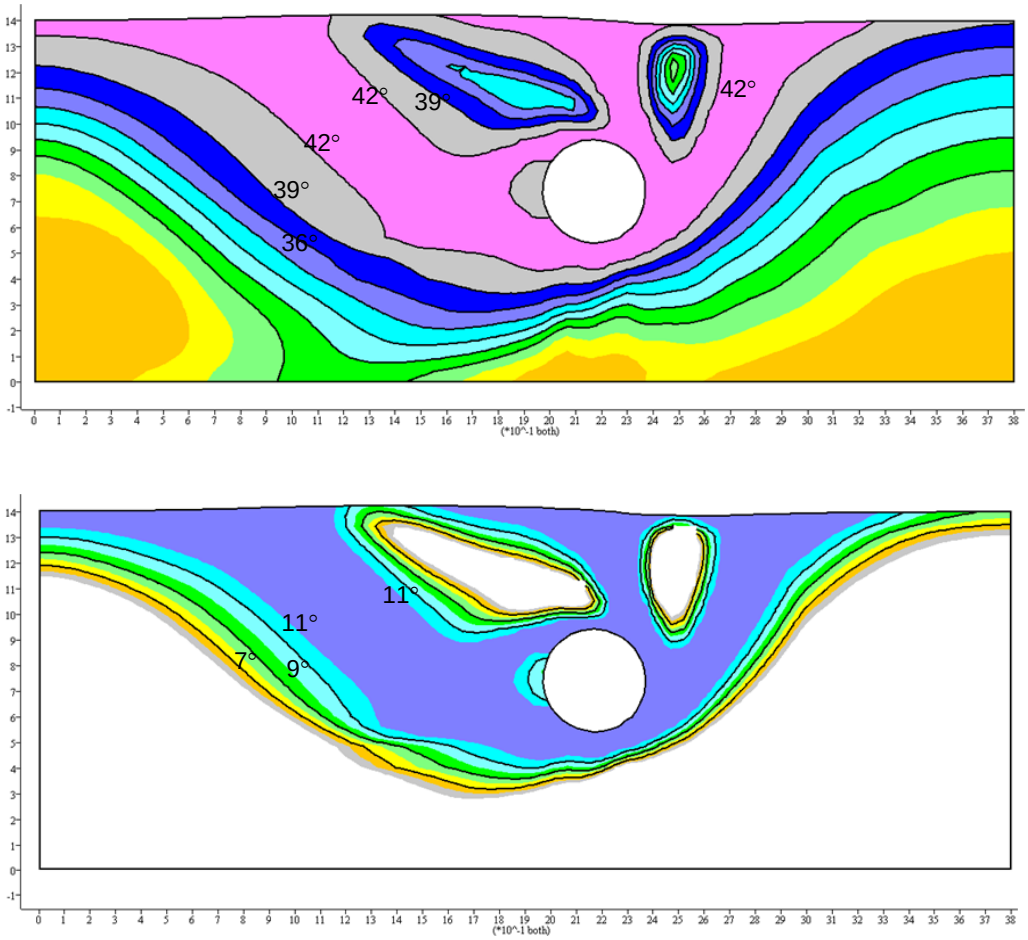

Figure 7.10: Distribution of mobilised friction and dilation angle by CYSOIL model at Y'=0.07D (failure condition) for Test 16-1.6-90H-MS-MS-GN.

7.2.1.5 Results of Numerical Simulation on Road Mulch Backfill

A comparison between the predicted and observed normalised lateral soil restraints, $N_{qh} = P / (\gamma \cdot D \cdot H \cdot L)$, versus normalised pipe displacement, Y' = Y / D, responses due to numerically simulated relative lateral seismic fault ground displacements on NPS18 (457-mm diameter) pipe specimen buried in road mulch with H/D = 1.9 is shown in **Figure 7.11**. Again, Mohr-Coulomb and CYSOIL constitutive models were used in the numerical model. The corresponding parameters used for the constitutive models are shown in

Table 7.1 and **Table 7.2**. The results of Tests 18-1.9-90H-RM-RM-GN-1 and 18-1.9-90H-RM-RM-GN-2 are also included in the same figure.

Similar to the case for tests with Fraser River sand backfill, an appropriate agreement in terms of fundamental characteristic behavior can be observed. Again, the predicted normalised lateral soil restraints, N_{qh}, versus normalised pipe displacement, Y', after initial yielding (N_{qh} of about 4.5) was stiffer than the actual data. For the Mohr-Coulomb model, a maximum normalised lateral soil restraint N_{qh} of about 11.2 was predicted by the numerical simulation. As for the CYSOIL model, a maximum normalised lateral soil restraint N_{qh} of about 10.15 was predicted. This range of predicted N_{qh} values was well within the observed values from full-scale testing (N_{qh} = 10.2 to 11). The normalised pipe displacements, Y', to failure predicted by both constitutive models were 20 to 35% lower than those recorded from the full-scale tests.

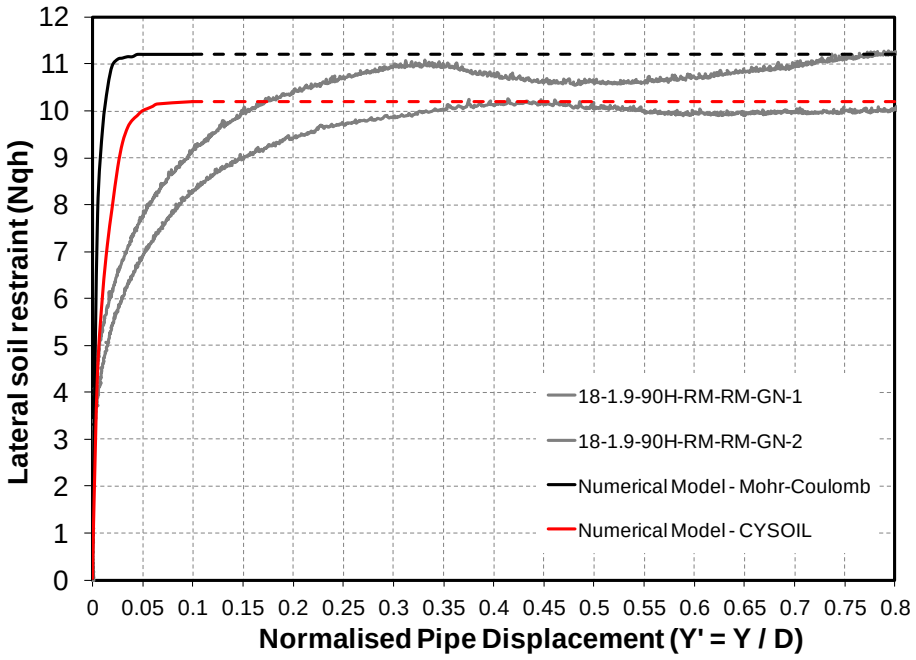

Figure 7.11: Simulation of Tests 18-1.9-90H-RM-RM-GN-1 and 1.9-90H- RM-RM -GN-2 using bilinear Mohr-Coulomb and CYSOIL models.

7.2.1.6 Results of Numerical Simulation on Crushed Limestone Backfill

The normalised lateral soil restraints N_{qh} = P / (γ·D·H·L) versus normalised pipe displacement Y' predicted by the Mohr-Coulomb and CYSOIL constitutive models on NPS16 (406-mm diameter) pipe specimen buried in crushed limestone with H/D = 1.6 are shown in **Figure 7.12**. The result of Test 16-1.6-90H-LM-LM-GN is also overlain in the same figure. Similar to the cases for Fraser River sand and road mulch backfills, all the curves were similar during the initial stages of loading. After loading continues, some elements started to yield and the predicted responses from the two constitutive models used in the numerical simulation deviated from each other. Here, the predicted curve by the Mohr-Coulomb model was very similar than that recorded during the experimental testing. The Mohr-Coulomb model, however, was not able to predict the peak N_{qh} of about 12 recorded during the full-scale test. Nevertheless, the after-peak normalised lateral soil restraint N_{qh} of about 10 was well captured by the model.

As for the CYSOIL model, yielding started at an N_{qh} of about 5.5 and then showed a nonlinear behaviour until it reached a maximum normalised lateral soil restraint N_{qh} of about 10. A comparison between the simulated normalised lateral soil restraints indicates that the Mohr-Coulomb model yielded a result that is in better agreement with the result from full-scale tests. However, because the parameters used in the constitutive models were selected on the basis of closely matching the result from the experimental testing, a set of parameters that produce a stiffer response for the CYSOIL model would have produce a better agreement too.

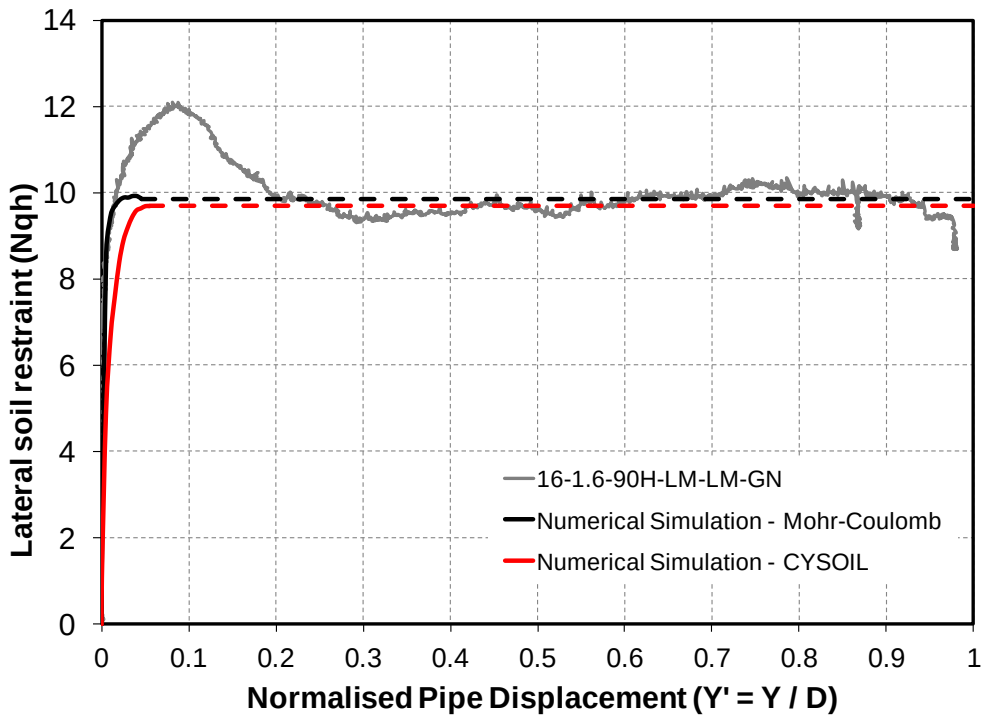

Figure 7.12: Simulation of Test 16-1.6-90H-LM-LM-GN using bilinear Mohr-Coulomb and CYSOIL models.

7.2.2 Numerical Simulation for Cases with Geotextile-lined Trench Wall

7.2.2.1 Mesh Configuration

The case of geotextile-lined pipeline trenches as shown in **Figure 7.13** was numerically simulated. This model represents tests with trench wall-pipe distance (S) of 0.5D and with sand and road mulch as backfill materials. As in the case with no trench conditions, the dimension and boundary conditions of the numerical model were selected similar to those of the testing chamber and the pipe specimen dimensions used for the full-scale tests. The geometric domain for modelling the soil-pipe interaction behaviour was discretized into uniform and fine grid elements. The discretization was selected so that the numerical results are not grid-sensitive. Beam elements with interface

properties were included in the model to represent the double interface (inner geotextile-outer geotextile and outer geotextile-backfill) along the trench wall.

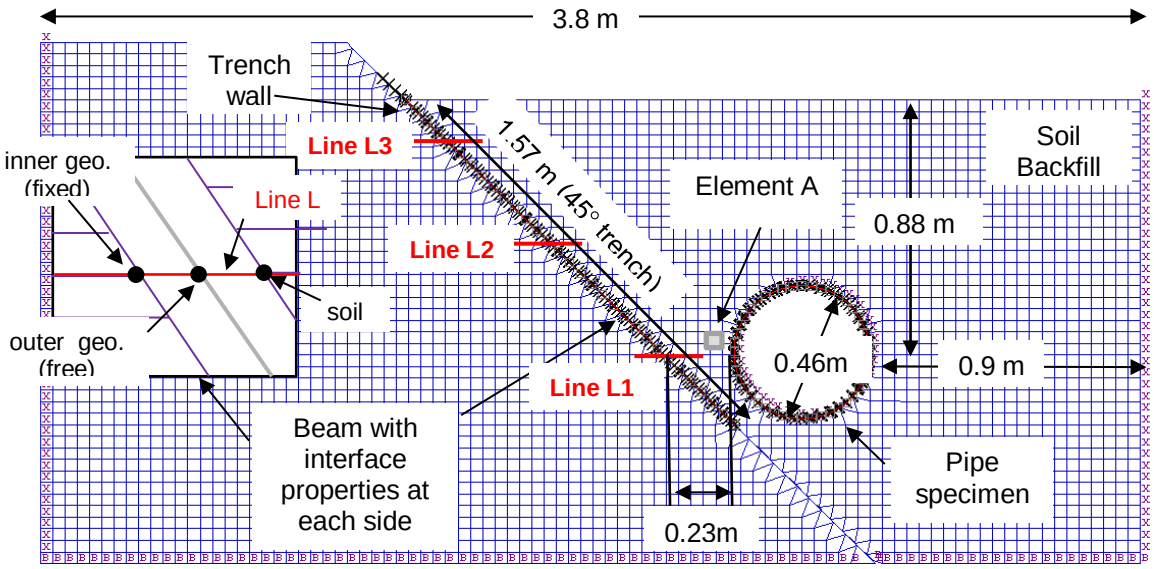

Figure 7.13: Grid configuration for simulating tests with NPS18 pipe specimen and trench conditions at 45°. Some nodes (at Line 1, Line 2 and Line 3) and soil element (Element A) selected to observe the mobilisation of responses at selected locations are also shown.

The number of elements in the model for simulating geotextile-lined pipeline trench conditions subjected to relative lateral ground displacements was equal to 3379 elements. Also, 44 beam elements were used to model the NPS18 pipe specimen. The interface parameters of pipe and soil were kept the same as in **Section 7.2.1.2** while new interface parameters were used to describe the interface between backfill material and outer geotextile interface as well as inner geotextile and outer geotextile interface along the sloped trench wall. Soil nodes on the lateral boundaries were restrained against lateral movement, but were allowed to move vertically. Soil nodes along the trench wall were restrained against lateral and vertical movement.

Histories for selected nodes were recorded to observe the mobilisation of responses at three different locations along the trench wall (Line 1, Line 2 and Line 3). For each line, the displacement response along the trench wall was recorded for a node in the inner geotextile (trench wall), in the outer geotextile, and for a node in the soil backfill. Note that these three nodes lie on the same space position for each line as they are located along the inclined plane of the trench. In addition, the history of volume change behavior for Element A was recorded. The locations of Line 1, Line 2, Line 3 and Element A are shown in **Figure 7.13**.

7.2.2.2 Simulation of Geotextile-Geotextile-Soil Interface

Beam elements with interface properties characterized by Coulomb sliding were used to model both the inner geotextile and outer geotextile interface and the outer geotextile and backfill soil interface along the trench boundary in accordance with the trench lining configurations used in the full-scale tests and described in **Section 3.4.4**. These interface elements allow for slippage when shear force between outer geotextile-soil or inner geotextile-outer geotextile exceeds F_{smax} as per **Equation [7.9]**.

FLAC uses the following formulation to determine normal (F_n) and shear forces (F_s) along the interface:

$$F_n^{(t+\Delta t)} = F_n^{(t)} - k_n \Delta u_n^{(t+(\frac{1}{2})\Delta t)} L \qquad [7.10]$$

$$F_s^{(t+\Delta t)} = F_s^{(t)} - k_s \Delta u_s^{(t+(\frac{1}{2})\Delta t)} L \qquad [7.11]$$

Where Δu_n and Δu_s are incremental relative displacements in the normal and shear directions, respectively; k_n and k_s are stiffnesses in the normal and shear directions, respectively; and L is the associated length between gridpoints.

The properties assigned to the interface elements to numerically simulate the soil-pipeline breakout behaviour of geotextile-lined pipeline trench conditions subjected to relative lateral ground displacements are described in **Table 7.3**. Interfaces were attached to both sides of beam elements along the trench wall to represent both inner geotextile and outer geotextile interface and outer geotextile and backfill soil interface.

Table 7.3: Interface Model Parameters Used in the Numerical Simulation

Interface	k_n[1] (kPa/m)	k_s[1] (kPa/m)	$\phi_{interface}$ (degrees)	Moment of Inertia for Beam (m^4)
Inner geotextile - outer geotextile	$3x10^6$	$3x10^6$	21	0
Outer geotextile - sand	$3x10^6$	$3x10^6$	32	0
Outer geotextile - road mulch	$3x10^6$	$3x10^6$	32	0

Note:
[1] $k_n=k_s=10*max\{(K+4/3G)/smallest\ width\ of\ adjacent\ element\}$

7.2.2.3 Results of Numerical Simulation on Sand Backfill

A comparison between the predicted and observed normalised lateral soil restraints, $N_{qh} = P / (\gamma \cdot D \cdot H \cdot L)$, versus normalised pipe displacement, Y' =Y/D, responses due to relative lateral ground displacements on NPS18 (457-mm diameter) pipe specimen buried in Fraser River sand with H/D = 1.9 and with trench wall is shown in **Figure 7.14**. The trench wall-pipe distance (S) is 0.5D. The results of Tests 18-1.9-90H-HB-MS-GY-45-0.5D-2 and 18-1.9-90H-HB-

MS-GY-45-0.5D-3, which correspond to trench walls lined with two and one geotextile, respectively, are also overlain in the same figure.

The numerical model includes Mohr-Coulomb and CYSOIL constitutive models to capture backfill sand behaviour. The corresponding parameters are shown in **Table 7.1** and **Table 7.2**, respectively.

The simulation was done only for the initial linear and transition region (Region 1) and plastic region (Region 2) of the normalised lateral soil restraint vs. pipe displacement relationship. Region 3, due to the effect of trench surface on pipeline response (hardening), was not captured in the numerical model. This appears to be partly due to the limitation of mesh geometry. FLAC's automatic rezoning option was tried to overcome this limitation. However, the results were not satisfactory due to the presence of interfaces in the problem. Nevertheless, the prediction of Region 2 (plateau, plastic region) of the normalised lateral soil restraints, N_{qh}, versus normalised pipe displacement, Y', was in good agreement with the physical model.

As can be seen in **Figure 7.14**, the predicted and measured responses compared reasonable well, in particular the prediction of the plateau, although the elastic-plastic transition region (Region 1) predicted by both Mohr-Coulomb and CYSOIL models were stiffer than those observed from the full-scale tests. However, it is evident that the constitutive models and the parameters used for both the soil and the interface elements provide results that are consistent for the most part with the fundamental characteristic behaviour of this soil-pipe interaction problem.

The maximum normalised lateral soil restraint N_{qh} predicted by both Mohr-Coulomb and CYSOIL models were very similar and were about 3% lower than the N_{qh} of about 6.4 measured from Test 18-1.9-90H-HB-MS-GY-45-0.5D-2. During the numerically simulated pipe lateral displacement, the maximum normalised lateral soil restraint was reached at a normalised pipe

displacement, Y', of 0.05D to 0.07D or about 33 to 45% lower than that recorded from the full-scale test.

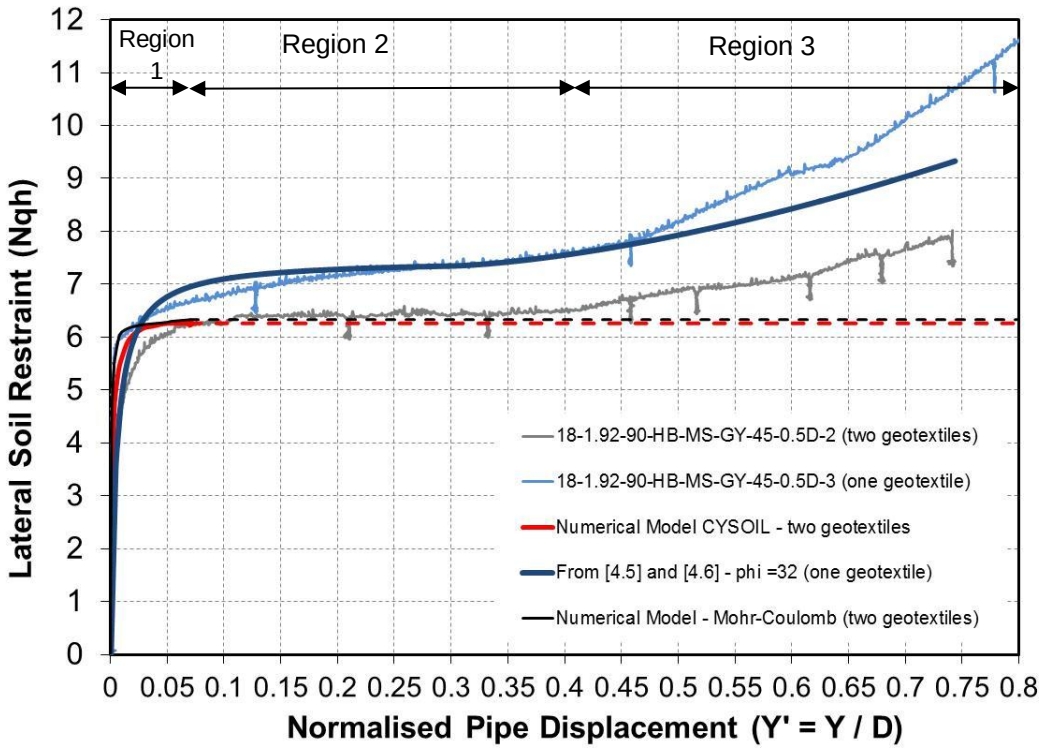

Figure 7.14: Simulation of Test 18-1.9-90H-HB-MS-GY-45-0.5D-2 using bilinear Mohr-Coulomb and CYSOIL models.

Patterns of soil backfill deformation, maximum shear strain and displacement fields at normalised pipe displacements, Y', of 0.001D, at 0.003D (Region 1) and at 0.05D (Region 2, plateau) predicted by the CYSOIL model simulating Test 18-1.9-90H-HB-MS-GY-45-0.5D-2 are illustrated in **Figure 7.15a**, **b**, and **c**, respectively. The magnitude and direction of displacement at each node is represented by an arrow. As shown in **Figure 7.15**, the predicted displacement field by the CYSOIL model at different stages of pipe displacement was seen to be in fair agreement with the patterns of soil backfill deformation observed during the corresponding full-scale test (see **Figure 4.26** and **4.40**).

Further, it can be seen that the size of the displacement vector along the trench wall started to increase at Y' = 0.003D (**Figure 7.15.b**) and is more evident at Y' = 0.05D (**Figure 7.15.b**). At this stage, the size of the displacement vector was constant along the slip flow in the shearing zone along the trench wall from the bottom to the top of the outer geotextile. This indicates a fully plastic condition along the trench wall. The normalised lateral soil restraints, $N_{qh} = P / (\gamma \cdot D \cdot H \cdot L)$, versus normalised pipe displacement, Y' =Y/D, curve shown in **Figure 7.14**, indicates that at Y' = 0.05D the N_{qh} is maximum (plateau).

As evidenced from **Figure 7.15c**, the largest values of maximum shear strain in the soil backfill (> 1%) were localized along a horizontal zone that extends from the bottom of the pipe to the trench wall and along a vertical zone that extends above the pipe. The smallest and constant values of shear strain were predicted for the soil elements located inside those horizontal and vertical zones.

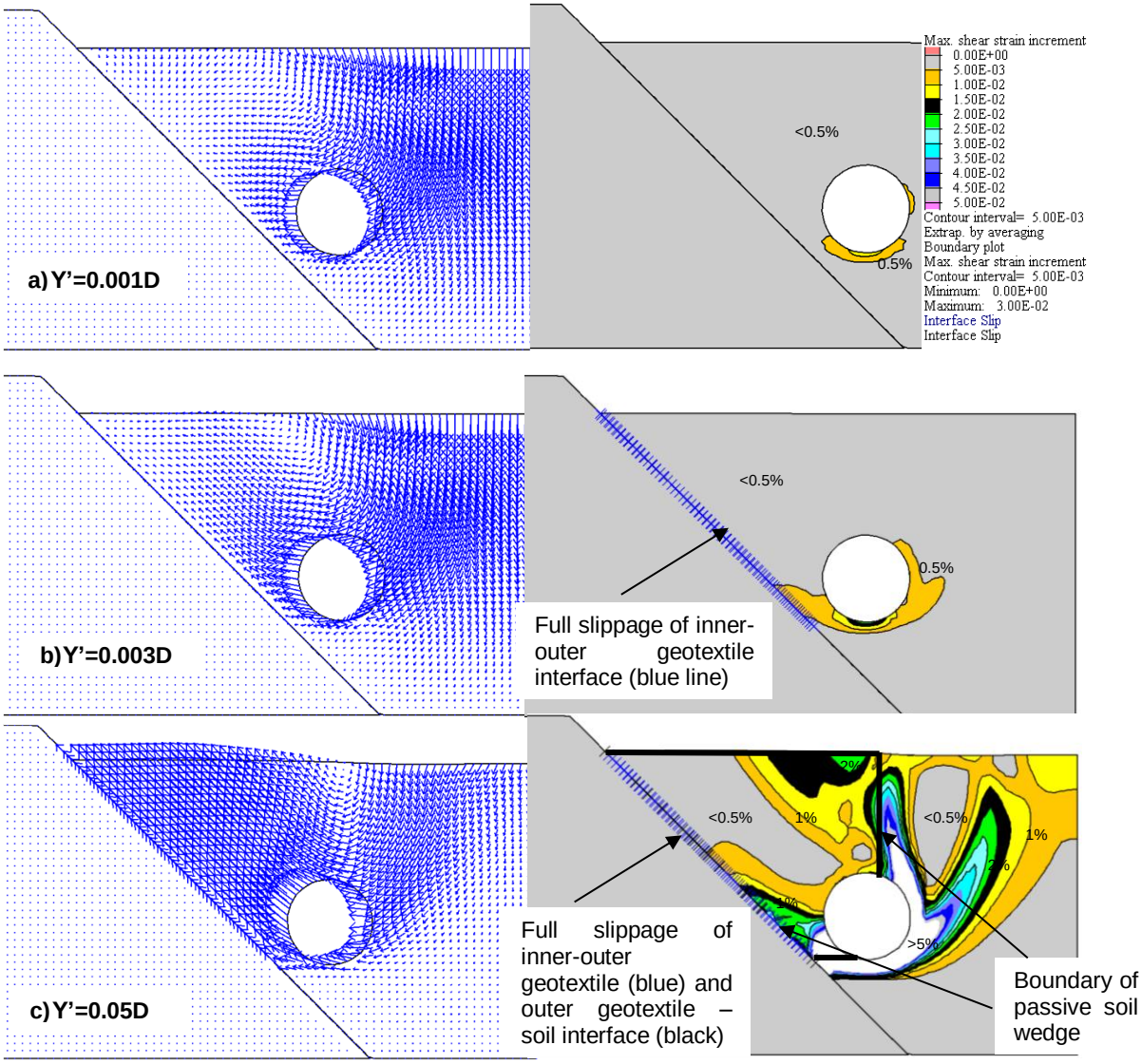

Figure 7.15: Displacement (left) and maximum shear strain (right) field by the CYSOIL model for Test 18-1.9-90H-HB-MS-GY-45-0.5D a) at Y'<0.002D; b) at Y=0.003D; c) at Y' = 0.05D (Region 2, plateau level).

Because in a limit equilibrium analysis all the deformation is assumed to occur along the boundaries of an assumed failure surface, the vertical and horizontal shear zones together with the slip flow in the shearing zone along the trench wall can in theory also be used to predict the plateau observed during the tests as discussed in **Section 4.7.3**.

The response for nodes along Line 1, L1, Line 2, L2, and Line 3, L3, as a function of normalised pipe displacement, Y', are shown in **Figure 7.16** through **Figure 7.20**. The following can be noted from these figures.

1. The condition of peak friction angle for the inner-outer geotextile interface (21 degrees), along the full length of the lined trench wall, was reached at a Y' of 0.003D and remain constant for further Y' (**Figure 7.16**). As expected, normalised pipe displacement above 0.003D produced no change in the peak friction angle for this interface. At Y' of 0.002D the peak frictional resistance was reached along the portion of the trench wall between Line 1 and Line 2.

2. For the outer geotextile-sand backfill interface, the peak friction angle (32 degrees), along a length of about a third of the total length of the lined trench wall, was reached at a Y' of 0.016D (**Figure 7.17**). The condition of peak friction angle increased progressively along the lined trench wall with further lateral pipe displacement. At Y' of 0.05D, the full length of the lined trench wall reached the 32 degrees condition.

3. During lateral pipe displacement larger than 0.002D to 0.003D, the history of displacement (in a direction along the trench wall) for nodes along L1, L2 and L3 showed a constant rate of increase until the end of the numerical simulation. For lateral pipe displacement less than 0.002D to 0.003D, the rate of increase was close to zero (**Figure 7.18** through **Figure 7.20**).

4. By relating the frictional resistance at Y' between 0.002D to 0.003D (**Figure 7.16**) with the normalised lateral soil restraint, N_{qh}, (**Figure 7.18** through **Figure 7.20**) it can be observed that in order to mobilise the inner-outer geotextile interface frictional resistance (21 degrees) along the full

length of the trench wall, a N_{qh} between 3.3 to 4.1 was required. This condition represents the onset of Coulomb sliding or slip (FLAC 7.0's manual) for the outer geotextile with respect to the inner geotextile. This level of N_{qh} was found to be similar to that recorded during the experimental testing (**Figure 4.41** and **Table 4.4** in **Chapter 4**).

5. The displacement history graphs (**Figure 7.18** through **Figure 7.20**) show that after Y'=0.003D large relative displacement developed between the inner geotextile (fixed) and the outer geotextile. This indicates that the outer geotextile was sliding as the pipe moved laterally. The figures also show that the displacement of the soil backfill was slightly larger than the outer geotextile displacement. This suggests that, in addition to the outer geotextile slip, relative displacement or deformation between the outer geotextile and the soil also developed (the displacement levels were computed along the direction of the trench wall; therefore, they are relative shear displacement).

6. Similarly, the normalised lateral soil restraint, N_{qh}, required to mobilise the outer geotextile-sand interface frictional resistance (32 degrees) along the full length of the trench wall was about 6.3 and occurred at a Y' of 0.05D. This condition occurred with the beginning of a plateau (Region 2) in the N_{qh} versus normalised pipe displacement, Y', graph and represents the onset of Coulomb sliding for the soil backfill with respect to the outer geotextile. This level of N_{qh} was found to be similar to that recorded during the experimental testing (N_{qh}=6.4, **Figure 4.41** and **Table 4.3** in **Chapter 4**).

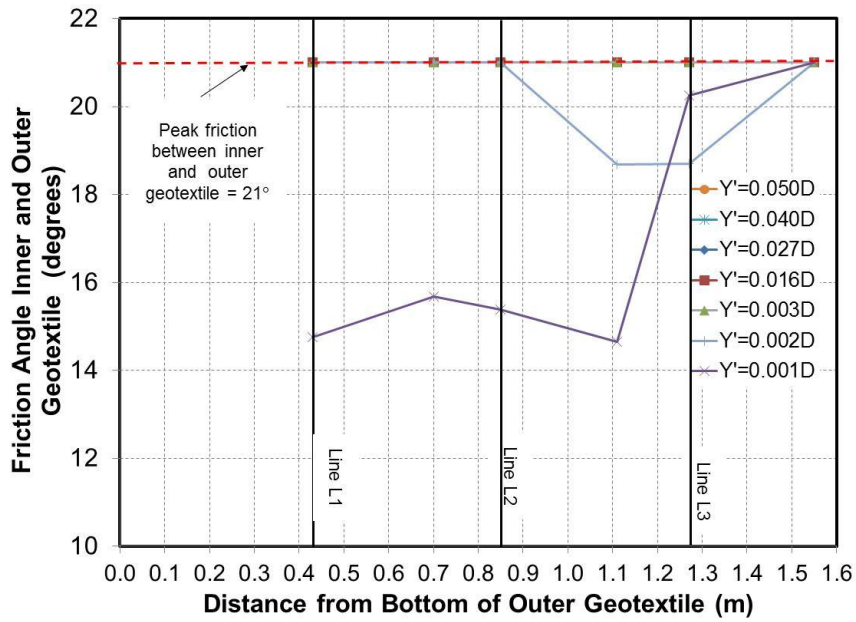

Figure 7.16: Mobilisation of inner-outer geotextile interface friction angle for Test 18-1.9-90H-HB-MS-GY-45-0.5D-2 using CYSOIL model.

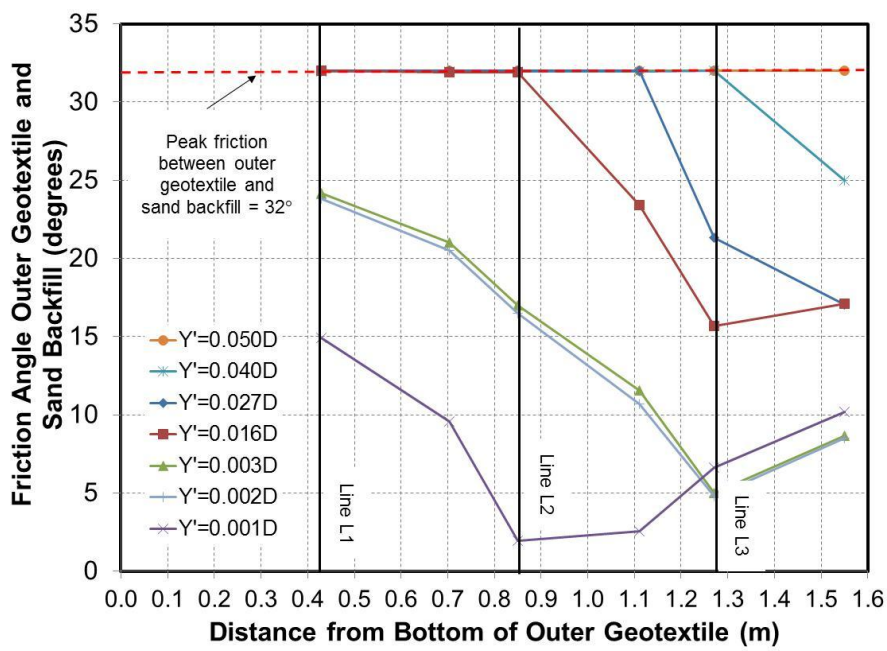

Figure 7.17: Mobilisation of outer geotextile-sand interface friction angle for Test 18-1.9-90H-HB-MS-GY-45-0.5D-2 using CYSOIL model.

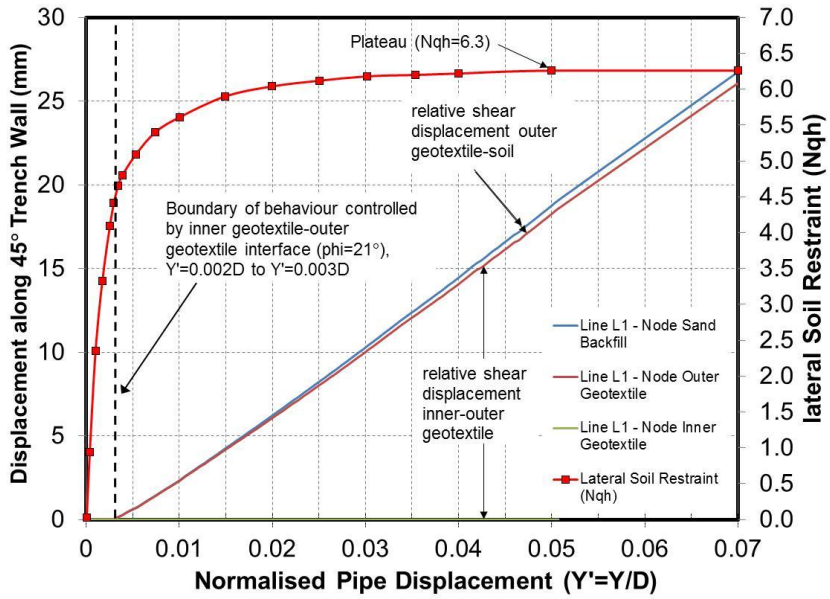

Figure 7.18: Evolution of inner geotextile, outer geotextile and sand backfill nodes along L1 for Test 18-1.9-90H-HB-MS-GY-45-0.5D-2.

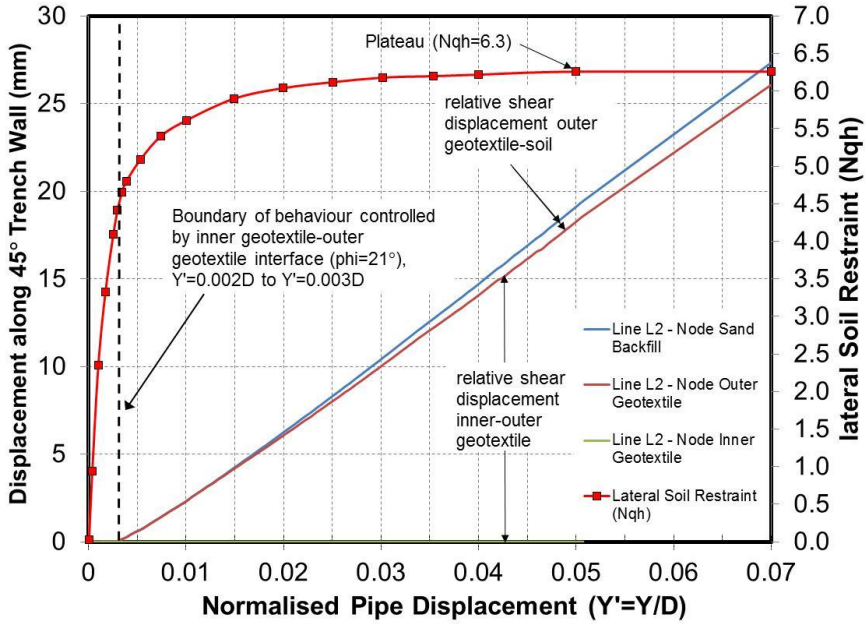

Figure 7.19: Evolution of inner geotextile, outer geotextile and sand backfill nodes along L2 for Test 18-1.9-90H-HB-MS-GY-45-0.5D-2.

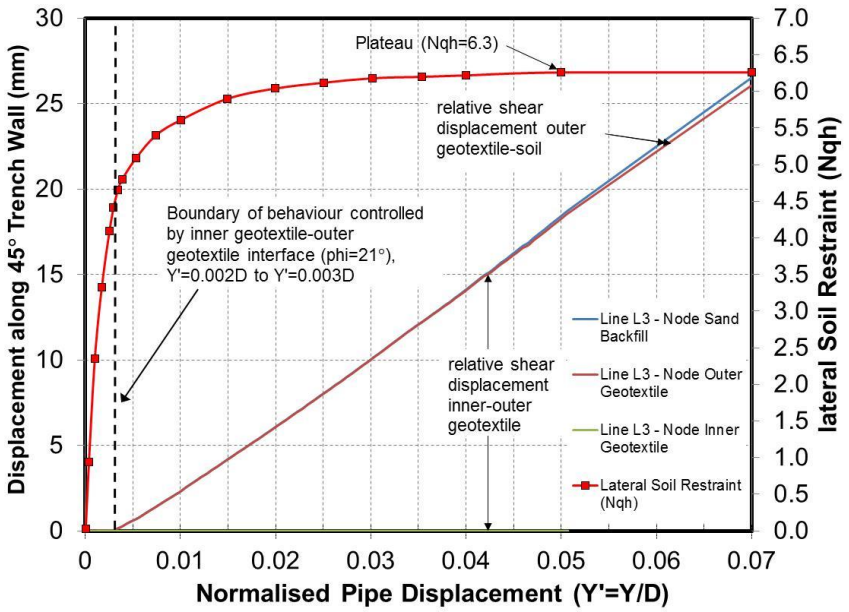

Figure 7.20: Evolution of inner geotextile, outer geotextile and sand backfill nodes along L3 for Test 18-1.9-90H-HB-MS-GY-45-0.5D-2.

The evolution of normal and shear forces along the trench wall interfaces as a function of normalised pipe displacement, Y', is shown in **Figure 7.21**. The figure shows that at Y', of 0.003D the shear force along the inner-outer geotextile interface started to deviate from the shear force along the outer geotextile-soil interface. This change appears to mark the boundary of a shift in shear resistance from that provided by the inner-outer geotextile interface to that provided by the outer geotextile-backfill soil interface.

The results from the numerical modeling suggest that the change in shear resistance progressively developed as the outer geotextile layer slid along the trench wall. The continuous sliding of the outer geotextile during lateral pipe displacement captured in the numerical simulation is in line with the results of Test 18-1.9-90H-HB-MS-GY-45-0.5D-2 presented in **Figure 4.29** and **Figure 4.41**.

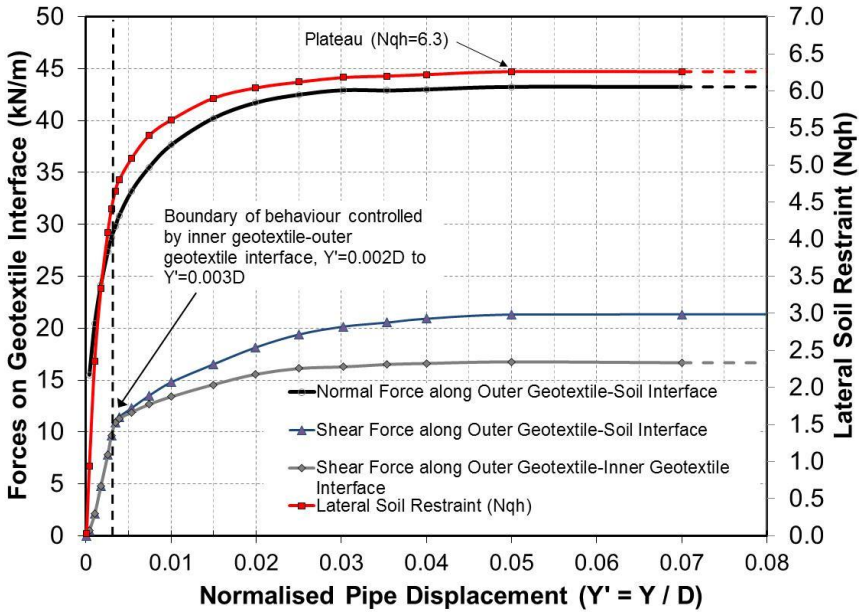

Figure 7.21: Normal and shear forces along the geotextile-geotextile and the soil-geotextile interfaces for Test 18-1.9-90H-HB-MS-GY-45-0.5D-2 using CYSOIL model.

The evolution of volume change behavior of Element A as a function of normalised pipe displacement, Y', is shown in **Figure 7.22**. As expected the volume change started at the beginning of lateral pipe displacement. The rate of volume change decreased with increasing levels of pipe displacement until it became zero at Y' of 0.05D (which coincide with the N_{qh} at the plateau or plastic region).

The observed volume change behavior evidenced that the role of soil deformability was active during the numerically simulated mobilisation of lateral soil restraint for a pipe specimen buried in a trench. The soil deformability was the reason not only for the mobilisation of the inner-outer geotextile resistance at Y' of 0.003D, but also was the reason for the mobilisation of the outer geotextile-soil interface resistance at Y' of 0.05D.

The role of soil deformability during normalised lateral pipe displacement, Y', larger than 0.3D or after the plateau has been reached (Region 3, hardening

region in the load-displacement relationships discussed in **Section 4.7**) was not evaluated in the current numerical simulation due to limitation of mesh geometry.

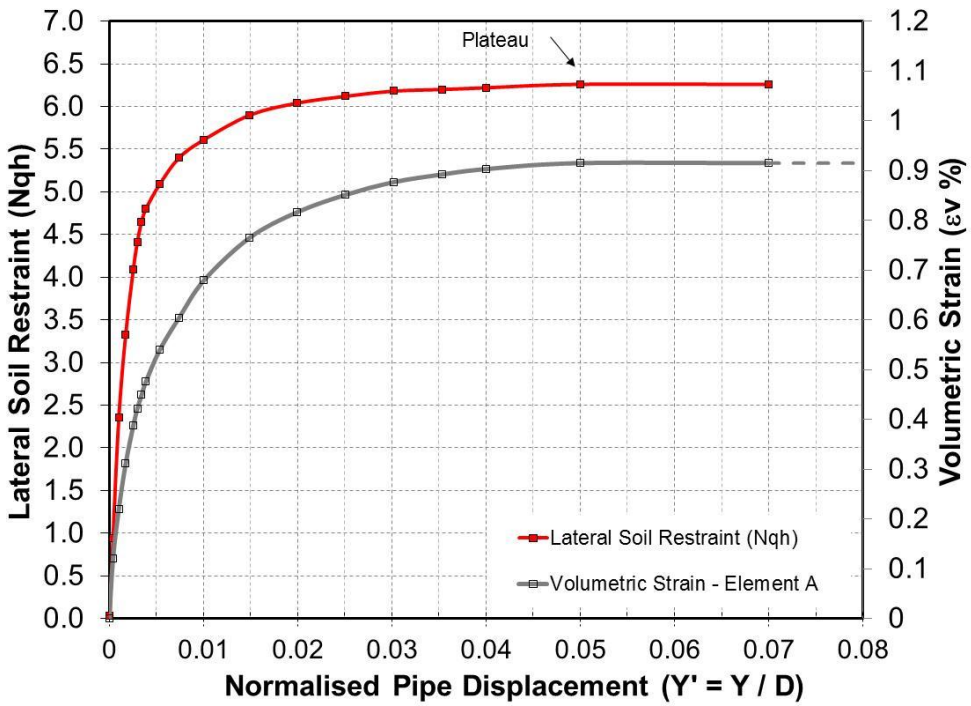

Figure 7.22: Volumetric strain – normalised pipe displacement relationship for Test 18-1.9-90H-HB-MS-GY-45-0.5D-2 using CYSOIL model.

The evolutions of mobilised friction predicted by the CYSOIL model at normalised pipe displacement of Y' of 0.001D and of 0.003D (Region 1, initial linear and transition region) and at Y' of 0.05D (Region 2, plastic region) for Test 1.9-90H-HB-MS-GY-45-0.5D-2 are shown in **Figure 7.23a**, **b** and **c**, respectively. In addition, the outer geotextile-soil interface slippage condition is observed only in **Figure 7.23.c**.

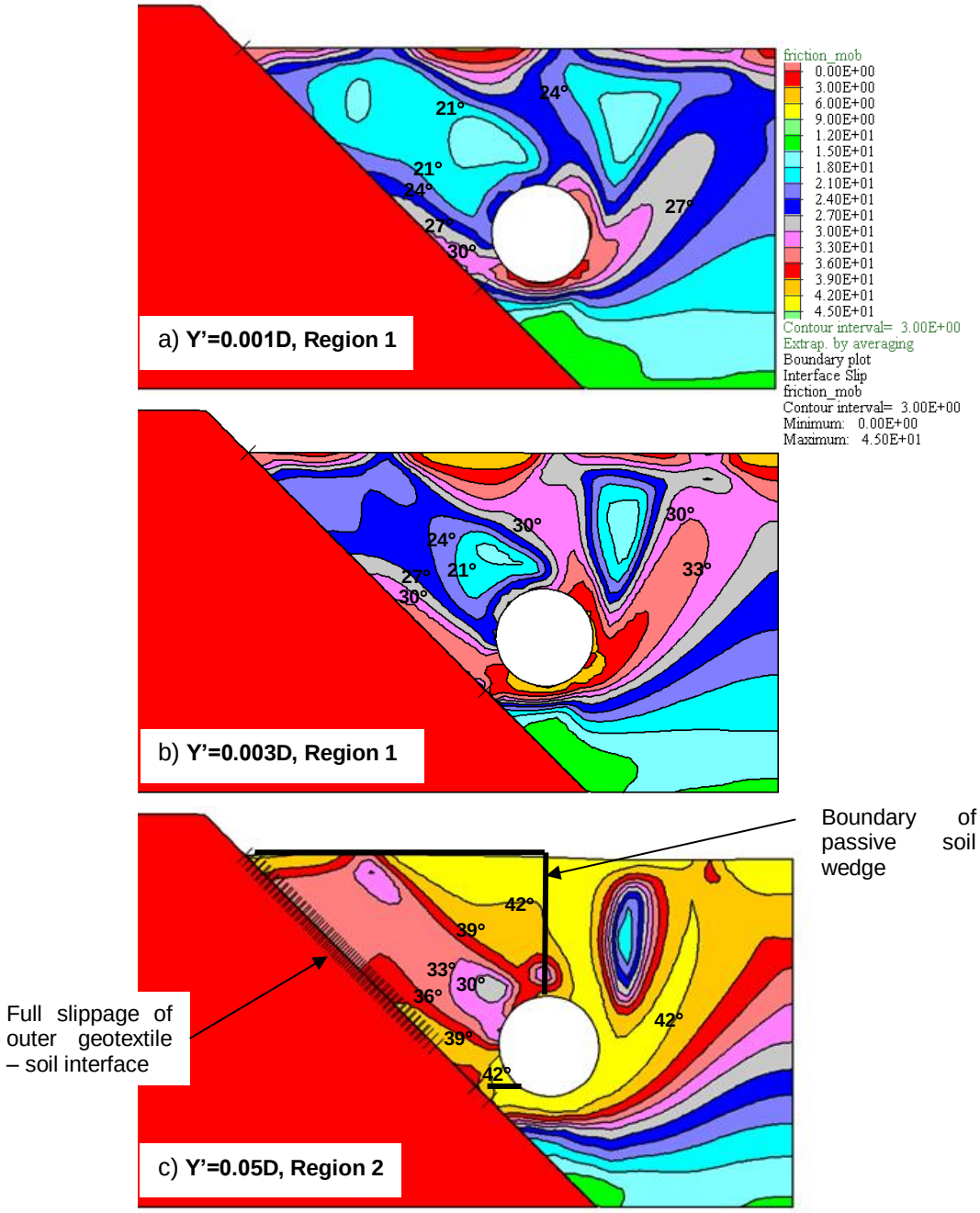

Figure 7.23: Spread of mobilised friction angle (ϕ_m) by CYSOIL model for Test 18-1.9-90H-HB-MS-GY-45-0.5D a) at Y'=0.001D; b) at Y'=0.003D; c) at Y' = 0.05D.

Furthermore, the distribution and magnitude of the mobilised friction angle were less than the peak friction, respectively, for the soil elements located inside the boundaries of the passive soil wedge depicted in **Figure 7.23.c** and discussed in **Section 4.7.3.1**. The fully mobilised peak friction angle was distributed along the boundary of this identified passive soil wedge located above and below the pipe. This is in agreement with the distributions of shear strains.

7.2.2.4 Results of Numerical Simulation on Road Mulch Backfill

Behaviour similar to the case with sand backfill was observed during the numerical simulation on road mulch backfill for Region 1 and Region 2. Therefore, only a comparison between the predicted and observed normalised lateral soil restraints, $N_{qh} = P / (\gamma \cdot D \cdot H \cdot L)$, versus normalised pipe displacement, Y' =Y/D, is presented in this part.

The results from the numerical simulations are shown in **Figure 7.24** for a NPS18 (457-mm diameter) pipe specimen buried in road mulch with H/D = 1.9 and with a trench wall-pipe distance (S) of 0.5D. The results from Tests 18-1.9-90H-RM-RM-GY-45-0.5D-1 and 18-1.9-90H-RM-RM-GY-45-0.5D-2, which correspond to trench wall lined with two geotextiles are also overlain in the same figure. A comparison for trench wall with a 35 degrees slope is shown in **Figure 7.25**.

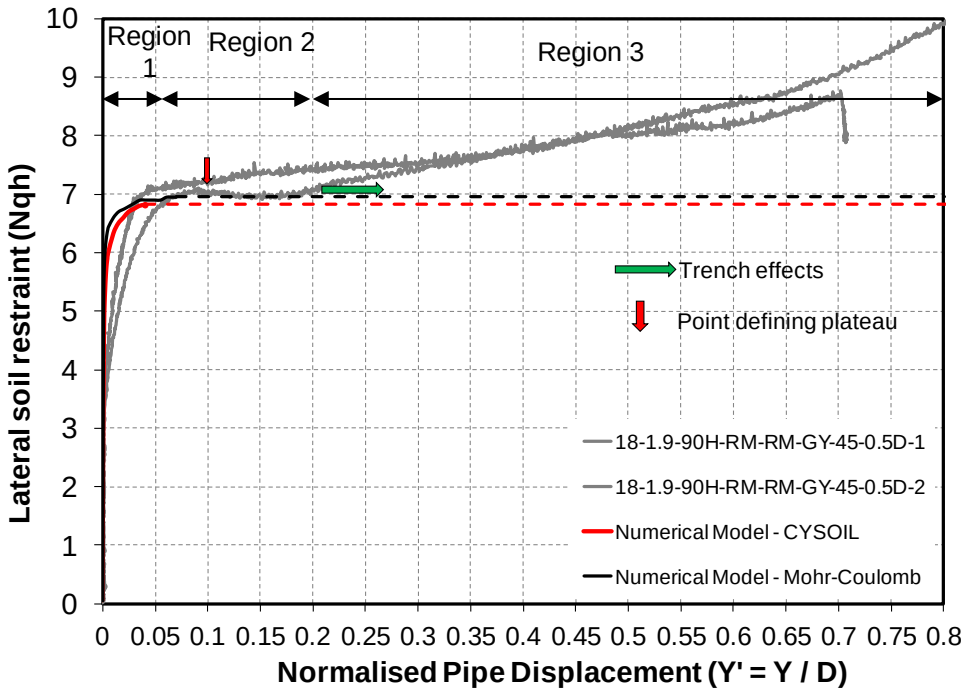

Figure 7.24: Simulation of Test 18-1.9-90H-RM-RM-GY-45-0.5D using bilinear Mohr-Coulomb and CYSOIL models.

Mohr-Coulomb and CYSOIL constitutive models were used to capture backfill soil behaviour during relative lateral ground displacement. The corresponding parameters are shown in **Table 7.1** and **Table 7.2**, respectively. As can be seen in **Figure 7.24** and **7.25**, the predicted responses are in satisfactory agreement with the measured lateral soil restraint-pipe displacement relationships up to Y' of 0.05D.

Similar to the case from Fraser River sand the elastic-plastic transition region predicted by both Mohr-Coulomb and CYSOIL models were stiffer than those observed from the full-scale tests. However, the constitutive models provided results that are consistent for the most part with the fundamental characteristic behaviour of this pipe specimen buried in road mulch. Soil behaviour at large normalised pipe displacements (Y' > 1D) and therefore the hardening region

of the lateral soil restraint-pipe displacement relationships could not be captured during the numerical simulation due to limitations of the mesh.

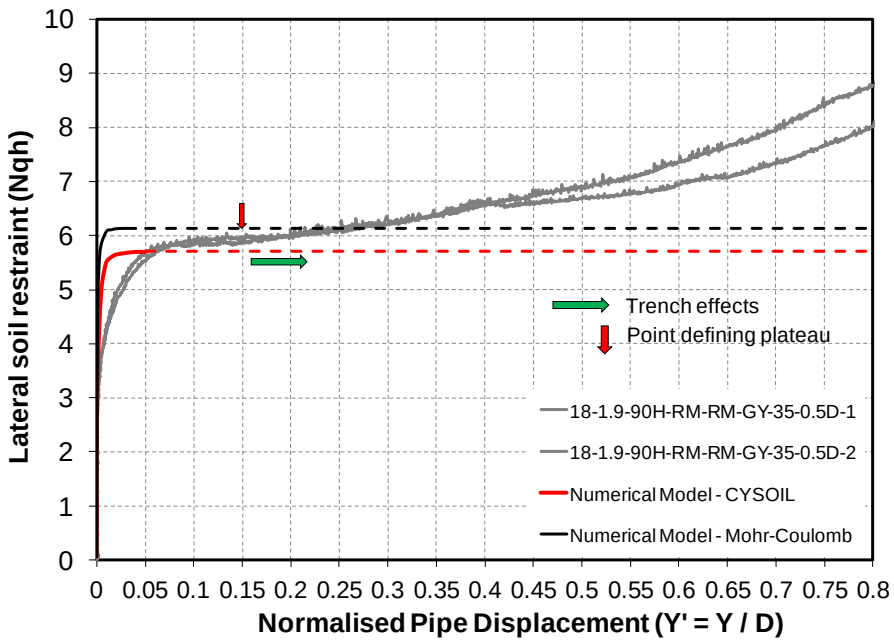

Figure 7.25: Simulation of Test 18-1.9-90H-RM-RM-GY-35-0.5D using bilinear Mohr-Coulomb and CYSOIL models.

7.2.2.5 Discussion on Interface Friction Angles for Geotextile-Lined Pipeline Trenches

Section 4.7.3 of **Chapter 4** has described that one common mitigation measure undertaken to reduce soil loads in situations of abrupt ground movement, such as those created by pipeline fault crossings, is the use of geosynthetic fabrics on sloped trench walls (PRCI 2004). This recommendation is based upon the condition that slippage in the form of contiguous soil blocks would be promoted due to the low frictional properties prevalent at the geosynthetic fabric interfaces.

However, the results of full-scale test, their data interpretation presented in **Section 4.7.3,** and the results of a simple mechanism based on limit

equilibrium are evidence that this condition does not occur during soil-pipeline breakout. In that section it was hypothesized that the observed additional horizontal soil resistance beyond what is necessary to induce slippage at the geotextile-geotextile interface may be due to deformation within the soil backfill. The results from the numerical simulation suggest that this may be the case as discussed in the next paragraphs.

Based on the results from the numerical modelling presented in **Figures 7.18** through **7.22,** the increase of N_{qh} occurred until the friction at the outer geotextile-soil interface was overcome (the plateau condition). This condition occurred even though the outer geotextile was sliding. The sliding of the geotextile was also observed during the full-scale tests.

Furthermore, the observed volume change behaviour during lateral pipe displacement (**Figure 7.22**) evidenced that the deformations internally occurring within the soil were very important for the mobilisation of lateral soil restraint. The deformations occurred only until the N_{qh} associated with the plateau was reached.

The impact of the deformations, internally occurring within the soil mass, on the N_{qh} value after the plateau condition was not evaluated in this numerical simulation. However, the observations from full-scale tests suggest that these deformations are the reason for the additional increase of N_{qh} value after the plateau condition or along the hardening region observed in the load vs. displacement curves (**Section 4.7**).

In addition, the degree of contribution of the backfill soil friction to the development of N_{qh} was evaluated based on the data presented in **Figure 7.26**. The friction angle along the trench wall interface for both inner-outer geotextile and outer geotextile-soil interfaces was kept constant with a value of 21°. No dilation angle was considered for the soil backfill. The curves from **Figure 7.26**, indicate that the level of maximum N_{qh} is not constant but rather

increases with the friction angle of the soil backfill. It is interesting to note that the N_{qh} corresponding to a soil backfill friction angle of 21° is very similar to the N_{qh} of 3.3 to 4.1 required to first displace the outer geotextile (**Figure 7.18** through **Figure 7.20**).

The above observations indicate that in order for the inner-outer geotextile interface friction angle to control the shear resistance along the trench wall, the soil backfill material has to be very loose and with a shear resistance similar to that one provided by the inner-outer geotextile interface. At the other end of the spectrum, the inner-outer geotextile interface friction angle would control the shear resistance if the soil backfill were rigid and therefore shear deformations occur only along the trench wall interface and not within the backfill soil.

The results of the numerical modeling showed that the N_{qh} at the plateau occurred when the maximum shear resistance of outer geotextile-soil interface was mobilised. However, other dissipation energy mechanisms were also occurring during the development of N_{qh}, which suggest a complex mechanism. Also the ongoing displacement of the outer geotextile also had an effect in the development of N_{qh} at the plateau. This effect can be observed in **Figure 7.14**.

By comparing the N_{qh} versus Y' from **Figure 7.14** from the experimental tests with one and two geotextiles it can be deduced that the use of two geotextiles (with the outer geotextile sliding) promotes a slightly less N_{qh} for the plateau (about 12% less) than the use of one geotextile. In addition, the use of two geotextiles promotes a larger plateau (it is present until Y' of about 0.3D). In contrast, the plateau is not well defined for the one geotextile case. This suggests a very complex mechanism for this soil-pipe system.

In view of the above, the simple limit equilibrium mechanism presented in **Section 4.7.3** only quantifies N_{qh} value for the plateau for the case of one

geotextile interface and therefore has limitations for the application of two geotextiles. It is recommended that, if possible, the N_{qh} value for the plateau be determined by doing numerical simulations.

However, regardless of the use of one geotextile, two geotextiles or no geotextile for lining the trench wall, a continuous increase in the levels of lateral soil restraint develops for pipelines buried in trenches with a trench wall-pipe distance of 0.5D. This increase can effectively be eliminated by simply placing the pipe at a distance larger than 1D and therefore promoting a failure through the soil. This recommendation was also presented in **Section 4.5.1**.

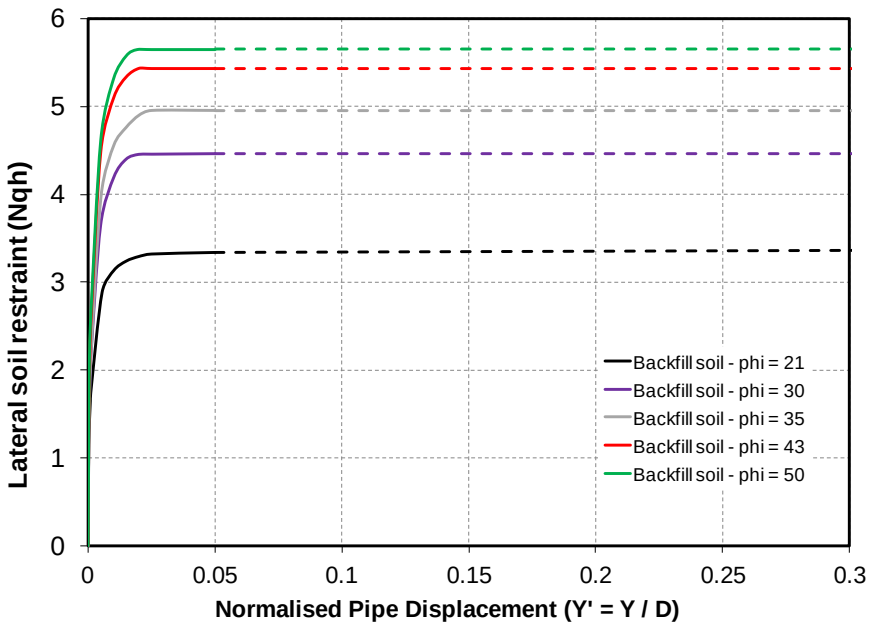

Figure 7.26: Mobilisation of N_{qh} for different soil backfill friction angles(ϕ'_p) – Friction angle along trench wall of 21° - Configuration for Test 18-1.9-90H-HB-MS-GY-45-0.5D using CYSOIL model.

7.3 Summary of the Chapter

Numerical simulations of the stages prior to ultimate failure and at collapse of a backfill soil mass that were observed and recorded during the full-scale soil restraint tests under lateral pipe displacement for plane cases (no trench) and for geotextile-lined trench cases have been presented and discussed in this chapter. The full-scale tests were numerically modelled according to the construction and specimen preparation sequence and conditions. The soil-pipe interaction problem was modelled assuming plane strain conditions. The Mohr-Coulomb model and a hyperbolic shear stress-strain relationship through the Cap-Yield (CYSOIL) model were selected as constitutive models for incorporating the soil backfill response in the numerical simulations. Material properties for the Fraser River sand were obtained directly from triaxial and direct shear tests carried out by Karimian (2006). Properties for the road mulch and crushed limestone backfills were obtained by calibrating the results from the model with those from full-scale testing. Outer geotextile-soil interface properties were obtained from direct shear tests results.

Results from the numerical analyses of the full-scale soil restraint tests under lateral pipe displacement for cases with no trench with different soil backfill materials were in good agreement with the patterns of behaviour observed during the stages prior to failure and at failure of the corresponding full-scale tests. Patterns of soil backfill deformation, maximum shear strain and displacement fields at failure condition from the numerical simulations were seen to be in fair agreement with the position of the log-spiral failure surface described in **Section 4.2.3** and observed from the full-scale tests.

The numerical models used for simulating the mobilisation of lateral soil restraint for cases of a pipe buried in a geotextile-lined trench with different backfill materials and with S=0.5D were shown capable of capturing the observed response of the physical models within a good range of accuracy until the plateau condition. Normalised lateral soil restraint values associated

with both the onset of outer geotextile movement and the plateau of the load-displacement relationships were correctly predicted by the numerical models.

Some of the key findings and observations from the numerical modeling of lateral soil restraint for a case of a pipe buried in a geotextile-lined trench with sand backfill and with S=0.5D are summarized below:

- The predicted displacement field by the CYSOIL model at different stages of pipe displacement was seen to be in fair agreement with the patterns of soil backfill deformation observed during the corresponding full-scale test.

- The evolution of normal and shear forces along the trench wall interfaces as a function of normalised pipe displacement, Y', showed that at Y', of 0.003D the shear force along the outer geotextile-soil interface started to deviate from the shear force along the inner-outer geotextile interface. This change marked the boundary of a shift in shear resistance from that provided by the inner-outer geotextile interface to that provided by the outer geotextile-backfill soil interface.

- The observed volume change behavior for soil Element A suggests that the role of soil deformability is active during the mobilisation of lateral soil restraint for pipelines buried in trench conditions. The soil deformability appears to be not only the reason for the mobilisation of the outer geotextile-soil interface resistance and the reaching of the plateau at small Y' (0.05D in numerical simulation, 0.1D to 0.2D in full-scale tests) but also for the increase on lateral soil restraint, N_{qh}, observed during the full-scale tests for Y' larger than 0.3D or after the plateau was reached.

- The numerical simulation showed that the soil deformations mobilised the outer geotextile-soil interface peak shear resistance. This peak shear resistance occurred when the lateral soil restraint reached the plateau of the load-displacement relationship. The outer geotextile was sliding during the development of N_{qh}. The plateau from the numerical simulation was similar to that observed during the full-scale tests of geotextile-lined pipeline trenches with trench wall-pipe distance (S) of 0.5D.

- In addition, the degree of contribution of the backfill soil to the development of lateral soil restraint was evaluated as a function of internal friction angle of the soil backfill for constant geotextile-geotextile interface friction angle. The results indicate that the level of N_{qh} at the plateau increased with the friction angle of the soil backfill. This behaviour corroborates the observations that deformations internally occurring within the soil provide an additional source of energy beyond what is necessary to induce slippage at the inner-outer geotextile interface during the development of lateral soil restraint due to relative lateral permanent fault displacement.

Chapter 8: Summary, Findings and Further Studies

Buried pipelines located in seismically active regions are potentially exposed to a variety of geotechnical earthquake hazards that primarily arise from different modes of ground displacement. Past experience suggests that the consequence of exposure to such hazards may include pipeline damage leading to unsafe conditions to the public and workers, loss of pressure integrity of pipeline contents, as well as impacts on the environment and economies.

For these reasons, proper identification of hazards and soil conditions, accurate estimation and characterisation of soil forces on buried pipelines, and development of mitigation measures to improve performance have become important considerations for reducing risk of damage to buried pipeline systems exposed to ground displacements. Along this line, the research work presented in this thesis focuses on characterizing levels of soil forces on shallow buried pipelines arising from different directions of ground displacements and on studying geotextile-based mitigation measures.

With this background, an existing full-scale testing chamber at the University of British Columbia was significantly modified to simulate the pipeline breakout from its soil embedment on one side of a strike-slip fault and on the footwall side of a reverse fault. This led to the characterisation of soil restraints in: (a) lateral; (b) horizontal oblique; and (c) vertical oblique directions. Furthermore, this work studied the influence of trench walls on the development of soil restraint on shallow buried pipelines and the effectiveness of reducing soil restraint using geotextiles.

This chapter is intended to summarize the findings and conclusions arising from this research work.

8.1 Testing Apparatus for Soil-Pipe Interaction

Although the mechanism and behaviour of lateral soil restraint on segments of pipelines buried in sand are fairly well understood, the behaviour of lateral soil restraint for granular materials other than sand has not been properly tested and verified due to the difficulty in conducting full-scale testing or in extrapolating to actual field conditions if the tests are conducted at a reduced scale. Likewise, soil restraint behaviour due to ground movement with direction different to pure lateral has not been fully studied or validated. Therefore, the first task of this dissertation was to design and build a full-scale testing chamber facility capable of applying different directions of displacement to pipe specimens and of providing continuous visual inspection during the tests. Towards this goal, details about the design and operation of the testing chamber, testing approach and instrumentation, properties of the materials used in the tests, and the type of tests conducted were described in **Chapter 3**, to establish the main aspects of the experimental work.

8.2 Lateral Soil Restraint on Buried Pipelines

Levels of lateral soil restraint on both NPS18 (457-mm diameter) and NPS16 (406-mm diameter) pipe specimens buried in dense moist sand, crushed sand and gravel mixture (road mulch) and crushed limestone backfills and in plain conditions (i.e. no trench) were presented in **Chapter 4**. Each pipe specimen was horizontally displaced to simulate the breakout of buried pipelines from their soil embedment on the fixed side of a strike-slip fault. Levels of lateral soil restraint on NPS18 pipe specimen buried in a trench excavated in dense granular “native” soil, backfilled with moist dense sand or road mulch were also presented. The effectiveness of a dual-layer geosynthetic fabric along a trench wall to provide a preferential failure surface was also investigated and discussed in this chapter.

The soil-pipe interaction behaviour under relative lateral ground displacement is a function of pipeline configuration (e.g. with trench or no trench), backfill soil properties and level of relative lateral ground displacement. This behaviour was described and presented in terms of three regions observed from the normalised soil restraint vs. pipe displacement results: initial linear and transition region (Region 1), plastic region (Region 2), and hardening region (Region 3).

The regions were presented to point out the different stages of lateral soil restraint mobilization during lateral permanent ground displacement and therefore apply the limit equilibrium approach only to Region 2 (plastic region). In this path, successful predictions of maximum lateral soil restraint on pipelines buried in granular geomaterials used in this study (sand, road mulch or crushed limestone) with no trench were obtained with the limit equilibrium approach proposed by O'Rourke et al. (2008). Likewise, the limit equilibrium approach predicted well values of lateral soil restraint for the plastic region for pipelines buried in geotextile-lined trenches.

The evaluation of the effectiveness of lining pipe trenches with geosynthetic fabrics as means to reduce lateral soil restraint on shallow buried pipelines yielded the following conclusions:

5. A sloped trench side-wall lined with two layers of geotextile fabric played a role in the variation of soil restraint with pipe displacement only when the pipe-trench wall distance is less than half a pipe diameter (0.5D). If the pipe was more than one diameter from the trench wall, the lateral soil restraint was simply controlled by the shear resistance of the backfill.

6. The test results indicated that the lateral soil restraint associated with the plastic region (Region 2) of the normalised lateral soil restraint vs. pipe displacement relationship for cases with a geotextile-lined trench

wall was not constant with lateral pipe displacement but rather it increased to values larger than those observed from cases with no trenches. This condition occurred regardless of geotextile sliding.

7. Patterns of soil deformability showed that the soil-pipe interaction for cases with geotextile-lined trench wall was associated with two distinct modes of instability of the backfill soil mass. One mode of instability was associated with the plastic region (Region 2) and showed that most of the appreciable shear deformation occurred along the edges of a passive wedge configuration, while the soil mass in front of the pipe and inside the wedge showed no significant shear deformation.

8. The second mode of instability of soil-pipe interaction for cases with geotextile-lined trench wall was associated with the hardening region (Region 3) of the normalised lateral soil restraint vs. pipe displacement relationship. In this mode the soil mass inside the soil wedge showed significant shear deformation. This mode of instability appears to represent a soil response governed by shearing through the backfill soil as the pipe moved upward and by shearing of a compressed soil mass due to the proximity of the pipe to the trench wall.

9. Based on the evaluation of test results, lining sloped pipeline trench walls with two layers of geotextile fabric as a means of reducing lateral soil restraint for pipeline crossing should be discouraged or its use limited to conditions governed by small relative soil-pipe displacements that may arise from thermal expansion, subsidence, or slope creep.

8.3 Combined Axial and Lateral Soil Restraints on Buried Pipelines

Current state of practice (ASCE 1984; PRCI 2004, 2009) for fault crossing design or similar geohazards assumes that soil restraints act independently (e.g., lateral and axial soil restraints react only to components of displacement

in the lateral and axial directions, respectively). In an effort to study this axial and lateral soil-pipe interaction coupling effects during relative oblique ground displacements, a series of full-scale horizontal oblique tests were conducted on several pipe specimens buried in moist sand. These were presented and described in **Chapter 5**.

The recorded horizontal oblique pipe displacement was resolved in components of axial and lateral pipe displacements with the aim of allowing direct comparison of the results from this work with those pipe displacements associated with purely axial and lateral maximum soil restraint values that exist in the literature. The results showed that the pipe displacements required to mobilise peak soil restraint in the axial direction and the lateral direction (perpendicular to the pipe axis) were in line with the pipe displacement ranges specified by PRCI (2004, 2009).

The analysis of the results showed the following:

7. The results from horizontal oblique tests showed a proportional decrease in lateral soil restraint as the oblique angles reduced from 90° (pure lateral) to 60°. Conversely, the axial soil restraint increased as the oblique angles changed from 90° to 60°.

8. Comparisons between the maximum horizontal oblique soil restraints from this testing program and the interaction envelops for oblique soil restraints proposed by Hsu et al. (2006), Phillips et al. (2004) and Daiyan et al. (2010, 2011) highlighted the importance of the pure axial soil restraint in the evaluation of the available oblique soil restraint envelops.

9. The current literature shows a large range for values of pure axial restraint soil. For example, Wijewickreme et al. (2009) values observed in pipes buried in dense soils were about 2 to 3 times higher than

those reported by Hsu et al. (2006), Dayian et al. (2010, 2011), and those calculated from the equation recommended by PRCI (2004).

10. A selection of the lower end of pure axial soil restraint values led to the coupled horizontal and axial soil restraint from the present work being much greater than that given by the relationship proposed by Hsu et al. (2006). Conversely, there would be a decrease in the difference in the data from the present work and the recommendations of Phillips et al. (2004) and Daiyan et al. (2010, 2011) if the lower end of pure axial soil restraint is used.

11. The horizontal oblique states measured from the present study were not sufficient to affirm or refute the recommended relationship of Hsu et al. (2006) or Daiyan et al. (2010, 2011). Therefore, this work provides limited clarification on whether or not soil restraints should be considered independent for fault crossing designs. The limited clarification was due to the difficulty in selecting an appropriate axial soil restraint value to anchor existing lateral-axial soil restraint interaction functions. No full-scale axial tests were conducted in this work.

8.4 Vertical Oblique Soil Restraint on Buried Pipelines

The design of pipelines for reverse/thrust fault crossings requires soil restraint properties to estimate pipeline segments performance. The results from a series of vertical oblique soil restraint tests were described and discussed in **Chapter 6**. Tests were carried out using a NPS16 (406-mm) diameter steel pipe buried in uniformly graded crushed limestone and in moist Fraser River sand with an H/D of 1.6. Uniform reverse/thrust angles of 35° and 45° degrees with respect to the horizontal were successfully simulated and achieved during the tests. A selected number of tests included a typical trench wall sloped at an angle of 45° degrees from the horizontal that was constructed inside the

soil testing chamber, and lined with geofabric in an effort to study the effectiveness of the geofabric to reduce vertical oblique soil restraints on buried pipes.

Currently, the design of pipeline segments crossing active reverse/trust fault environments are inferred on the basis of pure horizontal and vertical soil restraints; as such, the results from this work can provide valuable and improved understanding of shallow soil-pipe behaviour for assessing pipeline integrity for design conditions similar to those used in the tests. The following are some of the main findings yielded by this endeavour:

7. The vertical oblique soil restraint-displacement relationships indicated a generally continuous rise of soil restraint during the test reaching a peak value at relatively small pipe displacements (i.e., 0.1D to 0.18D). After the peak soil restraint was reached, a fairly constant-rate decrease in soil resistance with increasing pipe displacements was noted.

8. Soil restraints depend on the inclination of the pipe movement with respect to the soil mass. Peak soil restraint values diminished as the inclination of the angle of breakout of buried pipelines increased with respect to the horizontal. For example, the vertical oblique soil restraint derived from tests conducted with pipe displacement at a 35° angle from the horizontal was about 31% higher than that resulted from tests conducted where the pipe specimen was displaced at a 45° angle from the horizontal.

9. The results from vertical oblique soil restraint for trench walls lined with and without geotextile indicated that the peak vertical oblique soil restraints for the two configurations were similar. The maximum soil resistance was reduced only by about 12% due to geotextile lining of the trench indicating that the benefit derived from the introduction of a geosynthetic slip surface is minimal.

8.5 Numerical Simulation of Lateral Soil Restraint

The final goal of this dissertation was to virtually simulate the development of lateral soil restraint observed during the full-scale tests. The soil-pipe interaction problem was modelled by simulating the specimen preparation construction process and loading condition. A plane strain condition was used for the numerical modeling. Both, numerical simulation for conditions that include trench and no trench conditions were described and explained in **Chapter 7**.

Results from the numerical analyses for cases with trench and no trench with different soil backfill materials were in good agreement with the patterns of behaviour observed during the linear and transition stage (Region 1) and plastic stage (Region 2) of the corresponding normalised soil restraint versus pipe displacement relationship of the full-scale tests. Some of the key findings and observations from the numerical modeling for the case with trench conditions that provide additional evidence to the claim that geotextiles provide limited effectiveness as a mitigation option are summarized below:

- The evolution of normal and shear forces along the trench wall interfaces as a function of normalised pipe displacement, Y', showed that at Y', of 0.003D the shear force along the outer geotextile-soil interface started to increase above and to deviate from the shear force along the inner-outer geotextile interface. This change marked the boundary of a shift in shear resistance from that provided by the inner-outer geotextile interface to that provided by the outer geotextile-backfill soil interface.
- The results from the numerical modeling suggest that the change in shear resistance progressively developed as the outer geotextile layer slid along the trench wall. The continuous sliding of the outer geotextile

during lateral pipe displacement captured in the numerical simulation is in line with the results from full-scale tests.

- The numerical simulation showed that the soil deformations mobilised the outer geotextile-soil interface peak shear resistance. This peak shear resistance occurred when the lateral soil restraint reached the plateau of the load-displacement relationship. The plateau from the numerical simulation was similar to that observed during the full-scale tests of geotextile-lined pipeline trenches with trench wall-pipe distance (S) of 0.5D

- A comparison of the results of the experimental tests with one and two geotextiles showed that the use of two geotextiles (with the outer geotextile sliding) promoted a slightly less N_{qh} for the plateau (about 12% less) than the use of one geotextile. In addition, the use of two geotextiles promoted a larger plateau. In contrast, the plateau was not well defined for the one geotextile case. This suggests a very complex mechanism for this soil-pipe system.

- In view of the above, the proposed limit equilibrium mechanism presented in **Chapter 4** only quantifies N_{qh} value for the plateau for the case of one geotextile interface and therefore has limitations for the application of two geotextiles. It is recommended that, if required, the N_{qh} value for the plateau be determined by doing numerical simulations.

- However, regardless of the use of one geotextile, two geotextiles or no geotextile for lining the trench wall, a continuous increase in the levels of lateral soil restraint (above the plateau level, hardening region) develops for pipelines buried in trenches with a trench wall-pipe distance of 0.5D. This increase can effectively be eliminated by simply

placing the pipe at a distance larger than 1D and therefore promoting a failure through the soil.

8.6 Further Studies

The research undertaken herein has revealed additional work that can be undertaken to shed light in some of the shortcomings identified during this work:

To improve understanding on whether or not lateral and axial soil restraints react only to components of displacement in the lateral and axial directions, respectively, there needs to be some resolution to the question of what purely axial soil restraint should be used in plotting the axial-lateral soil restraint interaction curves for the full-scale tests conducted in this program.

One suggested alternative to answer this question is to conduct some tests at horizontal oblique angles ranging from 75° to 30° in loose sand (density of about 14 kN/m^3). The objective of using a lower sand density is to provide data for a soil material with a much lower value of peak axial soil load compared to dense sand.

Other alternative is to investigate further the discrepancies found for the peak values of axial soil restraint for dense sand conditions. Furthermore, some tests are recommended for a pipe located at an oblique angle of 45° and subjected to at least 300 mm of horizontal displacement to provide confirmation of the 45° tests performed in this study.

To develop a vertical-horizontal interaction relationship for the design of pipelines crossing thrust faults, it is recommended to carried out some full-scale tests at dip angles different than the ones used in this research. These additional tests can easily be performed in the fully redesigned soil-pipe interaction testing chamber. The effect of burial depth on the levels of vertical oblique soil restraint can be also evaluated.

Full-scale tests of pipe specimens buried in trench lined with one geotextile and different trench wall inclinations could shed light into the validation of the use of this friction angle to predict N_{qh} values.

References

Abdoun T. H., Ha, D., O'Rourke M., Symans M.D., O'Rourke T.,D., Palmer M.C., Stewart H. (2009) Factors influencing the behavior of buried pipelines subjected to earthquake faulting, *Soil Dynamics and Earthquake Engineering*, Volume 29, Issue 3, Pages 415-427.

Ahmadnia, A. A. (2012) Response of underground power transmission cables subjected to earthquake induced permanent ground deformations, Ph.D. Thesis, Department of Civil Engineering, University of British Columbia.

American Lifeline Alliance (2001) Guidelines for the design of buried steel pipe, <http://www.americanlifelinesalliance.org/pdf/Update061305.pdf>.

American Society of Civil Engineering (ASCE) (1984) Guidelines for the seismic design of oil and gas pipeline systems, Committee on Gas and Liquid Fuel Lifelines, ASCE, New York.

Anderson, C., Wijewickreme, D., Ventura, C., and Mitchell, A. (2004) Full-scale laboratory testing of soil-pipe interaction in branched polyethylene pipelines, *Experimental Techniques*, 29(2), 33-37.

Anubhav, P.K., Basudhar (2010) Modeling of soil–woven geotextile interface behavior from direct shear test results, *Geotextiles and Geomembranes* 28:4, 403-408.

Audibert, J. M. E., and Nyman, K. J. (1977) Soil restraint against horizontal motion of pipes, *Journal of the Geotechnical Engineering Division*, ASCE, 103 (GT10), 1119-1142.

Beaty, M. H. and Byrne, P. M. (1998) An Effective Stress Model for Predicting Liquefaction Behavior of Sand, *In Proc. Specialty Conf. Geotechnical*

Earthquake Engg. and Soil Dynamics, Seatle, ASCE GSP No. 75, Edited by Dakouluas, M. and Holtz, R.D., V. 1, pp. 766-777.

Bolt, B. A (2003) Earthquakes (5th edition) W. H. Freeman, New York.

Bolton, M. D. (1986) The strength and dilatancy of sands, *Geotechnique*, 36(1), 65-78.

Byrne, P. M., Cheung, H. and Yan, L. (1987) Soil Parameters for Deformation Analysis of Sand Masses, *Canadian Geotechnical Journal*, V. 24, (3), pp. 3 66-376.

Byrne, P. M., S. S. Park and M. Beaty (2003) Seismic Liquefaction, Proceedings of the 3rd International FLAC Symposium, Sudbury, Ontario, Canada, October 2003, pp. 321-331. R. Brummer et al.,eds. Lisse: A. A. Balkema.

Calvetti, F., Prisco, C., and Nova, R. (2004) Experimental and numerical analysis of soil-pipe interaction, *Journal of Geotechnical and Geoenvironmental Engineering*, ASCE, 130(2), 1292-1299.

C-CORE (2003) Extended model of pipe soil interaction, PRCI Report, Catalogue R-02-044-113.

C-CORE (2008) Pipeline Integrity for Ground Movement Hazards, final report prepared for United States Department of Transportation, C-CORE Report R-07-082-459.

Cluff L.S., Slemmons, D.B., and Waggoner (1970) Active Fault Zone Hazards and Related Problems of Sitting Works of Man, *Proceedings, Fourth International Symposium on Earthquake Engineering*, Vol. I. Roorkee, U.P., India, pp. 401-410.

Daiyan, N., Kenny, S., Phillips, R., and Popescu, R. (2010) Numerical investigation of oblique pipeline/soil interaction in sand, *Proceedings of the 8th International Pipeline Conference*, American Society of Mechanical Engineers.

Daiyan, N., Kenny, S., Phillips, R., and Popescu, R. (2011) Investigating pipeline-soil interaction under axial-lateral relative movements in sand, *Canadian Geotechnical Journal*, 48:1683-1695.

Danish Hydraulic Institute (DHI) and Ramboll and Hannemann (1985), Danish Submarine Guidelines, Danish Energy Agency.

Das B. M. (1985) Resistance of shallow inclined anchors in clay, *Proceedings, Uplift Behavior of Anchor Foundations in Soil*, ASCE, pp. 86-101

Das, B. M., Seeley, G. R. (1975) Load displacement relationship for vertical anchor plates, *Journal of Geotechnical Engineering Division*, 101(GT7), 711-715.

Desai, C. S., and Christian, JT. (1977) Numerical Methods in Geomechanics, New York: McGraw-Hill.

Duncan J. M., Byrne, P. M., Wong. K. S. and Marbry, P. (1980) Strength, Stress-Strain and Bulk Modulus Parameters for Finite Elements Analysis of Stresses and Movements in Soil Masses, Report No. UCB/GT/80-01, Un., Cal., Berkeley.

Foray, P., Balachowski L., and Colliat, J. L. (1998) Bearing capacity of model piles driven into dense overconsolidated sand, *Canadian Geotechnical Journal*, 35(2), pp 374-385.

Guo, P. J. (2005) Numerical modeling of pipe-soil interaction under oblique loading, *Journal of Geotechnical and Geoenvironmental Engineering*, 131(2), 260-268.

Guo, P. J., and Stolle, D. F. E. (2005) Lateral pipe-soil interaction in sand with reference to scale effect, J*ournal of Geotechnical and Geoenvironmental Engineering*, 131(3), 338-349.

Ha, D., O'Rourke, T., Symans, M., O'Rourke, M., Palmer, T., Stewart, M.H., (2008) Centrifuge Modeling of Earthquake Effects on Buried High-Density Polyethylene (HDPE) Pipelines Crossing Fault Zones, J*. Geotechnical and Geoenvironmental Engineering,* 134(10), 1501–1515.

Hansen, B.J. (1961) The ultimate resistance of rigid piles against transversal forces, Bulletin 12, Danish Geotechnical Institute, Copenhagen, Denmark.

Hardin, B., and Drenvich, V. P. (1972) Shear Modulus and Damping in Soils: Design Equations and Curves, *Soil Mechanics and Foundation Engineering,* ASCE Division, V. 98(SM7), pp. 667-692.

Hill R., (1950) The mathematical theory of plasticity, Clarendon Press. Oxford, England.

Hsu, T. W. (1994) Rate effect on lateral soil restraint of pipeline, *Soils and Foundations*, 33(4), 159-169.

Hsu, T. W., Chen, Y. J., and Hung, W. C. (1996) Soil resistant to oblique movement of buried pipes in dense sand, *Journal of Transportation Engineering*, 132(2), 175-181.

Hsu, T. W., Chen, Y. J., and Wy, C. Y. (2001) Soil resistant to oblique movement of buried pipes in dense sand, *Journal of Transportation Engineering*, 127(1), 82-87.

Hsu, T.-W. (1996) Soil restraint against oblique motion of pipelines in sand *Canadian Geotechnical Journal*, 33, 180–188.

Hsu, T-W, Chen, Y-J, and Hung, W-C, (2006) Soil Restraint to Oblique Movement of Buried Pipes in Dense Sand, *Journal of Transportation Engineering, American Society of Civil Engineers*, Vol. 132, No. 2.

Itasca, (2012) Fast Lagrangian Analysis of Continua (FLAC), Version 7, User's Guide, Itasca Consulting Group, Inc., Minneapolis, Minnesota.

Jardine, R. J., and Overy, R. F. (1996) Axial capacity of offshore piles driven in dense sand, *Proceedings, Offshore International Conference*, Houston, Texas, USA., 161-180.

Jung K. J., O'Rourke T., Olson N. (2012) Uplift Soil-Pipe Interaction in Granular Soil, *Canadian Geotechnical Journal*. doi:10.1139/cgj-2012-0357

Karimian H. (2006) Response of Buried Steel Pipelines subjected to Longitudinal and Transverse Ground Movement, Ph.D. Thesis, Deparment of Civil Engineering, University of British Columbia.

Karimian H., Wijewickreme D., Honneger D. (2006) Full scale laboratory testing to assess methods for reduction of soil loads on buried pipes subject to transverse ground movement, *Proceedings of 6th International Pipeline Conference*, Calgary, Canada.

Kennedy R.P., Chow A.,W., Williamson R., A. (1977) Fault movement effects on buried oil pipeline *Transportation Engineering Journal, ASCE*, 617-633.

Kennedy, R. P., Darrow, A. C., Short, S. A. (1979) Seismic design of oil pipeline systems, *Journal of the Technical Councils of ASCE*, 105(TC1), 119-133.

Konder, R. L., and Zelaski, J. S. (1963) A Hyperbolic Stress-Strain Formulation for Sands, *In Proc., Second Pan-American Conference, Soil Mechanics and Foundation Engineering*, V. 1, pp. 289- 324.

Konuk, I., Fredj, A., Yu, S. (2005) 3-Dimensional bifurcations of pipe-in-pipe structures, *Proceedings, 24th International Conference on Offshore Mechanics and Arctic Engineering*, 3, 747-753.

Kraft, L. M. (1990) Computing axial pipe capacity in sands for offshore conditions, *Geotechnique*, 9, 61-92.

Lee, K. L. (1970) Comparison of plane strain and triaxial tests on sand, *Journal of the Soil Mechanics and Foundation Division*, ASCE, Vol. 96, No. SM3, 901-921.

Lee, K.M., Manjunath V.R. (2000) Soil–geotextile interface friction by direct shear tests, *Canadian Geotechnical Journal*, 37: 238–252.

Lehane, B. and Cosgrove, H. (2000) Applying Triaxial Compression Stiffness Data to Settlement Prediction of Shallow Foundations, *Geotechnical Engineering Journal*, V. 142, Oct. 2000, pp. 191- 200.

Lehane, B. M., Jardine, R. J., Bond, A. J., and Frank, R. (1993) Mechanisms of shaft friction in sand from instrumented pile tests, *Journal of Geotechnical Engineering*, 119(1), 19-35.

Martin, C.M., Houlsby, G. T. (2001) Combined loading of spudcan foundations on clay: Numerical modeling, *Geotechnique*, 51(8), 687-699.

Matsuoka, H. and Nakai, T. (1977) Stress-Strain Relationship of Soil based on S.M.P, *In Proc., Constitutive Equations of Soils, Ninth Conference, Soil Mechanics and Foundation Engineering*, Tokyo, pp. 153-162.

Mayne, P. (2007) Cone Penetration Testing: A Synthesis of Highway Practice, NCHRP Synthesis 368, Transportation Research Board, National Cooperative Highway Research Program, 118p.

McAllister, E. W. (2001) Pipeline rules of Thumb handbook, Gulf Professional Publishing, 648 p.

Meyerhof G. (1973) Uplift resistance of inclined anchors and piles, *Proceeding of the 8th International Conference on Soil Mechanics and Foundation Engineering*, Moscow, Vol. 2, 167-172.

Monroy M., Wijewickreme D., Honegger D., (2012) Effectiveness of Geotextile-Lined Pipeline Trenches Subjected To Relative Lateral Seismic Fault Ground Displacements, *Proceedings 15th World Conference on Earthquake Engineering*, 2534, Lisbon, Portugal.

Newmark, M., Hall, W. J. (1975) Pipeline design to resist large fault displacement, *U.S. National Conference on Earthquake Engineering*, Ann Arbor, MI, Paper UILU-ENG-75-2011, 416-425.

Nova Gas Transmission (1995) Frictionless pipe wrap test results-ASC pipe/soil interaction test centre, Technical Report, July 18 1995, Nova Gas Transmission Ltd., Calgary, AB, Canada.

Nyman K.J. (1982) Soil response against the horizontal-vertical motion of pipes, Preprint 82-534, presented at ASCE National Convention, New Orleans.

O'Rourke et al. (2008), O' Rourke, T.D., (1988) Critical aspects of soil-pipeline interaction for large ground deformation, *Proceedings of the First Japan-U.S. Workshop on Liquefaction, Large Ground Deformation and their Effects in Lifeline Facilities*, Tokio, Japan, pp. 118-126.

O'Rourke T.D., Jezerski J. M., Olson N. A., Bonneau A.L., Palmer M.C., Stewart H.E., O'Rourke M. J. (2008) Geotechnics of pipeline system response to earthquakes, *Proceedings of the Geotechnical Earthquake Engineering and Soil Dynamics* IV. GSP(181).

O'Rourke T.D. (1998) An Overview of Geotechnical and Lifeline Earthquake Engineering, *Geotechnical Special Publication* No. 75, ASCE, Pakoulis P, Yegian M, Holtz D, eds, Reston, VA, 1392–1426.

O'Rourke, T. D. & Bonneau, A. (2007) Lifeline performance under extreme loading during earthquakes, *In Earthquake Geotechnical Engineering,* (ed. K. D. Pitilakis), pp. 407–432.

O'Rourke, T. D. (1988) Critical aspects of soil-pipeline interaction for large ground deformation, *Proceedings, 1st Japan-US Workshop on Liquefaction, Large Ground Deformation and Their Effects on Lifelines, Association for Development of Earthquake Prediction*, Japan, 118-126.

O'Rourke, T.D., Grigoriu, M.D., Khater, M.M. (1985) A state of the art review: seismic response of buried pipelines, *Decade of Progress in Pressure Vessel Technology*,(Sundararajan C,Editor) ASME.

O'Rourke, M.J., Liu, X., (1999) Response of buried pipelines subjected to earthquake Effects, Monograph Series, MCEER.

Ovesen N. K. (1964) Anchor slabs, calculation method and model tests, Bulletin 16, Danish Geotechnical Institute, Copenhagen.

Palmer, M.C., O'Rourke, T.D., Stewart, H.E., O'Rourke, M.J. and Symans, M. (2006) Large displacement soil-structure interaction test facility for lifelines, *Proc. 8th US National Conference on Earthquake Engineering*, San Francisco, CA.

Parkin, A., and Lunne, T. (1982) Boundary effects in the laboratory calibration of a cone penetrometer in sand, *Proc. 2nd European Symposium on Penetration Testing*, Amsterdam, Vol. 2, 761-768.

Parkin, A., Holden, J., Aamot, K., Last, N., and Lunne, T. (1980) Laboratory investigations of CPTs in sand, NGI Report S2108-9.

Paulin, M. J., Phillips, R., Clark, J. I., Hurley, S., Trigg, A. (1997) Establishment of a full-scale pipeline/soil interaction test facility and results from lateral and axial investigations in sand *Proceedings, 16th International Conference of Offshore Mechanics and Arctic Engineering*, Vol. 5, Pipeline Technology, 139-146.

Paulin, M.J., Phillips, R., and Boivin, R. (1996) An experimental investigation into lateral pipeline interaction, *International Conference on Offshore Mechanics &Arctic Engineering*, Florence, June 1996, vol. V, pp 313-323.

Paulin, M.J., Phillips, R., Clark, J.I., Trigg, A., and Konuk, I. (1998) A full-scale investigation into pipeline/soil interaction, *Proceedings, International Pipeline Conference*, Calgary, AB, ASME, 779-788.

Phillips, R., Nobahar, A., and Zhou, J. (2004) Combined axial and lateral pipe-soil interaction relationships, *Proceedings, International Pipeline Conference, Calgary*, AB, Canada.

Phillips, R., Nobahar, A., and Zhou, J. (2004) Trench effects on pipe-soil interaction, *Proceedings, International Pipeline Conference*, Calgary, AB, Canada.

Pipeline Research Council International, Inc. (PRCI), (2004) Guidelines for the Seismic Design and Assessment of Natural Gas and Liquid Hydrocarbon Pipelines, Catalogue No. L51927. Editors: Honegger, D. G., and Nyman D. J.

Pipeline Research Council International, Inc. (PRCI), (2009) Guidelines for Natural Gas and Liquid Hydrocarbon Pipelines in Areas Prone to Landslide and Subsidence Hazards, report prepared by C-CORE, D.G. Honegger Consulting, and SSD, Inc., Catalog No. L52292.

Popescu, R., Phillips, R., Konuk, I., and Deacu D. (1999) Numerical and physical modelling of pipe-soil interaction, *Proceedings, 52nd Canadian Geotechnical Conference*, Regina, SK, pp. 437-444.

Puebla, H., (1999) A constitutive model for sand and the analysis of the Canlex embankments, Ph.D. Thesis, Department of Civil Engineering, University of British Columbia.

Randolph, M. F., Dolwin, J., and Beck, R. (1994) Design of driven piles in sand, *Geotechnique*, 44(3), 427-448.

Rowe, P. W. (1962) The Stress-Dilatancy Relation for Static Equilibrium of an Assembly of Particles in Contact, Proc. Roy. Soc. A., 269, 500-527.

Rowe, R. K., and Davis, E.H. (1982) The behaviour of anchor plates in sand, *Geotechnique*, 32(1), 25-41.

Seed H. B., and Idriss, I. M. (1970) Soil Muduli and Damping Factors for Dynamic Response Analyses Report No. EERC 70-10, Earthquake Engineering Research Center, Berkeley.

Seed, H. B., Wong, R. T., Idriss, I. M., Tokimatsu, K. (1986) Moduli and Damping Factors for Dynamic Analyses of Cohesionless Soils, *Journal of Geotechnical Eng.*, *ASCE* V. 112(GT11), pp. 1016-1032.

Sivathayalan, S. (2000) Fabric, initial state and stress path effects on liquefaction susceptibility of sand, Ph.D Thesis, Department of Civil Engineering, University of British Columbia.

Talesnick, M., Horany, H., Dancygier, A., and Karinski, Y. (2008) Measuring Soil Pressure on a Buried Model Structure for the Validation of Quantitative Frameworks, Journal of Geotechnical and Geoenvironmental Eng., 134(6), pp. 855–865.

Tatsuoka, F. and S. Shibuya, (1992) Deformation Characteristics of Soils and Rocks from Field and Laboratory Tests, *Report of the Institute of Industrial Science*, University of Tokyo, Japan, Vol. 37, No. 1, 1992, 136 p.

Taylor, C.L., Cluff, L.S., (1977) Fault displacement and ground deformation associated with surface faulting, *Proceedings, Technical Council on Lifeline Earthquake Engineering,* ASCE. pp 338-353.

Terzaghi K. (1943) Theoretical soil mechanics, John Wiley and Sons, Inc., New York, NY: 510 p.

Trautmann C.H., and O'Rourke, T.D. (1983) Behaviour of pipe in dry sand under lateral and uplift loading, *Geotechnical Engineering Report*, 83-7, Cornell University, Ithaca, N.Y.

Trautmann, C.H., and O'Rourke, T.D. (1985) Lateral force displacement response of buried pipe, *Journal of Geotechnical Engineering*, ASCE, 111(9), 1077-1092.

Turner, J. E. (2004) Lateral force displacement behaviour of pipes in partially saturated sand, M.A.Sc. Thesis, Cornell University, Ithaca, N.Y.

Uthayakumar, M. (1996) Liquefaction of sands under multiaxial loading, Ph.D Thesis, Department of Civil Engineering, University of British Columbia.

Vanden Berghe, J-F., Cathie, D., Ballard, J-C. (2005) Pipeline uplift mechanisms using finite element analysis, *International Conference on Soil Mechanics and Foundation Engineering*, Osaka, Japan.

Weerasekara L., (2011) Pipe-soil interaction aspects in buried extensible pipes, Ph.D. Thesis, Department of Civil Engineering, University of British Columbia.

Weerasekara L., Wijewickreme D., (2008) Mobilization of soil loads on buried, polyethylene natural gas pipeline subject to relative axial displacement, *Canadian Geotechnical Journal*, 45, 9, 1237-1249.

Wijewickreme, D., Karimian, H., and Honegger, D., (2009) Response of Buried Steel Pipelines Subject to Relative Axial Soil Movement, *Canadian Geotechnical Journal*, Vol. 46, No. 7: 735-752.

Wook C., Tarek H. A., O'Rourke, M., Ha., D. (2007) Remediation for buried pipeline systems under permanent ground deformation *Soil Dynamics and Earthquake Engineering*, Volume 27, Issue 12, Pages 1043-1055.

Xie, X., Symans, M.D., O'Rourke, M.J., Abdoun T., O'Rourke, T.D., Palmer, M.C., Stewart H.E. (2012) Numerical modeling of buried HDPE pipelines subjected to strike-slip faulting, *Journal of Earthquake Engineering*, 15:1273–1296, 2011.

Yimsiri, S., Soga, K., Yoshizaki, K., Dasari, G.R., and O'Rourke, T.D. (2004) Lateral and upward soil-pipeline interactions in sand for deep embedment conditions, *Journal of Geotechnical and Geoenvironmental Engineering*, ASCE, vol. 130, no. 8.

APPENDICES

APPENDIX A: DIRECT SHEAR TEST RESULTS ON BACKFILL MATERIALS

Bottom of Shear Box Top of Shear Box

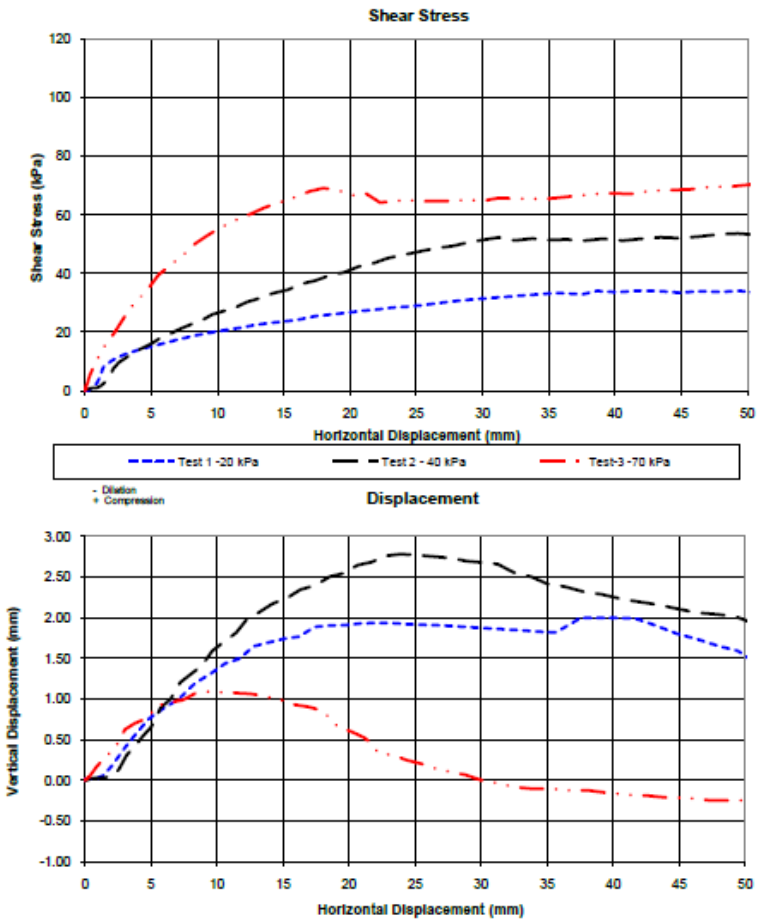

Figure A-1: Shear stress versus horizontal displacement – road mulch density=1,800 kg/m^3

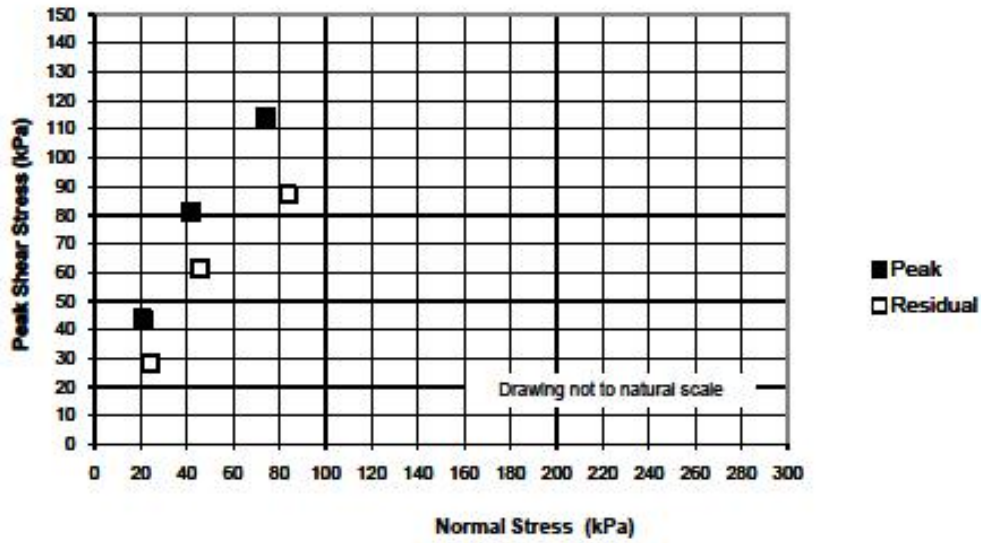

Bottom of Shear Box

Top of Shear Box

Figure A-2: Peak shear stress vs normal stress– crushed limestone - density=1,700 kg/m^3

APPENDIX B: DIRECT SHEAR TEST RESULTS ON BACKFILL-GEOTEXTILE INTERFACE

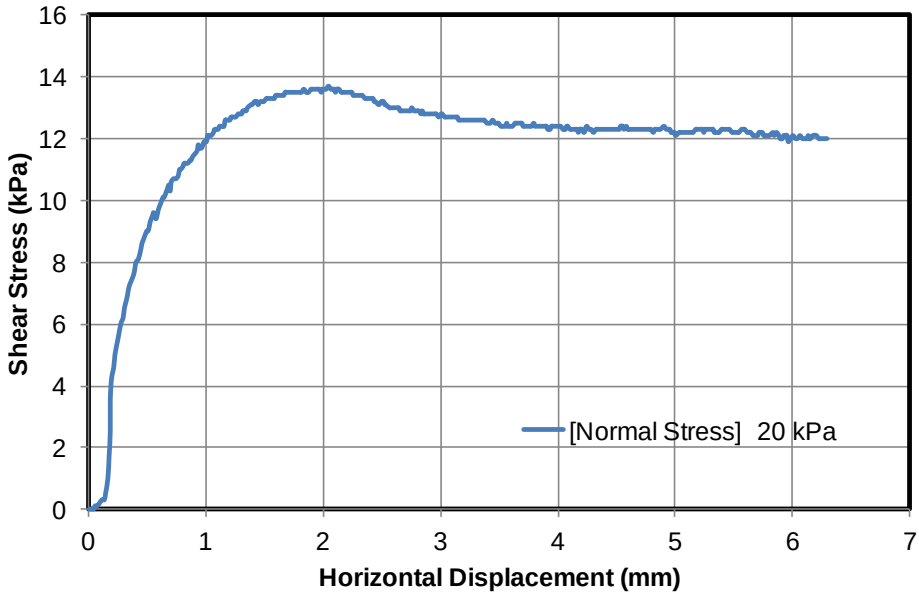

Figure B-1: Shear stress versus displacement – sand-geotextile interface density=1600 kg/m^3 (D_r = 75%) and normal stress of 20 kPa

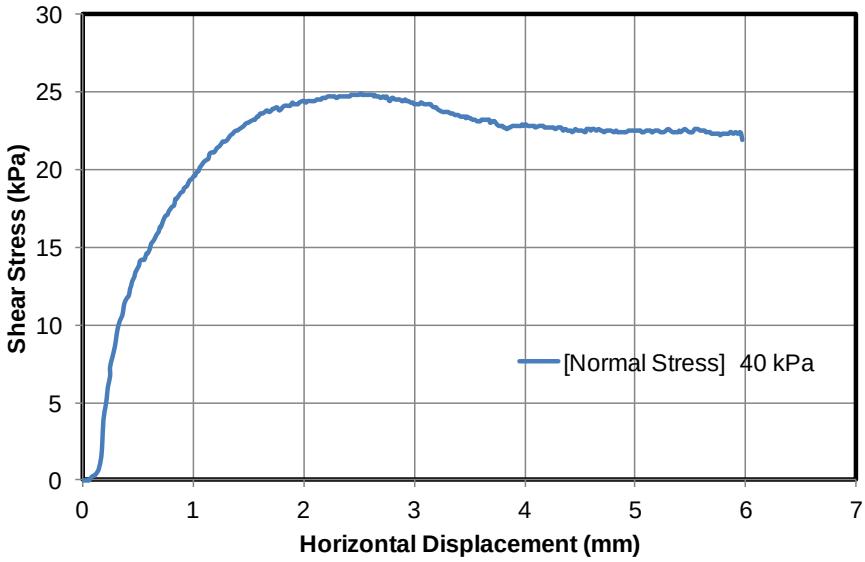

Figure B-2: Shear stress versus displacement – sand-geotextile interface density=1600 kg/m^3 (D_r = 75%) and normal stress of 40 kPa

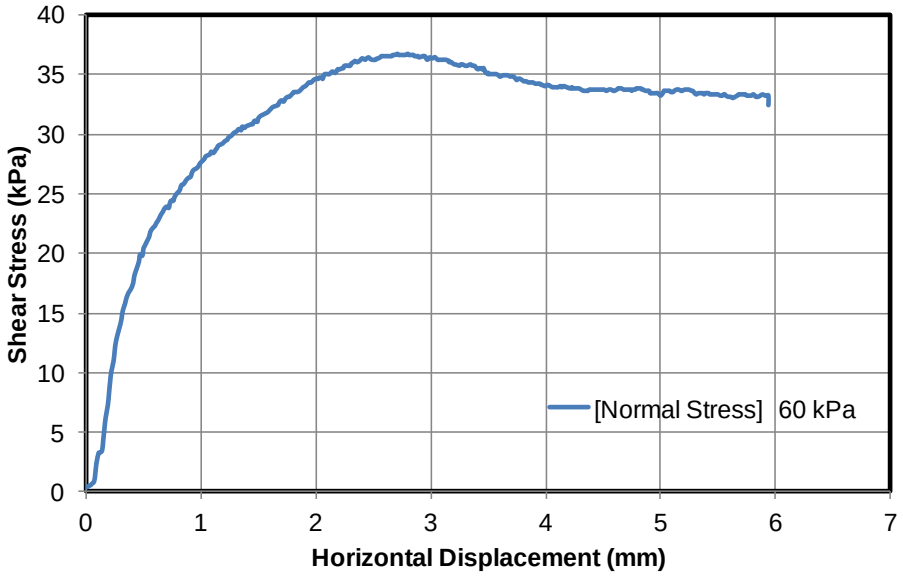

Figure B-3: Shear stress versus displacement – sand-geotextile interface density=1600 kg/m^3 (D_r = 75%) and normal stress of 60 kPa

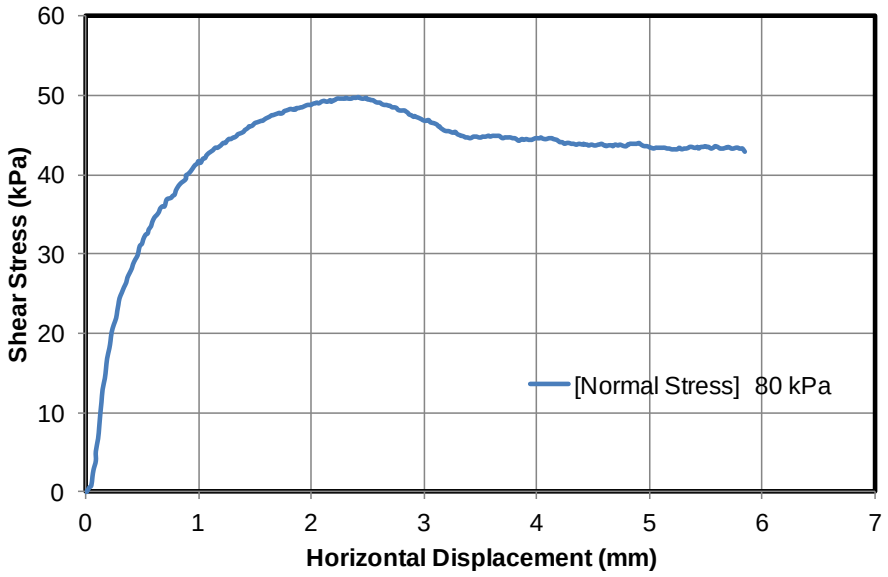

Figure B-4: Shear stress versus displacement – sand-geotextile interface density=1600 kg/m^3 (D_r = 75%) and normal stress of 80 kPa

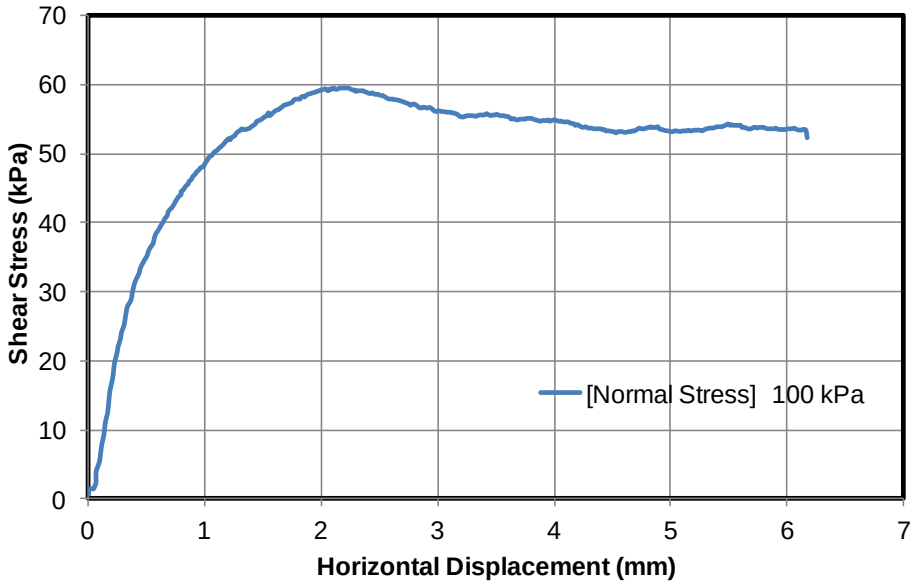

Figure B-5: Shear stress versus displacement – sand-geotextile interface density=1600 kg/m^3 (D_r = 75%) and normal stress of 100 kPa

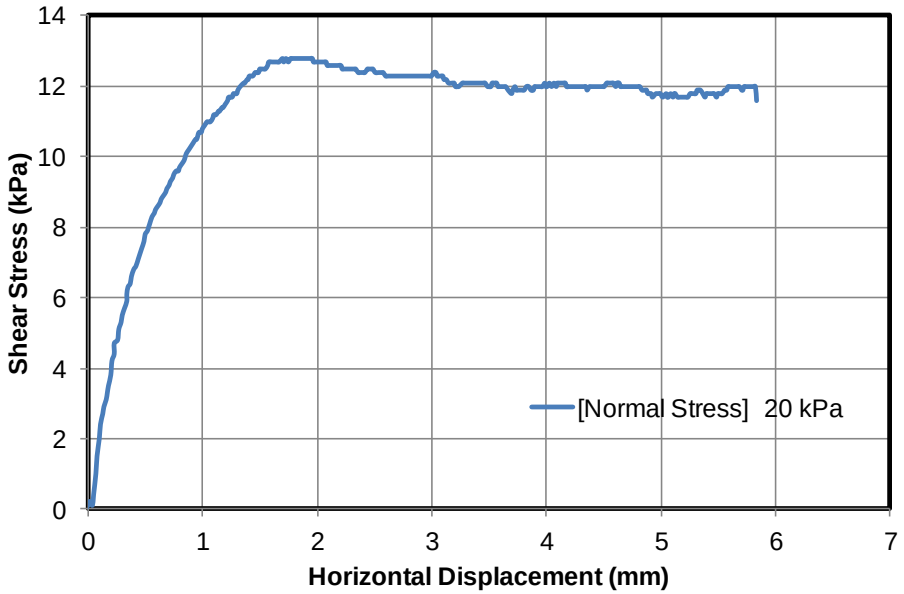

Figure B-6: Shear stress versus displacement – road mulch-geotextile interface density=1800 kg/m^3 and normal stress of 20 kPa

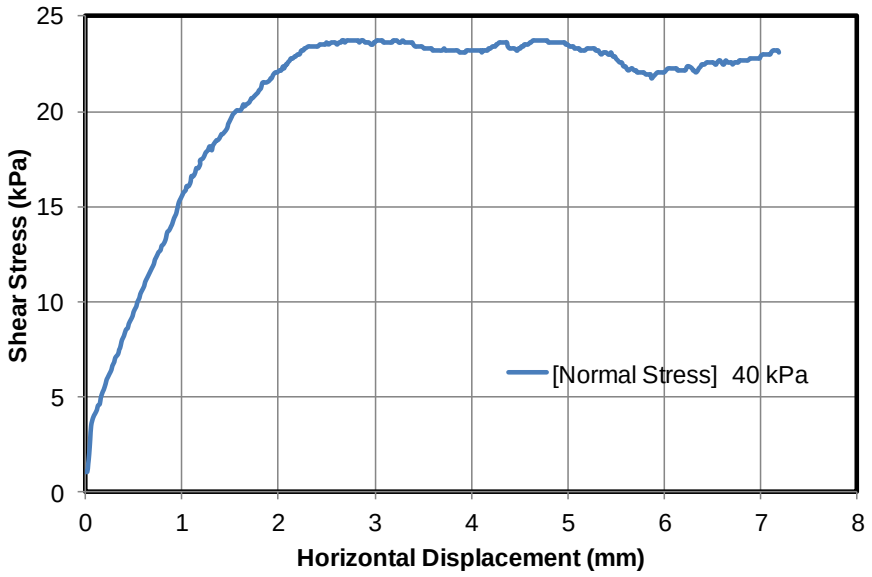

Figure B-7: Shear stress versus displacement – road mulch-geotextile interface density=1800 kg/m^3 and normal stress of 40 kPa

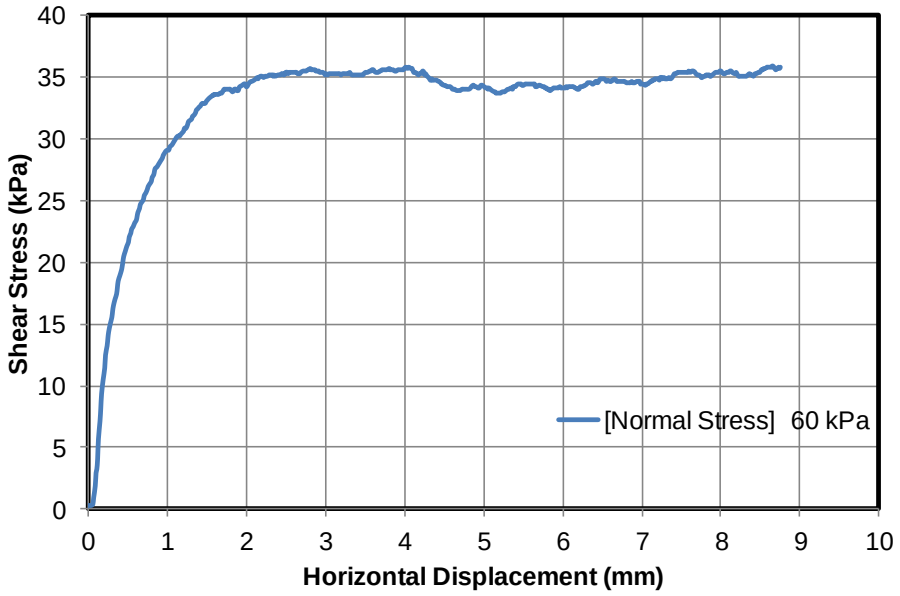

Figure B-8: Shear stress versus displacement – road mulch-geotextile interface density=1800 kg/m^3 and normal stress of 60 kPa

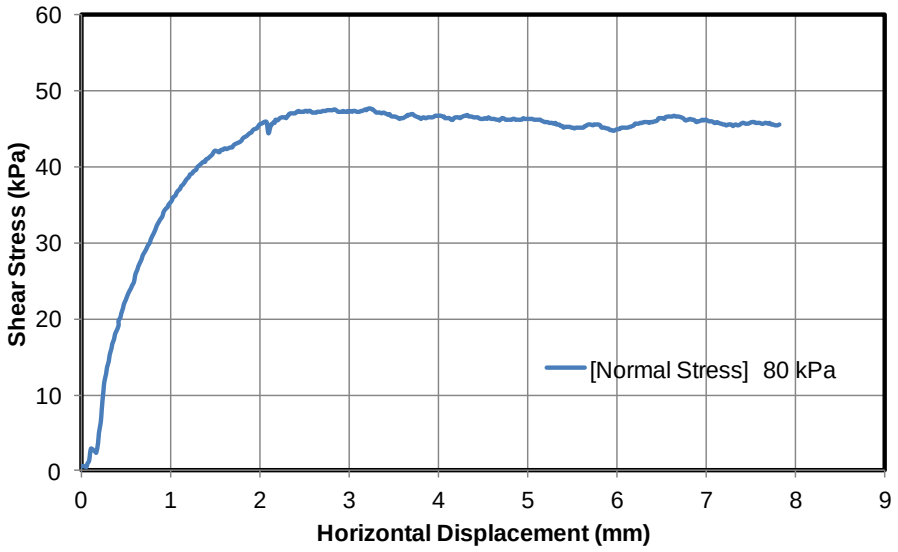

Figure B-9: Shear stress versus displacement – road mulch-geotextile interface density=1800 kg/m^3 and normal stress of 80 kPa

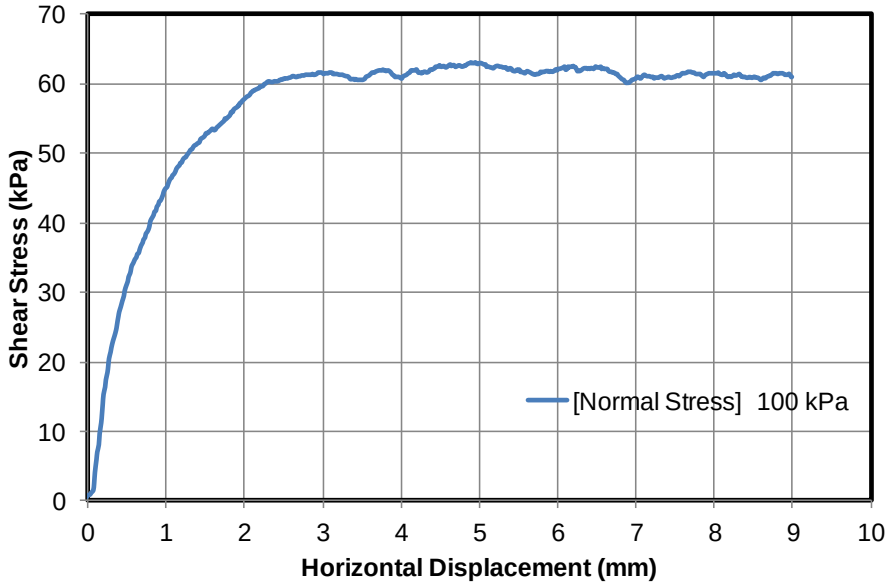

Figure B-10: Shear stress versus displacement – road mulch-geotextile interface density=1800 kg/m^3 and normal stress of 100 kPa

APPENDIX C-1: LATERAL SOIL RESTRAINT VS. PIPE DISPLACEMENT

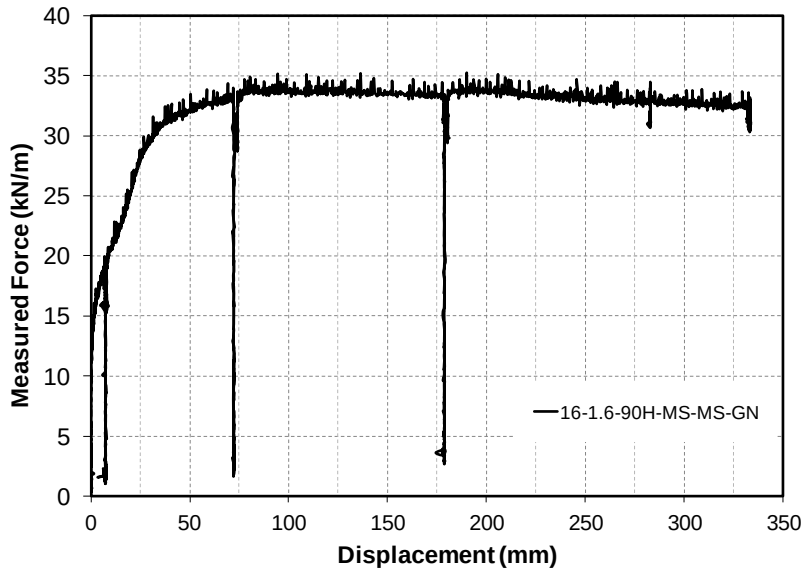

Figure C1-1: Lateral force vs. displacement, average dry density = 1,600 kg/m^3 (D_r=75%), NPS16 (406 mm), H/D=1.6

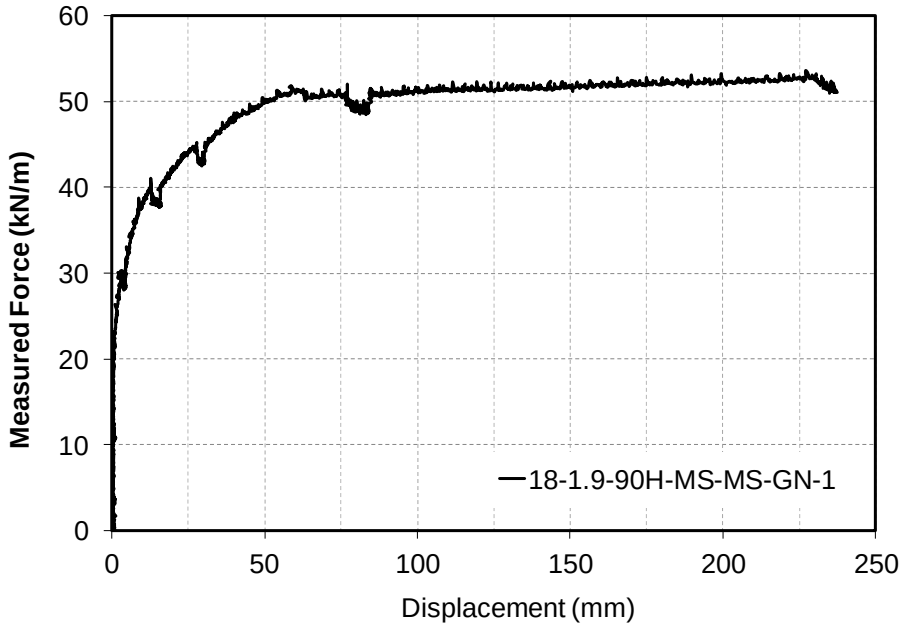

Figure C1-2: Lateral force vs. displacement, average dry density = 1,600 kg/m^3 (D_r=75%), NPS18 (457 mm), H/D=1.9

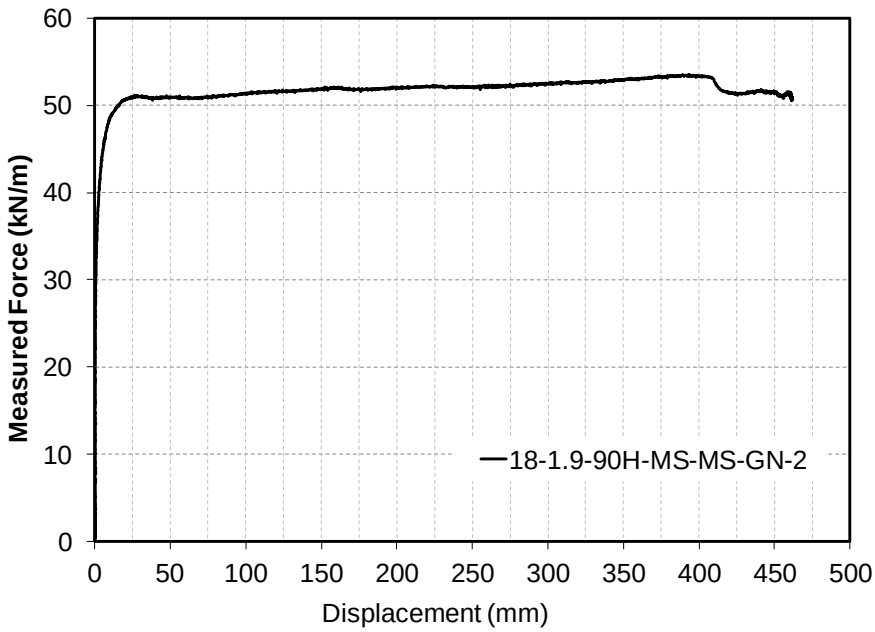

Figure C1-3: Lateral force vs. displacement, average dry density = 1,600 kg/m^3 (D_r=75%), NPS18 (457 mm), H/D=1.9

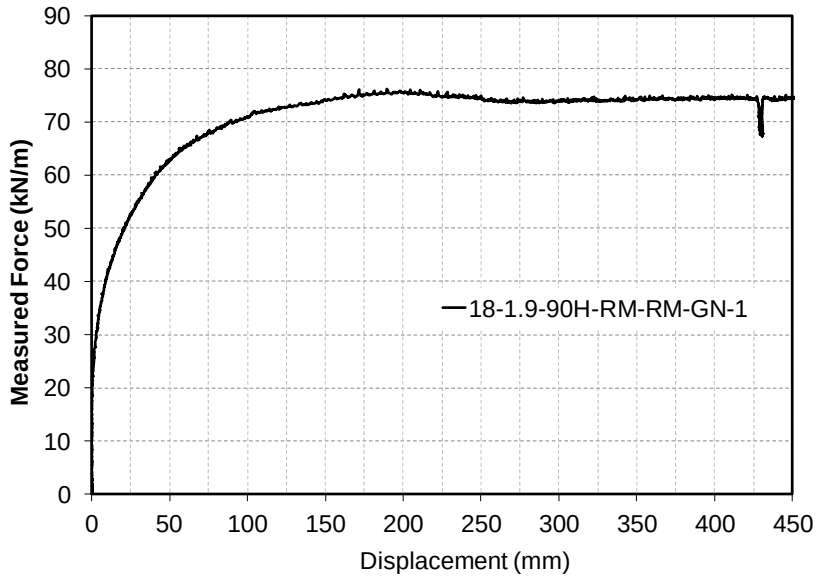

Figure C1-4: Lateral force vs. displacement, average dry density = 1,800 kg/m^3, NPS18 (457 mm), H/D=1.9

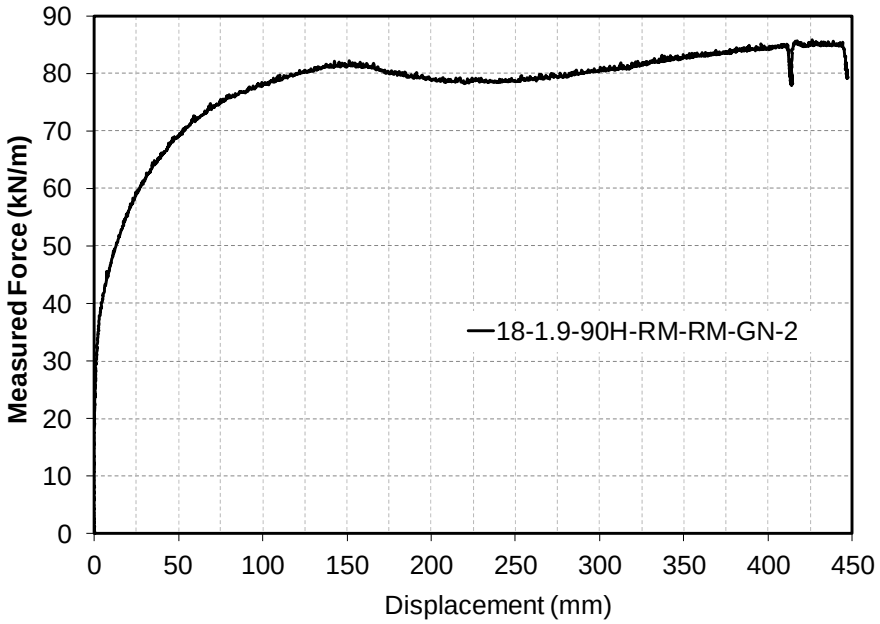

Figure C1-5: Lateral force vs. displacement, average dry density = 1,800 kg/m^3, NPS18 (457 mm), H/D=1.9

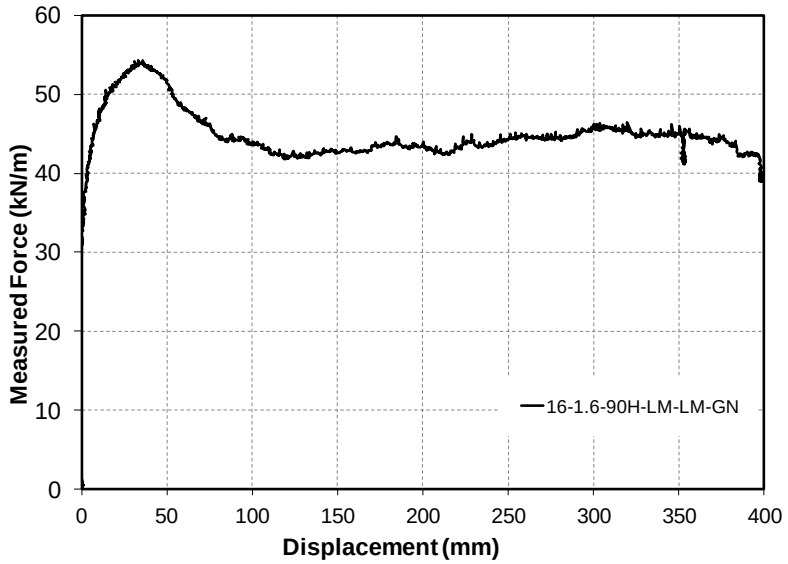

Figure C1-6: Lateral force vs. displacement, average dry density = 1,700 kg/m^3, NPS16 (406 mm), H/D=1.6

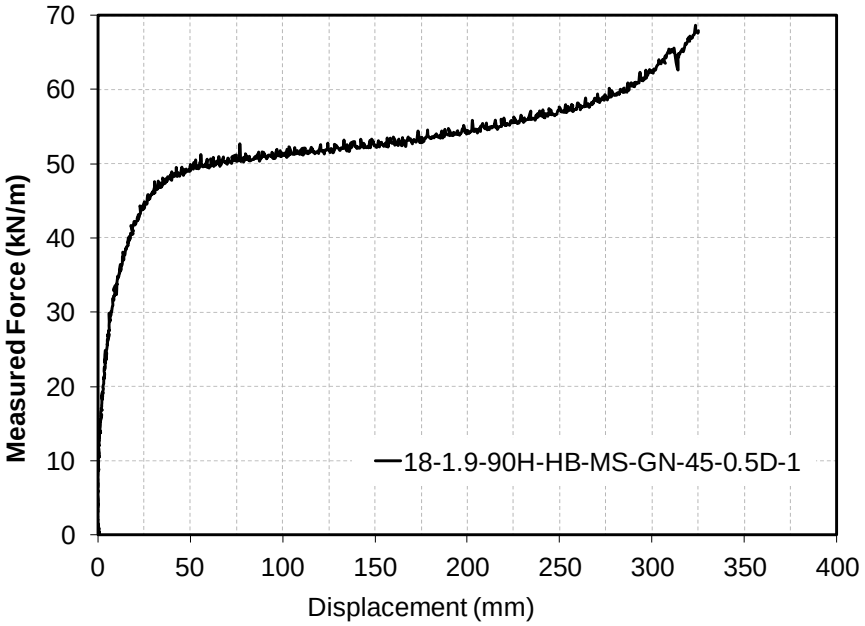

Figure C1-7: Lateral force vs. displacement, hard boundary (45°), no geotextile, NPS18 (457 mm), H/D=1.9, S=0.5D

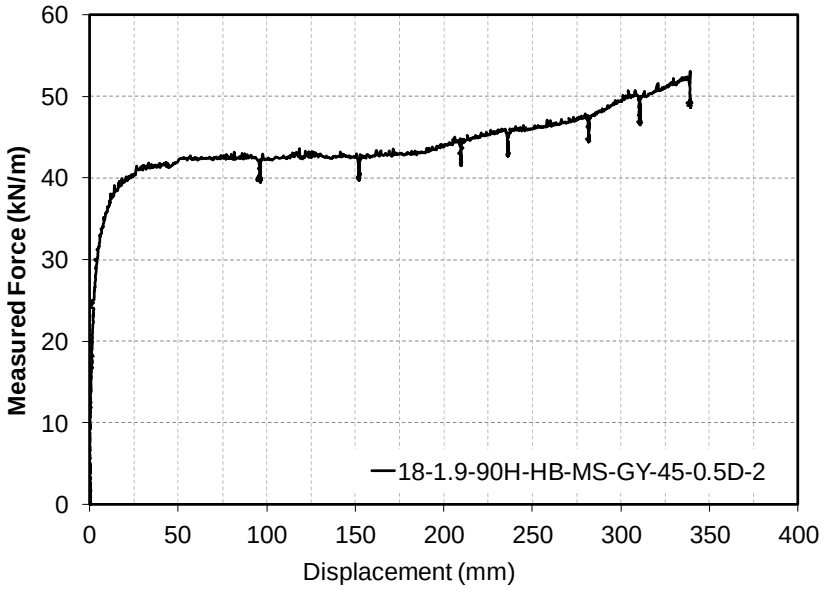

Figure C1-8: Lateral force vs. displacement, hard boundary (45°), sand- geotextile interface, NPS18 (457 mm), H/D=1.9, S=0.5D

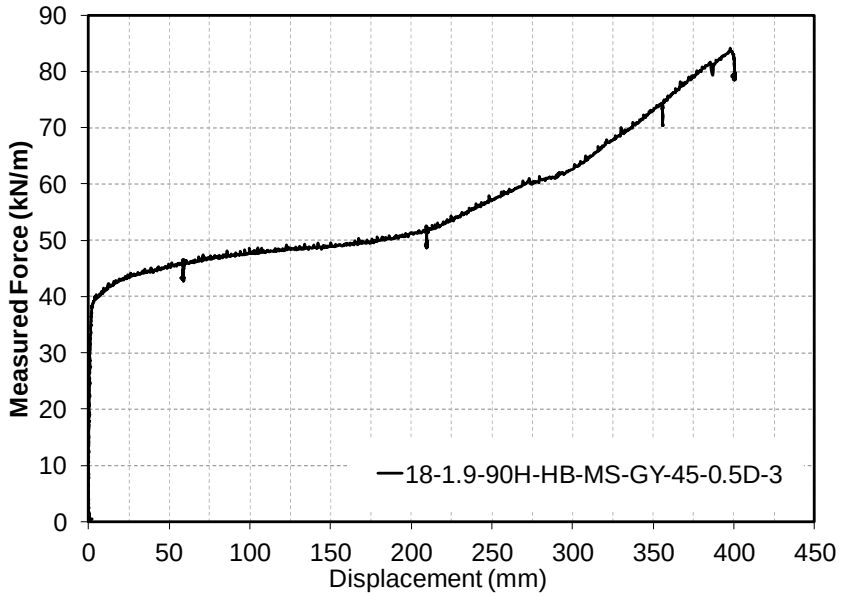

Figure C1-9: Lateral force vs. displacement, hard boundary (45°), sand- geotextile interface, NPS18 (457 mm), H/D=1.9, S=0.5D

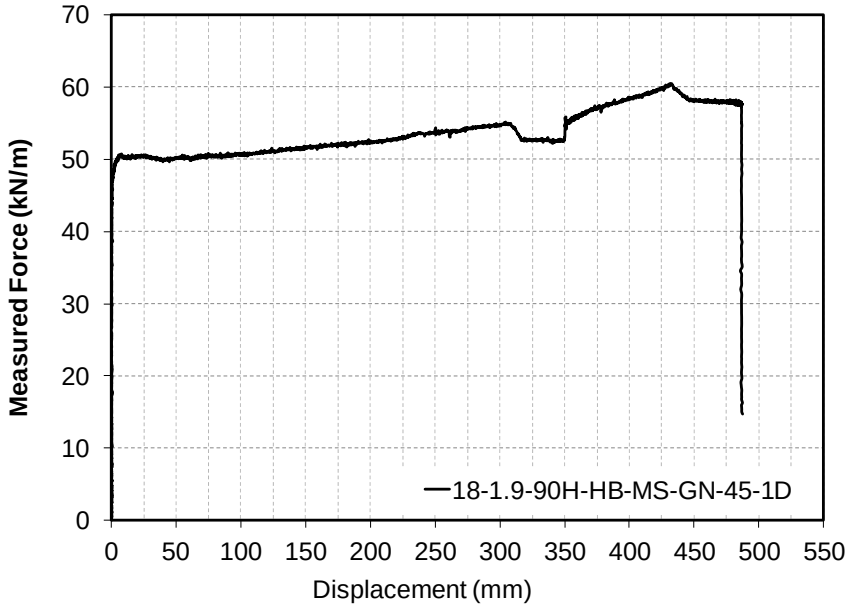

Figure C1-10: Lateral force vs. displacement, hard boundary (45°), no geotextile, NPS18 (457 mm), H/D=1.9, S=1.0D

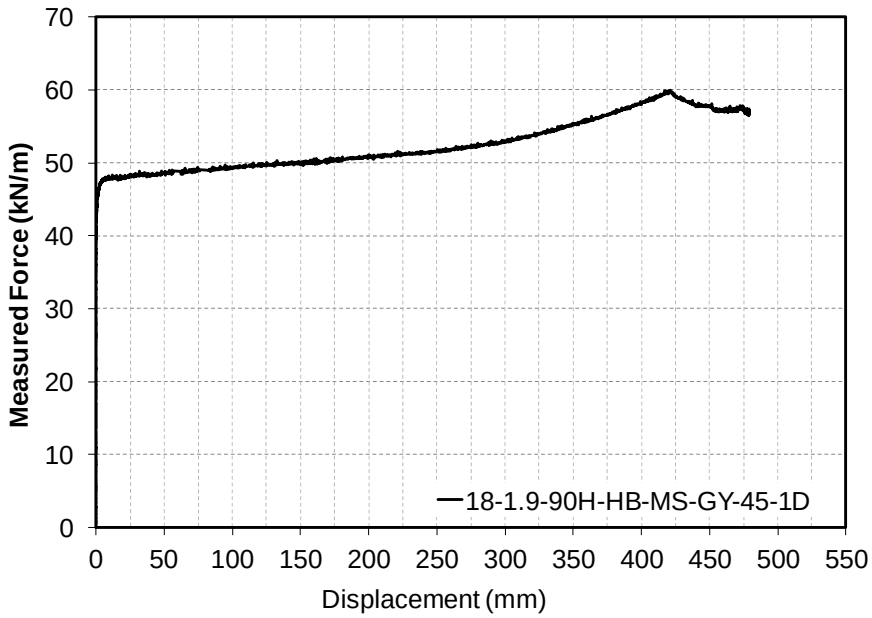

Figure C1-11: Lateral force vs. displacement, hard boundary (45°), sand- geotextile interface, NPS18 (457 mm), H/D=1.9, S=1.0D

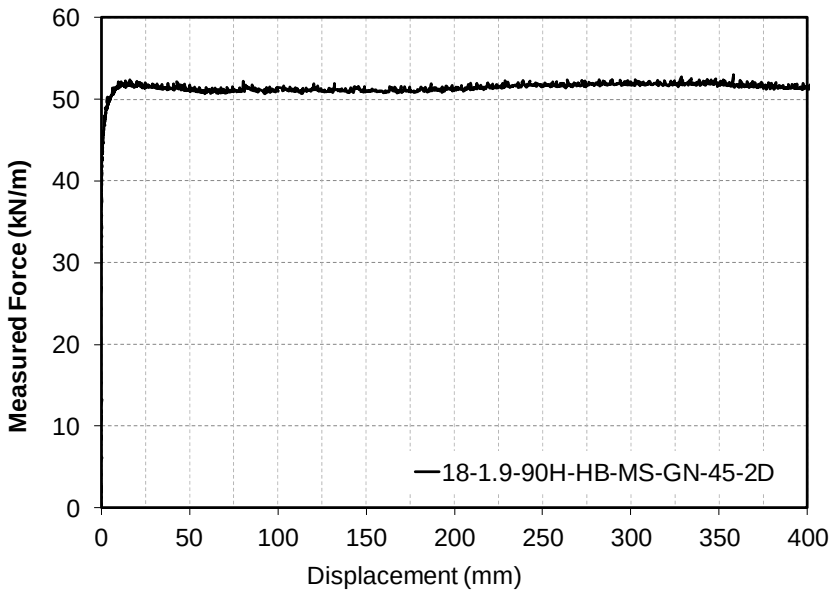

Figure C1-12: Lateral force vs. displacement, hard boundary (45°), no geotextile, NPS18 (457 mm), H/D=1.9, S=2.0D

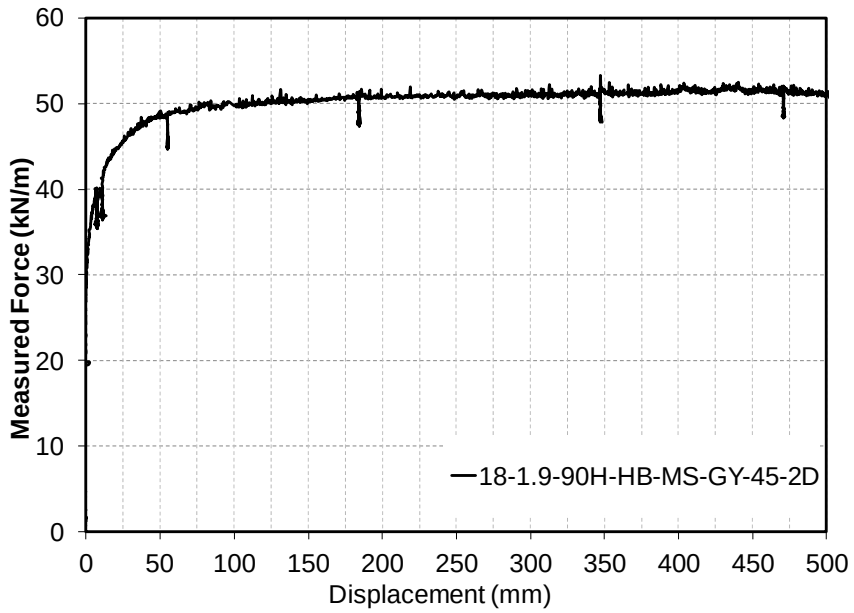

Figure C1-13: Lateral force vs. displacement, hard boundary (45°), sand- geotextile interface, NPS18 (457 mm), H/D=1.9, S=2.0D

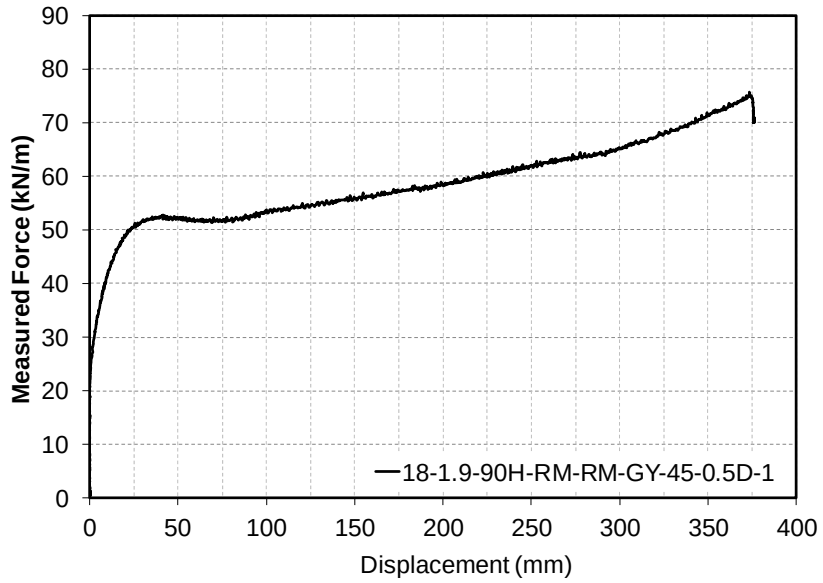

Figure C1-14: Lateral force vs. displacement, hard boundary (45°), road mulch-geotextile interface, NPS18 (457 mm), H/D=1.9, S=0.5D

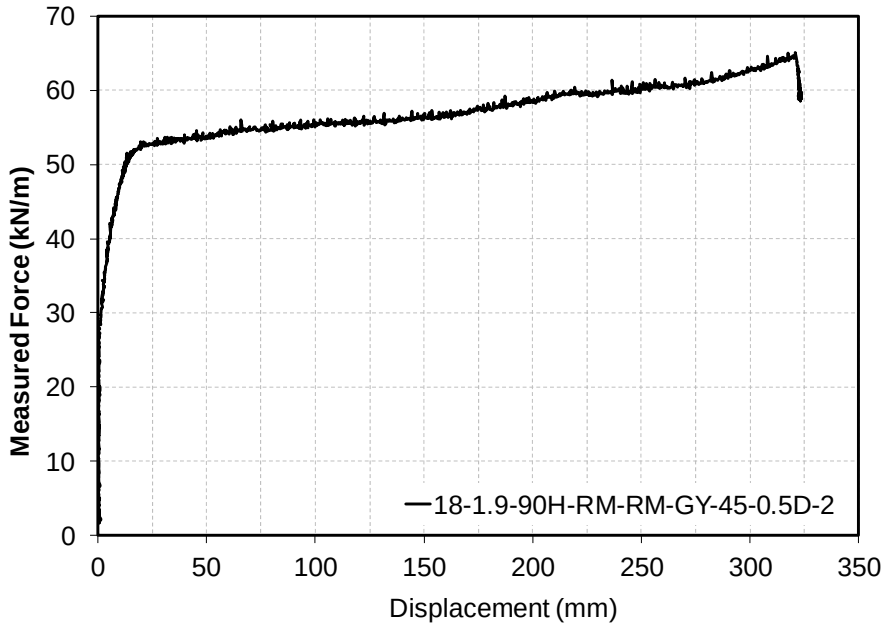

Figure C1-15: Lateral force vs. displacement, hard boundary (45°), road mulch-geotextile interface, NPS18 (457 mm), H/D=1.9, S=0.5D

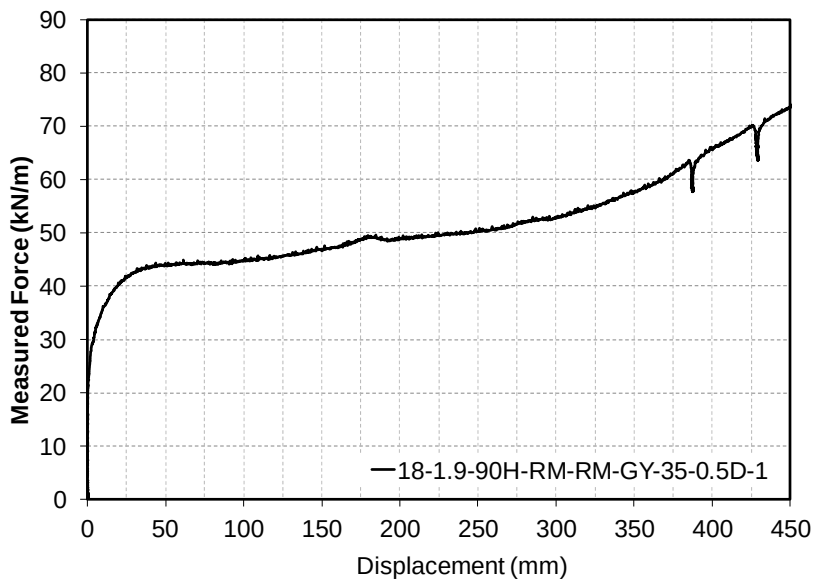

Figure C1-16: Lateral force vs. displacement, hard boundary (35°), road mulch-geotextile interface, NPS18 (457 mm), H/D=1.9, S=0.5D

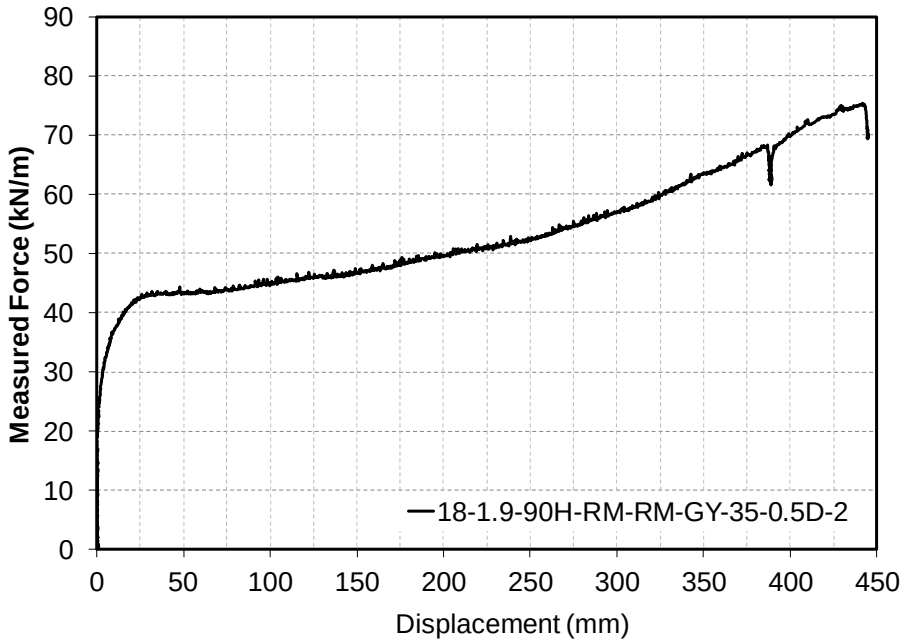

Figure C1-17: Lateral force vs. displacement, hard boundary (35°), road mulch-geotextile interface, NPS18 (457 mm), H/D=1.9, S=0.5D

APPENDIX C-2: HORIZONTAL OBLIQUE SOIL RESTRAINT VS. PIPE DISPLACEMENT

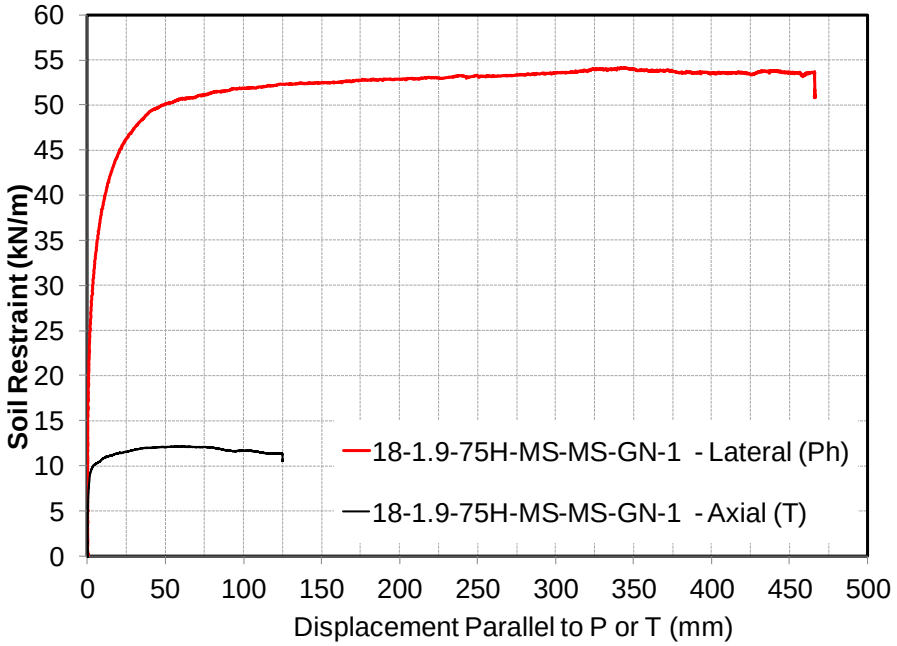

Figure C2-1: Horizontal oblique forces (75°) vs. displacement, average dry density = 1,600 kg/m^3 (D_r=75%), NPS18 (457 mm), H/D=1.9

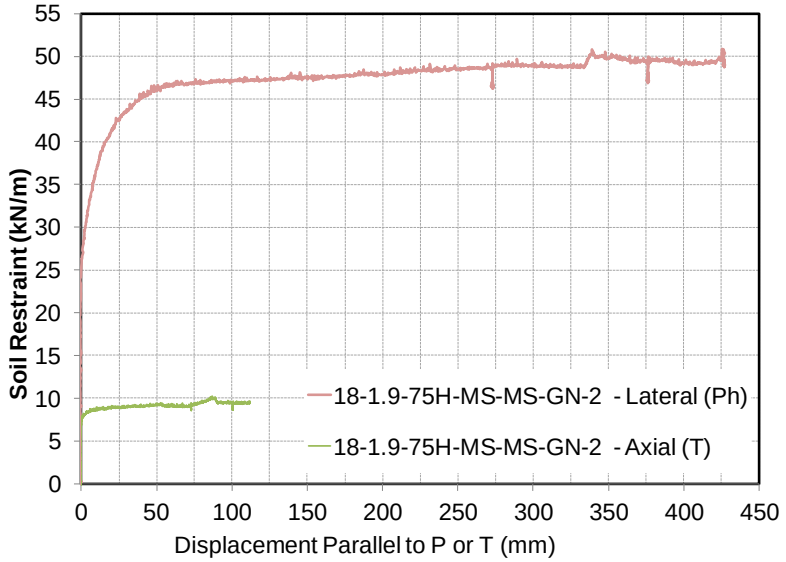

Figure C2-2: Horizontal oblique forces (75°) vs. displacement, average dry density = 1,600 kg/m^3 (D_r=75%), NPS18 (457 mm), H/D=1.9

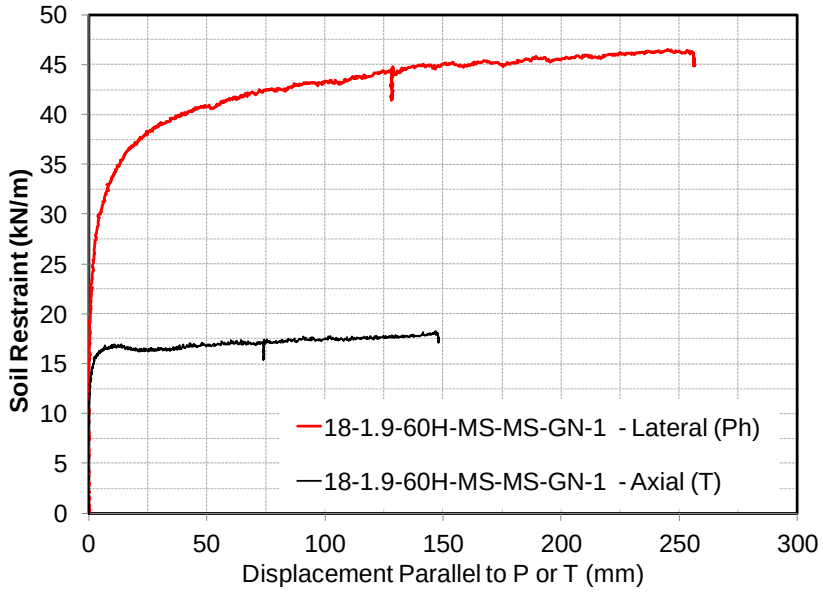

Figure C2-3: Horizontal oblique forces (60°) vs. displacement, average dry density = 1,600 kg/m^3 (D_r=75%), NPS18 (457 mm), H/D=1.9

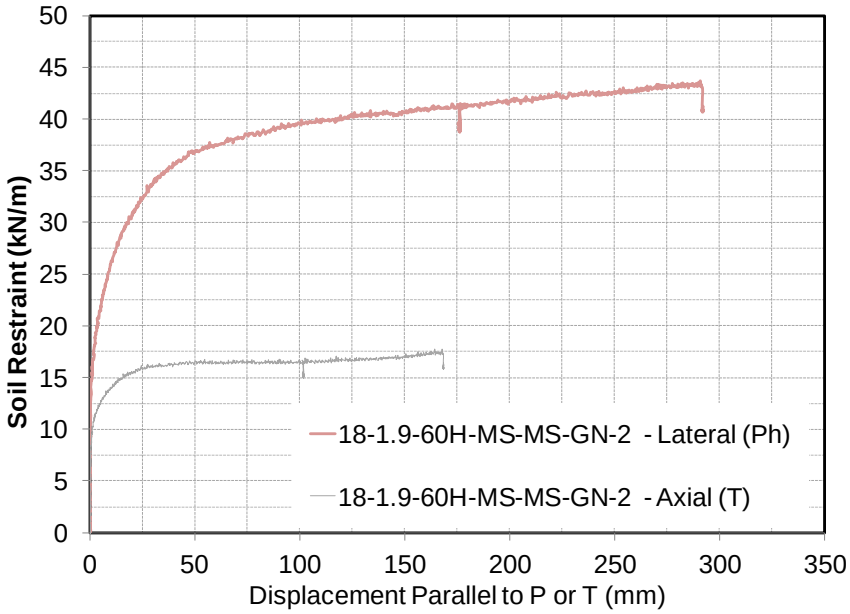

Figure C2-4: Horizontal oblique forces (60°) vs. displacement, average dry density = 1,600 kg/m^3 (D_r=75%), NPS18 (457 mm), H/D=1.9

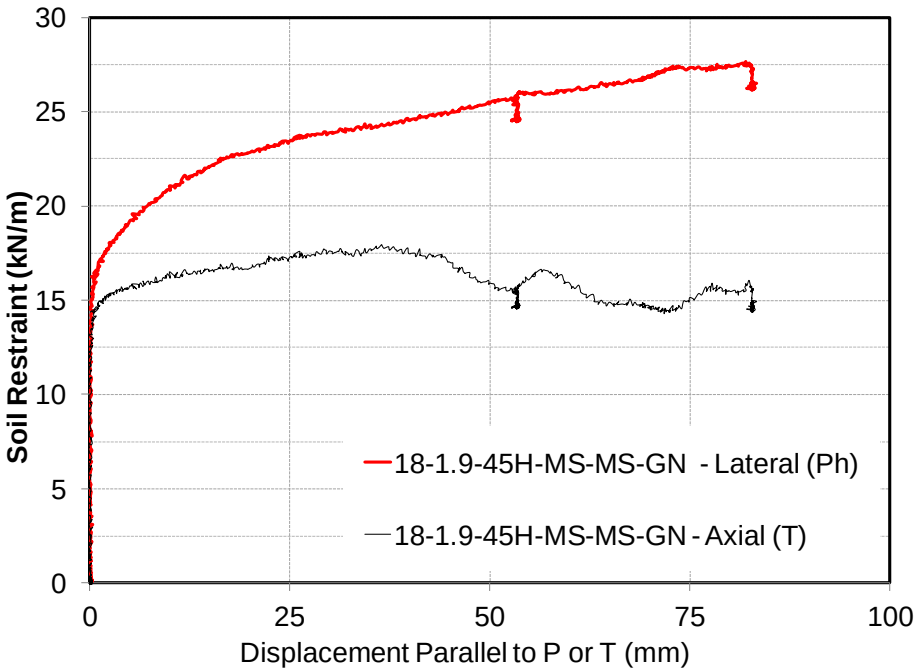

Figure C2-5: Horizontal oblique forces (45°) vs. displacement, average dry density = 1,600 kg/m^3 (D_r=75%), NPS18 (457 mm), H/D=1.9

APPENDIX C-3: VERTICAL OBLIQUE SOIL RESTRAINT VS. PIPE DISPLACEMENT

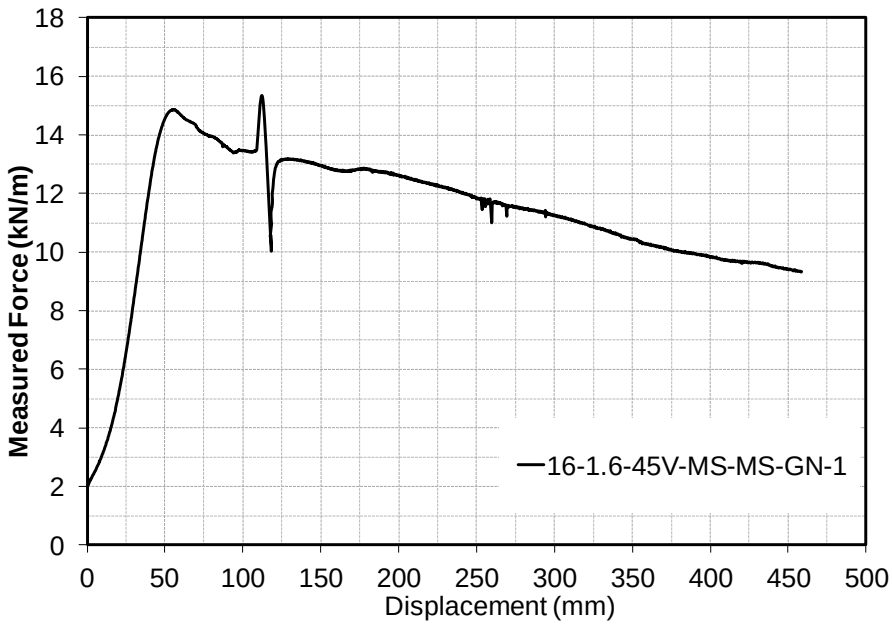

Figure C3-1: Vertical oblique forces (45°) vs. displacement, average dry density = 1,600 kg/m^3 (D_r=75%), NPS16 (406 mm), H/D=1.6

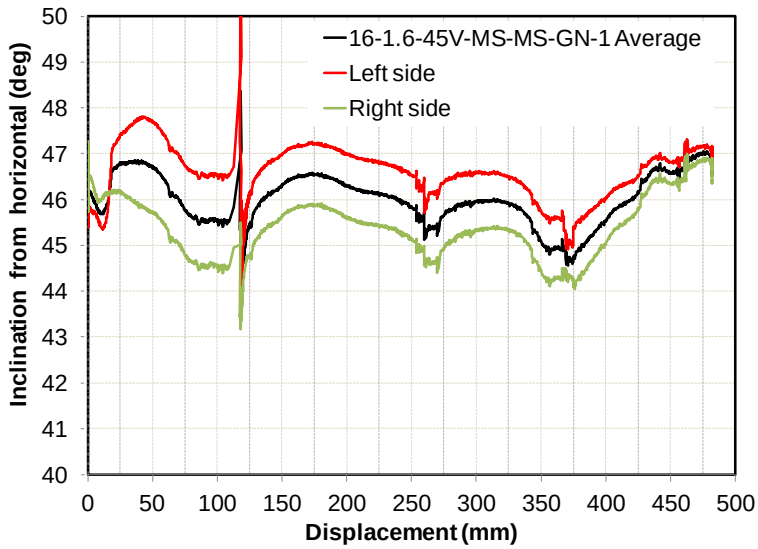

Figure C3-2: Puling angle vs. displacement, average dry density = 1,600 kg/m^3 (D_r=75%), NPS16 (406 mm), H/D=1.6

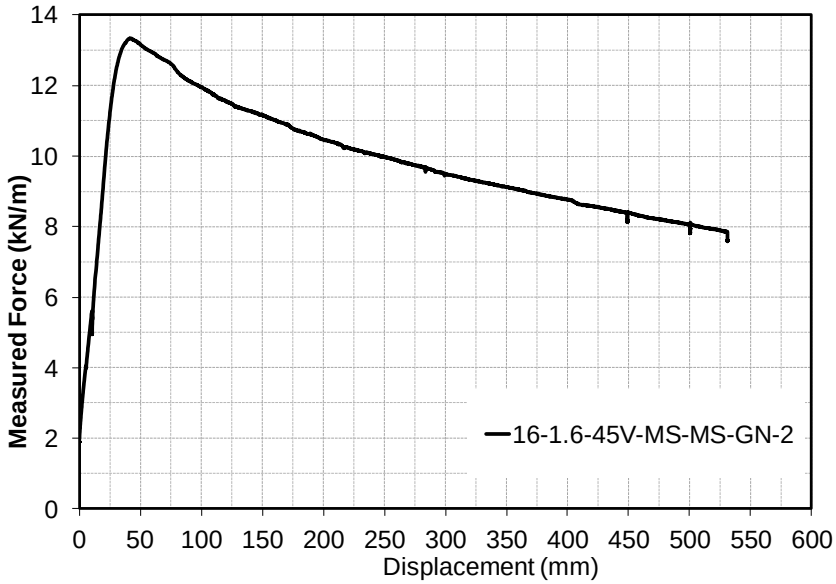

Figure C3-3: Vertical oblique forces (45°) vs. displacement, average dry density = 1,600 kg/m^3 (D_r=75%), NPS16 (406 mm), H/D=1.6

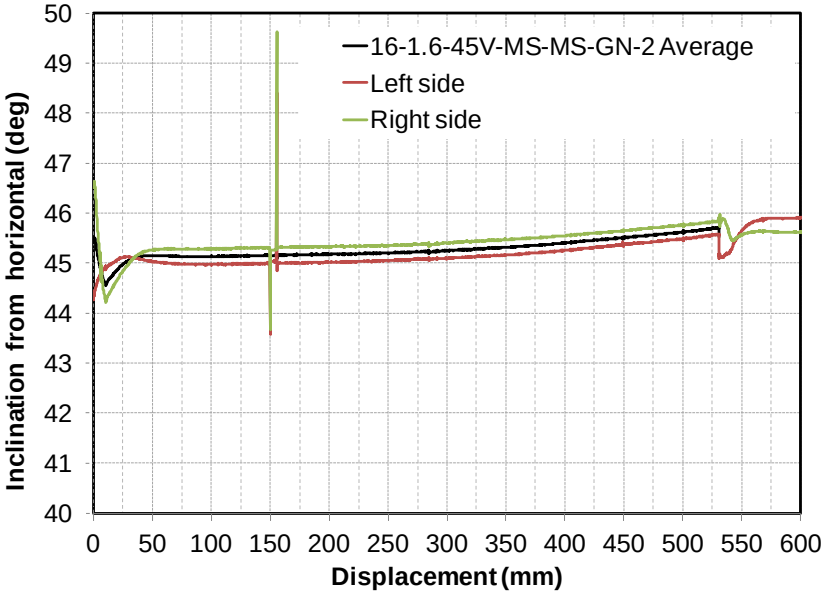

Figure C3-4: Puling angle vs. displacement, average dry density = 1,600 kg/m^3 (D_r=75%), NPS16 (406 mm), H/D=1.6

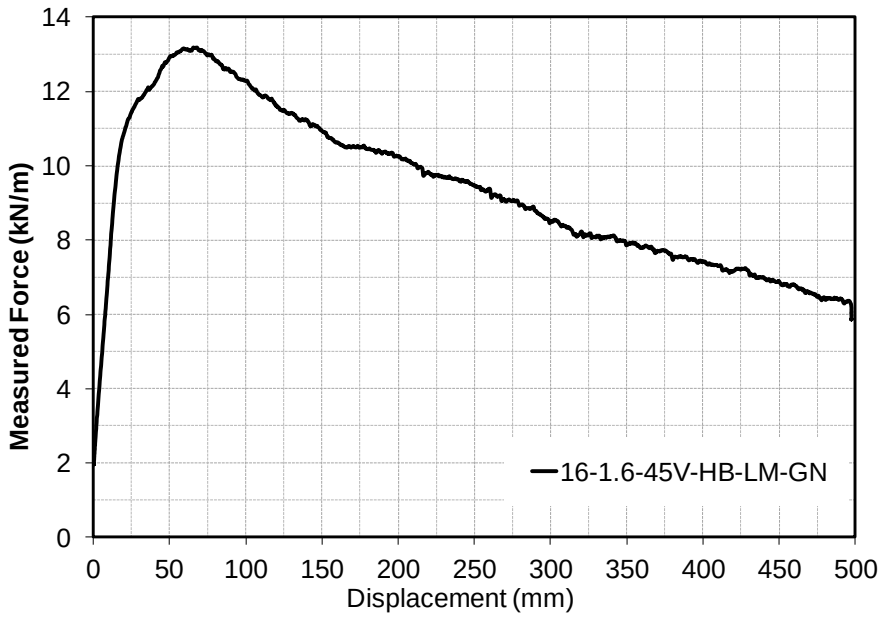

Figure C3-5: Vertical oblique forces (45°) vs. displacement, hard boundary (45°), NPS16 (406 mm), H/D=1.6

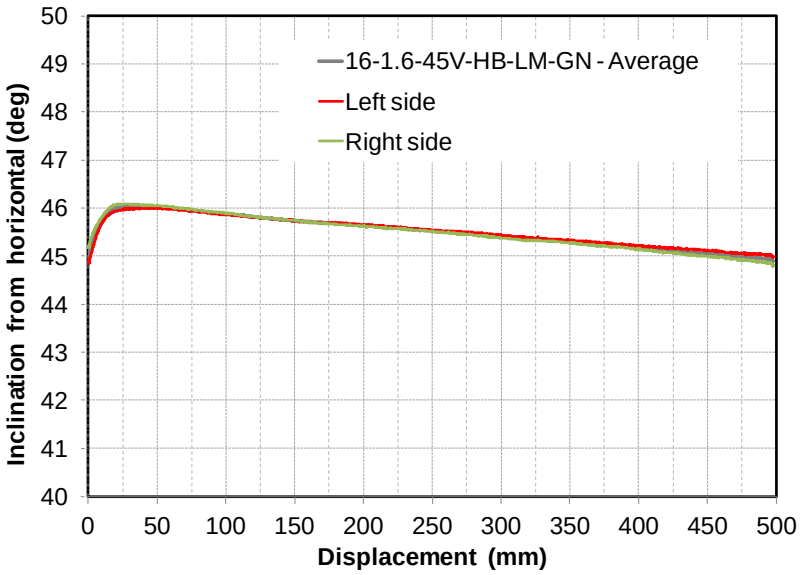

Figure C3-6: Puling angle vs. displacement, hard boundary (45°), average dry density = 1,700 kg/m^3, NPS16 (406 mm), H/D=1.6

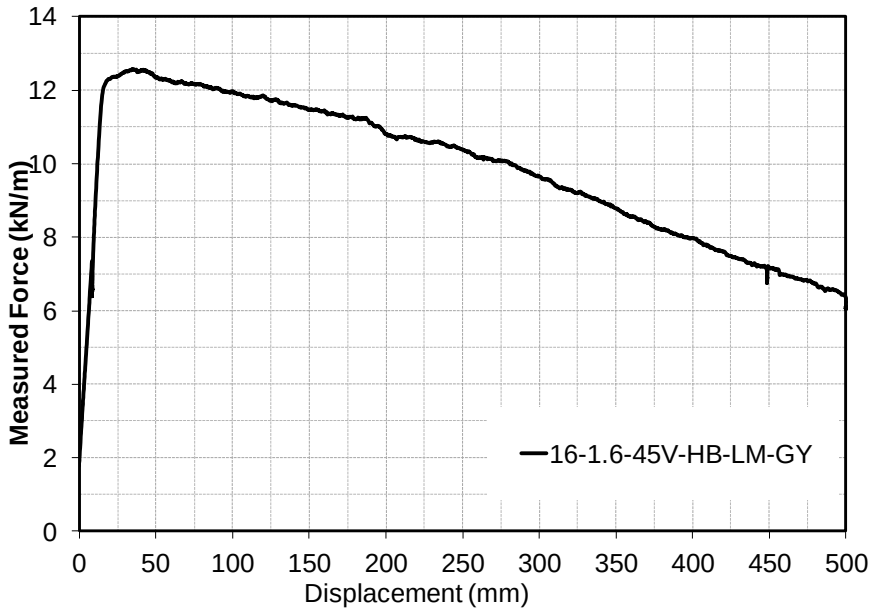

Figure C3-7: Vertical oblique forces (45°) vs. displacement, hard boundary (45°) w/geotextile, NPS16 (406 mm), H/D=1.6

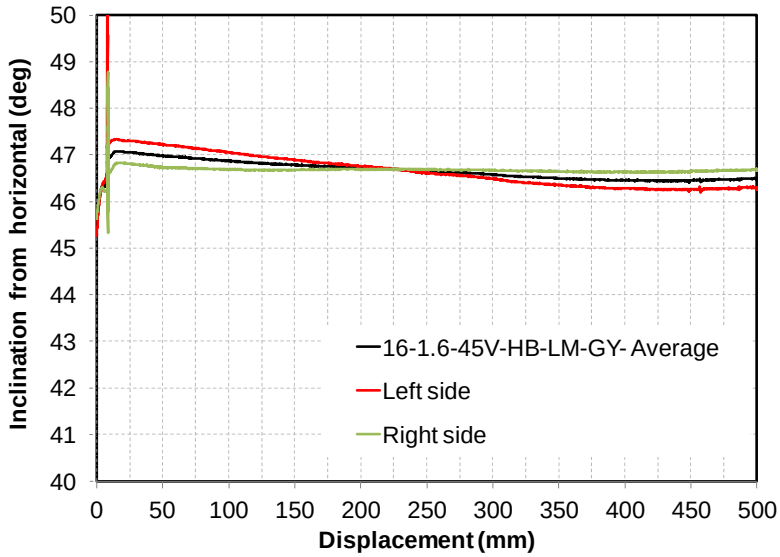

Figure C3-8: Puling angle vs. displacement, hard boundary (45°) with geotextile, NPS16 (406 mm), H/D=1.6

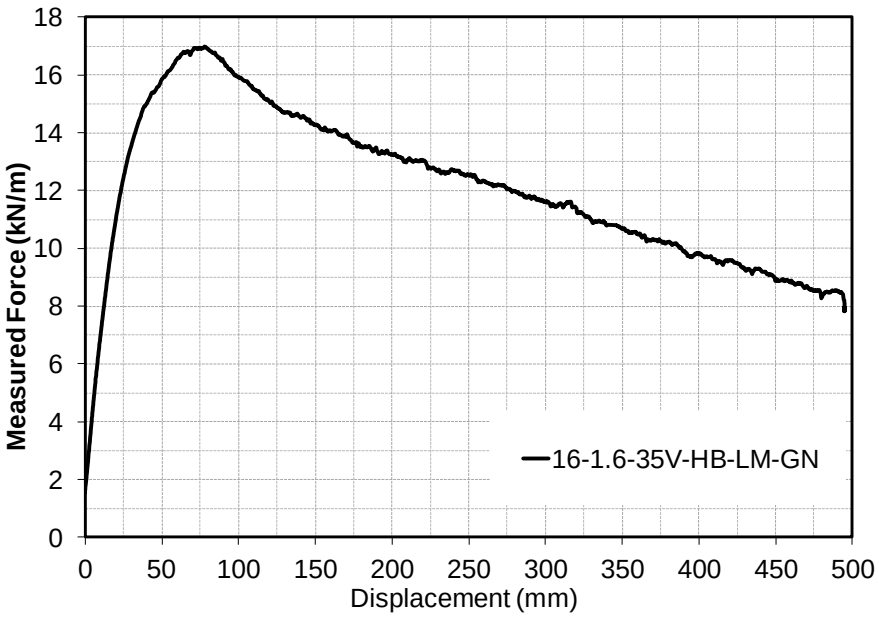

Figure C3-9: Vertical oblique forces (35°) vs. displacement, hard boundary (45°), NPS16 (406 mm), H/D=1.6

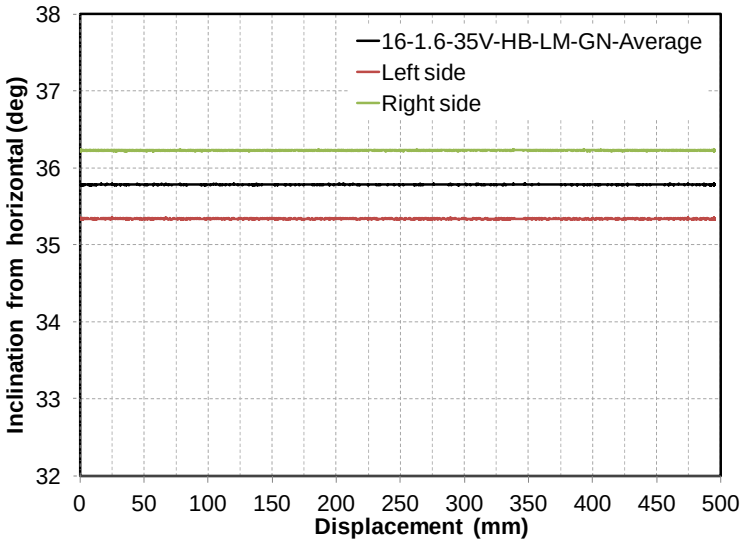

Figure C3-10: Puling angle vs. displacement, hard boundary (45°), average dry density = 1,700 kg/m^3, NPS16 (406 mm), H/D=1.6

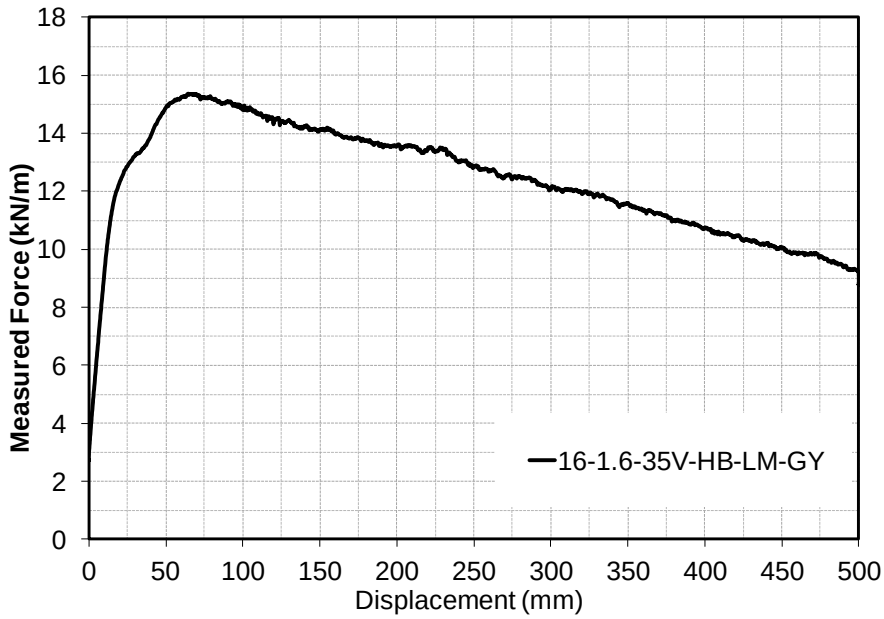

Figure C3-11: Vertical oblique forces (35°) vs. displacement, hard boundary (45°) w/geotextile, NPS16 (406 mm), H/D=1.6

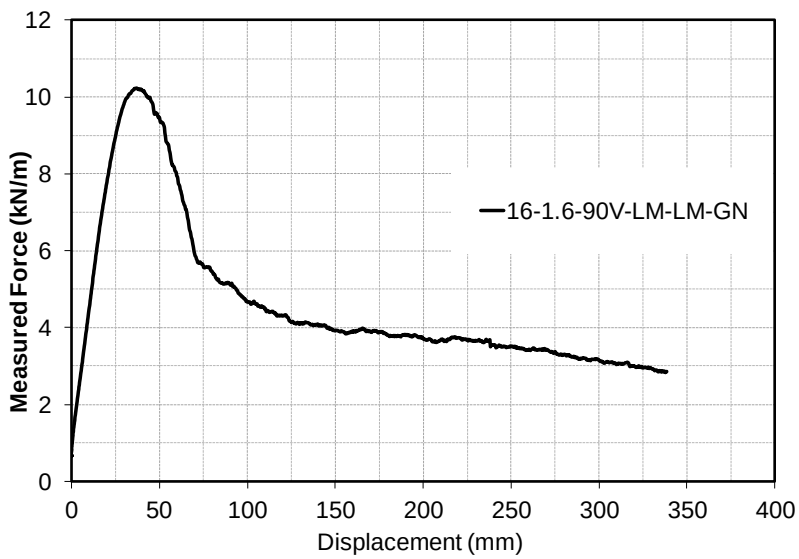

Figure C3-12: Vertical forces (90°) vs. displacement, average dry density = 1,700 kg/m^3, NPS16 (406 mm), H/D=1.6

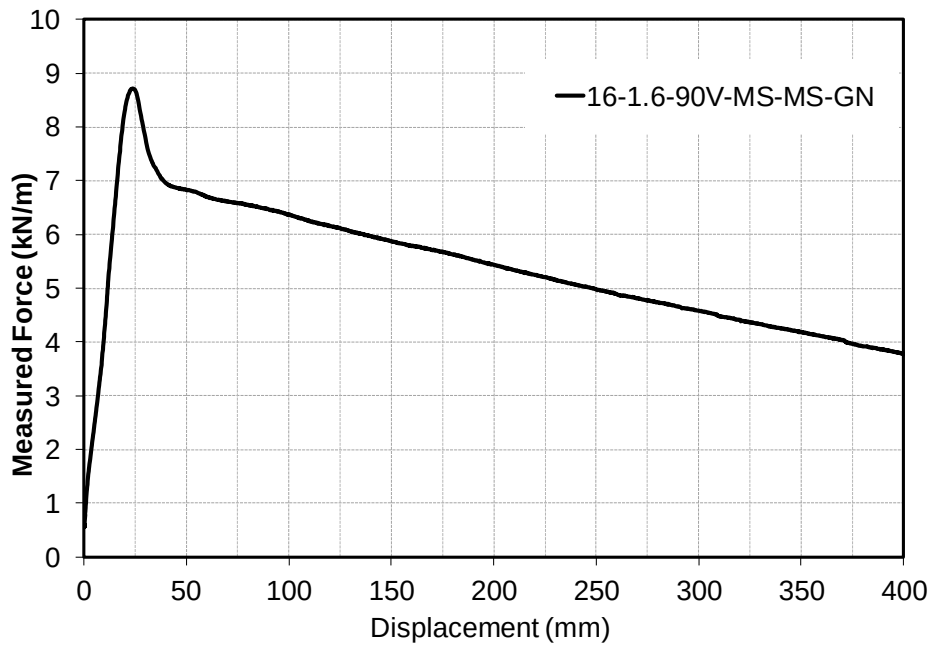

Figure C3-13: Vertical forces (90°) vs. displacement, average dry density = 1,600 kg/m^3, NPS16 (406 mm), H/D=1.6

APPENDIX D: CYSOIL MODEL

Both elastic and plastic deformation of soil elements are accounted for by the CYSOIL constitutive model. Principal stresses and directions are evaluated from the stress tensor and corresponding strain increments are decomposed in the form of plastic and elastic strains as presented in **Equation [D-1].**

$$\Delta e_i = \Delta e_i^e + \Delta e_i^p \quad i = 1,2,3 \qquad \text{[D-1]}$$

where the subscript “i” represents principal directions and superscripts “e” and “p” refer to the elastic and plastic part of the strain increment respectively. The relationship between elastic strains and principal stresses is described by Hooke’s law while flow rule controls the relation between plastic strains and principal stresses.

The Hooke’s law in incremental expression is as appear in **Equation [D-2]**:

$$\Delta\sigma'_1 = \alpha_1 \Delta e_1^e + \alpha_2(\Delta e_2^e + \Delta e_3^e)$$

$$\Delta\sigma'_2 = \alpha_1 \Delta e_2^e + \alpha_2(\Delta e_1^e + \Delta e_3^e) \qquad \text{[D-2]}$$

$$\Delta\sigma'_3 = \alpha_1 \Delta e_3^e + \alpha_2(\Delta e_1^e + \Delta e_2^e)$$

where:

$\alpha_1 = B^e + 4G^e / 3$

$\alpha_2 = B^e - 2G^e / 3$

and B and G are current, tangent elastic bulk and shear modulus of the material, respectively.

The failure envelope consists of a non-associated shear flow rule (Mohr-Coulomb) and an associated tensile flow rule (tension cut-off). The failure envelope as defined by Mohr-Coulomb yield function is expressed in a form consistent with the cap formulation and presented in **Equation [D-3]**:

$$f^s = Mp' - q + Nc \qquad \text{[D-3]}$$

where c is cohesion, $M = 6 \sin \phi_m / (3 - \sin \phi_m)$, and $N = 6 \cos \phi_m / (3 - \sin \phi_m)$. p' is the mean effective stress, $p' = -(\sigma'_1 + \sigma'_2 + \sigma'_3) / 3$, and q is a measure of shear stress, defined as:

$$q = -[\sigma'_1 + (\delta - 1)\sigma'_2 + \delta\sigma'_3] \qquad \text{[D-4]}$$

where $\delta = (3 + \sin \phi_m) / (3 - \sin \phi_m)$

In the FLAC formulation, the mobilized friction angle, ϕ_m, and cohesion, c, are given in terms of plastic shear-strain measure, γ^p, by means of a user-defined table. If no table is provided, it is assumed that friction and cohesion are constant, and equal to the input value of the friction property and cohesion property. The plastic shear strain, γ^p, is measured by a hardening parameter, whose incremental form is the second invariant of the incremental plastic deviatoric strain tensor as shown in **Equation [D-5]**:

$$\Delta\gamma^{p} = \left\{\frac{1}{2}(\Delta e_1{}^{ps} - \Delta e_m{}^{ps})^2 + \frac{1}{2}(\Delta e_m{}^{ps})^2 + \frac{1}{2}(\Delta e_3{}^{ps} - \Delta e_m{}^{ps})^2\right\}^{1/2}$$

[D-5]

Where $\Delta e_m{}^{ps} = \frac{1}{3}(\Delta e_1{}^{ps} + \Delta e_3{}^{ps})$

And Δe_j^{ps}, j = 1,3 are the principal plastic shear strain increments.

The evolution parameter for tensile yielding is the modulus of plastic tensile strain, e^{pt}. The increment of plastic tensile strain is defines as:

$$\Delta e^{pt} = \Delta e_3{}^{pt}$$

[D-6]

Where $\Delta e_3{}^{pt}$ is the increment of tensile plastic strain in the direction of the major principal stress. It is important to note that in FLAC tensile stresses are positive.

The potential function is nonassociative, and has the form:

$$g = M^* p' - q^*$$

[D-7]

where

$$q^* = [\sigma'_1 + (\delta^* - 1)\,\sigma'_2 + \delta^*\sigma'_3]$$

[D-8]

In **Equations [D-7]** and **[D-8]**, $\delta^* = (3 + \sin\psi_m) / (3 - \sin\psi_m)$, and $M^* = 6 \sin\psi_m / (3 - \sin\psi_m)$. Also the mobilized dilatancy angle, ψ_m, is given in terms of

plastic shear strain, γ^p, by means of a user-defined table. For more details on formulation and the modeling procedure of CYSOIL constitutive model refer to Section 1.6.10 of FLAC 7.0's manual.

As described in **Section 7.1.1**, the stress-strain curve for granular materials is usually approximated by a hyperbola (e.g. Kondner and Zelaski, 1963; Duncan et al., 1980, Matsuoka and Nakai, 1977; Beaty and Byrne, 1998; Puebla, 1999). The CYSOIL constitutive model is supplemented by a friction, strain hardening table to capture this hyperbolic behavior. In particular, CYSOIL adopts a hyperbolic incremental law similar to the one implemented in the UBCSAND model (Byrne et al. 2003):

$$d(sin\varphi_m) = \frac{G^p}{p'} d(\gamma^p)$$

[D-9]

Where p' is effective pressure, and the plastic shear modulus, G^p, is given by

$$G^p = \beta \cdot G^e (1 - \frac{sin\varphi_m}{sin\varphi_f} R_f)^2 \quad \varphi_m \leq \varphi_f$$

[D-10]

In the previous equation, G^e is the elastic tangent shear modulus, ϕ_f is the ultimate friction angle, R_f (the failure ratio) is a constant smaller than 1, and β is a calibration factor.

The elastic tangent shear modulus is a function of p', and we have

$$G^e = k_G{}^e \cdot P_a (\frac{p'}{P_a})^m$$

[D-11]

Where k_G^e is the elastic shear modulus number; m is the shear modulus exponent; and P_a is the atmospheric pressure. After some manipulation and integration of **Equation [D-9]**, the following expression is obtained (FLAC 7.0's manual):

$$\gamma^p = \frac{p\prime}{\beta \cdot k_G{}^e \cdot P_a (\frac{p'}{P_a})^m} \frac{sin\varphi_f}{R_f} \left[\frac{1}{1 - \frac{sin\varphi_m}{sin\varphi_f} R_f} - 1 \right]$$

[D-12]

The above expression was used in this study to generate the model input table of friction in terms of plastic shear strain.

The associated increment of irrecoverable volumetric strain, Δe^p, is related to the increment of plastic shear strain $\Delta\gamma^p$, through the shear-hardening flow rule of the form:

$$\Delta e^p = \Delta\gamma^p \sin \psi_m$$

[D-13]

Where ψ_m is the mobilized dilation angle.

Several different laws are available in the literature to characterize ψ_m. For the purpose of this research, an equation based on Rowe stress-dilatancy theory (1962) was used. According to this theory, there is a constant-volume stress ratio, ϕ_{cv}, below which the material contracts (i.e., for $\phi_m < \phi_{cv}$), while for higher stress ratios (i.e., for $\phi_m > \phi_{cv}$), the material dilates. The equation has the form shown in **Equation [D-14]:**

$$sin\, \psi_m = \frac{sin\phi_m - sin\psi_{cv}}{1 - sin\phi_m sin\psi_{cv}}$$

[D-14]

Where

$$sin\,\psi_{cv} = \frac{sin\phi_f - sin\psi_f}{1 - sin\phi_f sin\psi_f}$$

[D-15]

And ϕ_f and ψ_f are ultimate (known) values of friction and dilation, respectively.

APPENDIX E: ADDITIONAL PHOTOGRAPHS

PHOTO E-1.1	**Test 18-1.9-90H-HB-MS-GN-45-0.5D-1 : Prior to Testing – View from Left Side of the Soil Chamber**

PHOTO E-1.2	**Test 18-1.9-90H-HB-MS-GN-45-0.5D-1 – View from Left Side of the Soil Chamber**

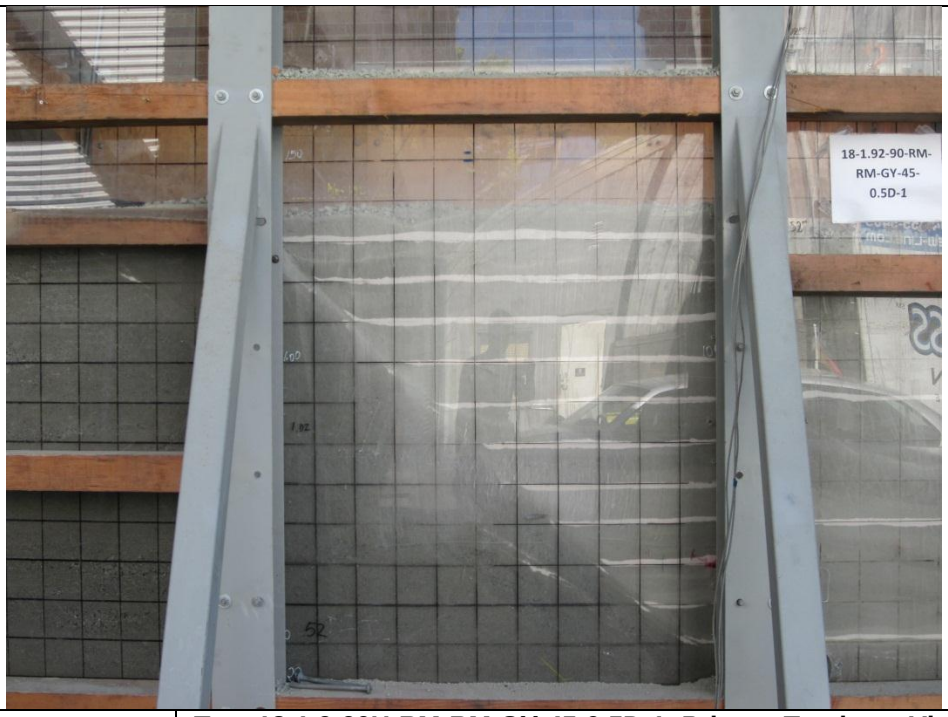

PHOTO E-1.3	**Test 18-1.9-90H-RM-RM-GY-45-0.5D-1: Prior to Testing – View from Left Side of the Soil Chamber**

PHOTO E-1.4	**Test 18-1.9-90H-RM-RM-GY-45-0.5D-1:– View from Left Side of the Soil Chamber**

PHOTO E-1.5	**Test 18-1.9-90H-RM-RM-GY-45-0.5D-2: Prior to Testing – View from Left Side of the Soil Chamber**

PHOTO E-1.6	**Test 18-1.9-90H-RM-RM-GY-45-0.5D-2:– View from Left Side of the Soil Chamber**

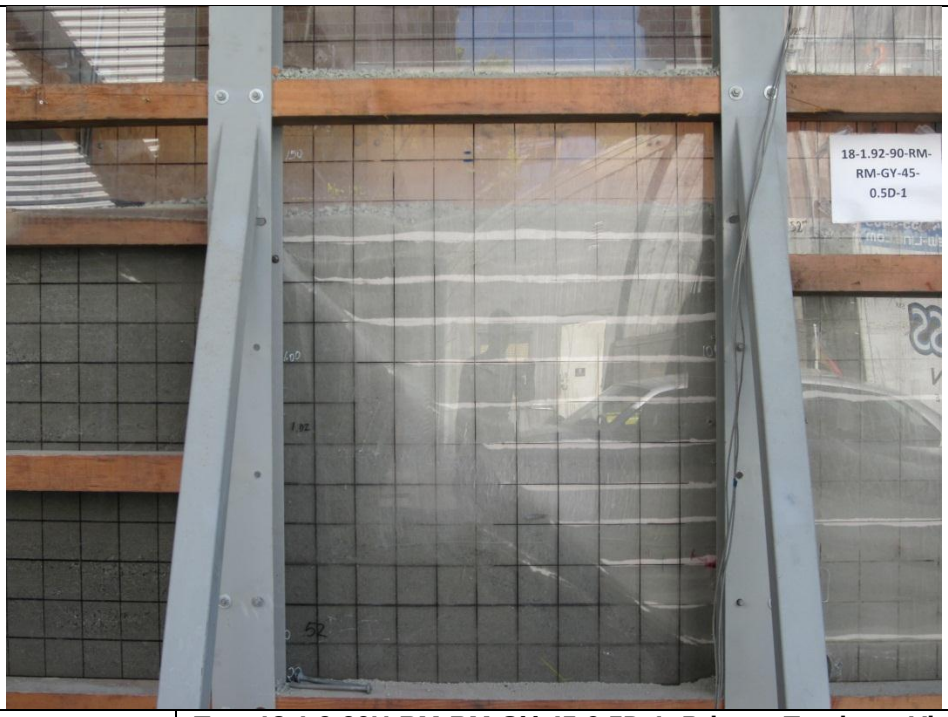

PHOTO E-1.7	**Test 18-1.9-90H-RM-RM-GY-45-0.5D-1: Prior to Testing – View from Left Side of the Soil Chamber**

PHOTO E-1.8	**Test 18-1.9-90H-RM-RM-GY-45-0.5D-1:– View from Left Side of the Soil Chamber**

PHOTO E-1.9	**Test 18-1.9-90H-RM-RM-GY-35-0.5D-1: Specimen Preparation – View from Left Side of the Soil Chamber**

PHOTO E-1.10	**Test 18-1.9-90H-RM-RM-GY-35-0.5D-1: After Test - View from Left Side of the Soil Chamber**

PHOTO E-1.11	**Test 18-1.9-90H-RM-RM-GY-35-0.5D-2: Before Test – View from Left Side of the Soil Chamber**

PHOTO E-1.12	**Test 18-1.9-90H-RM-RM-GY-35-0.5D-2: After Test - View from Left Side of the Soil Chamber**

PHOTO E-1.13	**Test 18-1.9-75H-MS-MS-GN-1: Test Preparation – View from Top Front of the Soil Chamber**

PHOTO E-1.14	**Test 18-1.9-75H-MS-MS-GN-1: After Test - View from Top Front of the Soil Chamber**

PHOTO E-1.15	**Test 18-1.9-75H-MS-MS-GN-2: Before Test – View from Top Front of the Soil Chamber**

PHOTO E-1.16	**Test 18-1.9-75H-MS-MS-GN-2: After Test - View from Top Front of the Soil Chamber**

PHOTO E-1.17	**Test 18-1.9-60H-MS-MS-GN-2: Test Preparation – View from Top Front of the Soil Chamber**

PHOTO E-1.18	**Test 18-1.9-60H-MS-MS-GN-2: After Test - View from Top Front of the Soil Chamber**

PHOTO E-1.19	**Test 18-1.9-45H-MS-MS-GN-1: Before Test – View from Top Rear of the Soil Chamber**

PHOTO E-1.20	**Test 18-1.9-45H-MS-MS-GN-1: After Test - View from Top Front of the Soil Chamber**

PHOTO E-1.21	**Test 16-1.6-45V-MS-MS-GN-1 : Prior to Testing – View from Front Side of the Soil Chamber**

PHOTO E-1.22	**Test 16-1.6-45V-MS-MS-GN-1 : Prior to Testing – View from Left Side of the Soil Chamber**

A. Before Application of Displacement

B. At 100 mm Average Displacement

C. At 230 mm Average Displacement

D. At 297 mm Average Displacement

PHOTO E-1.23	**Test 16-1.6-45V-MS-MS-GN-1 : Time Lapse – View from Left Side of the Soil Chamber**

PHOTO E-1.24	**Test 16-1.6-45V-MS-MS-GN-1 : End of Testing – View from Rear-Right Side of the Soil Chamber**

PHOTO E-1.25	**Test 16-1.6-45V-MS-MS-GN-1 : End of Testing – View from Left Side of the Soil Chamber**

PHOTO E-1.26	**Test 16-1.6-45V-HB-LM-GY : Prior to Testing – View from Front of the Soil Chamber**

PHOTO E-1.27	**Test 16-1.6-45V-HB-LM-GY : Prior to Testing – View from Left Side of the Soil Chamber**

PHOTO E-1.28	**Test 16-1.6-45V-HB-LM-GY : Prior to Testing – View from Rear Side of the Soil Chamber**

A. Before Application of Displacement

B. At Y'=0.25D

C. At Y'=0.65D

D. At Y'=1.23D

PHOTO E-1.29	**Test 16-1.6-45V-HB-LM-GY : Time Lapse – View from Left Side of the Soil Chamber**

PHOTO E-1.30	**Test 16-1.6-45V-HB-LM-GY : End of Testing – View from Front Side of the Soil Chamber**

PHOTO E-1.31	**Test 16-1.6-45V-HB-LM-GY: End of Testing – View from Left Side of the Soil Chamber**

PHOTO E-1.32	**Test 16-1.6-45V-HB-LM-GY: End of Testing – View from Rear Side of the Soil Chamber**

PHOTO E-1.33	**Test 16-1.6-35V-HB-LM-GY : Prior to Testing – View from Front Side of the Soil Chamber**

PHOTO E-1.34	**Test 16-1.6-35V-HB-LM-GY : Prior to Testing – View from Left Side of the Soil Chamber**

A. Before Application of Displacement

B. At Y'=0.34D

C. At Y'=0.72D

D. At Y'=1.23D

PHOTO E-1.35	**Test 16-1.6-35V-HB-LM-GY : Time Lapse – View from Left Side of the Soil Chamber**

PHOTO E-1.36	**Test 16-1.6-35V-HB-LM-GY : End of Testing – View from Front Side of the Soil Chamber**

PHOTO E-1.37	**Test 16-1.6-35V-HB-LM-GY: End of Testing – View from Left Side of the Soil Chamber**

APPENDIX F: SOIL PRESSURE SENSOR CALIBRATION

Sensor PT-1		Sensor PT-2		Sensor PT-3	
kPa	volt	kPa	volt	kPa	volt
0	-5.50E-03	0	-6.63E-01	0	-1.116
20	-6.67E-02	20	-7.26E-01	20	-1.179
40	-1.28E-01	40	-7.85E-01	40	-1.243
60	-1.86E-01	60	-8.45E-01	60	-1.305
80	-2.47E-01	80	-9.09E-01	80	-1.366
100	-3.07E-01	100	-9.69E-01	100	-1.428
120	-3.67E-01	120	-1.03E+00	120	-1.491
140	-4.29E-01	140	-1.09E+00	140	-1.553